Analysis of β-catenin signaling by a novel combinatory approach consisting of Co-Immunoprecipitation and DigiWest.

Dissertation

an der Mathematisch-Naturwissenschaftlichen Fakultät
der Eberhard Karls Universität Tübingen
zur Erlangung des Grades eines
Doktors der Naturwissenschaften
(Dr. rer. nat.)

vorgelegt von
Ragna Susan Häußler
aus Ravensburg

Tübingen
2016

Gedruckt mit Genehmigung der

Mathematisch-Naturwissenschaftlichen Fakultät der Eberhard Karls Universität Tübingen.

Tag der mündlichen Qualifikation:	**18.07.2016**
Dekan:	Prof. Dr. Wolfgang Rosenstiel
1. Berichterstatter:	Prof. Dr. Michael Schwarz
2. Berichterstatter:	Prof. Dr. Stefan Stevanović

Supervisor at the Eberhard Karls University, Tübingen

Prof. Dr. Michael Schwarz

and

Prof. Dr. Stefan Stevanović

Supervisor at the Natural and Medical Institute

at the University of Tübingen

Dr. Markus F. Templin

Der Wanderer muss nicht nur den Weg,
sondern auch den Horizont dahinter sehen.

Mustafa Kemal Atatürk

Acknowledgements

For reasons of data protection, the Acknowledgements are not included and published in the online version.

Table of contents

List of abbreviations

Abbreviation	Full name
~	approximately
3D	three dimensional
aa	amino acid
ac	acetylated
AFI	Assembled fluorescence intensities
BC1	β-catenin binding nanobody 1
BD	BD Biosciences
BioGRID	Biological General Repository for Interaction Datasets
bp	base pair
BSA	Bovine serum albumin
CA	California
CAN	Canada
CF	Capturing factor
cle	cleaved
Co-IP	Co-Immunoprecipitation
CV	Coefficient of variation
DigiWest	Digitalized Western Blot approach
dk	donkey
DMEM	Dulbecco's Modified Eagle's Medium
DMSO	Dimethylsulfoxide
DNA	Deoxyribonucleic acid
DTT	Dithiothreitol
e.g.	for example (lat. exempli gratia)
ECIP	Extracellular Immunoprecipitation
EDC	1-Ethyl-3-(3-dimethylaminopropyl)carbodiimide
EDTA	Ethylenediaminetetraacetic acid
ELISA	Enzyme-linked immunosorbent assay
EMT	Epithelial–mesenchymal transition
EtOH	Ethanol
F12	Nutrient Mixture F-12
FCS	Fetal calf serum
FIN	Finland
FpClass	data mining–based method for proteome-wide PPI prediction
GBP	GFP-binding protein
GER	Germany
gt	goat
H + L	Heavy and light chain of an antibody
H_2O_{dd}	Purified water (18.2 MΩ)
HAc	Acetic acid
HB	Hepatoblastoma
HCC	Hepatocellular carcinoma

Abbreviation	Full name
HD	Heidelberg
hu	human
ICIP	Intracellular Immunoprecipitation
IgG	Immunoglobulin G
IntAct	protein interaction database
IP	Immunoprecipitation
ITA	Italy
LDS	Lithium dodecyl sulfate
log_2	Logarithm with base 2
MA	Massachusetts
me3	trimethylated
MEME	Minimum Essential Medium Eagle
MeOH	Methanol
MES	2-(N-morpholino)ethanesulfonic acid
MFI	Median fluorescence intensity
mio	million
MO	Missouri
ms	mouse
MS	Mass spectrometry
MW	Molecular weight
n.a.	not available
n.d.	not derived
NDEA	N-nitrosodietylamine
NE	Nebraska
NH	New Hampshire
NHS	N-hydroxysuccinimide
NJ	New Jersey
NLD	Netherlands
NMI	Natural and Medical Science Institute at the University of Tübingen
NP-40	Nonidet P-40
NY	New York
OFF	inactivated signaling status
OH	Ohio
ON	activated signaling status
ONT	Ontario
p	phosphorylated
P/S	Penicillin/Streptomycin
PA	Pennsylvania
PBS	Phosphate buffered saline
PBST	Phosphate buffered saline with Tween 20
PE	Phycoerythrin
PMSF	Phenylmethanesulfonylfluoride
PPI	Protein-protein interaction

Abbreviation	Full name
PTM	Posttranslational protein modification
PVDF	Polyvinylidene fluoride
rb	rabbit
rpm	revolutions per minute
RT	Room temperature
rt	rat
SD	Standard deviation
SDS	Sodiumdodecylsulfat
SDS-PAGE	Sodiumdodecylsulfat-Polyacrylamid gel electrophoresis
spec.	species
Strep-PE	PE-labeled Streptavidin
sulfo-NHS	N-hydroxysulfosuccinimide
TBS	Tris-buffered saline
TBST	Tris-buffered saline with Tween 20
Tris	Tris(hydroxymethyl)-aminomethane
Triton X-100	4-(1,1,3,3-Tetramethylbutyl)phenyl-polyethylene glycol
Tween 20	Polyethylene glycol sorbitan monolaurate
TX	Texas
UK	United Kingdom
UniProtKB	UniProt Knowledgebase
USA	United States of America
UT	Utah
v/v	Volume per volume
vs.	versus
w/v	Weight per volume
WA	Washington
WB	Western blot
WI	Wisconsin

The established SI units were used. Abbreviations of amino acids were carried out according to the international three-letter code. Chemical compounds were abbreviated according to the periodic table and the corresponding empirical formula, if not listed above. Protein and gene names were shortened analog to UniProtKnowledgeBase (UniProtKB) protein database, except the β-catenin gene, *CTNNB1*, is written in capital letters both for the human and the murine gene variant. Gene names were written in italics according to the general convention.

Abstract

The canonical Wnt-/β-catenin pathway plays an important role in regulating central physiological processes, such as cell proliferation, cellular metabolism, differentiation and apoptosis. Aberrant mutational activation of central players in this signaling pathway is closely linked to the modulation of the signaling status of the pathway and disease formation such as carcinogenesis. To functionally analyze the signaling state of the Wnt pathway, a focus was put on the detection of protein-protein complexes comprising the central regulator β-catenin, since it exerts its regulatory role by forming protein complexes. Information on interaction partners of β-catenin in different complexes is instrumental to decode observed changes in cellular signaling.

To isolate these protein complexes consisting of β-catenin and differing interaction partners, classical Co-Immunprecipiation (Co-IP) was performed on various cell lines in which cell signaling was modulated by compound treatment in this thesis. Thereby, it was possible to characterize the state of signal transduction in these cell lines with a focus on the activity of the regulatory Wnt pathway. In addition, the approach was extended to allow the use of a recently developed class of intracellular binding molecules, called chromobodies. These binders can be expressed inside a cell and enable an „intracellular Co-Immunoprecipitation", which gives insight into *in vivo* conditions by detecting endogenous bound target proteins.

The protein complexes consisting of β-catenin and various interaction partners (e.g. α-catenin and GSK3 β) were precipitated and shown by immunoblotting. To obtain a higher resolution picture of the isolated β-catenin complexes, a novel Western blotting approach (DigiWest) could be employed. This Western blotting approach uses a bead-based microarray platform and allows probing of a low amount of precipitate with hundreds of antibodies and thereby a screening for interacting proteins.

By using this throughput technique, the efficient characterization of cell lines, e.g. tumor cells, was enabled. In addition, the analysis of novel and well-known interaction partners of β-catenin was facilitated.

In summary, a combinatory approach consisting of Co-IP and DigiWest was established. This approach is suitable for the detection and a wide ranging analysis of posttranslational protein modifications and protein-protein interactions as well as their impact on the surrounding signaling cascades. An additional advantage of the combinatory approach is the simplification of visualizing alterations between different sample types and drug treatments. It consitutes a versatile tool to study endogenous complexes and to identify dynamic protein-protein interactions in signaling cascades. This approach can generally be applied to analyze regulating pathways and to decipher cellular communication processes by precipitating proteins and their key interactions.

Zusammenfassung

Der kanonische Wnt/β-Catenin Signalweg spielt eine wichtige Rolle in der Regulation zentraler physiologischer Prozesse wie beispielsweise Zellproliferation, Zellstoffwechsel, Differenzierung und Apoptose. Abnorme Aktivierungen von Schlüsselmolekülen durch Mutationen wirken sich auf den Signalzustand dieses Signalweges aus und stehen in engem Zusammenhang mit der Entstehung von Krankheiten, beispielsweise Krebs. Um den Signalstatus des Wnt Signalweges funktional zu analysieren, wurde der Fokus auf die Detektion unterschiedlicher Proteinkomplexen mit β-Catenin gelegt, welches eine zentrale regulatorische Rolle bei der Bildung solcher Komplexe spielt. Detaillierte Kenntnisse über verschiedene Interaktionspartner von β-Catenin in unterschiedlichen Proteinkomplexen sind notwendig, um mögliche auftretende Veränderungen in der zellulären Signalgebung zu entschlüsseln.

Um diese aus β-Catenin und verschiedenen Interaktionspartnern bestehenden Proteinkomplexe zu isolieren, wurde in dieser Arbeit eine klassische Co-Immunopräzipitation (Co-IP) auf verschiedenen Zelllinien durchgeführt, deren zelluläre Signalgebung durch Behandlung moduliert wurde. Dadurch war es möglich, den Status der Signalübertragung, insbesondere des regulatorischen Wnt Signalwegs, in diesen Zelllinien zu charakterisieren. Zusätzlich wurde die Co-IP durch die Verwendung von kürzlich entwickelten intrazellulären Bindemolekülen, sogenannten Chromobodies, erweitert. Diese können innerhalb der Zelle exprimiert werden und ermöglichen eine „intrazelluläre Co-Immunopräzipitation“, welche durch die endogene Bindung an Zielproteine einen Einblick in den *in vivo* Zustand erlaubt.

Proteinkomplexe, bestehend aus β-Catenin und verschiedenen Interaktionspartnern (z.B. α-Catenin und GSK3 β), wurden präzipitiert und mittels Immunoblot detektiert. Um eine höhere Auflösung der isolierten β-Catenin-Komplexe zu erhalten, wurde ein neuer Western Blot Ansatz (DigiWest) eingesetzt. Dieser Ansatz ist an eine Bead-basierte Mikroarray-Plattform adaptiert, welche es ermöglicht, eine geringe Menge an Präzipitat mit hunderten von Antikörpern zu untersuchen und dabei nach Interaktionspartner zu suchen.

Durch die Verwendung dieses Durchsatzverfahrens ist eine effizientere Charakterisierung von Zelllinien möglich. Zudem können bekannte und neue Interaktionspartner von β-Catenin analysiert werden.

Zusammenfassend wurde eine kombinatorische Methode, bestehend aus Co-IP und und DigiWest, entwickelt, welche sich für die Entdeckung und weitläufige Analyse posttranslationaler Proteinmodifikationen und Protein-Protein-Interaktionen sowie deren Auswirkung auf die umgebenden Signalkaskaden eignet. Ein großer Vorteil dieser Kombination ist die einfachere Möglichkeit Veränderungen zwischen unterschiedlichen Probentypen und Behandlungen aufzuzeigen. Es wurde gezeigt, dass die Methode ein vielseitiges Werkzeug darstellt, um endogene

Komplexe zu untersuchen und dynamische Protein-Protein-Interaktionen in Signalwegen zu identifizieren. Diese Methode kann darüber hinaus allgemein für die Analyse regulierender Signalwege sowie für die Entschlüsselung zellulärer Kommunikationsprozesse durch die Präzipitation von Proteinen und ihren Schlüsselinteraktionen angewendet werden.

1. Introduction

1.1 Proteomics and protein-protein interactions

The concept that protein-protein interactions (PPIs) play a fundamental role in biological processes evolved considerably and continuously throughout the past decades [1]. Important insights into the complex biological interplay of regulatory and control mechanism of various organisms were gained. This correlates with the development of innovative technical approaches and the evolution of a broader understanding, which led to today's systems-wide approaches to analyze PPIs [1].

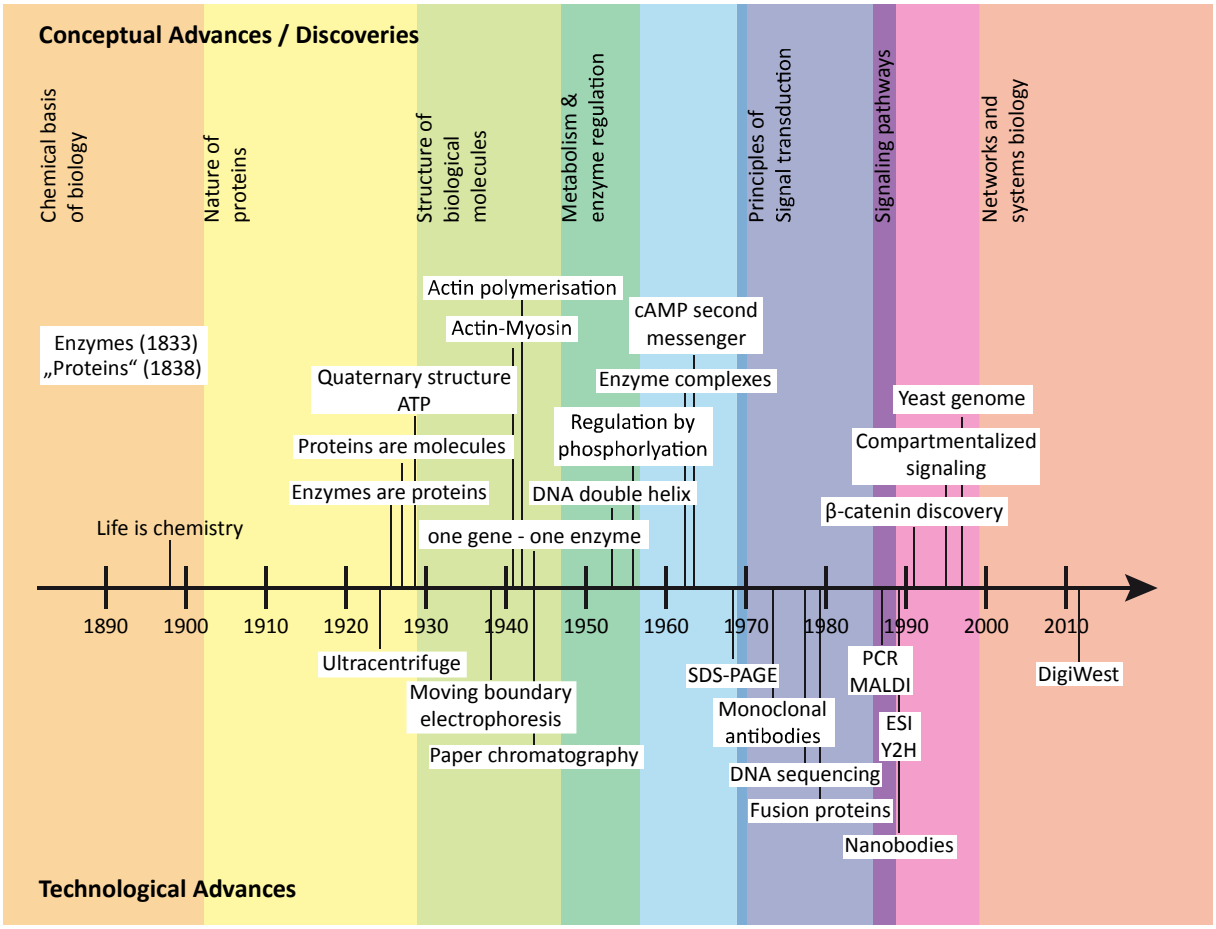

Figure 1: History of protein-protein interactions.
A timeline of protein-protein interaction research is shown. In the upper part, conceptual advances and discoveries are indicated, while in the lower part technological advances and inventions are indicated (altered from [1, 2]).

High throughput content analysis, also called the "omics" disciplines, paved the way to such a deeper understanding by providing a high-resolution data on biological processes: The study of the whole genome delivering information about gene structure and regulatory regions, developed into a new field of study, the genomics [3, 4]; the transcriptomics, creating maps of transcriptional regulation networks [5, 6], as well as large-scale protein expression data sets belonging to the proteomics [7].

The term proteome was coined in 1994 by Mark Wilkins [8] and followed by the creation of the term proteomics in 1997 [9]. Proteomics aims at achieving large-scale information about the protein entity, the proteome. The proteome is the set of proteins expressed by a genome at a certain time point and under specified conditions [10]. Compared to the lifelong maintained stability of the genome, the proteome is very dynamic and highly reliant on regulatory spatiotemporal processes [11], resulting in functional and physiological differences between various cells, which carry the same genome. Thus, proteomic studies facilitate a more distinct, but only momentary glance at what is actually happening [10]. Accordingly, the protein expression pattern of a defined cell and the interaction possibilities between proteins differ significantly depending on the phase of cell cycle and other internal and external influences. Therefore, a snapshot of the proteome at a given time and distinct location can be obtained at most [10].

As proteins are major protagonists in biochemical processes, their interactions play a key role in almost every type of biological process and at nearly every kind of cellular functioning [1, 12]. These processes and functions include signal reception and transduction, the transport machinery, regulation of gene expression, structuring of the cytoskeleton, DNA replication and many more. It has become apparent that intricate networks are formed by the interactions of proteins, which result in the formation of highly organized, dynamic cellular systems and the mediation of a vast range of regulatory functions in essentially every biological process [1, 13]. Due to this critical importance, the detection of PPIs is among the most informative ways of gaining information on a given protein. Starting in the 1940s, the importance of these interactions became apparent, as more and more PPIs were uncovered. By that it was also revealed, that proteins change their functions and effects, dependent on their complexation [1]. In various diseases, such as cancer, both alterations in the proteome and aberrant PPIs are observable and characteristic [10]. Those alterations modulate interactions qualitatively (all or none) and quantitatively (strength of interaction) [1]. To transmit signaling via PPIs and to establish complex intracellular signaling networks, individual proteins display nodes, which can respond to various input signals and control multiple effector outputs [14]. Due to this importance in developmental processes and disease progression, PPIs have been in the focus of research for many years and still are.

Thus, many proteomic projects aim at analyzing the changes in the proteome under different conditions and the resulting variations for the interacting networks of proteins [10, 15]. A deeper understanding of the interplay between different signaling cascades will make it easier to evaluate disease patterns correctly. The modulation of PPIs in order to utilize them as therapeutic targets, for example as an anticancer strategy, has become reality [15]. In cancer, PPIs have been shown to be involved in provoking tumorigenesis through regulating altered networks and present a working surface for the development of anticancer therapeutics [15].

Special biological databases, like UniProtKB, record knowledge about protein functions and their molecular properties [16]. Other databases collect published PPIs or even predict them, like “Biological General Repository for Interaction Datasets” (BioGRID) or the “FpClass” list. They try to mirror a complete map of the interactome, which is the entity of protein interactions, that may occur in a living organism [16]. These databases are used to verify observed interactions and interpret new occurring PPIs. By that, structuring of the large datasets of reported PPIs was possible and these databases proved to be indispensable tools in recent years.

1.2 Cancer and its association to Wnt signaling

Cancer is a disease, whose occurrence is increasing, due to factors like aging of the population as well as the increasing prevalence of established risk factors, such as smoking. For 2012 about 14.2 mio new cancer cases and 8.2 mio deaths based on cancer were estimated [17]. By that, cancer surpassed other illnesses like stroke in the number of deaths caused [10, 18]. In Germany, cancer is among the most frequent diseases with approximately 0.5 mio incidence per year. Additionally, it is the second most common cause of death [19]. Thus, cancer has become to a significant medical burden globally [10].

Many diseases are based on alterations in cellular signaling and deviations in the proteome. In cancer, most tumors harbor defined mutational alterations in genes encoding proteins, which act as central regulators in important signaling cascades. Ten main traits and enabling characteristics orchestrate the transformation from a normal state to malignancy, which were named "The Hallmarks of Cancer" [20]. One of these characteristics is the instability of the genome and the occurrence of mutational events. Often such mutations result in additional features, acquired by the cell, such as the ability to invade other tissues or modulate signaling in an inhibiting or activating manner [20-22]. As signaling pathways are not isolated, but interconnected in a complex network, already mutational changes in one signaling protein lead to wide ranging consequences. Thus, the understanding of the intricacy of signaling networks is crucial for speculating about tumor behavior and to achieve effective cancer therapies [14].

Known for their critical role in signaling transduction and complex interactions are pathways like MAPK (mitogen-activated protein kinase), Wnt (portmanteau of the *Drosophila* gene Wg (= Wingless) and mouse proto-oncogene int1 (= integration 1)) [23, 24], Hedgehog, TGF-β (Transforming growth factor beta), STAT (signal transducers and activators of transcription) and many more. They participate in the transmission of proliferation, differentiation, migration and survival signals [25-27]. Hence, in the development of cancer, a deregulation of these key pathways, caused by a mutational change, is frequently found [28, 29]. Such an observed deregulation of the Wnt pathway, for example the hyper-activation of Wnt/β-catenin pathway, is associated with many cancer forms [30-33].

The Wnt signaling pathway is an ancient and evolutionary conserved pathway in metazoan animals [34-36]. It is essentially involved in the regulation of cell fate determination, cell migration, cell polarity, stem/progenitor cell self-renewal and embryonic organogenesis [35, 37]. So far two main signaling branches have been discriminated downstream of the frizzled (FZD) receptor complex: the canonical or Wnt/β-catenin-dependent pathway and the noncanonical, β-catenin-independent pathway. The second branch can be further divided into Wnt/Ca^{2+} and Planar Cell Polarity pathways [35]. All subgroups of the Wnt pathway family are stimulated by a secreted Wnt glycoprotein, which binds extracellular to membrane receptors belonging to the FZD family [38]. For mediating the signal,

the assembly of additional co-receptors, such as LRP5/6 (low-densitiy-lipoprotein-related protein 5/6), is required [35, 38]. The signal is transduced to the cytoplasmic protein dishevelled (DVL) [28]. At this point, the three major branches of the Wnt signaling separate, but still require an intact function of DVL prior to this [28, 35]. Different Wnts exert reciprocal pathway inhibition by competing for FZD binding on the cell surface. Hence, through the specific binding and phosphorylation of unrelated co-receptors by different Wnts, distinct signaling pathways are activated [37]. In this thesis, the noncanonical Wnt pathways will be put aside, while the focus will be on the canonical Wnt/β-catenin signaling, which is also referred to as Wnt signaling from now on.

The key protein of the canonical Wnt signaling is β-catenin, which is responsible for the transduction of the Wnt signals into the nucleus. There β-catenin initiates the transcription of Wnt-specific target genes [36]. Generally, Wnt/β-catenin signaling is crucially implicated in tumorigenesis [39]. Besides this crucial role of deregulations of the pathway for the development of tumorigenesis, also an imbalance in the available amount of its key effector or an alteration of β-catenin, can lead to deregulations, which are linked to cancer [36].

Without a Wnt signal transduced from the membrane, the level of free, cytosolic β-catenin is kept at a low level. β-catenin is either bound to E-Cadherin, where it represents an integral structural component of cadherin-based adherens junctions (see Figure 2), or gets phosphorylated and thereby marked for its immediate degradation [36]. Responsible for this phosphorylation is a multiprotein complex, often called the β-catenin destruction complex [40]. This complex is composed of the scaffold proteins APC (Adenoma Polyposis Coli) and Axin, which present β-catenin to different kinases (GSK3 (glycogen synthase kinase 3), CK1 (Caseinkinase 1)) and phosphatases (PP2A, which is the protein phosphatase 2A). These are in charge of facilitating the phosphorylation at the N-terminus of β-catenin [36, 41, 42]. Subsequently to the phosphorylation, β-catenin gets ubiquitinated, mediated by β-TrCP (F-box/WD repeat-containing protein 1A) and the proteasomal degradation of the ubiquitin-conjugated β-catenin is carried out (see Figure 2) [36, 43-45].

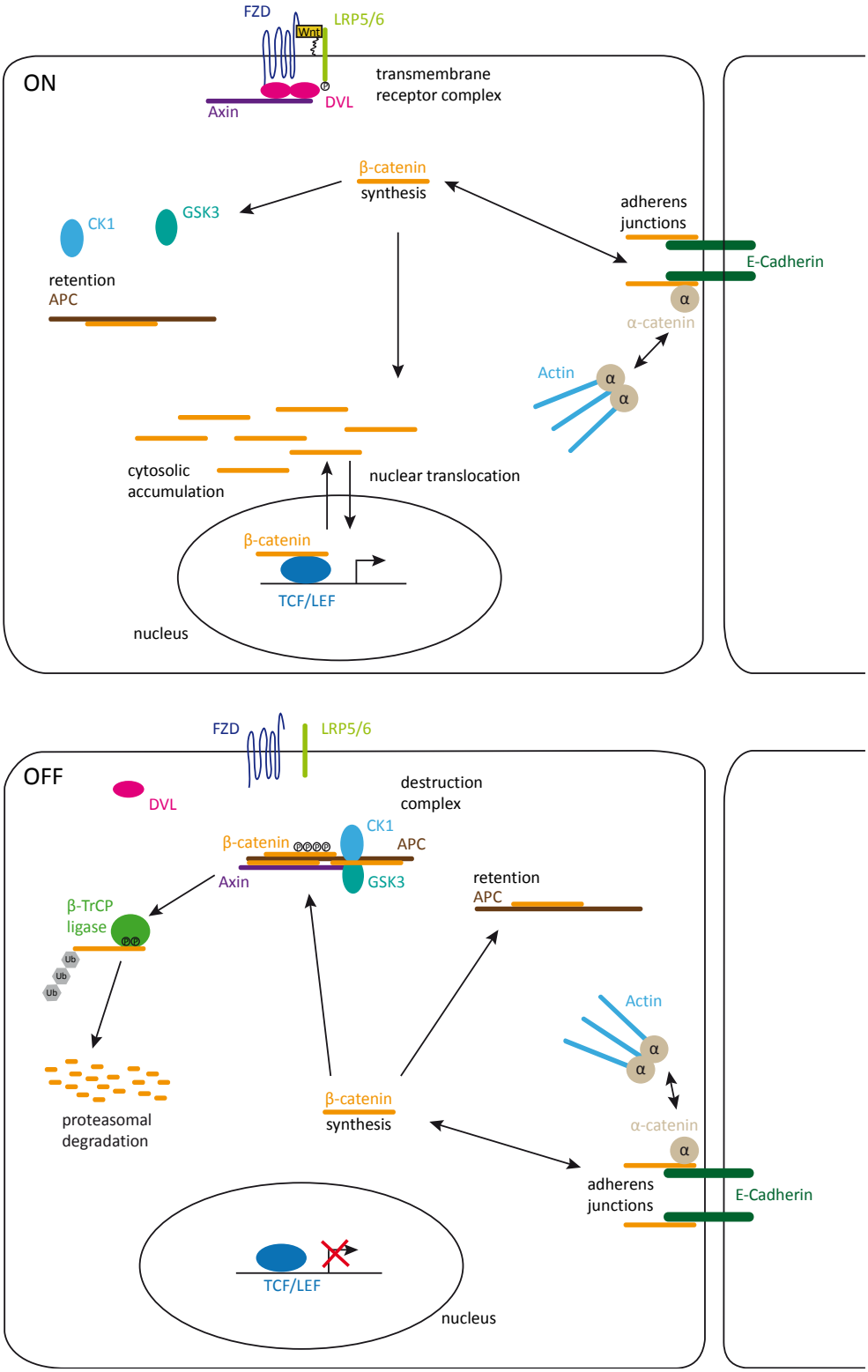

Figure 2: Canonical Wnt signaling.
The active (ON, upper image) and inactive (OFF, lower image) canonical Wnt pathway is represented. In active signaling, the Wnt ligand binds to the transmembrane complex, composed out of FZD and LRP5/6. This complex recruits DVL, which in turn recruits Axin. By that, the β-catenin destruction complex dissociates. Thus, the degradation of β-catenin is inhibited and the protein can translocate into the nucleus, after accumulating in the cytosol. There β-catenin acts as a transcriptional co-activator, binds to transcription factors and facilitates gene expression. In the absence of a Wnt ligand, the amount of cytosolic β-catenin is kept low, as it is permanently marked for degradation by the destruction complex. The destruction complex, composed of CK1, Axin, GSK3 and APC adds phosphate residues to the protein, which is followed by β-TrCP-mediated ubiquitination and proteasomal degradation of β-catenin (Figure adapted from [34, 36, 42]).

In the presence of a Wnt signal the β-catenin destruction complex gets inhibited. Binding of the ligand to the membranous FZD-LRP receptor complex induces association of the cytoplasmic protein DVL. DVL in turn is phosphorylated and activated [46-49]. By the multimerization of DVL, the formation of LRP-associated Wnt signalosomes is induced [50]. DVL subsequently recruits Axin, possibly together with associated kinases, like GSK3. Axin is an essential scaffolding structure in the destruction complex, thus the complex gets destabilized by its absence [51]. Additionally, the correct functioning of the Wnt signalosomes, composed of LRP6, DVL and Axin [37], leads to an inhibition of the GSK3 kinase activity [52]. As result of the destabilization of the complex and the inhibition of β-catenin phosphorylation, free non-phosphorylated β-catenin escapes the degradational machinery and is stabilized in the cytosol [53]. There, the stabilized protein accumulates and translocates into the nucleus. Nuclear β-catenin binds directly to transcription factors, most of which are members of the TCF/LEF family, and turns them from transcriptional repressors to transcriptional activators. This initiates transcription of Wnt-response genes, such as cJUN, TCF1, Axin2 and others (see Figure 2) [30, 36, 54, 55]. Within the nucleus the interaction of β-catenin with transcriptional co-activators additionally enhances or impairs its transcriptional activity [30].

It becomes apparent, that the key protein of the canonical Wnt pathway, β-catenin, forms complexes with a wide range of different proteins. This is caused, by its involvement at various subcellular locations, like its contribution to the cell-cell contact stabilization, its tightly controlled presence in the cytoplasm and its nuclear participation in the transcriptional regulation [56]. These PPIs facilitate β-catenin to step into direct crosstalk with other signaling cascades, provide a direct link to various transcription factors and by that affect its transcriptional output [36].

To gain a more comprehensive view on the Wnt signaling cascade, it is relevant to achieve insights not only in which interactions between β-catenin and other proteins occur, but also in how these spatially and temporally coordinated PPIs are built and which posttranslational modifications (PTMs) control these processes. Thus, the structure of β-catenin plays an important role.

β-catenin itself is a 781 aa long member of the armadillo protein family, which also comprises α-catenin, γ-catenin and δ-catenin [56]. It is composed out of a N-terminal domain (NTD), the armadillo domain (ARM), consisting out of 12 armadillo repeats (each approximately 40 aa long), followed by a conserved Helix-C and adjacent to that, the C-terminal domain (CTD) [56, 57] (see Figure 31). The ARM shows predominately a positive charge, while modifications, such as phosphorylation alter the local charge of β-catenin. The local charge of β-catenin is thought to have a distinct influence on its binding affinity to specific interaction partners [56]. Hence, its function can be regulated by PTMs, which are not always caused by signaling through the Wnt receptor [30, 58].

PTMs in general have a significant influence on the mediation of critical events involved in cellular responses. They affect and control enzymatic activity, protein conformation, occurrence of PPIs and

the cellular protein localization. Protein phosphorylation is one important example for such a modification, which affects approximately one third of all proteins and is one of the most studied PTMs overall [59, 60]. PTMs are mostly placed at so-called modular protein domains. These interaction modules mediate PPIs, but also serve to target signaling proteins to their substrate or distinct subcellular locations and to link proteins to multiprotein complexes and signaling cascades [14, 61].

β-catenin has a plethora of target sites for many different PTMs, like phosphorylations (some of them exemplary illustrated in Figure 31), but also ubiquitinations, acetylations and glycosylations [36]. These modifications modulate the operation mode and the different subcellular localizations of β-catenin (some of them exemplary listed in Table 39) [56, 62]. For example a C-terminal phosphorylation of β-catenin attenuates its binding to the cadherin-adhesion complex, while N-terminal phosphorylations often enhance its proteasomal degradation [56]. Also the association of β-catenin with TCF/LEF during transcriptional regulation is controlled by phosphorylation [56, 63].

The use of β-catenin as a therapeutic target in cancer seems to be of particular interest due to the large number of interaction partners that can prove to be valuable intervention points. But it was shown to be a formidable challenge to develop direct inhibitors of oncogenic β-catenin, as it holds an extensive main ligand interaction surface, which is shared between both positive and negative regulators. In addition, many other hindrances exist, which characterize β-catenin as an unattractive drug target, such as its promiscuity, which leads to difficulties in the drug design or the lack of a well-established enzymatic activator, which can be inhibited. Addressing other components of the Wnt/β-catenin pathway as therapeutic targets, could serve as an alternative [64, 65]. Therefore, it is important to gain a broader understanding of their molecular and cellular biological functioning as well as their interplay with different signaling cascades. High throughput experiments will simplify the investigation of the Wnt pathway and can additionally provide a detailed insight about changes, caused by stimuli or inhibitors. Thus, they can help to identify inter- and intramolecular interactions, which are necessary in order to understand the overall architecture of signaling networks [14]. This might lead to a more distinct evaluation and planning of target points for drug development.

1.3 Significance of liver and liver cell lines

The liver is a highly complex organ, whose differentiation and growth processes during development are modulated by Wnt/β-catenin signaling [66, 67]. Later in the adult liver, the canonical Wnt pathway regulates liver metabolism, regeneration and zonation [68, 69]. One of the most common solid tumors is primary liver cancer, predominantly hepatoblastoma (HB) and hepatocellular carcinoma (HCC) [70]. Constitutively activated Wnt/β-catenin signaling is observed in one third of HCCs, which is the most common form of liver cancer and one of the major causes of death worldwide [39, 71, 72]. The canonical Wnt signaling is frequently activated in this form of cancer. Already β-catenin itself, as the key player of the canonical Wnt signaling, plays a critical role in liver homeostasis and during liver regeneration [73]. It was shown that 50 % of mouse HCCs and 26 % of human HCCs have β-catenin-activating mutations [74]. Another form of liver cancer is hepatoblastoma (HB), which is the most frequent occurring form during childhood. It shows one of the highest known frequencies of mutations of the β-catenin gene, encoding for the key player in Wnt signaling [30, 39, 75], whereas for HCC also most commonly activating mutations in *CTNNB1* [39, 74] were observed. The link between Wnt signaling and carcinogenesis in the liver is important to analyze, in order to gain useful knowledge for future therapeutical research [39].
Thus, four different liver cell lines, derived from mouse or human were chosen, to get a closer insight to the changes in regulating signal transduction cascades:

1.3.1 Mouse hepatoma cell line 55.1c

The cell line 55.1c is a mouse hepatoma cell line (see Table 12), which was established from a mouse liver tumor of a C57BL/6J mouse. Tumor formation was induced by a single intraperitoneal injection of N-nitrosodietylamine (NDEA) [76]. After a followed feeding with 0.05 % phenobarbital (PB), this leads to a *CTNNB1* mutation in 80 % of the generated liver tumors in rodents [77]. Additionally, a constitutive, but non-maximum activation of β-catenin signaling is observed, that is due to a heterozygous deletion within exon 3 of *CTNNB1* [78]. The 55.1c cells seem to have a high protein expression in general.

1.3.2 Mouse hepatoma cell line 70.4

The second chosen mouse hepatoma cell line, 70.4, was established in parallel to the cell line 55.1c, out of identically generated mouse liver tumors (see Table 12). In this case, C3H/He mice were donors. In contrast to the 55.1c cells, 70.4 cells are wild type according to the expression of *CTNNB1* [76, 78], but harbor two different, independent p53 mutations.

1.3.3 Human hepatocellular carcinoma cell line HepG2

The cell line HepG2 was derived from liver tumor biopsies of a 15-year-old Caucasian boy. Its morphological characteristics and epithelia cell shape are compatible with liver parenchymal cells, without the presence of the hepatitis B viral genome [79, 80]. It is one of the most frequently used cellular models for *in vitro* liver cancer and toxicity studies, as it represents a well characterized liver cancer cell line [81]. This cell line was initially considered to be a representative of pediatric HCC, but is in fact an example of an epithelial hepatoblastoma [82]. Its hepatoblastoma characteristics were confirmed by the histopathological background, the original histology and recent molecular analyses [83]. Like many epithelial cell lines it shows a heterozygous deletion of exon 3 of the β-catenin gene [74, 82, 84, 85], which leads to the strong expression of a truncated β-catenin version (aa 25 – 140) and a small pool of wild type β-catenin [74, 85]. This results in a high activation of the canonical Wnt pathway.

1.3.4 Human hepatocellular carcinoma cell line HB35

HB35 is a human hepatocellular carcinoma cell line, which was established out of a liver neoplasm of a 4-year old, male donor. This cell line represents the first cell line derived from a pediatric HCC, without having a background of viral hepatitis or cirrhosis. It presents histological and biological characteristics of an epithelial liver tumor. As it is a rather novel cell line, whose characterization was first published in 2012, only little analysis was done so far. Because of the little characterization and the many preserved hepatocyte characteristics, HB35 represents an interesting liver cancer cell line. The cell line shows a heterozygous deletion of 49 bp in β-catenin exon 3 and the deleted area encodes a phosphorylation site of GSK3 β. Thus, β-catenin degradation is prevented and its accumulation within the cell is enhanced, whereby excessive Wnt/β-catenin signaling is observed [83].

1.4 DigiWest as screening tool for protein-protein interactions

The further evolution of research in life sciences resulted in experimental approaches, which are capable of handling and analyzing multiple samples and analytes in parallel. Microarray technology, which emerged throughout the past years, represents such a technique. It turned out to be a milestone for a plethora of different approaches in research, development and diagnostics [86], as its applications cover the area of genomics, transcriptomics and proteomics. It also offers the possibility of miniaturizing and parallelization [87], which results in less consumption of material, both of sample and reagents, but also in the possibility to achieve a high throughput for samples and analytes [88].

The commercially available Luminex technology provides such a microarray system, based on microspheres (beads). 500 different bead populations, containing three internal fluorescent dyes, are available. The addition of different amounts of the three fluorescent dyes is used as a specific color code to discriminate the beads and assign them to a distinct population. A flow cytometer is used as an readout system. This platform is capable of performing multiplexed immunoassays, which allow a the measurement of dozens to hundreds parameters in parallel with high sensitivity and reliability [89, 90]. In addition, less sample is consumed and fast assay times are possible, which allows automating and enhancing of the approach towards a high throughput technique [86].

The DigiWest is an optimization of the hitherto existing Western blot by transferring it to a bead-based microarray platform. It uses the advantages of the conventional Western blot protein detection method, such as providing a corresponding molecular weight, which allows the discrimination between specific and unspecific signals. Additionally, it avoids its main disadvantages: the detection of a very limited amount of analytes and the consumption of a proportionally high amount of sample volume [89, 91].

During DigiWest, hundreds of replicas of one Western blot are generated. Thereby, one initial Western blot lane results in a bead-mix, which still contains all original Western blot information on the protein size and attributes it to different distinct bead populations. Thus, results highly comparable to the classical Western blot can be achieved, but one experiment is capable of performing hundreds of antibody incubations [89, 91]. Especially in experimental setups with a limited amount of available material, the DigiWest provides a solution, which yet allows a broad testing of analytes. Co-Immunoprecipitation (Co-IP) samples are among such limited samples. The possibility to employ a technique like the DigiWest to screen Co-IP samples and thereby connecting these two approaches, offers the ability to screen a huge amount of analytes on a very limited amount of sample volume. At the same time, the DigiWest is a valid and less material consuming alternative for mass spectrometric approaches (MS), which became the method of choice for identifying PPIs lately [92-94]. As Co-IP is the most straightforward method for the detection of PPIs

[95], the linkage of Co-IP to DigiWest results in an alternate high throughput tool to screen for PPIs. This creates the great opportunity of achieving a higher understanding of the interactions between proteins, as well as a further investigation of their dynamics under different conditions [89]. That in turn allows the exploration of biological processes, such as interactions between signaling pathways or the influences of PTMs on these cascades.

1.5 From antibodies to nanobodies

The publication of mouse hybridoma technology in 1975 [96] represents a milestone in the development of the antibody technology and initiated the emergence of monoclonal antibodies in the therapeutical use [97]. Several monoclonal antibodies were approved or tested for biopharmaceuticals in the past years [97-99]. Besides that, antibodies have a high relevance in a wide range of biochemical applications, such as the identification and precipitation of proteins [100, 101], due to their high specificity and selectivity. This specificity turns them into excellent tools, that allows the identification of their addressed targets. They enable to draw conclusions about this molecule and its surrounding signaling cascades.

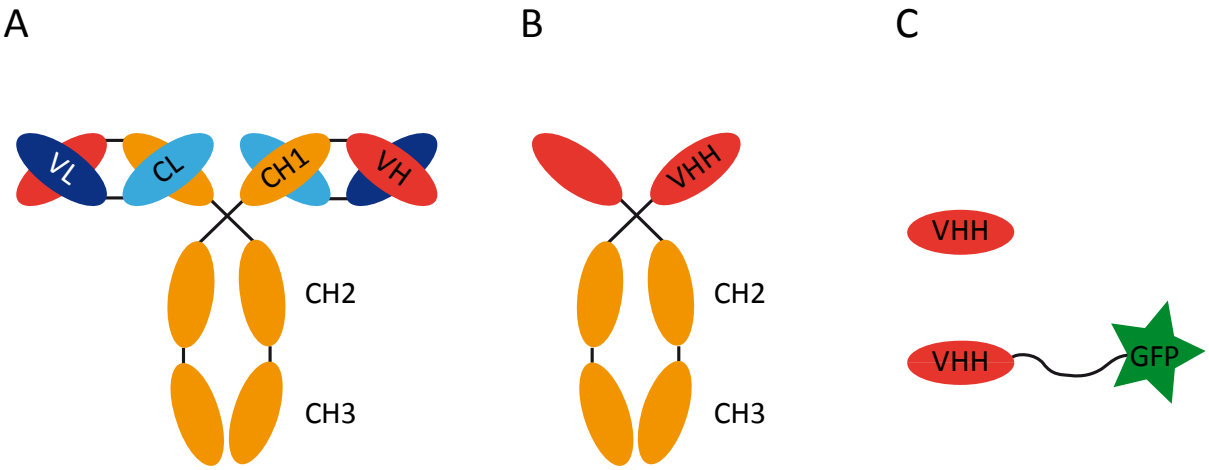

Figure 3: Schematic presentation of antibody IgG, heavy-chain camelid antibody, nanobody and chromobody.
A: A conventional heavy-chain antibody is represented. It consists out of two light chains with one variable domain (VL, dark blue) and a constant domain (CL, bright blue), as well as two heavy chains, with one variable domain (VH, red) followed by the first constant domain (CH1, orange), a hinge region and another two constant domains (CH2 and CH3, also orange).
B: A heavy-chain camelid antibody is shown. It is devoid of light chains as well as the first constant region CH1, while the VH domain is modified (now called VHH).
C: VHH is the smallest available intact antigen-binding fragment, derived of a camelid heavy-chain antibody, also called nanobody. This nanobody can be tagged by a GFP and results in a so-called chromobody
(Figure adapted from [102-105]).

Through the discovery of camelid heavy-chain antibodies at the end of the 1980s [2], a new category of antigen-binding molecules was identified, which were characterized by their small, but fully functional antigen binding fragment VHH (see Figure 3) [97]. The VHH domain, also called nanobody, is of small size (only about 15 kDa, roughly 120 aa), but shows a high affinity and selectivity for the addressed target [102, 106-108]. Additionally, nanobodies are of particular interest, as their generation is both easy and cheap [102, 105, 109], and they exhibit a high stability even under harsh, denaturing conditions [97]. These features enable them to penetrate tissue barriers [97], while conventional antibodies are too large to pass the cellular membrane and cannot fold correctly within

the reducing intracellular environment [107, 110]. It has been shown recently, that nanobodies can be selected as so-called intrabodies [105], which can be functionally expressed in living cells. This leads to significant advantages of nanobodies in several biotechnological and medical applications in comparison to conventional antibodies. One of these application is the possibility of targeting and precipitating proteins intracellularly, which to date is not feasible by using conventional antibodies [111].

Beyond the possibility to perform Co-IPs on cellular lysates, it is of high interest to be able to study endogenous protein-complexes and identify dynamic PPIs. By inducing the ectopical expression of protein fusion constructs inside a cell the validity of Co-IP approaches is frequently deteriorated [94]. As the cellular level and the distribution of many proteins underlie a complicated regulation, complexes containing these modified proteins might not describe the realistic characteristics of the endogenous protein [94, 112]. The utilization of nanobodies tagged by a fluorescent protein, facilitates the visualization of their binding to a specific protein, pointing to its subcellular location, but might also allow to modulate the proteins' target structure and subsequently its function [105, 108, 112-114]. Nanobodies fused to fluorescent proteins, like GFP, are called chromobodies (see Figure 3). They facilitate the endogenous protein detection and enable to trace dynamic re-localizations of the protein during fluorescence microscopy [108, 112]. Thus, nanobodies depict an useful class of novel molecules for biotechnological approaches and will emerge further. In addition, they also combine the beneficial characteristics of conventional antibodies with desirable properties of small-molecule drugs. This paved the way for designing nanobody-based therapeutical programs [102], where nanobodies can address highly potent therapeutic targets [111]. Their impact as an available pharmaceutical in clinics will therefore presumably experience an enormous rise.

2. Aim of the thesis

Quantitative and reliable data sets, which illustrate the momentary intracellular protein entity, the present protein-protein interactions and posttranslational modifications of proteins, are essential to characterize and decode the complexity of dynamic cellular signaling processes. It was revealed to be time and/or material consuming to accomplish a systematic pathway analysis for different cell types and under various treatments with conventional methods, like quantitative Western blots, Co-IPs and MS. Thus, high throughput methods, that go along with low material consumption, are required to simplify the analysis of complex cell signaling processes.

Co-IP is the most straightforward method for the detection of PPIs and is considered as a gold standard for the identification of protein functions and interactions as well as the protein complexation. As a subsequent approach to confirm PPIs, frequently traditional Western blots are performed, but these allow only limited testing and the verification of known or highly predicted interaction partners. On the contrary, subsequent MS-based analyses allow wide ranging, unbiased screening and are capable to identify *de novo* interactors. Thus, this approach is able to reveal important information on the cellular crosstalk and became the method of choice for PPI analysis lately. Still it shows some majors disadvantages, such as the complexity of the technique, the limited throughput and the high material consumption.

In this thesis, a combinatory approach is developed, which holds the capability of analyzing PPIs and unites both the advantages of the hitherto existing Western blot approach with the benefits of a high throughput tool. Hence, the recently developed DigiWest is connected to a prior performed Co-IP, with its high relevance for illustrating PPIs. As standard Co-IP requires a dissolving of the cellular structure, the development of intracellularly performed Co-IPs seems a promising way to gain deeper insights into *in vivo* conditions, as it reflects a system that is much closer to the authentic cellular networking. Thus, in a second step the DigiWest is combined with a novel intracellular Co-IP approach.

Via the wide ranging analysis of protein interactions, a new type of functional characterization of different cell lines, for example tumor cells, is enabled. The opportunity to characterize cell lines, provides novel information not only on the amount of expressed proteins within the cellular context and thereby goes well beyond a conventional expression analysis and the enhancement of mere knowledge about protein concentration. Analyzing complex formation around central proteins of important signaling cascades offers the recognition of new modulation points for aberrant cellular communication, which results in disease formation. In this thesis, the key player of the canonical Wnt pathway, the proto-oncogen β-catenin, and its PPIs are chosen to be analyzed in hepatoma cell lines after drug treatment.

Wnt/β-catenin signaling regulates central processes like the modulation of differentiation and growth processes during development in the liver. The key player of this pathway, β-catenin, participates not only in the canonical Wnt signaling, but also other cellular processes, such as cell-cell adhesion complexes. The deregulation of this pathway is crucially implicated in tumorigenesis, but also an imbalance or alteration of β-catenin itself is linked to the genesis of many common cancer forms, e.g. liver cancer. In addition, the functions of β-catenin as a cell adhesions molecule or as a transcriptional co-activator are highly dependent on its concentration, its PTMs and its ability to complex with other proteins. Via this complexation β-catenin is able to modulate central regulating complexes and provides a link between the canonical Wnt signaling and other important signaling cascades, like the MAPK pathway.

The goal of this thesis is to apply the at first developed combinatory high throughput approach, to focus on the various posttranslational modified variants of β-catenin and in parallel to screen for novel complex partners on different cell lines. By that, a more detailed understanding of the dynamics of β-catenin-mediated signaling and its extensive impact on the cellular crosstalk can be gained.

3. Materials and methods

3.1 Materials

3.1.1 Devices

Table 1: List of devices

Usage	Product	Distributor
Autoclave	Autoclave C	Webeco, Selmsdorf, GER
Burner	Gasprofi 1 micro	WLD TEC, Göttingen, GER
Centrifuges	5415D; 5417R (cooled); 5810R (cooled); Heraeus™ Pico™ 21 Universal 30F	Eppendorf, Hamburg, GER; Thermo Fisher Scientific, Waltham, MA, USA Hettich, Tuttlingen, Germany
Cutting machine	Silhouette SD Digital Craft Cutter	Silhouette America, Lehi, UT, USA
Electronic pipettes	Xplorer	Eppendorf, Hamburg, GER
Gel electrophoresis - System (SDS-PAGE)	XCell SureLock™ Mini-Cell	Life Technologies, Carlsbad, CA, USA
Ice Flaker	Scotman AF40	Frimont S.p.A., Pogliano Milanese, ITA
Incubator	Gas jacketed CO_2 incubator, BB 6220 CU	Heraeus Instruments, Hanau, GER
Laminar flow cabinet	Sterilbank UVF 6.12 F	BDK, Sonnenbühl, GER
LED Copy Board	A4	Amazon.com, Seattle, WA, USA
Magnet comb	KingFisher®™ 96 PCR head	Thermo Fisher Scientific, Waltham, MA, USA
Magnetic comb	KingFisher®™ 96 tip comb	Thermo Fisher Scientific, Waltham, MA, USA
Magnetic separator	DynaMag™ Spin	Life Technologies, Carlsbad, CA, USA
Magnetic stirrer	RCT basic	IKA®-Werke, Staufen, GER
Magnetpen	PickPen 8-M	Bio-Nobile, Turku, FIN
Micro centrifuge		Carl Roth, Karlsruhe, GER neoLab, Heidelberg, GER
Microsphere read out device	FLEXMAP 3D	Luminex, Austin, TX, USA
Multichannel pipettes	Research plus	Eppendorf, Hamburg, GER
Orbital Shaker	DRS-12	neoLab, Heidelberg, GER
Overhead mixing rotator	Rotator 2-1175	neoLab, Heidelberg, GER
pH meter	pH meter 766	Knick, Berlin, DE
Pipette Controller	PIPETBOY	INTEGRA Biosciences, Hudson, NH, USA
Pipettes	PIPETMAN Neo; Research plus Research Discovery Comfort	Gilson, Middleton, WI, USA; Eppendorf, Hamburg, GER; Eppendorf, Hamburg, GER; Starlab, Hamburg, GER
Pipetting robot	Biomek FX	Beckman Coulter, Brea, CA, USA
Plate shaker	Thermomixer comfort	Eppendorf, Hamburg, GER
Plate Shaker (16 plates)	TiMix 5	Edmund Bühler, Hechingen, GER

Usage	Product	Distributor
Platemagnet for microspheres	Magnetic Plate Separator	Luminex, Austin, TX, USA
Platform shaker	Polymax 2040	Heidolph, Schwabach, GER
Power supply unit	Power Ease 500	Life Technologies, Carlsbad, CA, USA
Reaction tube shaker	Thermomixer comfort	Eppendorf, Hamburg, GER
Rotating mixer for tubes	RM5	Assistent, Sondheim, GER
Scale	Explorer E12140	OHAUS, Pine Brook, NJ, USA
Scalpel		Martor, Solingen, GER
Shaker	Vortex Genie 2	Scientific Industries, Bohemia, NY, USA
Sonification bath	Sonorex RK 31 Transsonic T780/H	Bandelin, Berlin, GER; Elma, Singen, GER
Tweezers	Dumoxel® 5	EMS, Hatfield, PA, USA
Vacuum sealer	V.200	Landig + Lava, Bad Saulgau, GER
Water bath	1083	GFL, Burgwedel, GER
Water purification system	Milli Q Plus; arium® 611VF	Merck Millipore, Billerica, MA, USA; Sartorius Stedim Biotech, Göttingen, GER
Western Blot Documentation system	ODYSSEY Infrared Imaging System; ImageQuant LAS 4000 mini	LI-COR Biosciences, Lincoln, NE, USA; GE Healthcare, Chalfont St Giles, UK
Western Blot-System	XCell II Blot Module	Life Technologies, Carlsbad, CA, USA

3.1.2 Programs

Table 2: List of programs

Product	Distributor
Adobe Illustrator CS5	Adobe Systems, San José, CA, USA
Adobe Photoshop CS5	Adobe Systems, San José, CA, USA
DigiWest analysis tool (version 3.8.5.2, Excel-based)	NMI Reutlingen, Reutlingen, DE
DigiWest Viewer (Excel-based)	NMI Reutlingen, Reutlingen, DE
EndNote X7	Thomson Reuters, New York, NY, USA
etiLABEL	ETISOFT, Delmenhorst, GER
Image Reader LAS-4000	GE Healthcare, Chalfont St Giles, UK
Image Studio v4	LI-COR Biosciences, Lincoln, NE, USA
MeV Version 4.8.1, TM4 Microarray Software Suite [115, 116]	Dana-Farber Cancer Institute, Boston, MA, USA
MS Office 2010, MS Office 2013	Microsoft, Redmond, WA, USA
Silhouette Studio®	Silhouette America, Lehi, UT, USA
Windows XP, Windows 7	Microsoft, Redmond, WA, USA
XLfit 5.3.1.3	IDBS, London, UK
xPONENT Software Solutions IS 2.2	Luminex, Austin, TX, USA

3.1.3 Databases

Table 3: List of databases

Product	Distributor
BioGRID (Biological General Repository for Interaction Datasets) [117]	BioGRID Team
FpClass [118]	Princess Margaret Cancer Center, University Health Network, Toronto, ONT, CAN
IntAct database [119, 120]	The Molecular Interactions team, EMBL-EBI, Hinxton, UK
UniProtKB (UniProt Knowledgebase) [121]	UniProt Consortium

3.1.4 Consumables

Table 4: List of consumables

Usage	Product	Distributor
0.65 ml reaction tubes	Mμlti®-safety microcentrifuge tubes	Carl Roth, Karlsruhe, GER
1.5 ml protein LoBind tubes		Eppendorf, Hamburg, GER
1.5 ml reaction tubes		Vetter Laborbedarf, Ammerbuch, GER
10 cm cell culture dish	Falcon 3003	BD, Heidelberg, GER
15 ml tubes		Greiner Bio-One, Frickenhausen, GER
2 ml reaction tubes		Vetter Laborbedarf, Ammerbuch, GER
4 ml tubes		Greiner Bio-One, Frickenhausen, GER
50 ml tubes		Greiner Bio-One, Frickenhausen, GER
Calibration and Verification of the FLEXMAP	FLEXMAP 3D® Calibration Kit and Perfomance Verification Kit	Luminex, Austin, TX, USA
Calibration solutions for pH meter	Technical buffer solution pH 4.01, 7.00 and 9.21	Mettler-Toledo, Columbus, OH, USA
Cell scraper	Costar Cell Lifter	Corning Incorporated, Corning, NY, USA
Disposable bag		Sarstedt. Nümbrecht, GER
Filter paper	Whatman cellulose chromatography paper 3 mm	Sigma-Aldrich, St. Louis, MO, USA
Glass pasteur pipette		WU Mainz, Mainz, GER
Glass pipette	5 ml, 10 ml, 20 ml	Brand, Wertheim, GER
Glassware		Schott, Mainz, GER
Gloves	Micro Touch Hygrip; Safeskin Purple Nitrile; Nitrile gloves Rotiprotect-NITRIL Rotiprotect-LATEX	Ansell, Munich, GER; Kimberly-Clark, Dallas, TX, USA; VWR, Darmstadt, GER; Carl Roth, Karlsruhe, GER, Carl Roth, Karlsruhe, GER
Magnetic beads	Dynabeads® Protein G	Life Technologies, Carlsbad, CA, USA
Microplate sealing tape	Axygen® AxySeal	Corning Incorporated, Corning, NY, USA
Microplate, flat bottom	655101 – Greiner 96 well	Greiner Bio-One, Frickenhausen, GER
Microplate, half area flat bottom, non-binding surface	CLS3642 – Corning 96 well (Half Area Platte)	Corning Incorporated, Corning, NY, USA

Usage	Product	Distributor
Microspheres	MagPlex® Microspheres	Luminex, Austin, TX, USA
Needles	Sterican® Gr. 1, Gr. 14	Braun Melsungen, Melsungen, GER
Parafilm	PM-996	Bemis, Oshkosh, WI, USA
PCR comb	KingFisher®™ 96 tip comb	Thermo Fisher Scientific, Waltham, MA, USA
Pipetting tips	0.1 – 10 µl 1 – 200 µl; 1 – 200 µl (capillary tips); 1 – 300 µl; 100 – 1000 µl; 100 – 1200 µl; 100 – 5000 µl	Mettler-Toledo, Columbus, OH, USA Starlab, Hamburg, GER; VWR, Darmstadt, GER Starlab, Hamburg, GER; Starlab, Hamburg, GER; Biozym Scientific, Hessisch Oldendorf, GER neoLab, Heidelberg, GER
Polyacrylamid gels	NuPAGE Novex 4 – 12 % Bis-Tris Gels 1.0 mm 12, 15 and 17 well	Life Technologies, Carlsbad, CA, USA
Polyvinylidene difluoride membrane	Immobilon-P PVDF Membrane, 0.45 µm	Millipore Corporation, Billerica, MA, USA
Robot pipetting tips	4 – 220 µl; Biomek AP96 P250 Tips, Non-sterile	Beckman Coulter, Brea, CA, USA
Silicone tips for Magnetpen	QuickPick tips	Bio-Nobile, Turku, FIN
Sponge Pad	NuPage Novex Sponge Pad for Blotting	Life Technologies, Carlsbad, CA, USA
Sterile filter	Steritop 0.22 µm	Millipore, Eschborn, GER
Syringes	Injekt™ Syringe 10 ml, 5 ml	Braun Melsungen, Melsungen, GER
Vacuum bags	R-Vac	Landig + Lava, Bad Saulgau, GER

3.1.5 Chemicals

Table 5: List of chemicals

Product	Distributor
2-Mercaptoethanol	Sigma-Aldrich, St. Louis, MO, USA
2-Propanol 70 %	Carl Roth, Karlsruhe, GER
Bromophenol blue sodium salt	Carl Roth, Karlsruhe, GER
BSA Albumin Fraction V (protease-free)	Carl Roth, Karlsruhe, GER
CHIR 99021	Tocris Bioscience, Bristol, UK
DMEM	Life Technologies, Carlsbad, CA, USA
DMEM/F-12	Life Technologies, Carlsbad, CA, USA
DMSO	Sigma-Aldrich, St. Louis, MO, USA
DNAse I	AppliChem, Darmstadt, GER
DTT	Sigma-Aldrich, St. Louis, MO, USA
EDTA	Carl Roth, Karlsruhe, GER
EtOH 96 %	Carl Roth, Karlsruhe, GER
FCS	Life Technologies, Carlsbad, CA, USA
Glycerol	Sigma-Aldrich, St. Louis, MO, USA

Product	Distributor
HAc	Carl Roth, Karlsruhe, GER
HCl	Carl Roth, Karlsruhe, GER
Hepes	Carl Roth, Karlsruhe, GER
MeOH	Carl Roth, Karlsruhe, GER
MG132 (Z-Leu-Leu-Leu-al)	Sigma-Aldrich, St. Louis, MO, USA
$MgCl_2$	Sigma-Aldrich, St. Louis, MO, USA
Milk powder	Carl Roth, Karlsruhe, GER
Na_3VO_4	Sigma-Aldrich, St. Louis, MO, USA
NaCl	Carl Roth, Karlsruhe, GER
NaClO solution 12 %	Carl Roth, Karlsruhe, GER
NaF	Carl Roth, Karlsruhe, GER
$NaHCO_3$	Merck, Darmstadt, GER
NaN_3	Merck, Darmstadt, GER
NaOH	Carl Roth, Karlsruhe, GER
NP-40	Sigma-Aldrich, St. Louis, MO, USA
Penicillin	Biochrom, Berlin, GER
PMSF	AppliChem, Darmstadt, GER
Ponceau S	Carl Roth, Karlsruhe, GER
Protease Inhibitor (EDTA-free) Complete C	Roche Diagnostics, Mannheim, GER
Protease Inhibitor Mix M	Serva, Heidelberg, GER
SDS	Sigma-Aldrich, St. Louis, MO, USA
Streptomycin	Biochrom, Berlin, GER
Tris–HCl	Carl Roth, Karlsruhe, GER
Triton X-100	Merck, Darmstadt, GER
Trypsin-EDTA	Biochrom, Berlin, GER
Tween 20	Merck, Darmstadt, GER
Urea	Sigma-Aldrich, St. Louis, MO, USA

3.1.6 Reagents

Table 6: List of reagents

Reagent	Product	Distributor
Antioxidant	NuPAGE® Antioxidant	Life Technologies, Carlsbad, CA, USA
Biotinylation reagent	EZ-Link NHS-PEG12-Biotin	Thermo Fisher Scientific, Waltham, MA, USA
LDS Sample Buffer	NuPAGE® LDS Sample Buffer	Life Technologies, Carlsbad, CA, USA
MEME medium	Minimum Essential Medium Eagle	Sigma-Aldrich, St. Louis, MO, USA
MES Running buffer	NuPAGE® MES SDS Running Buffer (20x)	Life Technologies, Carlsbad, CA, USA
PBS	PBS (10x)	Thermo Fisher Scientific, Waltham, MA, USA

Reagent	Product	Distributor
Protein standard	SeeBlue® Plus2 Pre-Stained Standard	Life Technologies, Carlsbad, CA, USA
Reducing Agent	NuPAGE® Sample Reducing Agent	Life Technologies, Carlsbad, CA, USA
Roche buffer	Blocking Reagent for ELISA	Roche Diagnostics, Mannheim, GER
Sheath Fluid	LiquiChip System Fluid (10x)	Qiagen, Venlo, NLD
Transfer buffer	NuPAGE® Transfer Buffer (20x)	Life Technologies, Carlsbad, CA, USA

3.1.7 Buffer

Table 7: List of buffers

Buffer	Reagents and concentration	Distributor
Assay buffer	Roche buffer with 0.2 % milk powder, 0.05 % NaN_3, 0.05 % (v/v) Tween 20	Roche Diagnostics, Mannheim, GER and see chemicals
Dilution–buffer for Co-IP of HEK293T cells	10 mM Tris–HCl pH 7.4 150 mM NaCl 0.5 mM EDTA 2 mM PMSF 1 x Protease Inhibitor Mix M	
DMEM medium	6 g DMEM 1.22 g $NaHCO_3$ Ad 450 ml H_2O_{dd} pH 7.2	
DMEM/F–12 medium	6 g DMEM/F–12 1.22 g $NaHCO_3$ Ad 450 ml H_2O_{dd} pH 7.2	
Elution buffer DigiWest	1 % (v/v) Triton X–100, 8 M Urea in 100 mM Tris–HCl pH 9.5	
Laemmli buffer (4 x)	2 % SDS 10 % Glycerol 60 mM Tris–HCl adjust with HCl to pH 6.8 add 0.02 % Bromophenol blue sodium salt bring up to 95 ml with H_2O_{dd} add 5 ml 2-Mercaptopethanol	
Lysis–buffer for Co-IP of HEK293T cells	10 mM Tris–HCl pH 7.4 0.5 % NP-40 150 mM NaCl 0.5 mM EDTA 2 mM PMSF 1 x Protease Inhibitor Mix M 200 µg/ml DNAse I	
Lysis–buffer for Co-IP of the other cell lines	10 mM Hepes pH 7.6 0.5 % NP-40 100 mM NaCl 1 mM DTT 1 mM $MgCl_2$ 1 x Protease Inhibitors (EDTA-free) Phosphatase Inhibitors (50 mM NaF, 1 mM Na_3VO_4)	
PBST	0,1 % (v/v) Tween 20 in PBS	

Buffer	Reagents and concentration	Distributor
Ponceau staining solution	0,1 % (w/v) Ponceau S, 1 % HAc in H_2O_{dd}	
TBS	10 mM Tris–HCl 150 mM NaCl in H_2O_{dd} pH 7.4	
TBST	0,1 % (v/v) Tween 20 in TBS	

If no distributor is denoted, the source of supply for the individual buffer components can be obtained in the chemicals chapter (see 3.1.5).

3.1.8 Antibodies

3.1.8.1 Capturing antibodies for Co-IP

Table 8: Capturing antibodies for Co-IP

Analyte	Species	Binding site	Distributor	Product number	Dilution for Co-IP
β-catenin	ms	aa 571 – 781	BD Biosciences	610154	500
IgG1	ms		Sigma	M5284	400

All distributors for the capturing antibodies are listed beneath the primary antibody table in the appendix (see Suppl. Table A).

3.1.8.2 Nanotraps

Table 9: Nanotraps for Co-IP

Analyte	Binding site	Distributor
BC1-beads	aa 61 – 87	Prof. Dr. Rothbauer [112]
GFP-Trap®		ChromoTek, Planegg-Martinsried, GER

For generating the BC1-beads, a β-catenin-specific nanobody was immobilized on agarose beads. The BC1 nanobody binds β-catenin N-terminal close to the SSTS-motif (aa 61 – 87), presumably on a three dimensional epitope [112]. The GFP-Trap® represents a non-related nanobody against GFP, the GFP-binding protein (GBP), coupled to agarose beads. Nanobodies fused to fluorescent proteins are called chromobodies [108].

3.1.8.3 Primary antibodies

A complete list of all primary antibodies used for developing this screening approach can be found in the appendix (see Suppl. Table A). All antibodies in this list, which were used for ECIP on different liver cell lines are marked with *, while antibodies used for ECIP or ICIP on any kind of HEK293T cells are marked with **. For usage as a primary antibody in the conventional Western blot, the dilution was carried out as recommended by the manufacturer, with the dilution factor used for DigiWest

being five times lower as recommended for normal Western blotting. If different antibodies directed towards the same protein were used and had to be differentiated throughout the result and discussion chapter, their distinct NMI number was added in brackets to identify them in the antibody list. If two molecular weights are assigned to an antibody by the manufacturer, the antibodies were separated and examined as two individual analytes. Unless otherwise noted, these two peaks always correspond to different isoforms or cleaved versions of the same protein (see Suppl. Table B).

3.1.8.4 Detection antibodies

Table 10: List of detection antibodies for DigiWest.

Antigen	Conjugation	Species	Distributor
gt-IgG (H+L)	PE	dk	Jackson Dianova, Hamburg, GER
ms-IgG(H+L)	PE	dk	Jackson Dianova, Hamburg, GER
rb-IgG (H+L)	PE	dk	Jackson Dianova, Hamburg, GER
rt-IgG (H+L)	PE	gt	Jackson Dianova, Hamburg, GER
Streptavidin	PE	dk	Jackson Dianova, Hamburg, GER

Table 11: List of detection antibodies for Western blot.

Antigen	Conjugation	Species	Distributor
ms-IgG (H+L)	IRDye 800CW	dk	LI-COR Bioscience, Lincoln, NE, USA
ms-IgG (H+L)	IRDye 680RD	dk	LI-COR Bioscience, Lincoln, NE, USA
rb-IgG (H+L)	IRDye 800CW	dk	LI-COR Bioscience, Lincoln, NE, USA
rb-IgG (H+L)	IRDye 680RD	dk	LI-COR Bioscience, Lincoln, NE, USA

All used detection antibodies were diluted according to the manufacturers instruction.

3.1.9 Cell lines

For the identification of different β-catenin complexes, five different cell lines were used.

Table 12: Mouse hepatoma cell lines 70.4 and 55.1c.

Cell line	70.4	55.1c
Cell type	Hepatoma	Hepatoma
Species	mouse	Mouse
Source	Dr. Kress	Dr. Kress
Culture medium	DMEM/F–12 10 % FCS 1 % P/S	DMEM/F–12 10 % FCS 1 % P/S
Growth conditions	37°C, 5 % CO_2	37°C, 5 % CO_2
Mutation status	p53 mutation [76]	heterozygous β-catenin exon 3 deletion [78]; B-raf mutation

Both mouse hepatoma cell lines were established out of mice liver, induced by a single intraperitoneal injection of N-nitrosodietylamine (NDEA), but harbor different mutations [76, 78].

Table 13: Human hepatocellular carcinoma cell lines HB35 and HepG2.

Cell line	HepG2	HC-AFW1 (alternative name HB35)
Cell type	Hepatocellular carcinoma	Hepatocellular carcinoma
Species	human	Human
Source	DSMZ (Leibniz Institute DSMZ-German Collection of Microorganisms and Cell Cultures)	University Children's Hospital Tübingen, Pediatric Surgery
Culture medium	MEME 10 % FCS 1 % P/S 1 % Glutamine	DMEM 10 % FCS 1 % P/S [122]
Growth conditions	37°C, 5% CO_2	37°C, 5 % CO_2
Mutation status	heterozygous β-catenin exon 3-4 deletion [74, 79, 82, 85]	Heterozygous β-catenin exon 3 deletion [83]

Both human liver cell lines where generated out of liver tumors from young male donors. Both show a mutational deletion of β-catenin exon 3, so that an active Wnt/β-catenin signaling can be observed [79, 82-84]. To avoid confusion during the presentation of results, the cell line HC-AFW1 will be henceforth referred to as HB35 within this thesis.

Table 14: Human embryonic kidney cell line HEK293T.

Cell line	HEK293T	HEK293T_BC1	HEK293T_GFP
Cell type	Embryonic Kidney	Embryonic Kidney	Embryonic Kidney
Species	human	human	human
Source	ATCC (American Type Culture Collection)	ATCC (American Type Culture Collection)	ATCC (American Type Culture Collection)
Culture medium	DMEM 10 % FCS [123] 1 % P/S 1 % Glutamine	DMEM 10 % FCS [123] 1 % P/S 1 % Glutamine	DMEM 10 % FCS [123] 1 % P/S 1 % Glutamine
Growth conditions	37°C, 5 % CO_2	37°C, 5 % CO_2	37°C, 5 % CO_2
Mutation status	none	none, stabile transfected with the BC1-chromobody sequence	none, stabile transfected with the GFP plasmid

HEK293T cells was generated out of human embryonic kidney cells and shows an epithelioid character. The cell line shows no mutations associated with the Wnt/β-catenin pathway and is therefore, a relatively complete system to gain deeper insight in the mechanisms of this pathway [124].

3.2 Biomolecular and biochemical methods

3.2.1 Cell Culture

3.2.1.1 Growth conditions and general remarks

All working steps were performed under sterile conditions, in order to avoid contaminations. To ensure this, culture media, solutions and consumables were autoclaved at 121°C, 1 bar for 40 min. If heat sensitive, they were sterile filtered. Working materials were disinfected with 70 % EtOH before entering the sterile area underneath the clean bench and glassware was sterilized at 180°C for 4 h. All cell lines were cultivated in 10 cm cell culture dishes in the respective recommended growth medium (see Table 12 – Table 14) supplemented with 10 % (v/v) FCS and 1 % penicillin (10,000 U/ml) / streptomycin (10 mg/ml) solution at 37°C and 5 % CO_2 with almost saturated humidity. The growth medium was changed every second day.

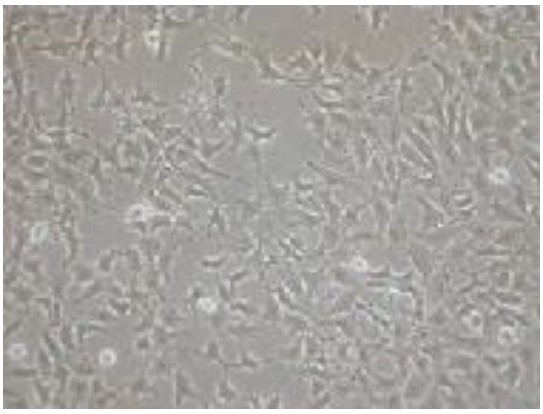

70.4

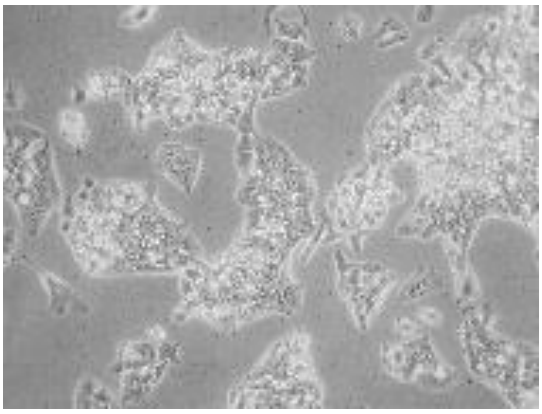

HepG2

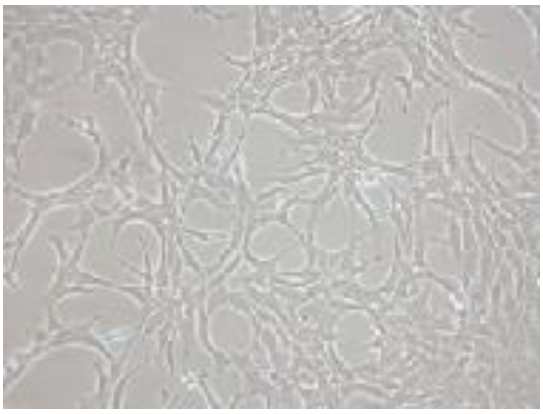

55.1c

HB35

Figure 4: Cells at maintenance culture.
Pictures were received from Eva Zeller, Toxicology department, Eberhard Karls University of Tübingen.

3.2.1.2 Cell Passaging

At 90 % confluence cells were subcultured; growth medium was aspirated and cells were washed with sterile PBS once. By adding 1 ml of trypsin-EDTA cells were detached from the cell culture dish. After incubating for 5 min in the incubator at 37°C, 9 ml of regular growth medium were added to stop enzymatic activity. It was required to disperse the cells by pipetting up and down, using a 10 ml syringe and an injection needle. To maintain a sustainment culture, a few drops of the cell suspension were added to a new cell culture dish, filled with fresh growth medium.

3.2.1.3 Drug treatment

At a confluence status of 70 - 80 % cells were treated for 24h with 10 ml treatment medium. The normal growth medium was supplied with less FCS (1 % (v/v) FCS) and supplemented with CHIR 99021 or MG132 at concentrations listed below. Untreated cells were used as a negative control (see Table 15). MG132 was solved in DMSO, as it is not soluble in water. Since it is known that a DMSO concentration above 1 % (v/v) is toxic [125]. It is recommended to stay below a concentration of 0.5 % – 1 % in cell culture in order to avoid cellular effects [126]. The used DMSO concentration of 0.0025 % (v/v) for the MG132 treatment is well below this concentration and since no cellular alterations were observed, no additional negative control was included.

Table 15: Treatment compounds, their mode of action and their final concentration.
CHIR 99021 and MG132 were dissolved according to the manufacturer's instructions.

Reagent	Mode of action	Final concentration
CHIR 99021	Inhibition of GSK3	10 µM
MG132	Inhibition of proteasome	1 µM
-	Negative control	

3.2.1.4 Cell harvesting

For harvesting, cell cultivation plates were placed on ice, and washed once with ice-cold PBS. Washing buffer was discarded, cells scraped off the plate in 1 ml of ice-cold PBS and collected into a 1.5 ml reaction tube. After centrifugation at 4°C and 600 g for 5 min, the supernatant was discarded and the cell pellets quick-frozen in liquid nitrogen. Cells were stored at -80°C.

3.2.2 Cell lysis under non-denaturating conditions

For cell lysis for ECIP or ICIP (see 3.2.3 and 3.2.4), two different lysis protocols were used.

Pellets of the cell lines (70.4, 55.1c, HepG2 and HB35), received from the Toxicology department, Eberhard Karls University of Tübingen, were homogenized in 200 µl of lysis buffer for Co-IP of other cells (10 mM Hepes pH 7.6, 0.5 % NP-40, 100 mM NaCl, 1 mM DTT, 1 mM $MgCl_2$, Protease Inhibitors (EDTA-free), Phosphatase Inhibitors (50 mM NaF, 1 mM Na_3VO_4)). The buffer system was adapted to

the protein extraction protocol described by Yakulov et al. [127] and thereby a better extraction of nuclear β-catenin was facilitated. This modification ensures compatibility to protein fractionation protocols, where nuclear and cytoplasmic fractions are generated.

The lysis procedure varied slightly for the HEK293T cells. Here the pellets were homogenized in 200 µl of lysis buffer for Co-IP of HEK293T cells (10 mM Tris-HCl pH 7.4, 0.5 % NP-40, 150 mM NaCl, 0.5 mM EDTA, 2 mM PMSF, 1 x Protease Inhibitor Mix M, 200 µg/ml DNAse I). For lysis, pellets were put on ice for 10 min and pipetted up and down for thirty times afterwards. This was repeated twice, before the lysate was centrifuged at 14000 rpm for 10 min at 4°C in a precooled centrifuge [112]. The supernatant was transferred into a new reaction tube and the protein solutions were adjusted to a total volume of 500 µl with the previously used lysis buffer, in case of the cells from the Toxicology department. If working with HEK293T, the volume was adjusted with dilution buffer (10 mM Tris/Cl pH 7.4, 150 mM NaCl, 0.5 mM EDTA, 2 mM PMSF, 1 x Protease Inhibitor Mix M) instead. This procedure was followed either by conventional Co-IP (see 3.2.3), ECIP (see 3.2.3.2) or ICIP (see 3.2.4).

3.2.3 Conventional Co-Immunoprecipitation

50 µl of lysate were taken and mixed with 4 x Laemmli buffer, to generate the input sample.

3.2.3.1 Co-IP on liver cell lines

For processing the four cell lines, received from the Toxicology department, either 1 µl of a β-catenin-specific antibody (dilution factor 1:500) or 1 µl of an identically concentrated monoclonal ms, IgG1-isotype control antibody (dilution factor 1:400), serving as a negative control, were added to each sample. Samples were mixed and left on ice for approximately 5 min. Afterwards 50 µl of magnetic protein G beads were washed in 50 µl of PBST three times and resuspended in lysis buffer, prior to adding to the lysate and incubated at 4°C overnight on an overhead mixing rotator. The used amounts of antibody and protein G beads for precipitation were determined according to the manufacturers protocol and in dependence on the ECIP and ICIP protocol (see 3.2.3.2 and 3.2.4). After incubation, the reaction tubes were put onto a magnetic separator, 50 µl of the supernatant was recovered and taken as the non-bound sample before mixing with 4 x Laemmli buffer. The remaining supernatant was discarded. The bead-pellet was gently washed with 500 µl of lysis buffer. This step was repeated twice. The bead-protein suspension was transferred into a new reaction tube, to avoid a carry over of sticky proteins attached to the reaction tube walls. After discarding the supernatant once more, the bound sample was generated by dissolving each bead-pellet in 100 µl 2 x Laemmli buffer. All samples (inputs, non-bounds, bounds) were denatured at 95°C for 10 min and 300 rpm on a reaction tube shaker. The workflow in detail is described in Figure 5.

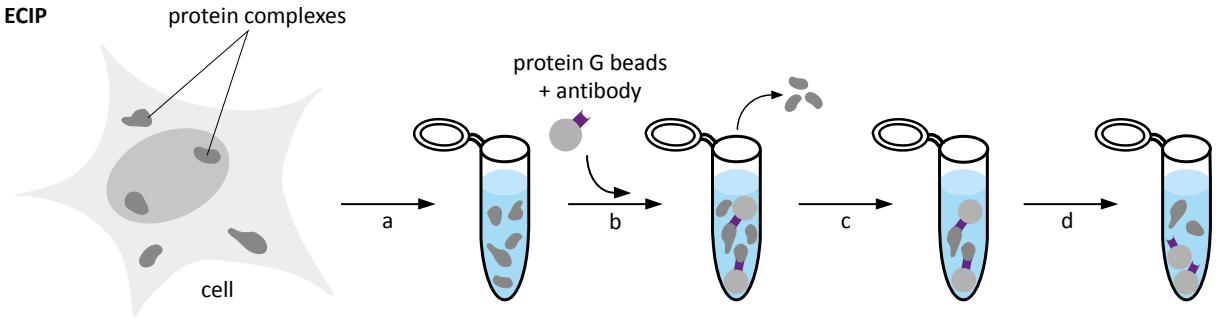

Figure 5: Workflow of Co-IP on other cell lines.
Cells were lysed, the input sample was taken (a); β-catenin protein complexes were captured by a β-catenin-specific antibody coupled to protein G beads overnight (b). Taking of the non-bound sample and washing (c); elution of protein complexes from the protein G beads, generating of the bound sample (d). (Figure adapted from ChromoTek, Planegg-Martinsried, GER).

3.2.3.2 ECIP on HEK293T samples

For processing of the HEK293T samples, 50 µl of BC1-beads or GFP-Trap® were added to each lysate and incubated at 4°C overnight on an overhead mixing rotator. GFP-Trap® as a nonrelated nanobody, was used as a negative control and the generated samples are referred to as GFP-bound [92]. After incubation, reaction tubes were centrifuged at 2500g at RT for 2 min and 50 µl of the supernatant was removed (non-bound sample) and mixed with 4 x Laemmli buffer. The remaining supernatant was aspirated with a needle and discarded. The bead-pellet was gently washed with 500 µl of dilution buffer; this step was repeated twice. Afterwards the bead-protein suspension was transferred into a new reaction tube. Another centrifugation step was performed and the supernatant discarded. The bound sample was generated by adding 100 µl 2 x Laemmli buffer to each bead-pellet. Samples were denatured at 95°C for 10 min and 300 rpm on a reaction tube shaker. This workflow in detail is shown in Figure 6.

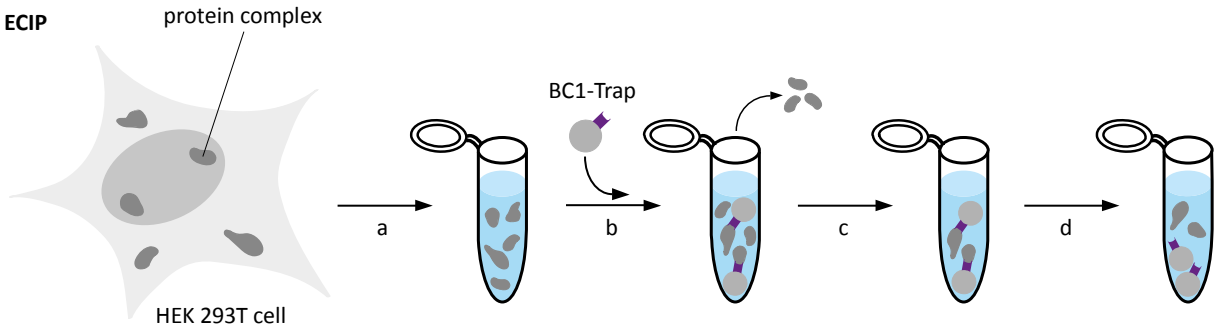

Figure 6: Workflow of ECIP on HEK293T cells.
Cells were lysed, the input sample was taken (a); β-catenin protein complexes were captured by the β-catenin-specific nanobody BC1 coupled to agarose beads overnight (b). Taking of the non-bound sample and washing (c); elution of protein complexes from the agarose beads, generating of the bound sample (d). (Figure adapted from ChromoTek, Planegg-Martinsried, GER).

3.2.4 Intracellular Co-Immunoprecipitation (ICIP)

Analog to 3.2.3, 50 µl of the 500 µl cell lysate (see 3.2.2) were taken and mixed with 4 x Laemmli buffer to receive the input sample. Subsequently 50 µl of GFP-Trap® were added to the stabile transfected HEK293T lysates. HEK293T cells stabile transfected with plasmid, carrying GFP, served as a negative control and were processed analog. After adding the GFP-Trap®, the lysates were incubated at 4°C overnight on an overhead mixing rotator. The ensuing procedure was identically performed as described in 3.2.3.2. Figure 7 gives a more detailed overview on the workflow.

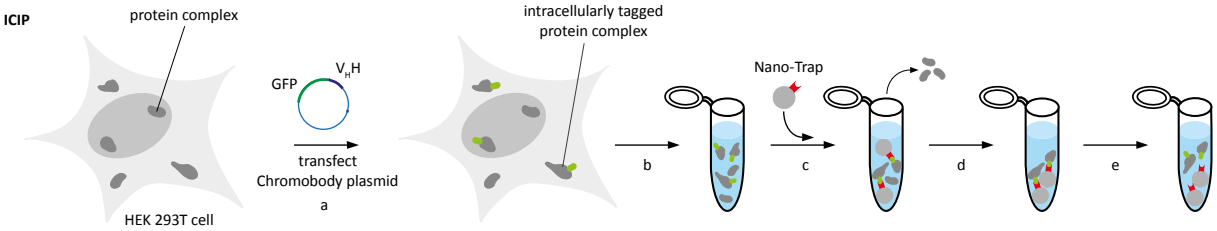

Figure 7: Workflow of ICIP on stable transfected HEK293T cells.
Cells were transfected with the chromobody plasmid (a); β-catenin protein complexes were bound by the intracellular expressed chromobody. Cells were lysed (b); protein complexes were captured via the fluorescent tag using the GFP-Trap® (c). Taking of the non-bound sample and washing (d), elution of protein complexes from the GFP-Trap®, generating of the bound sample (e). (Figure adapted from ChromoTek, Planegg-Martinsried, GER).

3.2.5 Polyacrylamid gel electrophoresis

The used gel electrophoresis system operates according to the principle of the discontinuous denaturing sodium dodecyl sulfate-polyacrylamide gel electrophoresis (SDS-PAGE), described by Laemmli [128]. The samples were mixed with 4 x Laemmli and denatured for 10 min at 75°C. 10 µl of the input samples (= 1 %), 20 µl of the bound samples (= 20 %) [112, 129] and 5 µl of a pre-stained marker, as a reference, were subsequently loaded onto a pre-cast NuPAGE gel. For checking the quality of the Co-IP additional 10 µl of the non-bound samples (= 1 %) were added onto the gel. All used gels were 4 – 12 % Bis-Tris gels with 12 – 17 wells and 1 mm thick. These gels contain a polyacrylamide-gradient from 4 to 12 %. Number of wells varied according to the experimental requirements. For DigiWest experiments, only 12 well gels were used. On gels, being destined for the DigiWest, additionally the molecular weight marker was applied twice and every second lane in between the samples was left empty, which was essential for the later blot cutting (see 3.3.2.1). The electrophoresis was run for approximately 1.5 h at 150 V in 800 ml 1 x NuPAGE MES buffer with 500 µl NuPAGE antioxidant per chamber, until the blue buffer front reached the bottom of the gel. For only checking the quality of the Co-IP procedure, gels were run shorter at 200 V. The successful performance of Co-IP was checked by proceeding with a conventional Western blot (see 3.2.6), before processing the samples in the DigiWest. If the blot was intended for specific immunological detection, it was proceeded into the microsphere-based DigiWest. (see 3.3.2).

3.2.6 Western blot

The proteins from the gel matrix were transferred onto a PVDF membrane using NuPAGE blotting system [130]. The transfer in transfer buffer with 10 % MeOH was carried out for 75 min at 30 V, 160 mA and RT.

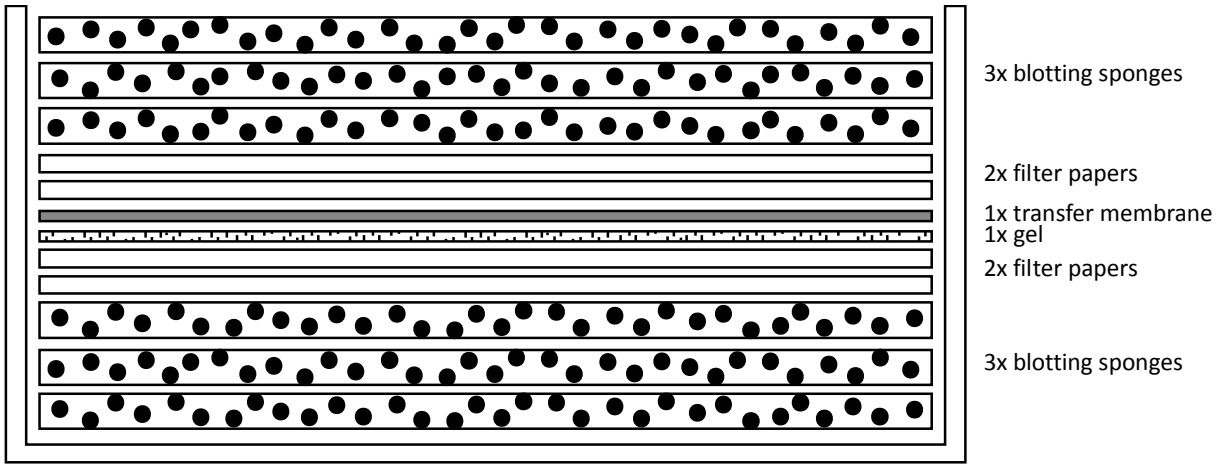

Figure 8: Western blot transfer setup.
The Western blot transfer setup consists out of three blotting sponges soaked with transfer buffer, two soaked Whatman papers, the gel, a PVDF membrane, activated in MeOH and rinsed with transfer buffer, two Whatman papers soaked with transfer buffer and again three soaked blotting sponges placed on top of each other.

After transferring the proteins, the membrane was washed in PBST for 15 min.

3.2.7 Ponceau S staining

The transfer efficiency was monitored by reversibly staining of the membranes with Ponceau S (10 min on an orbital shaker) to detect immobilized proteins on the membrane. After washing and decolorizing the membrane with H_2O_{dd} to an extent that protein bands were visible, they were detected by the ImageQuant LAS 4000 mini. For blots, which were processed further in the DigiWest, the lane positions were labeled with a pencil to guarantee a successful cutting of the membrane later on. Subsequently the membrane was completely destained by incubation in TBST or PBST for 30 min with exchanging the buffer several times.

3.2.8 Immunodetection

For blocking of free sites on the PVDF membrane 3 % BSA in TBST were added and incubated for 60 min on a rotating mixer. Blots were placed in 15 ml or 50 ml tubes and the incubation with primary antibodies was carried out in 1 % BSA in TBST overnight at 4°C on a rotating mixer (antibody dilutions see 3.1.8.3 and Suppl. Table A) [92]. Depending on the size of the membrane, 2.5 ml or 4 ml

of antibody dilution were used. Subsequently, the antibody solution was discarded and the membrane was washed three times for 5 min each with 10 ml of TBST to remove the unbound antibody. The species-specific, LI-COR IRDye labeled secondary antibodies diluted in 1 % BSA in TBST were applied and the membrane was incubated in the dark for 1 h at RT on a rotating mixer (antibody dilutions see Table 11). The earlier described washing was repeated three times and the membrane dried afterwards. Signal detection was performed at excitation wavelengths 685 nm and 785 nm on the ODYSSEY Infrared Imaging System; Images with a resolution between 42 – 337 µm were recorded. Via pre-scanning the optimal laser power setting (high intensity, but no saturated pixels), for the ensuing a high dynamic range, was determined. The Odyssey CLx was used due to the advantage of its multiplex analysis capacity. By selecting appropriate antibodies a simultaneous detection of two targets by using two different IR fluorophores is possible [131].

3.3 Microarray methods

The described microarray-based Western blots were performed on the microsphere-based, Luminex technology. The Luminex Flexmap 3D device was used, which is able to distinguish up to 500 different types of microspheres via their internal color-coding. Here, a 384-plex DigiWest bead mix was employed. The coupling conditions for generating such a 384-plex DigiWest bead mix were established and described in detail recently [89]; therefore, are only brieftly oulined here.

3.3.1 Preparation of magnetic microspheres

3.3.1.1 NeutrAvidin coating

NeutrAvidin coated Luminex MagPlex® beads provide an efficient binding matrix for biotinylated proteins. NeutrAvidin is a deglycosylated avidin, which has a strong affinity for biotin (dissociation constant ~ 10^{-14} M) [132]. Therefore, NeutrAvidin was coupled to Luminex MagPlex® beads with a KingFisher® 96 automated magnetic particle processor. In preparation of the coupling, the MagPlex® beads were vortexed firmly and treated with ultrasound to reduce bead agglomeration. Beads were provided in 96 well plates and placed together with the buffer plates into the KingFisher® 96. During the coupling process a covalent bond between primary amines and activated carboxyl groups on the surface of the Luminex beads is formed. These carboxyl groups can be activated with EDC and form a reactive sulfo-NHS-ester intermediate in the presence of sulfo-NHS. Primary amines and the intermediate react and form a covalent amide bond, which is later used by biotinylating proteins and coupling them to the MagPlex® beads in a second coupling step [133]. The beads covered with reactive sulfo-NHS-ester intermediates are washed and transferred into storage tubes.

3.3.1.2 Quality control of NeutrAvidin coupling

To guarantee a high biotin binding capacity, all bead populations were tested for functionality. In a first step a bead count of a mixture of all 400 bead IDs was generated. Eight replicas of 100 µl each were pipetted into an assay plate and the number of entities was counted on a Luminex Flexmap 3D. To ensure that all beads in a well are counted, the settings on the Luminex device were chosen accordingly. The measured number of beads was used for a backwards calculation to determine the bead concentration of each bead ID, which allowed the adjustment of each of the 400 bead sets to a concentration of 4000 beads/µl. The biotin binding capacity was monitored by incubating the generated bead mixture with a biotinylated c-Myc peptide (1 mg/ml concentration). The peptide was loaded onto the bead, the mixture was pipetted into 16 wells of a microplate and incubated with a dilution series of anti-c-Myc antibody. After washing, the beads were incubated with a PE-tagged, species-specific, secondary antibody and the plate was placed in the Luminex Flexmap 3D for

readout. The total intensity of the signal and the CV was measured for every bead ID. Only IDs with a CV below 3 % were selected for the later composed 384-plex DigiWest bead-mix.

3.3.1.3 Bead plate composition and preparation

Out of the 400 coupled bead sets, the best 384 bead IDs were chosen to compose four 96-plex bead plates with an ascending sorting of the bead ID. Criteria for exclusion were mainly due to technical problems, that prevented the specific classification for several bead IDs. But also a weak performance in the biotin binding capacity test or a low count (described in 3.3.1.2) led to an exclusion of bead IDs from the 384-plex. To create DigiWest bead plates with a defined number of beads per well, master plates with 200 µl/well per bead ID were pipetted in a first step. The master plates served as a source for the pipetting robot BioMek FX, which transferred between 20000 and 80000 beads/well into the correspondent DigiWest plates. For storage the plates were labeled, vacuum sealed and kept at 4°C in the dark.

3.3.2 Digitalized Western blot (DigiWest)

To carry on with the DigiWest procedure, blots were prepared as described above (see 3.2.5, 3.2.6 and 3.2.7). A summarized overview can be gained in Figure 9.

3.3.2.1 Membrane processing

The transferred proteins on the PVDF membrane were biotinylated by adding 20 ml of a 50 µM dilution of NHS-PEG12-Biotin (50 mM, 20 µl in DMSO) in PBST. Membranes were incubated for 1 h on an orbital shaker (30 shakes/min, 6° angle), at RT in the dark. Blots were subsequently washed in PBST three times and dried between Whatman papers overnight. For transferring the proteins onto beads according to their molecular size, the dried membranes were placed onto a printed Adobe Illustrator template and fixed with tape. To prevent rupture of the membrane while cutting, it was covered by an additional layer of paper. For cutting, the template with the fixed membrane was attached to the Silhouette cutting mat and inserted into the Silhouette SD cutting plotter. Lanes containing electrophoretically separated proteins, were cut into 96 equally sized, horizontal strips (7 mm wide, 0.5 mm high), linear from high to low molecular weight. Thereby a molecular range between 12 kDa and approximately 400 kDa was covered (see Figure 9).

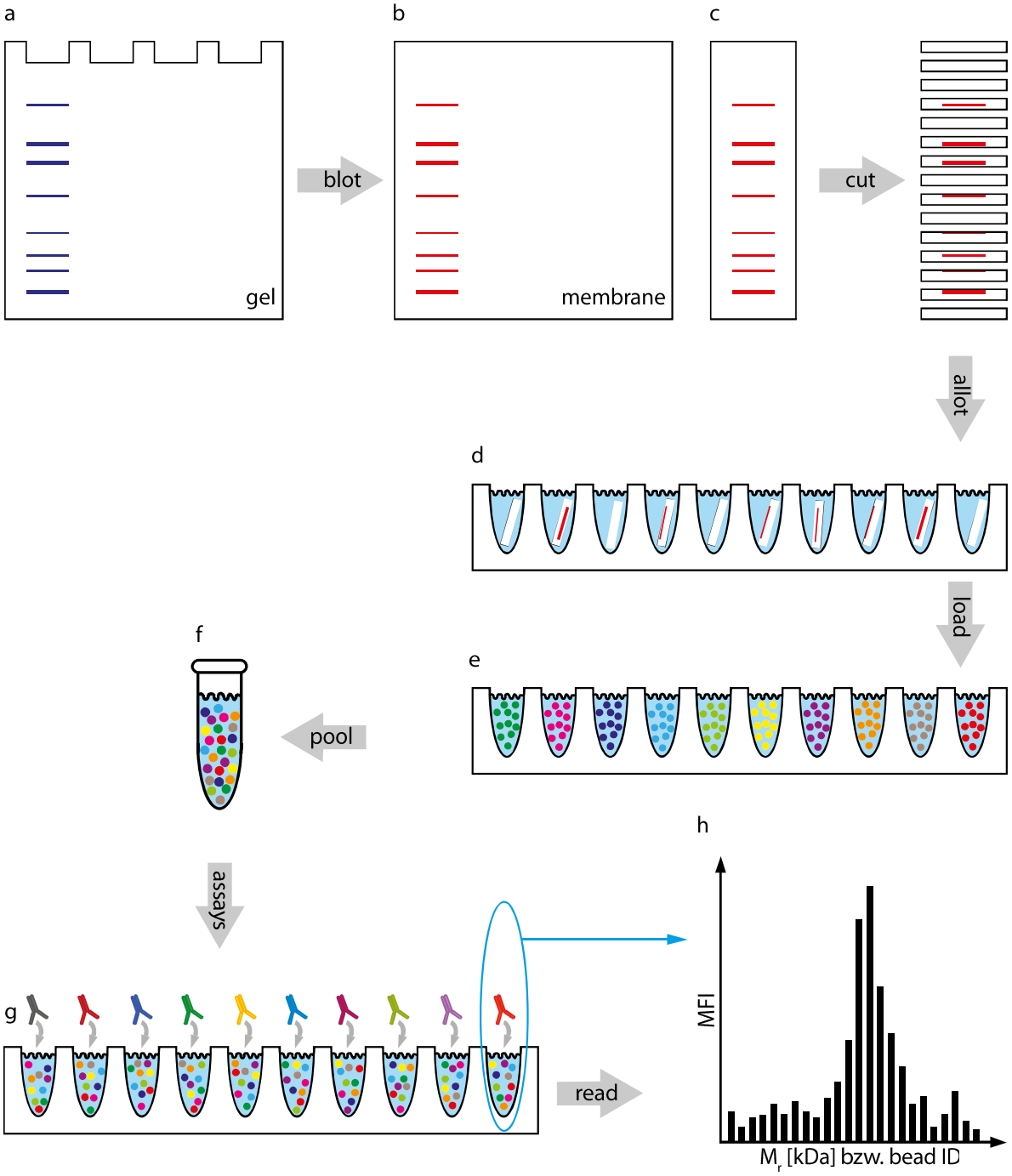

Figure 9: Schematic representation of the DigiWest assay design.
Proteins were separated via SDS-Page (a) and transferred onto a PVDF membrane via Western blotting (b). Each protein containing lane was cut into 96 strips corresponding to the molecular seize of the protein fractions, (c) strips were plucked and sorted into a 96 well microplate. Proteins were eluted from the strips (d). The proteins eluted from each strip were assigned to one of 96 specific Luminex MagPlex® bead IDs and coupled onto these beads (e). By pooling and mixing the different bead IDs, an original blot lane was represented (f). Immunoassays with one individual Western blot antibody per well can be performed (g). Subsequently the signal readout was carried out on a Luminex Flexmap 3D (h). The original Western blot was reconstituted. On the x-axis the 96 different bead IDs were arranged, while the y-axis represents the median of the median fluorescence intensity obtained for the species-specific, fluorescent, secondary antibody (Figure adapted from [89]).

3.3.2.2 Protein elution

These strips were plucked and sorted ascending into a 96 well microplate according to the molecular seize of the contained, immobilized protein fraction. Each lane was assigned to an individual microplate. 10 µl/well of elution buffer were added and it was insured that every strip was completely covered by buffer. Plates were sealed with plate sealing tape and incubated for 1.5 h at 1200 rpm on a plate shaker at RT to solubilize the bound proteins from the membrane again (see Figure 9).

3.3.2.3 Protein coupling to microspheres

After elution, 90 µl of 5 % BSA in PBST were added to each well. This led to a dilution of the denaturing elution buffer and facilitated the later immobilization of the eluted proteins onto the surface of the NeutrAvidin coated beads. Plates were placed on a shaker to mix the buffers briefly.

Stored DigiWest plates (see 3.3.1.3) were unwrapped and beads were transferred manually from the prepared DigiWest plates into the elution plates by using a KingFisher® 96 PCR magnet head mantled with a KingFisher® 96 tip comb. For coupling, the plates were sealed after the bead transfer with plate sealing tape and incubated for 18 h at 750 rpm and RT on a plate shaker. After coupling, the remaining biotin binding sites on the Luminex MagPlex® were blocked by adding 5 µl of deactivated NHS-PEG12-Biotin to each well and incubating for 1 h at 750 rpm and RT on a plate shaker. For generating the deactivated biotin reagent, NHS-PEG12-Biotin (50 mM, 20 µl in DMSO) was diluted in 6 ml TBST and left overnight at RT. Adding an excess of biotin to the wells, also leads to the prevention of bead aggregation.

As different Luminex MagPlex® microspheres can be distinguished by their various embedded color codes, it is possible to assign one distinct bead ID to a specified protein fraction of a distinct molecular weight range. By pooling the coupled beads from each 96 well plate, the bead collection leads to a bead mix, out of which an aliqot corresponds to the prior, original Western blot lane.

Due to the usage of a 384-plex, four different 96 well plates containing proteins coupled to beads presented four different Western blot lanes. These were pooled, mixed and could still be discriminated during the subsequent assay readout. For pooling, a KingFisher® 96 PCR magnet head manually mantled with a KingFisher® 96 tip comb was used to transfer the beads from four different plates into one. After pooling, the beads in the last remaining plate were collected into one well by usage of a magnetpen with 8 tips covered with corresponding silicone tips. The bead mixture was transferred into a reaction tube and washed in 500 µl Roche buffer on a magnetic separator three times (see Figure 9). Finally the washing buffer was discarded and the bead mix was resuspended in Roche buffer and adjusted to a concentration of 40 beads/ID/µl. The bead mixes were stored at 4°C in the dark.

3.3.2.4 DigiWest assay

For each assay an individual plate layout was designed, comprising the specific conditions like amount of samples/bead-mixes and the number of antibodies to be tested. DigiWest assays were run in a 96 well, half area microplate. 50 µl of assay buffer were provided into each well and a small aliquot of 5 µl of the generated bead mix (see 3.3.2.3) was added, to ensure an amount of 200 beads per ID per well. Before running regular assays, the quality of the protein loading onto the beads was tested by estimating the on-bead protein amount via detecting their biotinylated sites. Therefore, 5 µl of the bead mix were incubated with a dilution series of PE-labeled Streptavidin (Strep-PE, 4 µg/ml, 1 µg/ml and 0.25 µg/ml) for 1 h at 750 rpm and RT. After washing with PBST three times it was possible to simultaneously count the actual number of each bead ID during the readout. This resulted in the achievement of information about free biotins represented on the Luminex MagPlex® beads and the quality of the bead pooling. Bead sets passing this quality check were used to run regular assays. All detection antibodies were diluted in assay buffer in a five times higher concentration as recommended for conventional Western blot analysis. Before adding the diluted antibody, the microplates were placed on a magnet plate and the supernatant was fiercely discarded. 25 µl/well of the antibody dilution was added. The plates were covered with plate sealing tape and incubated overnight at 15°C and 750 rpm on a plate shaker. After incubation, the plates were washed with 100 µl PBST per well three times. The supernatant in between was discarded by placing the microplate on a magnet plate. PE-labeled, species-specific, secondary antibodies were also diluted in assay buffer, with a dilution factor of 1:200. The identical volume as used for the primary antibody was added to each well and the plate was incubated for 1 h at 23°C and 750 rpm on a plate shaker. The washing step was repeated identically. For the readout process, 100 µl of PBST were added to each well and the microplate was shaken up vigorously on a plate shaker at 1000 rpm for a couple of seconds to avoid a bead accumulation on the bottom of the wells. During readout on the Luminex FlexMap 3D, a minimum of 50 beads per ID were counted within a counting volume of 85 µl per well.

3.4 Presentation and analysis of data sets

3.4.1 Signal quantification

An in-house developed, Excel-based analysis tool (see 3.1.2) was used for quantification of the obtained antibody-specific signals. Herein both the result evaluation and the data analysis were performed. This tool allows the reconstruction of primary Western blot lanes, but is also capable to identify and quantify antibody-specific signals. An additional advantage of the digital DigiWest data generated by the Luminex FlexMap 3D, in comparison with the conventional Western blot analysis, is that no image processing and densiometrical analysis is needed for signal quantification.

Relative median fluorescence intensity (MFI) values are listed in the Luminex output files. Therefore, the MFI of each PE-labeled bead-ID out of a bead mix is measured. The analysis tool generates bar graphs visualizing the median fluorescence intensity out of 96 distinct obtained values for each initial Western blot lane (see Figure 10).

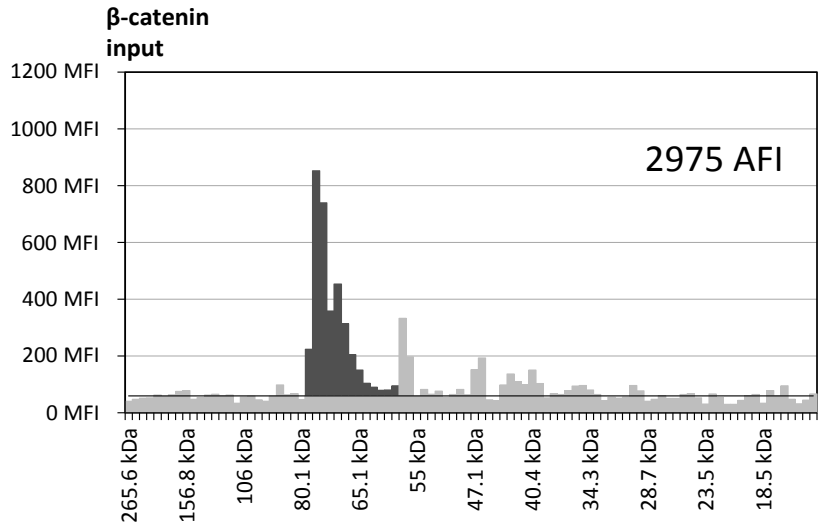

Figure 10: Exemplary bar graph for the target protein β-catenin.
This exemplary bar graph for the untreated β-catenin input was retrieved from the DigiWest analysis tool. On the x-axis the calculated molecular weight is plotted, while on the y-axis the median fluorescent intensity (MFI) is shown. The highlighted peak in dark gray shows the β-catenin-specific molecular weight (~75-82 kDa). This peak corresponds to the β-catenin-band observable in a conventional Western blot (see Figure 25). A baseline is calculated by using the local background and the highlighted peak area above this baseline is integrated. The integrated signal is based on relative fluorescence and is calculated as 2975 AFI (assembled fluorescence intensity).

These bar diagrams are equivalent to Western blot lanes and show antibody-specific peaks, which correlate with bands that can be observed in a classical Western blot. Within the analysis tool it is possible to evaluate a 384-plex incubated with 96 different antibodies. Additionally, the on-bead protein amount can be estimated using the test described earlier (see 3.3.2.4) and subsequent evaluation can be carried out by the analysis tool. An automatic subtraction of the assay-specific

background is implemented in the analysis tool. A defined molecular weight assigned to the x-axis of the generated bar graphs is used for assigning peaks the correct molecular weight. For this purpose, an Excel add-in (XLfit) is used to calculate the approximate molecular weight for each protein fraction. This can be achieved, by employing the measured positions of an external marker band, which was run and blotted together with the samples, or by selecting peak-positions of known proteins with a defined molecular weight, providing an internal marker.

For each tested antibody up to two different peaks can be selected and integrated. Based on their assigned molecular weight, a local maximum around this area is scanned automatically; the possibility to adjust the integrated area manually is implemented in the software tool. If two MWs were assigned to an antibody by the manufacturer and two peaks are observed, these were selected and integrated individually by the analysis tool.

The values of the integrated peaks are given in relative units, called assembled fluorescence intensity values (AFI). These values are used to perform further statistics or analysis.

3.4.2 Grayscale data representation

To obtain an intuitive way to analyze the created bar graphs and numerical values (see 3.4.1), the generated data can be transformed into a Western blot like graphic. This is done by a second in-house developed, Excel-based analysis tool, the DigiWest Viewer (see 3.1.2). The DigiWest Viewer facilitates the direct comparison of the DigiWest with a classical Western blot in an intuitive way. The background subtracted Luminex raw data is used to generate these Western blot mimics by normalizing it to values between 0 and 1. The provided data is converted into a grayscale map by applying a grayscale scheme from zero (white) to one (black). To smoothen the grayscale maps and for more visual similarity to the original Western blots, the arithmetic mean (from now onwards referred to as mean) between two neighboring values of the 96 distinct values for each lane is calculated. This mean value is inserted as an additional gray-shaded cell in between the two neighboring cells, taken for mean calculation (see Figure 11).

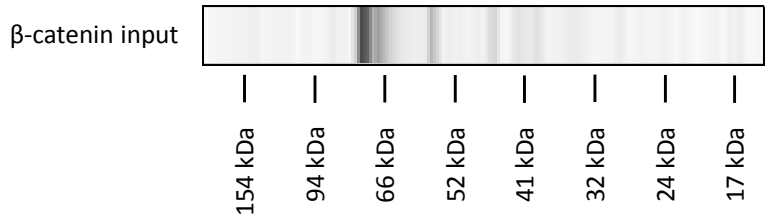

Figure 11: Western blot mimic for the target protein β-catenin.
The identical values used for the bar graph in Figure 10 were used to generate this grayscale Western blot mimic in the DigiWest Viewer. The main peak as well as minor side peaks were visualized as lanes. The molecular weights were taken from the original bar graph and rounded to a whole number.

The DigiWest Viewer facilitates the direct comparison of up to 16 different samples side by side. For this, data of the samples is individually exported from the DigiWest analysis tool and inserted into the DigiWest Viewer.

3.4.3 Data Evaluation

The peaks integrated in the DigiWest analysis tool can be exported and further analyzed to gain information about alterations in protein expression occurring after drug treatment and to identify PPIs with β-catenin. The integrated signal detected at the appropriate molecular weight, was defined as a specific signal and further analysis was done.

During the experiments, the cultured cells were subjected to different treatments (CHIR 99021 and MG132 for 24 h). But as different cell lines vary in their protein amount, the differences in protein content had to be adjusted using a normalization factor.

3.4.3.1 Strep-PE normalization

An incubation of the biotinylated samples with Strep-PE labels the free biotins on the bead-bound proteins. The measured Strep-PE signal represents freely available biotins from the bound proteins on the beads. A linear correlation between the Strep-PE signal and the protein amount loaded to the Luminex beads has been shown previously [89]. Thus, a relative on-bead protein determination can be performed and the derived factor can be used for data normalization [89]. In order to establish a basis to compare different cell lines, all lysates were normalized to the total amount of proteins coupled to the bead surface.

To estimate the total amount of proteins, the beads were incubated for 1 h with three different dilutions (4 µg/ml, 1 µg/ml and 0.25 µg/ml) of an anti-Strep-PE antibody, and signal was read out on the Luminex FlexMap 3D. By using integrals of all Strep-PE signals, generated of a fixed Strep-PE antibody concentration, the median was calculated. An individual normalization factor referring to each input sample was calculated by dividing the individual overall Strep-PE signal by this median. To ensure a stable individual normalization factor, the average of the three individual normalization factors for the same input sample, derived from the three different Strep-PE concentrations, was taken.

Hierarchical cluster analysis was used (euclidian distance (see Equation 1) as a measurement for detecting similarity and complete linkage as a clustering method) to generate heatmaps that allow the visualization of logarithmized data sets [134].

$$d_{ab}=\sqrt{\sum_{c}(e_{ac}-e_{bc})^2}$$

Equation 1: Formula of the Euclidian distance.

3.4.3.2 Comparable evaluation of cell line specific input samples

To create a comparable basis between the input data obtained for the different measured cell lines, the raw data values exported from the DigiWest analysis tool were normalized as described above (see 3.4.3.1). For the ECIP on HEK293T cells or the ICIP performed with stable transfected HEK293T cells, neither the normalization nor the comparable evaluation of the input samples was done.

For the inputs of the untreated samples, the normalized values were subsequently $\log_2$ transformed, in order to visualize the differences in between the four cell lines for all tested analytes, for signals obtained between the lower and the higher range.

To investigate the influences of treatment on the cells in comparison to the respective untreated input sample, a fold change was calculated out of the normalized input values. Therefore, each value obtained for an analyte was referred to its respective value received in the untreated input sample within the same cell line (see Equation 2).

$$\text{ratio} = \frac{\text{input (un)treated}}{\text{input untreated}}$$

Equation 2: Formula to investigate the influences of treatment.

After taking the logarithm to base 2, the derived values for the untreated sample were 0, while for CHIR 99021 and MG132 treatment increases, or decreases, were represented by positive or negative values respectively. Again a visualization of the alterations caused through treatment became possible both for a wide range of signal intensities on a linear scale.

3.4.3.3 Classification of protein-protein interactions

For the identification and classification of proteins as interaction partners of β-catenin, all peaks showing a signal intensity above 45 AFI in the bound samples were included in further calculations.

This cutoff limit at 45 AFI was derived from the averaged background level of approximately 11 AFI and the identification of signals as significant peaks, which was defined as four times above this background level. If duplicates (see 4.3) or triplicates (see 4.4) were analyzed, a two-step method was applied. For the two-step method, the sum of both exported AFIs had to be above 90 AFI (for duplicates) or 135 AFI (for triplicates). In order to receive more stability among the replicas and eliminate not reproducible signals, the deviation between the single values had to be smaller or equal to 10 AFI in addition. That led to the exclusion of inconsistent and unstable PPIs.

Additionally, unspecific binding of proteins to the immunoprecipitation matrix was observed for several proteins. To eliminate signals derived from unspecific binding, a second Co-IP was run simultaneously to the one, which employed a specific capturing antibody or nanobody against β-catenin. This control Co-IP used either an IgG1-isotype control antibody or the GFP-Trap® for capturing. Out of these two values, the specific and the unspecific one, the ratio was calculated. If the calculated ratio was below 1.5, the obtained binding was defined as unspecific and not included in further analysis. Again, a two-step method was applied to experiments where two or more replicas were analyzed in parallel. Here, the sum of the ratios had to be additionally above 2.9 (for duplicates) or 4.3 (for triplicates) and the deviation between the single ratios had to be below or equal to 0.2. All these criteria led to the elimination of random noise and instability among the individual replicas. Due to these main criteria, many unspecific bound proteins (e.g. histone deacetylases, GAPDH and PCNA) were identified and excluded from further analysis. The remaining possible interacting proteins were confirmed by manually reviewing and comparing the obtained bar graphs for each cell line individually. To acquire information about the proteins that were co-immunoprecipitated with the target protein β-catenin, the ratio between the β-catenin-specific bound and the respective input was built. With consideration of the enrichment throughout Co-IP and the differences in the amount of sample loaded onto the gel, a formula for the calculating capturing factor (CF) in percentage was derived (see Equation 3).

$$\text{capturing factor (CF)} = \frac{\frac{\text{bound}}{0.2}}{\frac{\text{input}}{0.01}} \cdot 100$$

Equation 3: Formula for calculating the capturing factor (CF).

The signal, obtained for the input sample, was divided by 0.01. This factor was introduced since only 1 % of the lysate was applied to the gel for electrophoresis. The bound sample was enriched 10 times by solving the bead pellet after Co-IP in 50 µl instead of the former 500 µl. Additionally, 10 µl of the precipitate mixed with 10 µl of Laemmli buffer were applied to the gel and used for generating DigiWest beads. Dividing the bound sample by 0.2 corresponds to 20 % of precipitate applied to the gel.

In experiments with several replicas (see 4.3 and 4.4), the mean of the individually calculated CFs was used to classify the strength of the PPI. For defining the strength of an interaction between the target protein β-catenin and its binding proteins, four limits were employed. If the result of the ratio between bound and input is below 0.1 %, the interaction was defined as weak. A binding factor between 0.1 % and 0.5 %, describes an interacting protein, which was referred to as a medium strong interactor. Above 0.5 %, the interacting protein was defined as a strong interactor. Very strong interactors exceed a CF of 10 %. An illustrating color scheme was chosen and is explained in the later

results chapter (see 4.2.2). If proteins did not show a signal in the input sample, but occurred as an interacting protein in the bound sample after passing the cutoff criteria, these antibodies were marked specifically with “+” in the later results. In this case, the obtained capturing factors are in general high and classified as very strong, which is due to the fact that the input value was set to the averaged background value of 11 to allow the calculation of a factor.

For one important antibody, anti-β-catenin 8E7, a signal occurred only in the CHIR 99021-treated samples of ECIP and ICIP (see 4.3.2 and 4.4.1). This led to difficulties during the calculation of fold changes to evaluate the authenticity of a signal and to gain information about the obtained increase after drug treatment. Thus, the mean of the unspecific background signals left and right of the received specific signals was calculated and their standard deviation (SD) determined. Signal intensities, which were three times higher than the SD, were assessed as specific signals, while signal intensities, which were ten times higher than the SD, were rated as quantifiable signals. By dividing the values calculated for the integrated peaks by three times of the SD of their averaged background, an estimation about the signal increase was achieved. This resulted in values which were specified “as greater than this calculated ratio”.

4. Results

Wnt signaling and β-catenin play a crucial role in cancerogenesis [26]. Both are of high interest in order to gain a deeper insight into aberrant signaling cascades. Due to the key role of β-catenin in multiple cellular processes, it cooperates with a large set of interaction partners in a spatially and temporally coordinated manner [112]. Co-IP is one of the most widespread methods to reveal these PPIs [112].

The combination of this technique with the recently developed high output tool, DigiWest, might lead to a novel screening approach requiring only a limited amount of sample volume while a larger number of PPIs can be detected.

4.1 Co-Immunoprecipitation and high throughput DigiWest

The Co-IP approach derives from the classical immunoprecipitation and is performed identically, but is expanded by additionally identifying the co-precipitated proteins during subsequent analysis [135]. These interacting proteins are typically confirmed in gel or on membranes after blotting by immunological methods [94, 136]. By combining this classical approach with the mentioned high throughput Western blot, the DigiWest, a promising screening tool is generated.

By employing this screening tool, the analysis of cellular signal transduction and specific signaling cascades of various cell lines is enabled. Especially alterations after drug treatment in the signaling state, which is focused on, can be observed, as well as the achievement of broad information on a specific pathway by covering different signaling intermediates. Beyond this, direct information of the modulation of cellular signaling by changes in protein complexes containing key players of specific signaling cascades, like the Wnt pathway and its central protein β-catenin, is obtained.

4.1.1 Analysis of cellular signal transduction in hepatoma cells

Four different hepatoma cell lines, two mouse and two human, were chosen for a first set of experiments in order to establish the combinatory approach and to demonstrate its feasibility. In the beginning a comprehensive characterization of signal transduction in these hepatoma cell lines was performed. The four cell lines (70.4, 55.1c, HepG2 and HB35) carry different known mutations, most of which are associated with Wnt/β-catenin signaling. The aberrant activation of the Wnt/β-catenin pathway is known to be an important central mechanism in cancer biology [137]. Just like modulating its crosstalk with a variety of other signaling cascades, such as the Hedgehog pathway [138] or the Hippo pathway [139], that play crucial roles in the development of cancer. The central role of Wnt signaling in cancer makes this pathway an attractive target for the development of novel therapeutic

strategies [139]. Hence, a broad proteomic analysis of cancer cell lines, carrying mutations in this pathway, can provide essential information for the development of therapeutic approaches.

4.1.1.1 Characterization of the Wnt/β-catenin pathway: identification of specific antibodies

To be able to characterize the Wnt/β-catenin pathway broadly, it was necessary to identify antibodies covering this pathway, which additionally facilitate to display possible crosstalk with other signaling cascades, PPIs and PTMs. This choosing was done by performing an extensive database and literature research.

During the early phase of this work, a total number of 344 antibodies were purchased and screened for specificity. All of these antibodies belonged to a list of interesting candidates, which was generated by reviewing relevant literature and by querying available databases, that list PPIs. Four different databases formed the basis for this work: FpClass is a data mining-based method for proteome-wide PPI prediction that achieves a good agreement with de facto detected PPIs in the experimental setup and proved to be better than previously used PPI prediction methods [118]. This method predicts 1721 possible interactions of β-catenin, of which 340 are listed with a total score above 0.75. This corresponds to a high predictive value, as the total score represents the probability of an interaction based on all evidence [118]. Three other databases, which list verified interaction partners of β-catenin were scanned: 1. BioGRID [117], providing 277 binary interactions for human β-catenin and 75 for mouse β-catenin; 2. UniProtKB [121], listing 65 binary interactions for human β-catenin and 13 for mouse β-catenin and 3. IntAct [119, 120], showing 551 interactions of human β-catenin and 155 of mouse β-catenin (see Table 16). After this extensive literature and database searching process, a first list was generated. A set of particularly interesting proteins, which occurred in several databases or with a high predicted interacting probability, were identified and all of the more than 1000 available antibodies were matched with this list.

Table 16: Predicted and verified interacting proteins for β-catenin.
(retrieved on the 24.01.2016)

Database	Amount of binary interactions	Amount of predicted interactions
FpClass		1721 in total 340 with a predicted score of > 0.75
BioGRID	277 for human 75 for mouse	
UniProtKB	65 for human 13 for mouse	
IntAct	551 for human 155 for mouse	

All screened tested antibodies are listed in the appendix (see Suppl. Table A). Antibodies, which showed a reproducible signal were processed in the further experimental development. Additionally,

antibodies which were of general interest were added. This led to a list of 190 antibodies, which are marked in the appendix (see Suppl. Table A) with *. If several antibodies addressed the same protein, the NMI number was added in brackets and serves as an unique identifier to for the antibody list (see Suppl. Table A). Antibodies, which had two molecular weights assigned by the manufacturer, were analyzed for presence of these two proteins and their peaks are treated as two individual proteins. Unless otherwise noted, these two peaks always correspond to different isoforms or cleaved versions of the same protein (see Suppl. Table B). From the 190 antibodies, corresponding to 213 peaks, tested on the four screened cell lines, for approximately 160 proteins or peaks, a signal was obtained in at least one of the untreated cell lysates (Figure 15). 52 antibodies or bar graphs without any signal were excluded from the graphical data presentation.

4.1.1.2 Protein expression analysis – normalization strategy

As different cell lines express differing amounts of proteins, a normalization had to be performed to adjust the raw values and in order to establish a basis to compare the four cell lines and the individual influences of treatment. Individual normalization factors for each of the lysates were calculated by using the total amount of proteins coupled to the bead surface as determined by measuring the Strep-PE signals (see 3.4.3.1). The normalization factors varied between 0.48 and 7.68. All obtained raw values were normalized with their corresponding normalization factor.

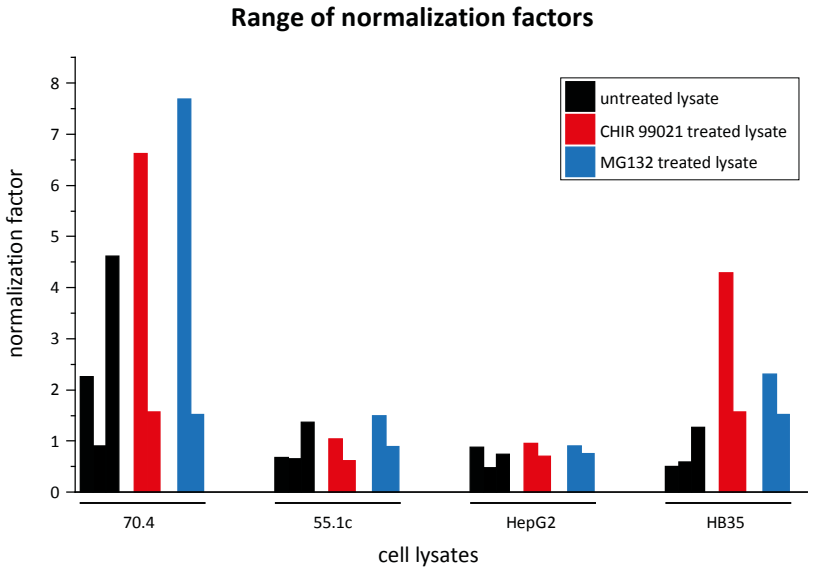

Figure 12: Range of normalization factors of the different cell lines.
The normalization factors ranged between 0.48 and 7.68 for the individual cell lines and treatments. This range is plotted in the bar graphs. For cell line 70.4 these factors are overall higher, than in comparison to the other cell lines.

The normalization factors determined, show a wide range of variety (see Figure 12). As different cell lines show differences in their expression of proteins, the variations in the amount of proteins loaded to the DigiWest beads and the thereof derived range in the normalization factors can be explained. Cell line 70.4 shows overall small signal intensities, which have to be adjusted in order to be able to compare this cell line to cell lines, with a higher protein expression and higher signal intensities.

After normalization of the raw data, median centering and $\log_2$ transformation of 16, randomly chosen analytes was performed. This set of data was suitable to perform cluster analysis to detect differences and similarities of the normalized samples.

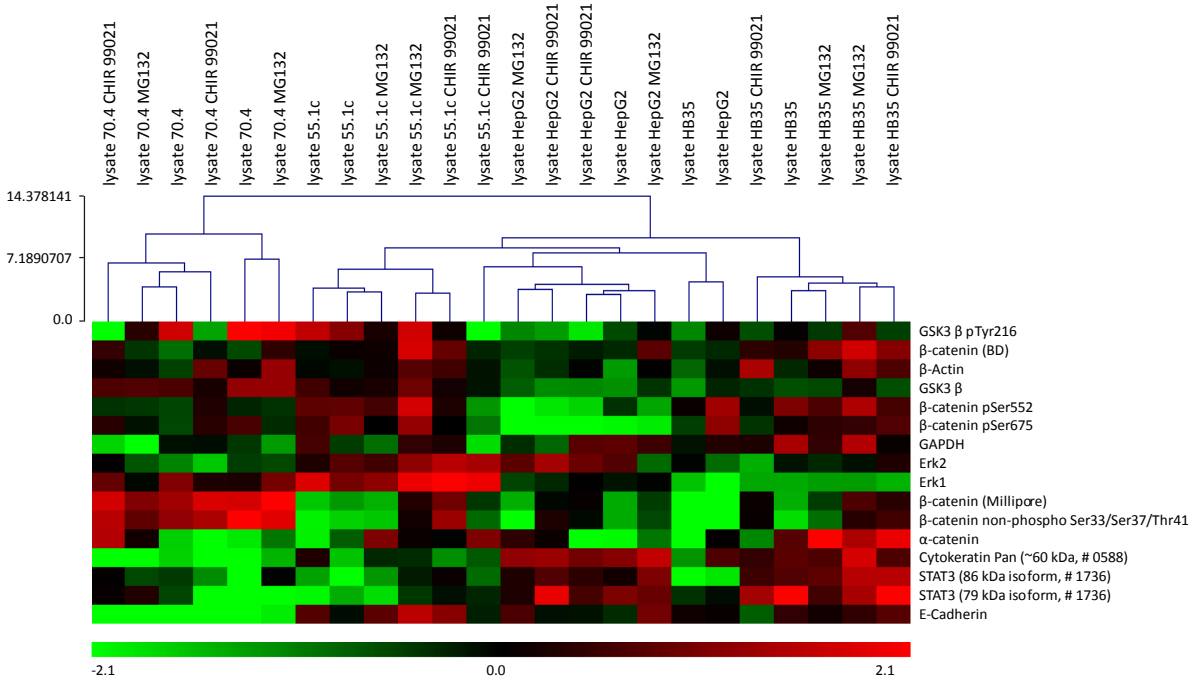

Figure 13: Clustering of analytes after normalization.
The raw data of 16, randomly chosen analytes was normalized by the corresponding normalization factor, median centered and $\log_2$ transformed. The derived data set was suitable to perform cluster analysis. A hierarchical clustering with euclidean distance and complete linkage was applied.

In the clustering (see Figure 13) all 70.4 derived samples are separated from the remaining cell lines, which is presumably due to its different mutation status compared to the other three cell lines, carrying a heterozygous *CTNNB1* deletion. In addition, a clear separation of human and mouse cell lines is visible and the cell lines are largely clustered in groups. The clustering shows, that the characteristics of the individual cell lines and their response to treatment remained unchanged through normalization.

To additionally prove the accuracy of the strategy chosen for the normalization, the housekeeping proteins, β-Actin and GAPDH, were looked at. Housekeeping genes are ubiquitously expressed in all tissues and cell types [140]. Thus, they should be equally and high expressed independently from the mutational status of the cell line and lead to a similar amount of synthesized protein. After

multiplying the raw values with the corresponding normalization factor, the logarithm with base 2 was taken and similar values for the different cell lines were obtained (see Table 17). A log_2 transformation is used in order to visualize differences in between the cell lines for all tested analytes and to cover a wide signaling range both in the lower and the higher area.

Table 17: Housekeeping proteins after Strep-PE normalization and log_2 transformation.
The log_2 transformed values of the Strep-PE normalized housekeeping proteins β-Actin and GAPDH are represented. Additionally, the normalized raw values are listed in brackets underneath.

Analyte	70.4 lysate	55.1c lysate	HepG2 lysate	HB35 lysate
β-Actin	17.06 (136625.07)	16.81 (114772.65)	16.83 (116684.50)	16.11 (70542.45)
GAPDH	16.15 (72522.82)	16.12 (71074.39)	16.90 (122559.77)	16.45 (89340.40)

In previous studies, it was shown that β-Actin and GAPDH are among the most consistent proteins [141]. Hence it can be assumed that this way of normalization is valid, as these two housekeeping proteins show similar values for all cell lines.

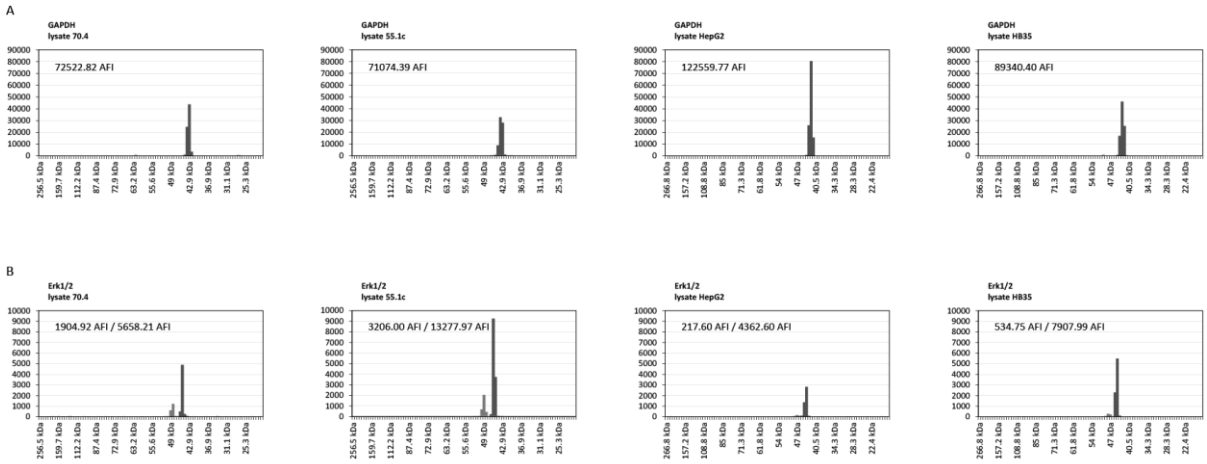

Figure 14: Representation of the normalized DigiWest output graphs.
Two proteins are represented exemplarily as normalized DigiWest output graphs. On the x-axis the molecular weight between ~15 kDa and ~300 kDa is represented, while on the y-axis the signal intensity in MFI values is shown. For GAPDH the y-axis is set to a maximum of 90000 MFI; for Erk1/2 it is set to 10000 MFI. The normalized values in AFIs, measured for the integrated peaks, are added to the respective peak and written inside the graph.
A: GAPDH, which serves as a control for normalizing the data is shown. For normalization, a normalization factor was generated by building the ratio between the specific over all Strep-PE signal for each bead population and the median of all derived over all Strep-PE signals.
B: The same normalization factor was applied to every measured analyte. Erk1/2 is depicted as an example.

The normalization for GAPDH is additionally represented in normalized DigiWest output graphs (see Figure 14 A). For the cell lines 70.4 and 55.1c similar signal intensities are calculated by normalizing the data (72522.82 AFI vs. 71074.39 AFI). Also the signal for HB35 is very alike

(89340.40 AFI). Only the signal obtained for HepG2 is higher compared with the other three cell lines (122559.77 AFI). HepG2 are cells, which are chosen in many experimental setups as a standard cell line, due to their good and fast growing behavior. It is possible that they gained the ability to express a higher level of GAPDH at some point. The second analyte, which is exemplary represented, is Erk1/2 (see Figure 14 B). Alterations between the four cell lines are clearly visible, especially for the lower peak at ~45 kDa, representing Erk2. The cell line 55.1c shows the highest Erk2 peak (signal intensity of 13277.97 AFI), while for HepG2 cells the lowest signal was detected (4362.60 AFI). The same can be obtained in Figure 15, where the normalized data is represented after log_2 transformation in a redscale color scheme.

4.1.1.3 Molecular diversity of the examined cell lines.

Cell lines exhibit considerable differences in their characteristics, like their growth rate or their internal signaling status. These differences exist not only between different species or tissues, but also within the same organism and the same tissue between normal and altered cells, e.g. cancer cells, due to varieties in their mutational status [142]. Thus, it is especially important to have the possibility to derive a normalization factor, as described earlier (see 4.1.1.2), in order to compare the generated lysates of the four cell lines used in this thesis.

In Figure 15, the differences in between cells lines, displayed by the DigiWest, are depicted. To visualize the differences in between the four cell lines for all tested antibodies, both for the lower and the higher range, the normalized raw values were again logarithmized to base 2 and a redscale color scheme from zero (white) to the maximum value (= 17.06, intense red) was applied. This led to an intense red colorization for extremely high AFIs, measured for some antibodies, and to white cells marked with n.d., if no signal was obtained.

Figure 15 shows, that the DigiWest is able to visualize similarities and discrepancies between different cell lines, more generally speaking, between variable sample types. High signal intensities were obtained for some of the tested antibodies. As mentioned above a focus was set on proteins, which are known to participate in β-catenin signaling. Thus, many of the tested analytes were directed against familiar complex partners of the key protein β-catenin, like GKS3 β, α-catenin or E-Cadherin. In addition, many analytes were screened, which are associated with important signaling pathways, such as the MAPK pathway, or are known transcriptional and epigenetic regulators.

Assigned category	Analyte	Modification	70.4 lysate	55.1c lysate	HepG2 lysate	HB35 lysate
1	β-catenin (BD)		12.52	13.23	12.80	12.63
	β-catenin (Millipore)		12.43	9.38	8.50	8.41
	β-catenin	non-pospho Ser33/Ser37/Thr41	9.65	5.04	4.41	4.33
	β-catenin	pSer552	9.64	10.74	11.26	10.04
	β-catenin	pSer675	10.34	10.74	10.90	9.21
	β-catenin	pThr41/pSer45	5.50	3.36	4.95	3.91
2	β-Actin		17.06	16.81	16.83	16.11
	GAPDH		16.15	16.12	16.90	16.45
3	DKK1 (# 1593)		n.d.	n.d.	8.56	n.d.
	DVL2 (# 0687)		n.d.	6.34	n.d.	n.d.
	DVL2 (# 1739)		n.d.	4.87	2.52	n.d.
	DVL3 (# 0686)		n.d.	5.14	4.91	n.d.
	Evi (50 kDa isoform)		6.07	6.58	5.10	3.82
	Evi (60 kDa isoform)		5.60	8.36	8.78	5.02
	Frizzled4		11.18	9.47	11.55	8.96
	Frizzled7		6.70	n.d.	5.85	5.26
	LGR5		n.d.	n.d.	n.d.	10.76
	LRP6 (# 1750)	pSer1490	n.d.	5.24	4.77	n.d.
	LRP6 (HD)		n.d.	4.74	4.69	2.94
	SFRP2 (# 1414)		9.40	14.62	13.75	10.17
	Wnt1		6.95	n.d.	n.d.	n.d.
	Wnt11		n.d.	4.74	5.41	n.d.
	Wnt16		7.55	n.d.	n.d.	n.d.
	Wnt7b		n.d.	5.51	n.d.	5.32
4	APC		5.27	3.98	4.47	3.81
	Axin1		5.50	5.10	4.41	4.59
	Axin2 (95 kDa isoform, # 0956)		n.d.	n.d.	3.99	n.d.
	CK1 α		n.d.	8.36	7.27	6.38
	CK1 δ		10.92	9.61	9.58	8.79
	CK1 ε		7.11	8.15	8.33	6.95
	CK2 α		8.39	8.36	8.13	7.64
	GSK3 α	pTyr279	7.89	8.22	8.46	7.21
	GSK3 β	pTyr216	10.43	8.90	7.94	6.68
	GSK3 β		12.35	11.29	10.85	9.87
	GSK3 β	pSer9	8.04	6.81	8.57	6.89
	PP2A C		n.d.	10.85	8.09	6.03
5	α-catenin		8.08	9.25	10.05	7.45
	E-Cadherin		5.70	9.06	9.23	9.29
6	ATF4		n.d.	8.99	n.d.	9.22
	Bax		5.80	8.52	7.02	5.50
	Bcl2		n.d.	5.08	n.d.	n.d.
	Bcl9		n.d.	5.72	5.26	n.d.
	Bcl-xL		7.77	10.71	10.11	7.05
	cJUN (43 kDa isoform, # 1187)		7.31	6.86	7.02	7.24
	cJUN (# 1162)	pSer63	5.18	3.78	3.82	3.46
	cJUN (# 1744)	pSer63	n.d.	3.70	4.33	3.14
	cJUN (HD)		n.d.	3.77	4.22	3.41
	eIF2 α		7.90	12.15	11.25	9.54
	eIF2 α	pSer51	8.28	7.48	7.00	10.34
	eIF4E		11.56	12.56	10.74	11.77
	FoxM1 (# 0949)		5.35	3.85	9.35	3.86
	FoxO3a	pThr32	n.d.	3.98	n.d.	n.d.
	FoxO4	pThr28	5.08	5.18	3.41	3.00
	GATA4		n.d.	n.d.	6.25	n.d.
	GLI1		6.18	4.46	4.35	n.d.
	HIF1 α		n.d.	3.63	n.d.	n.d.
	HNF1A		8.91	9.70	8.02	9.40
	KLF5		8.60	10.22	9.43	7.06
	MTA2		3.48	4.36	n.d.	6.45
	Pontin52		2.69	3.79	n.d.	4.38
	Rb		n.d.	5.36	6.03	4.78
	Smad1		8.81	9.64	5.71	5.13
	Smad2		9.02	10.38	8.74	8.23
	Smad2	pSer245/pSer250/ pSer255	n.d.	6.90	5.50	3.33
	Smad3		8.05	7.93	5.50	4.62
	Smad3	pSer423/pSer425	6.88	4.98	n.d.	n.d.
	Smad3 (# 0879)		8.32	8.73	6.96	8.48
	Smad4		n.d.	7.98	7.30	5.02
	Smad5		n.d.	7.85	n.d.	n.d.
	Src		13.10	12.63	11.42	11.63
	Src	pTyr527	13.19	11.85	11.93	12.20
	Src	pTyr416	6.82	6.63	6.44	4.78
	TAZ (# 1626)		9.66	11.32	14.34	14.44
	TAZ (# 1737)		n.d.	4.63	n.d.	3.99
	TCF1 (# 1673)		5.99	4.50	4.82	3.86
	TCF1 (# 1746)		n.d.	3.97	3.46	n.d.
	TCF4 (50 kDa isoform, # 1727)		7.19	n.d.	n.d.	n.d.
	TCF4 (50 kDa isoform, # 1753)		n.d.	n.d.	8.55	8.13
	TCF4 (60 kDa isoform, # 1481)		6.13	3.26	5.63	8.35
	TCF4 (60 kDa isoform, # 1727)		n.d.	n.d.	7.90	n.d.
	TCF4 (60 kDa isoform, # 1753)		n.d.	n.d.	10.46	7.20
	TCF4 (70 kDa isoform, # 1481)		5.93	4.36	3.91	3.46
	TCF7L2 (30 kDa isoform)		n.d.	n.d.	2.26	2.82
7	14-3-3 ε		7.41	13.13	8.81	10.97
	14-3-3 ζ δ		9.84	13.45	10.89	11.49
	A-Raf		7.37	7.36	7.27	n.d.
	BMP4		n.d.	n.d.	8.33	8.23
	CD133		5.88	5.61	5.75	6.95
	c-Raf		8.02	8.01	7.12	8.36
	DUSP1		8.78	9.83	10.16	10.06
	DUSP16		n.d.	n.d.	9.15	n.d.
	DUSP4		10.35	11.81	10.42	9.73
	DUSP5		14.04	n.d.	13.61	n.d.
	DUSP6		8.50	9.15	11.20	10.96
	DUSP7		8.88	n.d.	n.d.	n.d.
	DUSP9		8.64	7.28	11.89	11.60
	Elk-1		7.92	9.63	8.99	8.70
	Erk1		10.90	11.65	7.77	9.06
	Erk2		12.47	13.70	12.09	12.95
	Erk3		4.50	3.26	n.d.	n.d.
	Ha-ras		13.08	14.40	13.00	12.97
	IMP		5.08	3.70	3.52	n.d.
	JNK/SAPK (46 kDa isoform)		7.01	7.20	8.13	6.45
	JNK/SAPK (54 kDa isoform)		8.35	7.46	9.06	10.57
	JNK1 (46 kDa isoform)		n.d.	7.39	6.63	5.34
	JNK1 (54 kDa isoform)		n.d.	5.63	5.44	4.91
	MAPKAPK-2		n.d.	6.68	5.88	5.44
	MAPKAPK-3		n.d.	5.67	7.90	5.48
	MAPKAPK-5		n.d.	5.38	5.69	n.d.
	MDM2 (60 kDa isoform)		4.99	4.88	3.41	5.81
	MDM2 (90 kDa isoform)		5.64	4.21	5.07	n.d.
	MEK1		n.d.	10.78	n.d.	n.d.
	MEK2		6.91	9.41	9.41	7.71
	MEKK3		5.76	3.70	4.35	3.09
	MKK4		n.d.	9.97	6.99	6.45
	MKK6		7.04	8.13	7.30	7.17
	MKK7		7.29	6.83	6.99	5.60
	Mnk1		6.85	6.21	6.31	4.13
	MSK1 (61 kDa isoform)	pThr589	n.d.	2.70	n.d.	n.d.
	p38/MAPK		9.09	9.84	9.50	9.41
	p38/MAPK α		n.d.	7.92	7.27	5.40
	p38/MAPK γ		n.d.	n.d.	5.56	n.d.
	p38/MAPK δ		n.d.	n.d.	8.65	7.61
	Ras		7.31	9.33	7.78	9.40
	SPRY2		n.d.	9.42	7.59	5.52
	TAK1		5.64	5.50	4.87	3.65
8	STAT3	pSer727	5.99	5.67	8.12	6.58
	STAT3 (79 kDa isoform, # 1736)		5.99	8.73	10.07	9.75
	STAT3 (86 kDa isoform, # 1736)		6.19	7.51	8.73	8.13
	STAT3 (79 kDa isoform, # 1192)	pTyr705	6.08	6.09	4.07	5.87
	STAT3 (79 kDa isoform, TK # 054)		10.09	9.21	11.11	10.39
	STAT4	pTyr693	3.17	n.d.	3.52	3.04
9	DNMT1		8.12	6.96	8.04	6.93
	Ezh2		8.91	9.94	8.62	7.72
	HDAC1 (# 1165)		5.99	7.47	4.35	5.63
	HDAC2		5.50	5.07	5.71	3.25
	HDAC3		8.32	7.77	5.47	4.21
	HDAC6 (# 0739)		7.01	9.58	11.34	10.85
	HELLS		n.d.	7.41	9.57	8.50
	LSD1		9.74	9.80	10.00	10.56
	PRMT4		9.97	9.64	9.04	8.07
10	Cytokeratin Pan (~55 kDa, # 0474)		11.28	15.03	17.00	16.34
	Cytokeratin Pan (~46 kDa, # 0474)		n.d.	5.91	10.65	8.57
	Cytokeratin Pan (~57 kDa, # 0261)		n.d.	n.d.	16.99	15.53
	Cytokeratin Pan (~60 kDa, # 0588)		10.19	14.20	16.46	14.60
	Vimentin		9.60	12.30	5.11	2.59
11	FAK		6.99	6.36	7.61	5.96
	FAS		6.64	4.95	n.d.	n.d.
	p21		5.93	n.d.	7.59	8.95
	p53		9.99	n.d.	7.64	7.98
	p53	pSer15	7.29	4.31	4.47	4.62
	PARP (116 kDa isoform, # 1358)		n.d.	n.d.	5.70	5.04
	PARP (24 kDa isoform, # 1358)		n.d.	5.63	4.96	n.d.
	PCNA		10.37	15.03	13.38	14.58
12	PTCH1		n.d.	n.d.	4.14	3.53
	PTCH2		6.85	n.d.	4.41	3.53
13	ILK1		13.16	11.46	9.80	9.39
	LATS1		n.d.	n.d.	n.d.	5.17
	MOB1		n.d.	6.18	n.d.	n.d.
	Mst1		n.d.	6.16	6.55	5.64
	YAP (# 1605)		6.13	5.16	4.78	4.40
	YAP/TAZ		n.d.	5.63	n.d.	n.d.
	Yes		n.d.	n.d.	6.73	6.37

Figure 15: Overview of all available tested antibodies, which showed a signal, on lysates of different cell lines.
The shown proteins were sorted into thematically related:
Category 1: The target protein β-catenin; Category 2: Housekeeping proteins; Category 3: Proteins associated with membranouse Wnt-signal transduction; Category 4: Proteins participating in the β-catenin destruction complex; Category 5: Proteins present in the membrane-associated β-catenin complex; Category 6: Transcriptional regulators and factors; Category 7: Proteins associated with MAPK signaling; Category 8: Proteins associated with JAK/STAT signaling; Category 9: Epigenetic regulators; Category 10: Tumor markers; Category 11: Apoptosis; Category 12: Hedgehog pathway: Category 13: Hippo pathway.
The presented values were calculated by normalizing the raw data with the total amount of protein loaded onto the beads and taking the logarithm with base 2. In brackets the molecular weight and the distinct NMI number are noted, if needed for differentiation. A signal below the detection limit is represented with n.d. and a white cell, while the intensity of the received raw signal is visualized with an analog intensification of red. 153 antibodies, detecting 163 individual peaks, which were used on the four different cell lysates, are seen in this figure. Proteins, which did not show a signal were not included in the graph.

Transcriptional regulators and factors are proteins, which bind to DNA sequences and influence the transcriptional activity thereby. They can act in a promoting or inhibiting way either individually or within a bigger protein complex. Due to their vital role in a large variety of cellular processes, their alteration has substantial effects on the development of diseases, such as cancer [143], as it often results in inactivity or an increased activity of transcription. On the other hand, epigenetic regulators, such as histone deacetylases and methyltransferases, play a fundamental role in the accessibility of the DNA for regulatory proteins [144].

Besides the high similarities between the different cell lines after normalization for the housekeeping proteins (see Table 17), also several β-catenin antibodies (BD, pSer552 and pSer675) as well as antibodies detecting other proteins such as eIF4E, Erk2, Ha-ras, LSD1 and Src (pTyr527) show similar and high signal intensities (mean > 10) (see Figure 16).

Analyte	Modification	70.4 lysate	55.1c lysate	HepG2 lysate	HB35 lysate
LSD1		9.74	9.80	10.00	10.56
β-catenin	**pSer675**	10.34	10.74	10.90	9.21
β-catenin	**pSer552**	9.64	10.74	11.26	10.04
eIF4E		11.56	12.56	10.74	11.77
Src	**pTyr527**	13.19	11.85	11.93	12.20
β-catenin (BD)		12.52	13.23	12.80	12.63
Erk2		12.47	13.70	12.09	12.95
Ha-ras		13.08	14.40	13.00	12.97

Figure 16: Visualization of high signal intensities obtained for the different lysates.
Calculation and presentation of the values was done analog to Figure 15. Analytes are ordered by their mean in an ascending manner. All presented signals are around or above 10 for each individual cell line, which corresponds to a high signal intensity. Additionally, the similarity between the values for different analytes in the four cell lines is high after normalization according to the colorization of the cells.

Those similarities can also be obtained with lower signal intensities for additional 19 proteins, e.g. APC, CK1 ε, Elk-1, HNF1A, MKK7, p38/MAPK and YAP (# 1605) (see Figure 17).

Analyte	Modification	70.4 lysate	55.1c lysate	HepG2 lysate	HB35 lysate
cJUN (# 1162)	**pSer63**	5.18	3.78	3.82	3.46
APC		5.27	3.98	4.47	3.81
Axin1		5.50	5.10	4.41	4.59
YAP (# 1605)		6.13	5.16	4.78	4.40
CD133		5.88	5.61	5.75	6.95
MKK7		7.29	6.83	6.99	5.60
FAK		6.99	6.36	7.61	5.96
cJUN (43 kDa isoform, # 1187)		7.31	6.86	7.02	7.24
JNK/SAPK (46 kDa isoform)		7.01	7.20	8.13	6.45
MKK6		7.04	8.13	7.30	7.17
DNMT1		8.12	6.96	8.04	6.93
CK1 ε		7.11	8.15	8.33	6.95
c-Raf		8.02	8.01	7.12	8.36
GSK3 α	**pTyr279**	7.89	8.22	8.46	7.21
CK2 α		8.39	8.36	8.13	7.64
Elk-1		7.92	9.63	8.99	8.70
HNF1A		8.91	9.70	8.02	9.40
p38/MAPK		9.09	9.84	9.50	9.41
DUSP1		8.78	9.83	10.16	10.06

Figure 17: Visualization of lower signal intensities obtained for the different lysates.
Calculation and presentation of the values was done analog to Figure 15. Sorting is done ascendingly by the mean. The values for the analytes show high similarities between the different cell types, although the signal intensities are lower than in Figure 16.

Besides the listed similarities, the DigiWest also reveals differences, between the four cell lines. Some proteins are detected only in a single cell line, e.g. Bcl2, DUSP16, DUSP7, GATA4, HIF1 α, LGR5, MEK1 and Wnt16 (see Figure 18), while others show a significant difference between mouse and human cells (see Figure 19). Examples for these differences are amongst others BMP4, Cytokeratin Pan (~57 kDa, # 0261), Erk3, p38/MAPK δ and PTCH1.

Analyte	Modification	70.4 lysate	55.1c lysate	HepG2 lysate	HB35 lysate
Bcl2		n.d.	5.08	n.d.	n.d.
DUSP16		n.d.	n.d.	9.15	n.d.
DUSP7		8.88	n.d.	n.d.	n.d.
GATA4		n.d.	n.d.	6.25	n.d.
HIF1 α		n.d.	3.63	n.d.	n.d.
LGR5		n.d.	n.d.	n.d.	10.76
MEK1		n.d.	10.78	n.d.	n.d.
Wnt16		7.55	n.d.	n.d.	n.d.

Figure 18: Exemplary visualization of signals occurring only in one cell line.
Calculation and presentation of the values was done analog to Figure 15. Several analytes detect a signal only in one of the cell lines, eight exemplary analytes were picked to illustrate that.

Individual signals, which occur only in one cell line (see Figure 18), have to be seen as significant. The different mutational status of the cell lines form the basis of these distinctions and the expression of a protein in just one cell line is a consequence of this genetic difference. The DigiWest is able to detect these differences and visualize them in a direct comparison.

Analyte	Modification	70.4 lysate	55.1c lysate	HepG2 lysate	HB35 lysate
BMP4		n.d.	n.d.	8.33	8.23
Cytokeratin Pan (~57 kDa, # 0261)		n.d.	n.d.	16.99	15.53
Erk3		4.50	3.26	n.d.	n.d.
p38/MAPK δ		n.d.	n.d.	8.65	7.61
PTCH1		n.d.	n.d.	4.14	3.53

Figure 19: Visualization of several signals derived only for mouse or human cell types.
Calculation and presentation of the values was done analog to Figure 15. Several analytes detect signals only for one of the two species, of which the cell lines were derived. The signals observed vary in their intensity.

In Figure 19 represents species-specific detection of proteins by antibodies. The antibodies addressing BMP4, p38/MAPK δ and PTCH1, are verified by manufacturer for human, but not for mouse. It is possible, that they are not able to identify the murine protein. On the other hand, it is possible, that the addressed proteins were not present in the mouse samples and thus cannot be detected by the antibody. This is likely to be the case for Cytokeratin Pan (~57 kDa, # 0261) and Erk3, which both are verified to recognize human and murine proteins, but only detect a protein in one of the species here.

In addition to the detected and presented similarities and discrepancies, many others can be found by the DigiWest and are visualized in the overall graphic above (see Figure 15).

4.1.2 Modulation of protein levels by drug treatment

To analyze β-catenin and its binding partners two drugs, known to influence the stability of β-catenin, were applied. Both CHIR 99021 and MG132 are inhibitors, which lead to an enrichment in the amount of available proteins. CHIR 99021 as a GSK3 inhibitor simulates the ON status of the canonical Wnt/β-catenin signaling by prohibiting the phosphorylation of β-catenin by GSK3. Thus, preferentially non-phosphorylated β-catenin is enriched. MG132 on the other side inhibits the proteasome and blocks the degradation of proteins that use this pathway. Therefore, no specific β-catenin variant should be enriched, but the entity of β-catenin available in the cell be increased.

Based on earlier experiments, a set of antibodies was defined, which recognize different epitopes of β-catenin. Additionally, all antibodies that either showed a signal in the untreated bound sample or were of a particular interest, were tested further on the treated samples.

Again, the raw data values were normalized with the corresponding normalization factor calculated by the obtained total Strep-PE signal, as described above (see 4.1.1.2). To visualize these effects, every treated lysate was referred to its corresponding untreated lysate. By calculating the ratio between treated and untreated lysates, fold change values were derived. Of these, the logarithm to base 2 was taken, to be able to present them equally distributed on either side of the baseline ($\log_2 = 0$). It was possible to visualize increase and decrease in protein expression after treatment on a color map, starting with a white colorization for no obtained signal (value = 0), intense red for a high signal increase and intense dark green for a decreased signal intensity (Figure 25). Colorization was done individually for each cell line, as the calculated maximal and minimal values vary among the different cell lines and the colorization would have been distorted otherwise.

Proteins that didn't show a signal in any of the samples, leading to a white cell for all eight columns, were extracted from the image. Of the 117 tested antibodies with 133 possible signals to derive, 119 signals remained and were visualized in Figure 20.

Assigned category	Analyte	Modification	70.4 lysate		55.1c lysate		HepG2 lysate		HB35 lysate	
			CHIR 99021	MG132	CHIR 99021	MG132	CHIR 99021	MG132	CHIR 99021	MG132
1	β-catenin (BD)		0.48	0.99	0.75	1.68	0.11	1.09	0.87	2.23
	β-catenin (Millipore)		0.03	0.59	2.22	1.58	2.21	1.65	2.33	2.90
	β-catenin	pSer552	0.59	-0.11	-0.56	0.95	-3.08	-2.69	-0.21	1.35
	β-catenin	pSer675	-0.26	-0.97	-1.01	0.21	-3.65	-3.12	0.09	0.96
	β-catenin	pThr41/pSer45	-5.50	-5.50	-3.36	1.39	-1.11	-1.11	1.51	-3.91
	β-catenin	non-pospho Ser33/Ser37/Thr41	-1.46	-1.00	3.02	1.90	2.29	1.78	2.53	2.77
2	β-Actin		0.76	1.14	0.69	0.86	0.09	0.15	2.25	2.03
	GAPDH		0.36	-0.82	0.74	0.90	0.43	0.21	0.41	1.65
3	DVL1		n.d.	n.d.	6.80	n.d.	n.d.	n.d.	n.d.	n.d.
	DVL2 (# 1739)		n.d.	n.d.	2.28	2.91	2.88	-2.52	5.68	n.d.
	Evi (50 kDa isoform)		4.25	4.32	1.19	2.34	2.06	-5.10	4.80	-3.82
	Evi (60 kDa isoform)		2.74	4.16	-0.70	0.22	-1.89	-0.77	1.94	-5.02
	Frizzled4		-11.18	-11.18	3.58	3.40	0.17	-0.06	-8.96	3.06
	Frizzled7		1.23	-6.70	6.19	6.39	0.84	0.01	-5.26	-5.26
	LRP6 (# 1750)	pSer1490	6.73	7.40	0.85	1.35	1.40	1.10	6.10	5.30
	LRP6 (180 kDa isoform, # 1567)	pSer1490	n.d.	7.80	5.52	6.76	4.69	5.87	5.68	5.53
	LRP6 (210 kDa isoform, # 1567)	pSer1490	n.d.	n.d.	n.d.	4.98	4.64	4.49	n.d.	5.30
	LRP6 (HD)		n.d.	6.26	0.82	1.37	1.77	1.13	3.56	2.92
	Wnt1		-6.95	-6.95	3.65	n.d.	5.67	n.d.	n.d.	n.d.
	Wnt11		n.d.	n.d.	-4.74	1.31	0.57	-0.10	7.62	6.99
	Wnt16		-7.55	-7.55	7.37	n.d.	9.73	11.75	n.d.	n.d.
	Wnt3A		n.d.	n.d.	n.d.	6.87	n.d.	n.d.	n.d.	n.d.
	Wnt7b		n.d.	n.d.	1.63	-5.51	n.d.	8.14	-5.32	3.36
4	APC		-5.27	-5.27	-3.98	1.07	-4.47	-0.53	2.10	1.20
	Axin1		1.40	1.53	-1.23	0.73	-4.41	-4.41	-4.59	-4.59
	Axin2 (95 kDa isoform, # 956)		n.d.	6.64	n.d.	n.d.	-0.25	1.17	n.d.	n.d.
	Axin2 (98 kDa isoform, # 956)		n.d.	6.26	n.d.	n.d.	3.52	3.65	n.d.	n.d.
	CK1 α		6.98	7.80	0.19	-0.09	-3.63	-3.18	0.04	-1.00
	CK1 δ		0.20	1.29	1.57	2.26	0.70	1.42	2.46	1.91
	GSK3 α	pTyr279	-0.58	0.72	-3.70	0.65	-8.46	-1.11	-7.21	1.14
	GSK3 β	pTyr216	-4.00	-0.62	-0.97	0.63	-2.07	-0.20	0.47	1.80
	GSK3 β		-0.99	0.03	0.03	0.78	-0.84	-0.13	0.86	1.46
	GSK3 β	pSer9	-1.31	0.19	-2.50	0.36	-2.77	-3.30	-6.89	1.62
5	α-catenin		-0.96	0.94	0.73	0.85	-2.27	-1.04	1.45	3.98
	E-Cadherin		-5.70	1.49	1.22	1.63	-0.23	0.89	-0.90	0.28
6	ATF4		n.d.	n.d.	-8.99	-0.58	n.d.	n.d.	-0.80	0.03
	Bcl9		n.d.	n.d.	0.57	1.36	1.18	0.87	n.d.	n.d.
	CDK2		n.d.	6.53	n.d.	4.39	n.d.	3.65	n.d.	n.d.
	cJUN (43 kDa isoform, # 1187)		1.04	4.55	0.53	2.27	2.21	2.50	-0.28	2.87
	cJUN (# 1162)	pSer63	-5.18	4.85	0.53	2.94	1.76	3.22	2.96	4.82
	cJUN (# 1744)	pSer63	n.d.	8.75	1.27	2.69	1.20	2.34	3.35	3.28
	eIF2 α		4.36	4.18	1.78	1.58	2.07	1.64	2.54	3.13
	eIF2 α	pSer51	0.21	-1.63	-0.23	-0.08	3.38	1.53	-3.11	-4.49
	eIF4E		-1.18	-1.88	-0.20	-0.67	-0.15	0.91	-3.03	-1.37
	FoxO3a	pSer413	n.d.	n.d.	n.d.	n.d.	n.d.	3.43	5.91	n.d.
	GATA4		n.d.	6.53	4.92	5.94	3.63	3.01	n.d.	6.46
	GLI1		-6.18	0.76	-4.46	-0.55	-0.82	-0.50	6.01	5.38
	HNF1A		0.80	0.72	-1.80	0.39	1.59	1.68	-0.81	-2.70
	MTA2		n.d.	8.72	2.13	2.42	2.71	3.11	-3.48	4.35
	Pontin52		n.d.	7.47	3.07	2.56	1.64	2.01	5.91	n.d.
	Rb		8.09	n.d.	-5.36	-5.36	-6.03	-6.03	2.74	-4.78
	Smad1		-1.13	2.21	0.81	2.08	0.36	2.02	-5.13	3.05
	Smad2		0.41	0.68	0.91	0.97	-0.81	-0.01	-8.23	0.25
	Smad2	pSer245/pSer250/ pSer255	n.d.	8.19	-0.19	1.47	3.36	3.02	2.94	3.58
	Smad3	pSer423/pSer425	0.24	0.97	-1.01	0.93	3.85	5.30	6.85	5.30
	Smad3 (# 0879)		-8.32	-8.32	-0.27	0.89	0.68	0.38	-8.48	-0.48
	Smad3 (# 1237)		-8.05	-0.78	-1.96	0.33	-1.97	-5.50	1.29	1.05
	Smad4		6.98	8.70	1.25	2.56	0.27	1.25	1.08	3.64
	Smad5		7.98	8.26	2.03	1.83	4.11	5.30	7.14	6.70
	Snail		n.d.	n.d.	n.d.	n.d.	5.19	n.d.	7.49	n.d.
	SOX17 (30 kDa isoform)		n.d.	n.d.	n.d.	n.d.	6.24	n.d.	n.d.	n.d.
	SOX17 (44 kDa isoform)		n.d.	n.d.	n.d.	n.d.	6.51	n.d.	n.d.	n.d.
	Src		-1.13	-0.21	-0.59	0.05	0.77	1.05	-0.28	0.31
	Src	pTyr416	1.08	0.98	-2.48	-1.40	-0.91	-1.79	2.67	1.74

Assigned category	Analyte	Modification	70.4 lysate		55.1c lysate		HepG2 lysate		HB35 lysate	
			CHIR 99021	MG132	CHIR 99021	MG132	CHIR 99021	MG132	CHIR 99021	MG132
6	Src	pTyr527	-0.81	0.55	-0.24	0.71	0.63	0.80	0.14	0.86
	TAZ (# 1626)		-2.84	-1.81	-6.01	-4.88	-1.01	-0.85	-5.42	-2.14
	TAZ (# 1737)		n.d.	n.d.	1.08	-4.63	6.01	5.34	3.47	3.15
	TCF1 (# 1673)		-5.99	-5.99	-0.19	1.22	-0.18	-4.82	-3.86	1.43
	TCF1 (# 1746)		6.73	n.d.	2.03	2.43	0.80	0.85	5.68	6.07
	TCF4 (50 kDa isoform, # 1753)		-7.19	-7.19	n.d.	n.d.	n.d.	n.d.	n.d.	n.d.
	TCF4 (50 kDa isoform, # 1727)		n.d.	n.d.	7.93	8.41	-7.90	-0.25	n.d.	n.d.
	TCF4 (60 kDa isoform, # 1481)		0.18	1.06	1.93	1.32	-0.26	-0.08	-8.35	-2.68
	TCF4 (60 kDa isoform, # 1727)		-5.93	-5.93	-4.36	-0.19	0.03	1.66	3.10	-3.46
	TCF4 (60 kDa isoform, # 1753)		n.d.	n.d.	n.d.	n.d.	-0.11	0.76	-7.20	3.14
	TCF4 (70 kDa isoform, # 1481)		n.d.	n.d.	n.d.	n.d.	1.64	1.17	-8.13	1.75
	TCF7L2 (30 kDa isoform)		n.d.	n.d.	n.d.	4.67	2.38	-2.26	2.98	-2.82
	TCF7L2 (50 kDa isoform)		n.d.	n.d.	n.d.	5.54	4.11	4.24	n.d.	4.53
7	14-3-3 ζ δ		-1.83	-3.31	-0.54	-1.50	0.59	-0.34	-4.58	-1.23
	A-Raf		-7.37	1.00	1.68	1.65	-0.40	0.13	8.37	8.61
	c-Raf		-1.29	0.62	0.36	0.00	0.40	1.66	-0.90	-3.83
	DUSP1		-8.78	1.01	0.51	0.61	-0.33	-0.14	0.11	0.37
	DUSP4		4.22	-10.35	1.10	0.94	2.69	-0.44	0.40	1.43
	DUSP6		1.09	-0.20	-0.64	-0.49	-3.42	-3.38	-2.69	-5.66
	DUSP9		-8.64	-8.64	-7.28	0.47	0.16	-0.65	0.40	-2.23
	Elk-1		0.56	1.88	-0.03	-0.30	-0.60	-0.91	0.14	0.19
	Erk1		0.02	0.76	1.56	1.00	2.93	2.88	0.22	0.32
	Erk2		-1.15	-0.09	0.80	0.44	1.77	0.01	-1.41	-0.12
	Ha-ras		-1.20	-1.18	-0.53	-0.22	0.82	0.55	-0.67	0.08
	JNK/SAPK (46 kDa isoform)		-7.01	1.32	2.48	2.60	-0.34	-0.01	2.56	3.11
	JNK/SAPK (54 kDa isoform)		-0.76	0.82	1.92	2.74	4.34	1.71	0.55	-0.82
	MAPKAPK-5		6.54	7.90	2.72	2.57	2.30	3.17	8.17	9.39
	MDM2 (60 kDa isoform)		-4.99	-4.99	-4.88	-4.88	-3.41	-3.41	-5.81	-5.81
	MDM2 (90 kDa isoform)		1.00	2.21	1.31	1.99	1.88	0.63	6.35	5.11
	MKK7		-7.29	1.49	0.68	0.89	-1.56	-1.69	1.71	1.49
	MSK1 (61 kDa isoform)	pThr589	n.d.	n.d.	2.17	1.69	n.d.	4.02	n.d.	n.d.
	MSK1 (85 kDa isoform)	pThr589	n.d.	n.d.	3.39	4.39	n.d.	n.d.	n.d.	n.d.
	p38/MAPK		-0.58	-1.56	-0.02	-0.77	-0.33	-0.97	-2.45	-0.45
8	STAT3	pSer727	1.20	1.71	1.00	0.73	0.61	0.19	-6.58	1.69
	STAT3 (79 kDa isoform, # 1192)	pTyr705	-6.08	-6.08	-1.56	-6.09	0.39	1.17	0.93	-0.34
	STAT3 (79 kDa isoform, # 1736)		1.69	-5.99	1.30	0.98	0.67	0.96	1.77	1.78
	STAT3 (86 kDa isoform, # 1736)		3.32	4.44	3.25	2.96	2.29	2.96	3.04	4.04
	STAT3 (79 kDa isoform, TK # 054)		-0.58	-0.34	0.43	-0.12	-1.00	-0.78	-0.22	0.58
	STAT4		n.d.	n.d.	4.76	n.d.	5.46	n.d.	8.21	n.d.
	STAT4	pTyr693	-3.17	-3.17	n.d.	n.d.	1.33	-3.52	-3.04	2.92
9	Ezh2		0.01	0.87	-0.66	0.00	-1.47	-1.16	-1.38	0.02
	HDAC1 (# 1165)		-5.99	0.66	-0.90	-1.19	0.12	-0.92	0.37	0.22
	HDAC2		1.04	1.76	-1.10	0.87	-0.15	-0.50	2.94	2.54
	HDAC3		-1.78	-1.05	-0.42	-0.22	-0.36	-0.49	2.28	1.58
	HDAC6 (# 739)		0.11	1.39	-0.80	-0.75	-2.35	-1.32	-1.94	-2.04
	HELLS		n.d.	8.80	0.00	0.01	-2.54	-2.29	-1.27	-0.17
	LSD1		0.05	1.00	0.06	0.18	-0.28	0.62	-2.33	-0.81
	PRMT4		-1.81	-1.60	-0.98	0.02	-2.03	-0.74	0.20	1.41
10	Cytokeratin Pan (~46 kDa, # 474)		8.19	12.99	7.16	8.09	5.22	6.53	6.96	9.21
	Cytokeratin Pan (~55 kDa, # 474)		-11.28	-2.14	-1.68	-5.79	-1.39	0.01	-2.75	0.44
	Cytokeratin Pan (~60 kDa, # 588)		1.68	4.13	0.44	1.26	0.31	0.96	1.65	2.99
	Vimentin		2.89	4.73	-0.77	-0.28	-1.47	-0.94	3.68	2.87
11	PCNA		0.86	0.85	0.30	-0.80	1.64	-1.55	-2.66	-0.92
12	PTCH2		0.20	0.18	4.65	5.98	-0.88	-0.56	2.66	-3.53
13	ILK1		-2.02	-1.86	-0.18	0.16	-0.52	-0.58	-0.12	0.12

Figure 20: Overview of all measured proteins and protein variants on the cell lines, which showed differences in abundance after treatment.
The shown proteins were sorted into thematically related:
Category 1: The target protein β-catenin; Category 2: Housekeeping proteins; Category 3: Proteins associated with membranouse Wnt-signal transduction; Category 4: Proteins participating in the β-catenin destruction complex; Category 5: Proteins present in the membrane-associated β-catenin complex; Category 6: Transcriptional regulators and factors; Category 7: Proteins associated with MAPK signaling; Category 8: Proteins associated with JAK/STAT signaling; Category 9: Epigenetic regulators; Category 10: Tumor markers; Category 11: Apoptosis; Category 12: Hedgehog pathway: Category 13: Hippo pathway.
The increase or decrease in protein concentration after treatment with CHIR 99021 and MG132 is shown within a 3-color scale. White representing cells with no signal detected, marked with n.d.; intense red visualizing the highest increase and intense green the highest decrease. Colorization was done for each cell line individually. In brackets the molecular weight and the distinct NMI number are listed, if needed for differentiation. The represented factors were calculated by normalizing the raw data with the total amount of protein loaded onto the beads. After calculating, the ratio between treated and untreated sample and the logarithm with base 2 was taken. Proteins, which did not show a signal or remained unchanged after treatment, compared to the untreated sample, were not included in the graph.

In Figure 20 above, the increases and decreases in protein expression in the different cell types after treatment with CHIR 99021 or MG132 are shown. The differences in the amount of the housekeeping proteins are low, indicating a good quality of the prepared sample extracts (see Figure 21).

Analyte	Modification	70.4 lysate		55.1c lysate		HepG2 lysate		HB35 lysate	
		CHIR 99021	MG132	CHIR 99021	MG132	CHIR 99021	MG132	CHIR 99021	MG132
β-Actin		0.76	1.14	0.69	0.86	0.09	0.15	2.25	2.03
GAPDH		0.36	-0.82	0.74	0.90	0.43	0.21	0.41	1.65

Figure 21: Housekeeping proteins after treatment in the different cell lysates.
The housekeeping proteins β-Actin and GAPDH are suitable to serve for the normalization of the different samples. Calculation and presentation is done analog to Figure 20.

The signals obtained for GAPDH are similar between the different cell lines and treatments, which confirms the way of normalizing the raw values. The second used housekeeping protein, β-Actin, shows some variation after treatment, as the calculated values for HB35 are around two after treatment.

Some proteins show increased values after treatment in all screened cell lines, prominent examples are Cytokeratins, MAPKAPK-5 and Smad5. The reverse is also observed, resulting in a decreased signal after treatment, visible in all samples. Examples are MDM2 (60 kDa isoform) and TAZ (# 1626) (see Figure 22).

Analyte	Modification	70.4 lysate		55.1c lysate		HepG2 lysate		HB35 lysate	
		CHIR 99021	MG132	CHIR 99021	MG132	CHIR 99021	MG132	CHIR 99021	MG132
Cytokeratin Pan (~46 kDa, # 474)		8.19	12.99	7.16	8.09	5.22	6.53	6.96	9.21
Smad5		7.98	8.26	2.03	1.83	4.11	5.30	7.14	6.70
MAPKAPK-5		6.54	7.90	2.72	2.57	2.30	3.17	8.17	9.39
TAZ (# 1626)		-2.84	-1.81	-6.01	-4.88	-1.01	-0.85	-5.42	-2.14
MDM2 (60 kDa isoform)		-4.99	-4.99	-4.88	-4.88	-3.41	-3.41	-5.81	-5.81

Figure 22: Visualization of analytes which increased or decreased after treatment in all cell lines similarly.
The analytes having the clearest enrichment or reduction after treatment with CHIR 99021 and MG132 for all samples similarly are shown. Calculation and presentation is done analog to Figure 20.

Analyte	Modification	70.4 lysate		55.1c lysate		HepG2 lysate		HB35 lysate	
		CHIR 99021	MG132	CHIR 99021	MG132	CHIR 99021	MG132	CHIR 99021	MG132
β-catenin (BD)		0.48	0.99	0.75	1.68	0.11	1.09	0.87	2.23
β-catenin (Millipore)		0.03	0.59	2.22	1.58	2.21	1.65	2.33	2.90
β-catenin	pSer552	0.59	-0.11	-0.56	0.95	-3.08	-2.69	-0.21	1.35
β-catenin	pSer675	-0.26	-0.97	-1.01	0.21	-3.65	-3.12	0.09	0.96
β-catenin	pThr41/pSer45	-5.50	-5.50	-3.36	1.39	-1.11	-1.11	1.51	-3.91
β-catenin	non-pospho Ser33/Ser37/Thr41	-1.46	-1.00	3.02	1.90	2.29	1.78	2.53	2.77

Figure 23: Behavior of β-catenin after treatment for the different lysates.
The antibodies against total β-catenin or active β-catenin show an increase after both treatments, CHIR 99021 and MG132, in all cell lines, except 70.4. Antibodies directed against C-terminal phosphorylations show a decrease in the amount of detected β-catenin only for HepG2 and minor alterations otherwise. Calculation and presentation is done analog to Figure 20.

Figure 23 comprises the effects of treatment on the amount of β-catenin detected in the cell lysates. The antibodies addressing total β-catenin show a slight increase for both treatments, CHIR 99021 and MG132, in all cell lines. Thereby it varies, if the enrichment for CHIR 99021 or MG132 treatment is higher. For the anti-β-catenin antibody directed against the active variant of the protein, unphosphorylated at Ser33/Ser37/Thr41, a minor decrease is visible for 70.4 cells and a high increase, especially after CHIR 99021 treatment for the other cell lines. β-catenin phosphorylated at Ser552 or Ser675, both located C-terminally, show only a small change under any treatment. Only HepG2 cells show a decrease in the amount of the phosphorylated protein for both treatments.

For many proteins, differences are found after treatment or between the various cell lines. In Figure 24, a few analytes, showing the discrepancies between the treatments or the cell lines, are listed.

Analyte	Modification	70.4 lysate		55.1c lysate		HepG2 lysate		HB35 lysate	
		CHIR 99021	MG132	CHIR 99021	MG132	CHIR 99021	MG132	CHIR 99021	MG132
A-Raf		-7.37	1.00	1.68	1.65	-0.40	0.13	8.37	8.61
Axin1		1.40	1.53	-1.23	0.73	-4.41	-4.41	-4.59	-4.59
Evi (50 kDa isoform)		4.25	4.32	1.19	2.34	2.06	-5.10	4.80	-3.82
GSK3 α	pTyr279	-0.58	0.72	-3.70	0.65	-8.46	-1.11	-7.21	1.14
GSK3 β	pSer9	-1.31	0.19	-2.50	0.36	-2.77	-3.30	-6.89	1.62
STAT3 (79 kDa isoform, # 1192)	pTyr705	-6.08	-6.08	-1.56	-6.09	0.39	1.17	0.93	-0.34
TAZ (# 1737)				1.08	-4.63	6.01	5.34	3.47	3.15

Figure 24: Diverse behavior of various analytes after treatment for the different lysates.
Analytes showing the most striking discrepancies in behavior after treatment are picked from Figure 20 and outlined separately. Calculation and presentation is done analog to Figure 20.

The first protein listed in Figure 24, A-Raf, shows minor changes for most of the signals after treatment. Noticeable is a high decrease in the signal intensity (-7.37) for CHIR 99021-treated 70.4 cells, while HB35 cells show a contrary high signal increase for both treatments (> 8), compared to the untreated sample. The signal observed for Axin1 shows little deviation after treatment in the mouse cells, but a striking decrease in the human cells for both treatments. Noticeable is the identical value, calculated for both treatments in HepG2 and HB35 cells (-4.41 and -4.59). Here, no peak was detected in the treated samples, which results in identical values after referring the treated to the untreated sample by building ratios. The third selected protein, Evi (50 kDa isoform) shows another peculiarity: for both mouse cell lines, an increased signal is obtainable for CHIR 99021 and MG132 treatment, which is higher for 70.4 cells (> 4), while the human cell lines show an increase of Evi (50 kDa isoform) only after CHIR 99021 (2.06 and 4.80) and a strong decrease after MG132 treatment (< -3.5). For GSK3 α (pTyr279) and GSK3 β (pSer9) a decrease in the signal, received after CHIR 99021 treatment compared to the untreated sample is obtained for all cell lines. This decrease is stronger for the human cell types. For the MG132 treatment, only HepG2 cells show a decreased signal, while all other cell lines show a slightly increased signal in comparison with the untreated cells. STAT3 (pTyr705, 79 kDa isoform, # 1192) shows a decreased signal intensity especially for the mouse cells, the identical value calculated for both treatments in 70.4 (-6.08) is due to the missing peak in the untreated sample. Values for STAT3 (pTyr705, 79 kDa isoform, # 1192) detected in human cells are colored in a pale color, which implies that signals obtained for treated and untreated sample don't differ much and the calculated and logarithmized ratio is between -1 and 1. The last protein, TAZ (# 1737) shows no signal in 70.4 lysate, represented by white cells in Figure 24. In the 55.1c cell line, a slight increase after CHIR 99021 and a stronger decrease after MG132 treatment is observed. Striking however is the intense increase for both human cell lines after treatment, always slightly higher for CHIR 99021 than for MG132 treatment.

4.1.3 Summary

A modulation of protein amount after drug treatment in the different cell lysates is observed. In addition, differences between the cell lines and their individual response to treatment were apparent.

The increased amount of β-catenin detected after treatment by antibodies against total β-catenin, was an expected reaction of the cell lines to drug treatment. For CHIR 99021 it is known, that the active variant of β-catenin accumulates in the cytosol; this was visible, as higher amounts of β-catenin, unphosphorylated at the SSTS-motif, were detected by specific antibodies (see Figure 23). For MG132, all β-catenin variants are expected to increase, since this drug leads to the inhibition of the proteasomal degradation pathway. The general increase of different β-catenins is indeed seen

and is especially visible for total β-catenin (see Figure 23). GSK3 was exemplarily chosen to visualize the effects of drug treatment on interacting proteins of β-catenin. This kinase regulates a great variety of proteins [145], thus inhibition of GSK3 by a specific inhibitor such as CHIR 99021, led to major alterations of several proteins, which are influenced by the kinase activity of GSK3 (see Figure 20). Another example for visualizing the response of the screened cell lines towards drug treatment, was the increase of Cytokeratins upon MG132 treatment (see Figure 22). The intracellular accumulation of Cytokeratins after application of MG132 was shown before [146]. Cytokeratins belong to the group of proteins, which use the proteasomal degradation way, inhibited by MG132.

Several results were confirmed, which were expected based on reviewing literature. Additionally, novel effects were obtained, which lack an explanation so far, and have to be put into greater context.

The quality of the material, used during screening to obtain differences in between cell lines and alterations upon differing drug treatment, was verified. This led to further analysis in terms of performing Co-IPs on these cell lines.

4.2 Targeted Co-Immunoprecipitation of hepatoma cell lines

After analyzing the signaling state of four different cell lines and being able to both visualize differences between cell lines and modulations in the detected proteins caused by drug treatment, the cell lysates were processed further. A Co-IP addressing β-catenin was performed to detect PPIs as well as changes in the amount of captured proteins and dynamic alterations of the PPIs under drug treatment.

4.2.1 Isolation of β-catenin containing protein complexes

The immunoprecipitate (bound sample) generated during Co-IP was first analyzed for the presence of the target protein β-catenin. For this analysis, the total cell lysate as described above, was used for the precipitation reaction. It will be referred to as input sample from now on. The bound fraction (or bound) represents the protein complexes precipitated with β-catenin, while the non-bound fraction (or non-bound) is the by Co-IP material depleted supernatant.

For performing Co-IPs, it is important to use a well characterized high-quality monoclonal antibody recognizing a defined epitope to dissect real interactions from unspecific binding and to avoid interference with potential binding partners [112]. An antibody against total β-catenin (BD), recognizing the target protein at its C-terminus (aa 571 – 781), was used to address a wide range of β-catenin variants. At the N-terminus many activating mutations are located [147], as a central regulatory domain of β-catenin, the SSTS-motif, is found here. Especially in HCC or HB cell lines, mutations in this region occur frequently [74]. Some of the cell lines (55.1c, HepG2 and HB35) harbor a mutation here, which could affect the binding of a capturing antibody addressing this region. Binding of the BD antibody at the C-terminus is not directly affected by these mutations and it is able to address many of the posttranslationally modified β-catenin variants as well as N-terminally truncated proteins.

To check the quality of the Co-IP, Western blots were performed that demonstrated the success of the Co-IP (see Figure 25). For this analysis, 1 % of the input, 1 % of the non-bound and 20 % of the bound samples of each cell line were loaded onto a gel (loading volumes as described in 3.2.5). After gel electrophoresis and blotting, the blots were incubated with the capturing antibody against β-catenin and a control antibody addressing GAPDH.

In both blots, no GAPDH signal (red) was detected in the precipitates, which demonstrates the efficiency of washing. GAPDH is not interacting with β-catenin and a fluorescent signal in the bound fraction would imply a carry over of unspecific proteins into the precipitate. The β-catenin signal (green) is seen in all lanes (Figure 25 A); an enrichment after Co-IP is visible in the precipitate for all cell lines, although there is still an intense, yet reduced signal visible in the non-bound lane. This indicates that the amount of available β-catenin in the lysate is too high to be depleted completely

during Co-IP performance. Due to the high amount of β-catenin available in the cells, a complete β-catenin harvesting is difficult to achieve. The incomplete harvesting has to be taken into consideration. We assumed that the different β-catenin complexes are addressed and precipitated in equal proportions and a representative sample was generated. Thus, the Co-IP samples were used for further analysis. In the corresponding Co-IP control (see Figure 25 B), no β-catenin signal was obtained in the bound fraction. Here, IP was performed with an IgG1-isotype control antibody to detect unspecific protein binding to the bead surface during Co-IP. Such an unspecific binding signal is visible for the bound lane of the cell line 55.1c. Here a signal at approximately 70 kDa is detected, which did not reoccur during the performance of the DigiWest assays. This fluorescent signal might be caused by overfilling the well containing the non-bound sample during loading and a thereof derived contamination of the bound lane. Signals seen at a molecular weight of approximately 50 kDa and 25 kDa are derived from the secondary species-specific antibody detecting mouse antibodies and fragments of it. In this case, the heavy and light chains of the capture-antibody used during the Co-IP performance are detected; this signal was not taken into account.

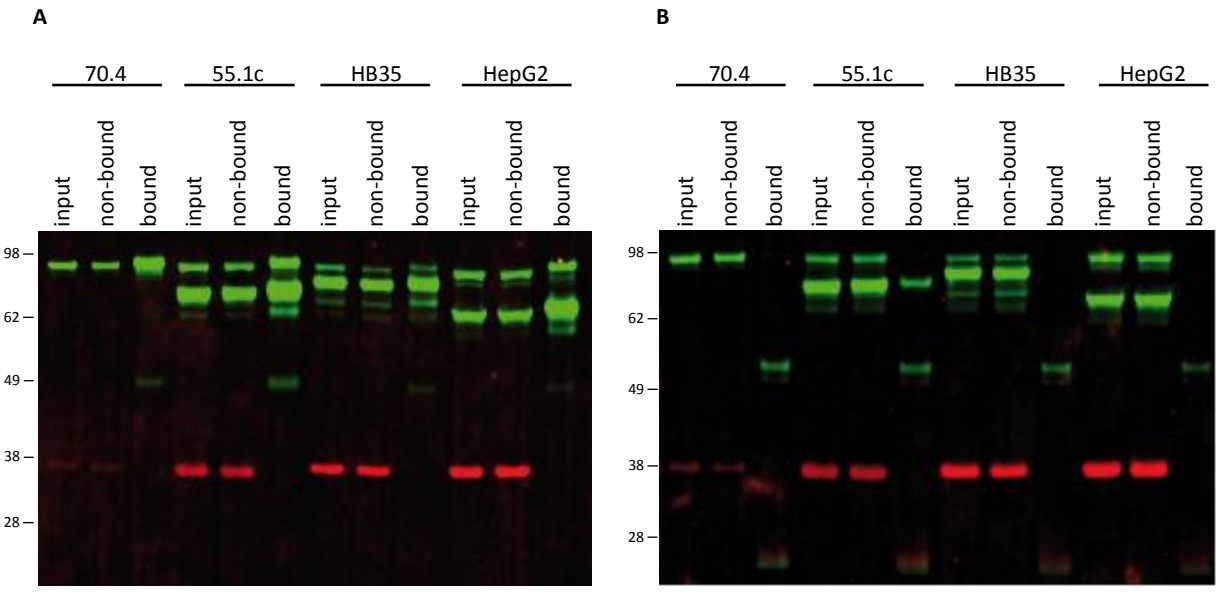

Figure 25: Control Western blot for the Co-IP.
All samples were processed as described earlier (see 3.2.2 and 3.2.3). To check the quality of the Co-IP, all samples were applied onto a NuPAGE gel (1 % input, 1 % non-bound and 20 % bound sample) and a Western blot with subsequent immunoblotting and -detection was performed. Blots were incubated with anti-GAPDH (red band at ~38 kDa) and anti-β-catenin (BD, green band at ~92 kDa). A shows the enrichment of β-catenin during Co-IP in the bound lane, while no GAPDH signal is obtained. B represents the negative control of the Co-IP performed with an IgG1-isotype control antibody, to eliminate unspecific protein binding. No β-catenin or GAPDH signal appear in the bound lane.

The Western blots show truncated β-catenin variants, indicated by the additional lower green bands on the blot; they are observed in the cell lines 55.1c, HB35 and HepG2. This is caused by the

heterozygous deletion of the N-terminal region of *CTNNB1* and the existence of additional truncated β-catenin variants in these cells.

It was shown previously, that signals obtained by the well-established Western blot method and the novel DigiWest approach are comparable [91]. This was proven here. For the combination of Co-IP and DigiWest, both Western blots and DigiWests were run in parallel (see 4.3.1). The reproducibility of the results for biological duplicates (see 4.3) or triplicates (see 4.4) was shown later.

In a first analysis the different β-catenin pools, which were precipitated during the Co-IP with an antibody recognizing the C-terminus of total β-catenin (BD), were looked at. Assays with eight different antibodies against β-catenin were performed. The antibodies differed in having distinct binding sites on the protein or were recognizing different PTMs.

The integrated and exported peak values from the DigiWest analysis tool provided the basis to estimate the amount of the different captured β-catenin variants and to calculate a capturing rate. This capturing rate provides information about the strength of precipitation of the target protein β-catenin and later also about the strength of interaction between β-catenin and the co-immunprecipitated interaction partners. A formula for calculating the capturing factor (CF) was derived in consideration of the enrichment through the Co-IP and the differences in the amount of sample loaded onto the gel (see Equation 3). The CF was denoted in percentage (for further details on the calculations, see 3.4.3.3). Six anti-β-catenin antibodies remained for further analysis (see Table 18). All CFs, along with the obtained raw values for the differently treated input and bound samples, are listed in the appendix (see Suppl. Table C – Suppl. Table F).

Table 18: Caught β-catenin variants on the different cell lines.
The capturing rate for the different β-catenin antibodies is represented, calculated as described in 3.4.3.3, Equation 3. Additionally, the raw values (input/bound), of which the CFs were derived, are displayed below. For some antibodies, no signal was obtained. These antibodies were either excluded completely from the table (e.g. two antibodies recognizing a β-catenin variant phosphorylated at Ser33/Ser37/Thr41) or the cell was marked with "-".

Analyte	Modification	70.4	55.1c	HepG2	HB35
β-catenin (BD)	-	18.01 (2596/9349)	22.68 (14047/63725)	2.78 (8037/4464)	5.31 (12678/13472)
β-catenin (Millipore)	-	24.26 (2434/11812)	28.51 (969/5525)	2.83 (410/232)	5.62 (680/764)
β-catenin	non-p Ser33/ Ser37/Thr41	66.47 (354/4706)	113.33 (48/1088)	-	9.75 (40/78)
β-catenin	pThr41/pSer45	13.75 (20/55)	-	-	-
β-catenin	pSer552	41.30 (353/2916)	47.18 (2497/23560)	4.30 (2775/2384)	14.56 (2102/6121)
β-catenin	pSer675	41.31 (572/4726)	61.84 (2491/30807)	4.61 (2161/1994)	13.18 (1179/3107)

Both antibodies against total β-catenin (BD and Millipore) show a similar percentage of capturing within the same cell line. Anti-β-catenin non-phospho Ser33/Ser37/Thr41 recognizes an active β-catenin variant, which is unphosphorylated at the SSTS-motif. The detected capturing rate was high in both mouse cell lines, while for HepG2 the obtained signal was very low (below the determined cutoff levels) and for HB35 the signal intensity was also much lower in comparison to the murine cell lines (input: 40 AFI, bound: 78 AFI). All cell lines, apart from HepG2, showed a higher enrichment for the unphosphorylated β-catenin variant, when compared to the rate of total β-catenin (factor > 1.5). β-catenin pThr41/pSer45 was only detected in cell line 70.4 and a CF was calculated. This was caused by the very low signal intensities (between 15 and 55 kDa) received for the integrated signal peaks for this antibody in all cell lines. As the cutoff limit was defined at a minimum of 45 AFI in the bound samples (see 3.4.3.3), only cell line 70.4 surmounts this limit and a CF of 13.75 was derived from the calculated bound/input ratio. The cutoff limit was defined at 45 AFI, as the averaged background level was approximately at 11 AFI and signals four times above this background average were identified as significant peaks. For the C-terminal phosphorylation forms of β-catenin at Ser552 and Ser675, similar capturing rates were detected within the same cell line. Yet, it is interesting to note that these signals displayed a fold change of two or higher when compared to the CFs derived for total β-catenin.

4.2.2 Co-precipitated β-catenin interaction partners

Besides the semi-quantitative detection of different β-catenin variants, it was possible to screen for interacting proteins, starting with the final screening list (see 4.1.1.3), containing 189 antibodies and 179 antibody-based signals pointing to possible interactors of β-catenin. Among the screened analytes were proteins, whose interaction with β-catenin is well-documented, like α-catenin or GSK3 β. Furthermore, less charaterized or only predicted interaction partners of β-catenin were seen. All bound signals with an intensity above 45 AFI were included into further calculations (see 3.4.3.3). Additionally, an unspecific binding of proteins during Co-IP was identified by building the ratio of specific values over values, measured for the negative control; only ratios above 1.5 were considered to be indicative of an interaction. To determine actual interactors, the capturing rate, defining the strength of an interaction between β-catenin and a binding protein, was calculated (see 3.4.3.3, Equation 3 and 4.2.1). To classify this strength of interactions, four distinct limits were defined to evaluate the received CF during analysis. According to this classification, a colorization of the cells, containing the CFs, was done (see 3.4.3.3 and Table 19).

Table 19: Definition criteria for the strength of a PPI.
The classification and colorization for defining the strength of a PPI are visualized.
Green illustrates a weak interaction, with a calculated ratio beneath 0.1 %. Interactions between 0.1 % and 0.5 % are marked in yellow and referred to as a medium interaction. A strong interaction above 0.5 % is represented in lighter red, while an intense red indicates a very strong interaction with a CF > 10 %.

$x = \left(\frac{\frac{bound}{0.2}}{\frac{input}{0.01}} \cdot 100\right)$	**Strength of PPI**
x < 0.1 %	weak
0.1 % < x < 0.5 %	medium
0.5 % < x	strong
x > 10 %	very strong

After analyzing the results for all cell lines, only one protein was consistantly found in all precipitates: α-catenin. All other observed PPIs showed variations for the different cell lines. In some cases, proteins were only detectable in the precipitate, when they were enriched during Co-IP. These interaction partners are specifically marked with "+". In this case, the obtained capturing factors are high and classified as very strong. This is due to the fact that the input value was set to the averaged background value of 11 to allow the calculation of a factor. Although it is not always consistent with the signals obtained in raw data. The values depicted for CFs in the following chapters, are always given as percentage of capturing, calculated and classified with the mentioned criteria (see 3.4.3.3, Equation 3 and Table 19), but the percent sign was omitted in the following chapters.
The interacting proteins for each of the different cell lines were arranged into eight possible, defined groups, describing either β-catenin comprising complexes or are based on a common characteristic, like participation in a specific pathway or a shared function. It has to be mentioned, that most proteins have different functions and could be assigned to several of the groups below.

1. Housekeeping proteins
2. Proteins associated with membranous Wnt signal transduction
3. Proteins participating in the β-catenin destruction complex
4. Proteins present in the membrane-associated β-catenin complex
5. Transcriptional regulators and factors
6. Proteins associated with MAPK signaling
7. Proteins associated with JAK/STAT signaling
8. Epigenetic regulators
9. Tumor markers

α-catenin, as the only protein that was detected as an interaction partner in all untreated cell lines, was assigned to the group of proteins present in the membrane-associated β-catenin complex (see Figure 2).

Table 20: Co-immunoprecipitated proteins together with β-catenin in all cell lines.
The CFs and raw values for α-catenin are represented, the red background indicates α-catenin as a strong interactor of β-catenin. A more intense red color shows the difference between a strong and very strong interaction. CFs were calculated with the formula described in 3.4.3.3, Equation 3.

Analyte	Modification	70.4	55.1c	HepG2	HB35
α-catenin		7.29 (120/175)	16.20 (888/2878)	0.55 (1200/133)	1.14 (350/80)

α-catenin [148, 149] was defined as a strong interactor with the cutoff limits, specified above. The amount of α-catenin enriched through Co-IP is highest for 55.1c cells. α-catenin was classified as a very strong interactor (CF = 16.20) in these cells. Already in the raw data, a high amount of this protein was detected in the input sample. Another possibility could be a better recognition of the murine α-catenin by the antibody than of the human variant.

4.2.2.1 Protein-protein interactions in the cell line 70.4

The 70.4 cell line is the only cell line which carries no mutational activation of the Wnt pathway, but a p53 mutation instead [76]. Here only few PPIs with β-catenin were detectable. As mentioned before (see 4.2.1, Table 18), β-catenin was captured with a high CF (18.01 for the BD antibody (input signal of 2596 AFI and 9349 AFI for the bound); 24.26 for the Millipore antibody (input: 2434 AFI, bound: 11812 AFI); both recognizing total β-catenin (see Table 21)). Besides the captured target β-catenin and its binding partner α-catenin (see Table 20) as an interactor, eight more interactors were identified (see Table 21), which all were classified as strong or very strong. No medium or weak interacting proteins could be found.

The cell line 70.4 showed only few interacting proteins in the untreated samples, thus the proteins are only sorted and listed, but the characteristics of the groups are described in the next chapters.

Table 21: Co-immunoprecipitated proteins in 70.4.
The CFs and raw values for cell line 70.4-specific β-catenin interacting proteins are represented, calculated with the formula described in 3.4.3.3, Equation 3. The colorized background indicates the strength of the PPI (see Table 19). In brackets the molecular weight and the distinct NMI number are listed, if the analytes need to be differentiated. Proteins, which were only detected in the bound sample, are marked with a "+". If more than one protein was assigned to a category, they were sorted in an ascending order.

Analyte	Modification	CF (AFI input/AFI bound)	Captured only in bound sample
Proteins associated with membranous Wnt signaling			
Wnt11		20.45 (11/45)	+
Proteins comprising the β-catenin destruction complex			
APC		26.18 (17/89)	
Proteins associated with the membrane-associated β-catenin complex			
β-Actin		4.77 (60390/57646)	

Analyte	Modification	CF (AFI input/AFI bound)	Captured only in bound sample
Proteins associated with the membrane-associated β-catenin complex			
α-catenin		7.29 (120/175)	
Transcriptional regulators and factors			
GLI1		7.50 (32/48)	
Elk-1		8.93 (107/191)	
Proteins associated with MAPK pathway			
DUSP6		2.56 (160/82)	
Proteins associated with JAK/STAT signaling			
STAT4		28.64 (11/63)	+
Tumor markers			
Vimentin		6.78 (343/465)	

Wnt11 [38, 150] was a strong interaction protein (CF of 20.45). It has to be pointed out that Wnt 11 is marked with a "+", which means that it showed no signal in the input sample and only a small peak (45 AFI) was obtained for the bound sample. Another very strong interacting protein, APC [41, 151, 152], was caught together with β-catenin (CF of 26.18). The third group "proteins associated with the membrane-associated β-catenin complex" is represented with two members for cell line 70.4, both being classified as strong interactors. β-Actin [153-155] (CF of 4.77) and α-catenin with a 1.5 times higher CF (CF = 7.29). GLI1 [156], which is an effector of hedgehog signaling and additionally a transcription factor, and the transcription factor Elk-1 (ETS domain-containing protein) [29, 157] are strong interacting proteins (CFs of 7.50 and 8.93). Both belonging to the group of "transcriptional regulators and factors". The obtained PPI for β-catenin in 70.4: DUSP6 (dual specificity phosphatase 6) [29, 158], associated with the MAPK signaling, is classified as strong (CF of 2.56). STAT4 [159], associated with the JAK/STAT pathway, is a very strong interacting protein (CF = 28.64). It is also a protein, with no signal detectable in the input sample, but it emerges as a complex partner of β-catenin in the bound sample with a raw value of 63 AFI, which led to its classification as a very strong interactor. The last group contains the tumor markers received for 70.4 cells, with only one protein: the intermediate filament Vimentin [160-163], with a capturing rate of 6.78, portraying it as a strong interacting protein.

4.2.2.2 Received protein-protein interactions in 55.1c cells

A high number of PPIs was detected for cell line 55.1c. Additionally, the highest signal for detecting β-catenin was achieved here. This cell line harbors a heterozygous β-catenin exon 3 deletion and an

additional b-raf mutation [78]. The BD antibody led to a CF of 22.68 derived from an input signal of 14047 AFI and a bound signal of 63725 AFI, while the Millipore anti-β-catenin antibody resulted in a CF of 28.51 (input: 969 AFI, bound: 5525 AFI) (see 4.2.1, Table 18). Thus, the input signal detected by the BD antibody was approximately five times higher for 55.1c cells than it was for the 70.4 cells (see Table 22). In total 33 interacting proteins were found, which are displayed in in the tables below, ordered by the categories defined in 4.2.2.1. No weak interacting proteins were identified. Three medium interactors were found and 30 strong ones, of which 16 are further classified as very strong.

Table 22: Co-immunoprecipitated proteins in 55.1c.
The CFs and raw values for β-catenin interacting proteins caught in cell line 55.1c are shown. Calculation, representation and sorting were done analog to Table 21.

Analyte	Modification	CF (AFI input/AFI bound)	Captured only in bound sample
Proteins associated with membranous Wnt signaling			
Evi (60 kDa isoform)		4.49 (503/452)	
LRP6 (# 1750)	pSer1490	5.78 (58/67)	
Wnt7b		38.36 (70/537)	
Wnt3a		47.73 (11/105)	+
Proteins comprising the β-catenin destruction complex			
CK1 α		2.32 (480/223)	
GSK3 α	pTyr279	8.56 (436/746)	
GSK3 β		10.97 (3653/8018)	
APC		11.74 (23/54)	
GSK3 β	pTyr216	15.09 (696/2100)	
Axin2 (# 1724)		40.91 (11/90)	+
Axin1		75.80 (50/758)	
Proteins associated with the membrane-associated β-catenin complex			
α-catenin		16.20 (888/2878)	
E-Cadherin		21.31 (781/3328)	
Transcriptional regulators and factors			
eIF4E		0.11 (8820/189)	
Smad4		0.93 (387/72)	
Smad5		1.32 (355/94)	

Analyte	Modification	CF (AFI input/AFI bound)	Captured only in bound sample
Transcriptional regulators and factors			
Smad3 (# 0879)		1.53 (618/189)	
HNF1A		1.61 (1211/391)	
Src		2.02 (9241/3738)	
TCF4 (70 kDa isoform, # 1481)		12.83 (30/77)	
TAZ		14.09 (3726/10502)	
TCF4 (60 kDa isoform, # 1727)		133.64 (11/294)	+
Proteins associated with MAPK pathway			
JNK/SAPK (54 kDa isoform)		1.52 (256/78)	
MKK7		2.44 (166/81)	
A-Raf		2.94 (240/141)	
MAPKAPK-5		4.45 (64/57)	
MDM2 (60 kDa isoform)		10.47 (43/90)	
DUSP6		11.29 (831/1876)	
Proteins associated with JAK/STAT signaling			
STAT3 (79 kDa isoform, TK # 054)		0.42 (862/73)	
Epigenetic regulators			
Ezh2		0.38 (1435/109)	
HDAC2		8.47 (49/83)	
Tumor markers			
Vimentin		16.38 (7346/24060)	
Cytokeratin (~46 kDa, # 0474)		65.33 (92/1202)	

Evi (60 kDa isoform), also known as G protein-coupled receptor 177 (GPR177) or Wntless [164], fits into both categories “transcriptional regulators and factors” and “proteins, associated with membranous Wnt signal transduction”. As it modulates Wnt in a positive feedback loop [164], it was filed into the latter group. Together with the phosphorylated LRP6 [49, 152, 165, 166], it represents a strong interactor (CFs of 4.49 and 5.78). Wnt3a [53] and Wnt7b [167] are ligands of the Wnt pathway family, which bind to receptor proteins like LRP5/6 and FZD, both in turn build a complex and

facilitate Wnt signaling [152, 167]. Wnt3a and Wnt7b count as very strong interacting proteins (CFs above 35), but for Wnt3a signal was only obtained in the bound sample (peak size of 105 AFI).

All proteins listed in the second group, are part of the β-catenin destruction complex, which targets β-catenin by phosphorylation at the SSTS-motif, leading to degradation by the proteasome. The found proteins can bind to Axin1 and its homolog Axin2 (also called Axil or Conductin) [36, 152, 168]. For Axin1 and Axin2 the highest capturing ratios are obtained. The CF for Axin1 is 75.80, categorizing it as very strong interactor. Axin2, also a strong interacting protein of β-catenin, was only detectable in the bound sample with a value of 90 AFI, resulting in a CF of 40.91. CK1 α [49, 169] is the kinase, which performs the initial phosphorylation at Ser45, before GSK3 starts to phosphorylate further sites on the SSTS-motif. Both, CK1 α and GSK3 α (pTyr279) [170, 171], were detected as strong interacting proteins (CFs of 2.32 and 8.56), while GSK3 β and GSK3 β (pTyr216) [171-173] were classified as very strong interactors (CFs above 10). APC represents another strong interactor (CF = 11.74), which is also part of the destruction complex, but is also able to bind β-catenin directly. It influences the binding affinity of β-catenin to the destruction complex [41, 152].

β-catenin also exists in a membrane-associated complex together with E-Cadherin [36, 149, 174, 175] and α-catenin. Both represent very strong interactors in 55.1c cells (CFs of 16.20 and 21.31). α-catenin provides a possible link to the cytoskeletal β-Actin, which was not detectable in this case.

Additionally, various transcription factors and transcriptional regulators were captured in 55.1c lysate. One medium, five strong and three very strong PPIs were detected after Co-IP. The only medium interactor (CF = 0.11) is eIF4E (Eukaryotic translation initiation factor 4E) [176, 177]. The CFs of the strong interacting proteins vary from 0.93 to 2.02. Three members of the Smad family (Mothers against decapentaplegic homolog): Smad4 and 5, as well as Smad3 (# 0879) [178-182] were identified as strong interactors. Additionally, the transcription factor HNF1A (hepatocyte nuclear factor 1 homeobox A) [183] and the proto-oncogen Src (a tyrosine kinase) [184-186] were captured. Three very strong interactors, two isoforms of TCF4 with different MWs, detected by different antibodies and TAZ (WW domain-containing transcription regulator protein 1) [187], were found. For TCF4 (60 kDa isoform, # 1727) [36, 54, 55] a signal occurs only in the bound sample (294 AFI), but not the input sample. This results in an extremely high CF of 133.64, while the signals of the other two proteins lead to CFs of 12.83 and 14.09.

The MAPK pathway is an important and intensively studied signaling pathway, which is deregulated in various diseases, e.g. cancer [188]. For cell line 55.1c six proteins were immunoprecipitated with β-catenin, which are in some way associated with MAPK signaling. Among these six proteins, four strong and two very strong interactors were found. JNK/SAPK (the 54 kDa isoform of the cJUN N-terminal and stress activated protein kinases, also called MAPK8) [189, 190], MKK7 (dual specificity mitogen-activated protein kinase 7) [190-195], A-Raf (Ser/Thr-protein kinase A-Raf) [196, 197] and

MAPKAPK-5 (MAP kinase-activated protein kinase 5) [198] were classified as strong interacting proteins (CFs between 1.52 and 4.45). Additionally, two very strong interactors, MDM2 (the 60 kDa isoform or cleaved version of mouse double minute 2 homolog) [199, 200] (CF of 10.47) and again DUSP6 (CF = 11.29), were captured.

One medium interactor, STAT3 (79 kDa isoform, TK # 054) [201, 202] (CF of 0.42), associated with the JAK/STAT signaling, was detected. This pathway is activated by cytokines and growth factors and can mediate their signals directly to target gene promoters in the nucleus. By that, it provides a mechanism for transcriptional regulation, which works without a second messenger. Beyond that, MAPKs can phosphorylate STATs and modulate their functioning [203].

The histone deacetylase HDAC2 [204-207] and the histone-lysine N-methyltransferase Ezh2 [208] can both be addressed as epigenetic regulators, due to their capability of transferring functional groups posttranslational to histones and other proteins. By doing that, they are able to modify the proteins' activity and its function.

Vimentin is an accepted marker for EMT (Epithelial–mesenchymal transition) and generally a biomarker in tumor detection. It shows a CF of 16.38, indicating it as a strong interactor of β-catenin. The Cytokeratin family also comprises various tumor markers [209] and the obtained CF of 65.33 for a ~46 kDa-variant is assessed as very strong. As all Cytokeratin antibodies were Pan antibodies recognizing a variety of different Cytokeratins, the evaluated peak is marked by noting the specific MW in brackets.

4.2.2.3 β-catenin interactors in the cell line HepG2

The human HepG2 cell line carries a heterozygous β-catenin exon 3-4 deletion [74, 79, 82, 85]. In comparison to the 55.1c cells, a decrease for both antibodies recognizing total β-catenin (see 4.2.1, Table 18) was seen in HepG2 cells. The BD antibody directed against β-catenin resulted in a CF of 2.78 (input: 8037 AFI, bound: 4464 AFI) and the Millipore antibody showed even smaller raw values (input: 410 AFI and bound: 232 AFI), although the detected CF of 2.83 was almost identical (see Table 23). For the cell line HepG2, it was possible to detect 14 PPIs, among which one weak, two medium, five strong and six very strong interactors were found.

Table 23: Co-immunoprecipitated proteins in HepG2.
The CFs and raw values for β-catenin interacting proteins caught in cell line HepG2 are shown. Calculation, representation and sorting were done analog to Table 21.

Analyte	Modification	CF (AFI input/AFI bound)	Captured only in bound sample
Housekeeping proteins			
GAPDH		0.01 (138556/386)	

Analyte	Modification	CF (AFI input/AFI bound)	Captured only in bound sample
Proteins associated with membranous Wnt signaling			
LRP6 (180 kDa isoform, # 1567)	pSer1490	24.09 (11/53)	+
Wnt7b		32.27 (11/71)	+
Proteins comprising the β-catenin destruction complex			
CK1 δ		0.27 (867/46)	
GSK3 β		0.59 (2085/244)	
GSK3 β	pTyr216	1.15 (278/64)	
Proteins associated with the membrane-associated β-catenin complex			
α-catenin		0.55 (1200/133)	
E-Cadherin		1.64 (679/223)	
Transcriptional regulators and factors			
eIF4E		0.14 (1930/54)	
HNF1A		1.02 (293/60)	
FoxO3a	pSer413	24.55 (11/54)	+
ATF4		41.82 (11/92)	+
Snail		53.18 (11/117)	+
Proteins associated with JAK/STAT signaling			
STAT4		23.64 (11/52)	+

GAPDH is one of the housekeeping proteins, which was used for normalization earlier. It was detected here as a weak interactor. It is seen as a false positive since the huge signal obtained in the input sample (138556 AFI) is a likely cause for the comparatively small carry over into the bound sample (386 AFI).

Only two interacting proteins, which are associated with the membranous Wnt signaling were detected in the bound samples for HepG2 cells. Both, LRP6 (pSer1490, 180 kDa isoform, # 1567) and Wnt7b, were classified as very strong interactors, but their raw values (53 and 71 AFI) in the bound are rather small, resulting in a very high CF.

For HepG2, only three proteins of the β-catenin destruction complex were captured during Co-IP. CK1 δ was a medium interactor (CF = 0.27) belonging to the CK1 kinase family. Like CK1 α, it is capable of phosphorylating β-catenin at Ser45 [49, 169]. Additionally, total GSK3 β and the Tyr216

phosphorylated, active form of GSK3 β were detected as strong interacting proteins (CFs of 0.59 and 1.15).

Similar to the caught members of the membrane-associated complex in 55.1c, α-catenin and E-Cadherin are captured for HepG2 as well. Both are classified as strong interactors with CFs above 0.5.

Five proteins were sorted into the category "transcriptional regulators and factors" for HepG2 cells. One medium, one strong and three very strong PPIs were obtainable. Similar to the received interactors in 55.1c, again eIF4E was captured with a medium strength of interaction (CF = 0.14) and HNF1A, classified as a strong interactor (CF of 1.02). Additionally, three novel interacting proteins were detected with a very strong interaction: The transcription factors FoxO3a (pSer413) (Forkhead box O3) [210-212] and ATF4 (Activating transcription factor 4) [213, 214], as well as the transcriptional repressor Snail [36, 215]. They show CFs between 24.55 and 53.18, but for these three proteins only signals in the bound samples, ranking between 54 and 117 AFI, were measured.

Only one interacting protein captured for HepG2 was assigned to the category "proteins associated with JAK/STAT signaling", which is STAT4. STAT4 was also only detected in the bound sample, not the input sample, with a peak intensity of 52 AFI, which led to its classification as a very strong interactor (CF = 23.64).

4.2.2.4 Interactors of β-catenin in HB35 cells

HB35, a recently established cell line with a known heterozygous β-catenin exon 3 deletion [83], shows a variety of PPIs. This cell line showed in general a high capturing rate for β-catenin, as the BD and the Millipore antibody have CFs of 5.31 (input: 12678 AFI, bound: 13472 AFI) and 5.62 (input: 680 AFI, bound: 764 AFI) (see Table 24). Thus, the input signal for the BD antibody was approximately 1.5 times higher than observed in HepG2 cells. Of the 16 detected interacting proteins, three interactions were classified as low strength, three as medium and 11 as strong or very strong (see Table 24).

Table 24: Co-immunoprecipitated proteins together with β-catenin in HB35.
The CFs and raw values for β-catenin interactors in cell line HB35 are shown. Calculation, representation and sorting were done analog to Table 21.

Analyte	Modification	CF (AFI input/AFI bound)	Captured only in bound sample
Housekeeping proteins			
GAPDH		0.02 (178263/848)	
Proteins comprising the β-catenin destruction complex			
GSK3 α	pTyr279	3.34 (295/197)	

Analyte	Modification	CF (AFI input/AFI bound)	Captured only in bound sample
Proteins comprising the β-catenin destruction complex			
GSK3 β		10.80 (1868/4036)	
GSK3 β	pTyr216	20.76 (204/847)	
Axin1		23.96 (48/230)	
Proteins associated with the membrane-associated β-catenin complex			
β-Actin		0.04 (140755/1250)	
α-catenin		1.14 (350/80)	
E-Cadherin		4.32 (1246/1077)	
Transcriptional regulators and factors			
eIF4E		0.05 (6969/74)	
Src	pTyr527	0.10 (9362/188)	
Smad2		0.78 (598/93)	
cJUN (43 kDa isoform)		1.28 (301/77)	
TCF1		10.69 (29/62)	
TAZ (HD)		15.19 (27/82)	
Snail		84.09 (11/185)	+
Proteins associated with JAK/STAT signaling			
STAT3 (79 kDa isoform, TK # 054)		0.17 (2679/92)	
STAT3 (86 kDa isoform, # 1736)		0.61 (475/58)	
Epigenetic regulators			
LSD1		0.16 (3015/97)	
Tumor markers			
Cytokeratin (~55 kDa, # 0474)		0.01 (140930/277)	

As described in the results for the HepG2 cell line, GAPDH was detected as a weak false positive interactor. Its classification as an interacting protein is explained with the huge signal obtained for the input (178263 AFI) and a carry over into the bound fraction (848 AFI).

Four proteins of the β-catenin destruction complex were detected and rated as strong or very strong PPIs: Phosphorylated GSK3 α (pTyr279) is a strong interactor (CF = 3.34), while GSK3 β, GSK3 β (pTyr216) and Axin1 are very strong interacting proteins, with CFs between 10.80 and 23.96. Thereby a similar distribution, as seen before for 55.1c cells (see 4.2.2.2), was obtained. While

GSK3 α showed a lower CF as GSK3 β, the CF calculated for the activated, phosphorylated form of GSK3 β was even higher.

All three tested proteins, belonging to the group "associated with the membrane-associated β-catenin complex" showed interactions. β-Actin was classified as a weak interacting protein (CF of 0.04), while the CFs for α-catenin and E-Cadherin were high (CF = 1.14 and 4.32), which defined them as strong interactors.

Seven of the detected proteins were assigned to the group of the "transcriptional regulators and factors". eIF4E occurred as a weak interactor (CF of 0.05); Src (pTyr527) was found with a medium strength (CF = 0.10), while Smad2 [178, 216] and the transcription factor cJUN (43 kDa isoform) [36, 217-219] are strong interacting proteins (CFs of 0.78 and 1.28). Three very strong interactors, TCF1 (CF = 10.69) [36, 54, 55], TAZ (HD) (CF = 15.19) and Snail (CF = 84.09) [36, 215] were detected. Interestingly Snail was not detectable in the input sample, but showed a bound signal of 185 AFI.

Two different isoforms of STAT3, detected with two different antibodies, were obtained for HB35 cells: STAT3 (79 kDa isoform, TK # 054), a medium strong interacting protein (CF of 0.17) and STAT3 (86 kDa isoform, # 1736) as a strong interactor (CF = 0.61).

For the 55.1c cells, the epigenetic regulators HDAC2 and Ezh2 were identified as PPIs. Here another epigenetic regulator, the lysine-specific histone demethylase 1A (LSD1) [127, 220], was identified as a medium interactor (CF of 0.16).

One tumor marker was found, which belongs to the Cytokeratin family. Since it represents a weak interaction (CF = 0.01), it might present a weak false positive caused by a carry over (input: 140930 AFI, bound: 848 AFI).

4.2.3 Changes in β-catenin precipitation by drug treatment

As described (see 4.1.2) samples from differently treated cells were generated and compared. The applied inhibitors, CHIR 99021 and MG132, led to changes in the distribution of the available and captured β-catenin variants during Co-IP and the CFs were calculated as described earlier (see 3.4.3).

CHIR 99021 inhibits GSK3 in a highly specific and potent manner [221, 222] and leads to activated Wnt signaling. When Wnt signaling is active, GSK3 is inhibited in general [222]. The inhibition of GSK3 leads to an accumulation of unphosphorylated β-catenin in the cytosol and its further translocation into the nucleus [36]. MG132 on the other side is a potent proteasome inhibitor, which blocks the ubiquitin-proteasomal degradation of ubiquitinated proteins [223, 224]. As β-catenin is among the proteins, targeted towards this degradation pathway [45], it gets enriched together with other proteins using this inhibited degradation way.

Table 25: Caught β-catenin variants and their enrichment after treatment in 70.4.
The CFs and raw values are represented for both treatments in comparison to the untreated sample. Calculation is done analog to Table 18. For some antibodies, no signal was obtained. These were either directly excluded in the table or the cell was marked with "-".

Analyte	Modification	untreated	CHIR 99021	MG132
β-catenin (BD)		18.01 (2596/9349)	30.01 (1239/7437)	44.76 (1519/13598)
β-catenin (Millipore)		24.26 (2434/11812)	38.17 (846/6459)	40.30 (1076/8672)
β-catenin	non-p Ser33/ Ser37/Thr41	66.47 (354/4706)	250.11 (44/2201)	231.54 (52/2408)
β-catenin	pThr41/pSer45	13.75 (20/55)	-	-
β-catenin	pSer552	41.30 (353/2916)	55.86 (181/2022)	89.32 (96/1715)
β-catenin	pSer675	41.31 (572/4726)	67.76 (163/2209)	84.07 (86/1446)

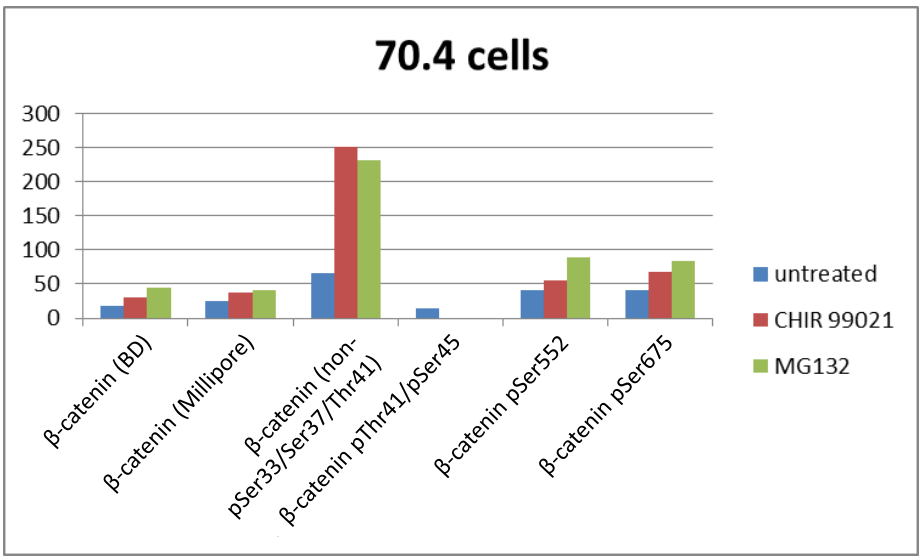

Figure 26: Caught β-catenin variants and their enrichment after treatment in 70.4.
The CFs listed in Table 25, are represented for both treatments (CHIR 99021 in red; MG132 in green) in comparison to the untreated sample (blue). For some antibodies with no signal obtained, no bar is displyed.

Antibodies detecting total β-catenin (BD and Millipore) showed similar capturing rates after both treatments. The raw values reveal that peak intensity decreased after treatment; however, the signal obtained after Co-IP for the bound fraction is proportionately increased. Thus, higher CFs are obtained. Anti-β-catenin non-phospho Ser33/Ser37/Thr41 showed a higher CF (= 66.47), which almost quadruples for CHIR 99021 treatment (CF = 250.11) and is nearly as high after MG132 treatment (CF = 231.54). Only in the untreated sample for the 70.4 cells, the signal for β-catenin pThr41/pSer45 was found above the cutoff limit of 45 AFI (see 4.2.3), for the treated samples, the signals are below this defined limit. Both antibodies recognizing C-terminal phosphorylations of β-catenin (Ser552 and Ser675) recorded an increase after treatment. The increase for MG132

treatment was much higher than for CHIR 99021, although the raw values obtained from the peaks after CHIR 99021 treatment were only slightly higher than for MG132 (see Suppl. Table C).

Table 26: Caught β-catenin variants and their enrichment after treatment in 55.1c.
The CFs and raw values are represented for both treatments in comparison to the untreated sample. Calculation and presentation of data are analog to Table 18.

Analyte	Modification	untreated	CHIR 99021	MG132
β-catenin (BD)		22.68 (14047/63725)	12.21 (15515/37887)	18.11 (20615/74652)
β-catenin (Millipore)		28.51 (969/5525)	21.79 (2955/12880)	33.23 (1320/8773)
β-catenin	non-p Ser33/ Ser37/Thr41	113.33 (48/1088)	109.22 (255/5570)	155.79 (82/2555)
β-catenin	pSer552	47.18 (2497/23560)	28.47 (1114/6343)	41.97 (2206/18517)
β-catenin	pSer675	61.84 (2491/30807)	38.01 (810/6157)	53.34 (1317/14049)

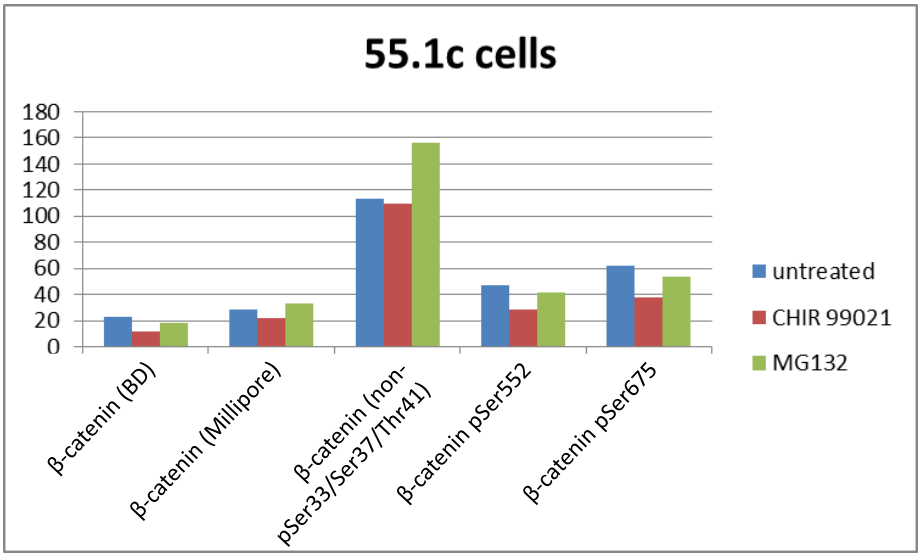

Figure 27: Caught β-catenin variants and their enrichment after treatment in 55.1c.
The CFs listed in Table 26, are represented for both treatments (CHIR 99021 in red; MG132 in green) in comparison to the untreated sample (blue). For some antibodies with no signal obtained, no bar is displayed.

For 55.1c cells, five of the employed β-catenin antibodies gave a signal in the bound fraction. Total β-catenin, detected using the BD antibody, showed a decrease in the detected CF for both treatments. For CHIR 99021 this decrease was also clearly visible in the raw values, which declined from a signal above 60000 AFI to approximately 38000 AFI (see Suppl. Table D). For the MG132 the raw values increased, but the portion of β-catenin captured within the addressed complexes still resulted in a lower CF (= 18.11) for MG132 treatment than for the untreated sample. For the Millipore antibody against the total β-catenin, the signal decreased for the CHIR 99021 treatment, but increased for the MG132 treatment. Looking into the raw data, the CHIR 99021-treated sample

showed a 2.5-fold increase in the recognition of β-catenin in the CHIR 99021-treated sample (~13000 AFI) compared to the untreated sample (~5500 AFI), while for MG132 the obtained signal in the bound stays around 9000 AFI. The CFs derived from the signals of the anti-β-catenin non-phospho Ser33/Ser37/Thr41 were similar for the untreated and CHIR 99021-treated sample (CFs of approximately 100), but for MG132 treatment the CF (= 155.79) was notably increased. The raw values showed a 5.5 times higher value for the obtained bound signal after CHIR 99021 treatment, than for the untreated sample, but also the protein amount measured in the input increased simultaneously. Antibodies against C-terminal phosphorylations showed both for the CFs and the raw values a decrease after CHIR 99021 treatment. For MG132 treatment, the decrease was also existent, but not as strong. The CFs for phosphorylation at Ser675 were higher than for the phosphorylated Ser552 variant.

Table 27: Caught β-catenin variants and their enrichment after treatment in HepG2.
The CFs and raw values are represented for both treatments in comparison to the untreated sample. Calculation and presentation of data are analog to Table 18.

Analyte	Modification	untreated	CHIR 99021	MG132
β-catenin (BD)		2.78 (8037/4464)	15.76 (8021/25290)	27.49 (16848/92633)
β-catenin (Millipore)		2.83 (410/232)	25.10 (1752/8796)	31.36 (1271/7972)
β-catenin	non-p Ser33/ Ser37/Thr41	-	192.13 (108/4150)	142.78 (81/2313)
β-catenin	pSer552	4.30 (2775/2384)	42.79 (303/2593)	104.14 (422/8789)
β-catenin	pSer675	4.61 (2161/1994)	37.52 (159/1193)	75.57 (245/3703)

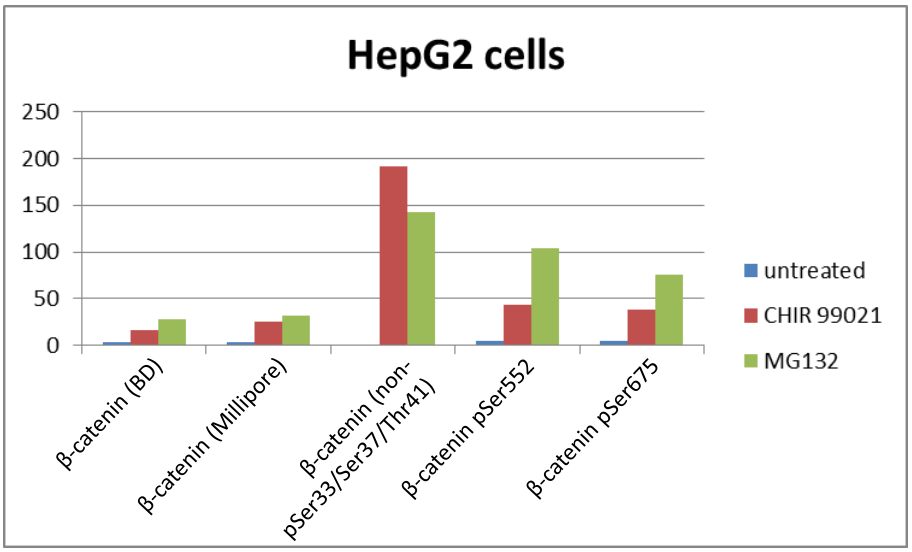

Figure 28: Caught β-catenin variants and their enrichment after treatment in HepG2.
The CFs listed in Table 27, are represented for both treatments (CHIR 99021 in red; MG132 in green) in comparison to the untreated sample (blue). For some antibodies with no signal obtained, no bar is displayed.

The CFs for HepG2 cells were in general lower than for the mouse cell lines. A high increase of β-catenin was observed: The BD antibody showed approximately 5.6 times higher CF for the CHIR 99021 (= 15.76) and a circa 9.9 times higher CF for the MG132 treatment (= 27.49), while the Millipore antibody showed an increase as well, but the difference between the CFs of the two treatments (CF = 25.10 and 31.36) was less pronounced. Non-phosphorylated β-catenin was only detected after treatment. CHIR 99021 treatment led to high values for the CF (= 192.13) and the raw value (4150 AFI, see Suppl. Table E), a lower increase was observed for MG132 (CF = 142.78, 2313 AFI). The CFs for the C-terminal phosphorylated β-catenin variants were eight to ten times higher after CHIR 99021 treatment than without treatment. For MG132 treatment, this factor rose up to 16 to 22 times. Both the CFs and the raw values for the Ser552 phosphorylation show, that a higher amount of this posttranslational modified variant is detected, than of the pSer675 variant.

Table 28: Caught β-catenin variants and their enrichment after treatment in HB35.
The CFs and raw values are represented for both treatments in comparison to the untreated sample. Calculation and presentation of data are analog to Table 18.

Analyte	Modification	untreated	CHIR 99021	MG132
β-catenin (BD)	-	5.31 (12678/13472)	15.54 (2710/8423)	13.42 (12872/34538)
β-catenin (Millipore)	-	5.62 (680/764)	17.38 (401/1394)	19.64 (1098/4313)
β-catenin	non-p Ser33/ Ser37/Thr41	9.75 (40/78)	54.44 (27/294)	106.53 (59/1257)
β-catenin	pSer552	14.56 (2102/6121)	29.81 (212/1264)	25.99 (1166/6061)
β-catenin	pSer675	13.18 (1179/3107)	36.36 (147/1069)	32.41 (497/3222)

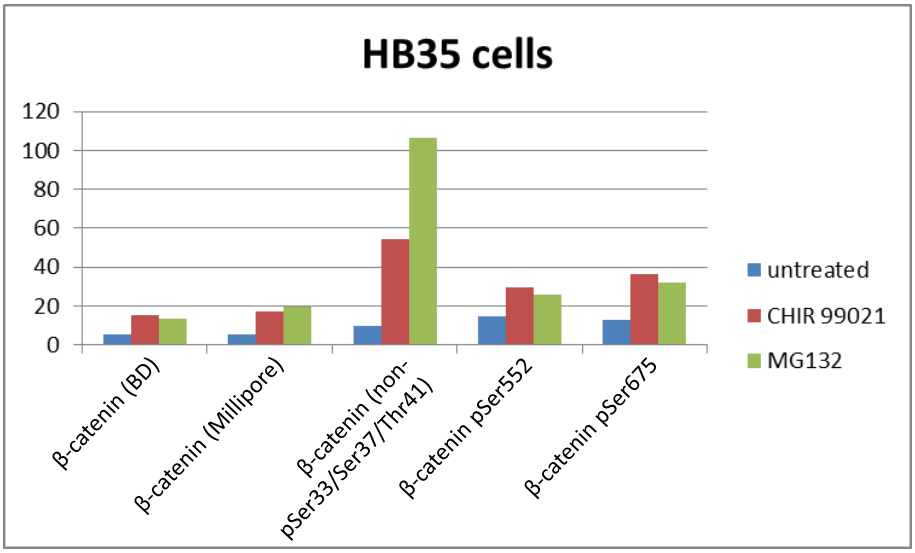

Figure 29: Caught β-catenin variants and their enrichment after treatment in HB35.
The CFs listed in Table 28, are represented for both treatments (CHIR 99021 in red; MG132 in green) in comparison to the untreated sample (blue). For some antibodies with no signal obtained, no bar is displayed.

HB35 cells showed increased CFs for both total anti-β-catenin antibodies after treatment; the CFs in the untreated samples for both analytes were similar (between 5 and 6). Unphosphorylated β-catenin, detected by the non-phospho Ser33/Ser37/Thr41 antibody, showed an increase; the rise after MG132 treatment was approximately double the increase observed for CHIR 99021. The antibodies binding the phosphorylated C-terminus of β-catenin, showed similar CF values for both antibodies, dependent on the treatment. In contrast to the other three cell lines, in HB35 no clear distinction between the two treatments was observed for these two antibodies.

4.2.4 Effect drug treatment on β-catenin protein complex formation

Besides changes in the captured β-catenin pools, changes in the amount of other proteins detected after treatment with CHIR 99021 and MG132 were found. A comparison of the alterations of interaction partners of β-catenin found upon treatment is given below. Interacting proteins, which were detected only after treatment, are discussed in detail. Proteins, which occurred as interactors of β-catenin only in the untreated samples without persisting after treatment, are listed, but are not discussed further. Ratios for the PPIs were calculated as before and the sorting into categories (see 4.2.2.1) was performed analog.

4.2.4.1 Altered protein-protein interactions in cell line 70.4

For cell line 70.4, the capturing of β-catenin increased after treatment (see 4.2.3). For CHIR 99021 the rise of the CF was approximately two (BD antibody) and 1.5 times (Millipore antibody). The increase observed for MG132 was slightly higher: 2.5 times for the BD antibody and 1.7 times for the Millipore antibody. However, the amount of β-catenin available in the input sample, decreased for both treatments (1239 AFI and 846 AFI for CHIR 99021; 1519 AFI and 1076 AFI for MG132) (see 4.2.3, Table 25). 19 interactions were detected, 15 were seen after treatment only, while four were already detected in the untreated sample. The categories for the detected PPIs are shown in Table 29.

Table 29: Co-immunoprecipitated proteins in 70.4 after treatment.
The CFs and raw values for cell line 70.4-specific β-catenin interacting proteins are represented. Calculation, representation and sorting were done analog to Table 21.

Analyte	Modification	untreated	+	CHIR 99021	+	MG132	+
Proteins associated with membranous Wnt signaling							
Wnt11		20.45 (11/45)	+	-		-	
DVL1		-		40.00 (11/88)	+	-	
Evi (50 kDa isoform)		-		-		1.49 (175/52)	
LRP6 (210 kDa isoform, # 1567)	pSer1490	-		-		21.36 (11/47)	+

Analyte	Modification	untreated	+	CHIR 99021	+	MG132	+
Proteins associated with membranous Wnt signaling							
Wnt7b		-		-		31.36 (11/69)	+
DVL2 (# 1739)		-		-		138.64 (11/305)	+
Proteins comprising the β-catenin destruction complex							
CK1 δ		-		1.07 (336/72)		1.61 (615/198)	
APC		26.18 (17/89)		-		-	
GSK3 β		-		-		0.43 (694/60)	
Proteins associated with the membrane-associated β-catenin complex							
β-Actin		4.77 (60390/57646)		0.47 (34895/3304)		0.01 (39159/81)	
α-catenin		7.29 (120/175)		25.48 (21/107)		15.07 (68/205)	
Transcriptional regulators and factors							
GLI1		7.50 (32/48)		-		-	
Elk-1		8.93 (107/191)		-		-	
cJUN (# 1744)	pSer63	-		-		7.68 (56/86)	
cJUN (HD)		-		-		8.15 (84/137)	
Proteins associated with MAPK pathway							
DUSP6		2.56 (160/82)		-		-	
A-Raf		-		21.82 (11/48)	+	-	
Proteins associated with JAK/STAT signaling							
STAT4		28.64 (11/63)	+	35.45 (11/78)	+	24.09 (11/53)	+
STAT3 (86 kDa isoform, # 1736)		-		2.45 (110/54)		473.23 (206/19497)	
STAT3 (79 kDa isoform, # 1736)		-		-		2495.00 (11/5489)	+
Tumor markers							
Vimentin		6.78 (343/465)		0.88 (871/153)		-	
Cytokeratin (~46 kDa # 0474)		-		6.82 (44/60)		-	
Cytokeratin (~55 kDa, # 0474)		-		-		42.05 (73/614)	
Cytokeratin (~60 kDa, # 0588)		-		-		68.93 (2665/36739)	

As a result of CHIR 99021 treatment, DVL1 (dishevelled1) [48, 219, 225] appeared as a new and very strong interacting protein in 70.4 cells (CF of 40). This protein belongs to the category of proteins

being associated with membranous Wnt signaling. MG132 treatment resulted in the identification of four interactors: The 50 kDa isoform of the Evi protein emerged as a strong interactor (CF = 1.49), while LRP6 (pSer1490, 210 kDa isoform, #1567), Wnt7b and DVL2 were classified as very strong PPIs (CFs between circa 20 and approximately 140). Both forms of DVL, DVL1 and DVL2, can link the membrane-bound Wnt receptor complex to the cytosolic β-catenin destruction complex. For all new, very strong interacting proteins, a signal was obtainable only in the enriched bound sample (raw values between 47 and 305 AFI).

APC was the only member of the β-catenin destruction complex detected in 70.4 in untreated cells. After treatment this protein was not seen anymore, but new interactors were detected. Both treatments showed CK1 δ as an interacting protein with a CF above one. GSK3 β was found only in MG132-treated cells, as a medium interactor (CF of 0.43).

The occurrence of α-catenin and β-Actin, participating in the membrane-associated β-catenin complex, was consistent throughout different treatments of 70.4 cells. The CF for α-catenin was circa 3.5 times higher for CHIR 99021 treatment (CF = 25.48) and approximately double for MG132 (CF = 15.07) compared to the untreated sample. The interaction with β-Actin, on the other hand, decreased both for the detected CFs and the obtained raw values. After CHIR 99021 treatment, it still represented a medium interacting protein (CF = 0.47), while for MG132 treatment the PPI is weak (CF = 0.01).

The PPIs obtained for GLI1 and Elk-1, both transcriptional regulators found in the untreated sample, did not reoccur after treatment. cJUN and its activated phospho-variant, cJUN (pSer63), were found to be strong interactors of β-catenin after MG132 treatment (CFs of 7.68 and 8.15) instead.

The DUSP6 interaction in the untreated sample, was not obtained after treatment. Yet, one other protein associated with the MAPK signaling, A-Raf, occurred as a very strong interactor in the CHIR 99021-treated bound sample (CF of 21.82).

STAT4 was only detected in the bound samples as a β-catenin complex partner and not visible in input, yet seen for the treated and untreated bound samples. Additional proteins that appeared as strong or very strong interactors after treatment were the two STAT3 isoforms. The 86 kDa isoform of STAT3 (# 1736) was visible after CHIR 99021 and MG132 treatment as a strong interactor (CF of 2.45) or a very strong interactor (CF = 473.23), while the 79 kDa isoform of STAT3 (# 1736) was a very strong interacting protein only after MG132 treatment (CF = 2495.00). This 79 kDa isoform, only showed a strong signal in the bound sample (5489 AFI), but not in the input.

Vimentin remained as a strong interacting protein (decreased CF of 0.88 after CHIR 99021 treatment), but disappeared for MG132 treatment. Two different peaks were measured in the differently treated cells for the Cytokeratin Pan (# 0474) antibody. For CHIR 99021 the Cytokeratin with a MW of ~46 kDa represented a strong interactor (CF = 6.82), while the interaction for

the ~55 kDa-sized Cytokeratin was increased for MG132 and classified as very strong (CF = 42.05). Additionally, another Cytokeratin (~60 kDa, # 0588) was rated as a very strong PPI (CF = 68.93) in the MG132-treated sample.

4.2.4.2 Modulation of β-catenin interactions in 55.1c by drug treatment

In 55.1c cells a decrease in the capture of β-catenin after treatment was observed for CHIR 99021 and MG132. The CF for CHIR 99021 dropped to 0.5 (BD antibody) and to 0.8 (Millipore antibody). MG132 resulted in a 0.8 fold decrease (BD antibody), while the Millipore antibody detected a 1.2 times increase. Both treatments measured an increase in the obtained raw values (see 4.2.3, Table 26). 13 PPIs were detected only after treatment and 17 interactions, which already occurred in the untreated sample, could be confirmed. The interacting proteins were assigned to seven of the eight categories (see 4.2.2.2); no interactions with the "epigenetic regulators" were found.

Table 30: Co-immunoprecipitated proteins in 55.1c after treatment.
The CFs and raw values for cell line 55.1c-specific β-catenin interacting proteins are represented. Calculation, representation and sorting were done analog to Table 21.

Analyte	Modification	untreated	+	CHIR 99021	+	MG132	+
Proteins associated with membranous Wnt signaling							
Evi (60 kDa isoform)		4.49 (503/452)		10.80 (193/417)		12.17 (254/618)	
Wnt7b		38.36 (70/537)		181.63 (135/4904)		38.18 (11/84)	+
LRP6 (# 1750)	pSer1490	5.78 (58/67)		-		-	
Wnt3a		47.73 (11/105)	+	-		-	
Evi (50 kDa isoform)		-		18.88 (209/789)		-	
Frizzled4		-		-		10.51 (4960/10430)	
Proteins comprising the β-catenin destruction complex							
GSK3 α	pTyr279	8.56 (436/746)		20.23 (22/89)		3.38 (312/211)	
GSK3 β		10.97 (3653/8018)		5.72 (2442/2795)		4.84 (2856/2767)	
CK1 α		2.32 (480/223)		1.31 (360/94)		-	
GSK3 β	pTyr216	15.09 (696/2100)		-		5.42 (493/534)	
Axin1		75.80 (50/758)		-		40.39 (38/307)	
APC		11.74 (23/54)		-		-	
Axin2 (# 1724)		40.91 (11/90)	+	-		-	

Analyte	Modification	untreated	+	CHIR 99021	+	MG132	+
Proteins associated with the membrane-associated β-catenin complex							
α-catenin		16.20 (888/2878)		7.77 (968/1504)		18.88 (732/2764)	
E-Cadherin		21.31 (781/3328)		6.27 (1191/1493)		11.39 (1102/2511)	
β-Actin		-		13.24 (176674/467673)		12.13 (138494/335905)	
Transcriptional regulators and factors							
HNF1A		1.61 (1211/391)		2.68 (288/122)		6.06 (726/880)	
TCF4 (60 kDa isoform, # 1727)		133.64 (11/294)	+	8.29 (234/388)		11.70 (227/531)	
Smad5		1.32 (355/94)		1.00 (902/181)		-	
Smad3 (# 0879)		1.53 (618/189)		0.25 (2394/119)		-	
Src		2.02 (9241/3738)		1.35 (4022/1085)		-	
TAZ		14.09 (3726/10502)		-		25.43 (58/295)	
Src	pTyr527	-		1.62 (2982/968)		0.68 (4024/550)	
Elk-1		-		18.46 (742/2740)		18.74 (428/1604)	
Src	pTyr416	-		39.71 (17/135)		10.20 (25/51)	
eIF4E		0.11 (8820/189)		-		-	
Smad4		0.93 (387/72)		-		-	
TCF4 (70 kDa isoform, # 1481)		12.83 (30/77)		-		-	
ATF4		-		381.36 (11/839)	+	-	
Proteins associated with MAPK pathway							
DUSP1		-		27.20 (1236/6724)		25.30 (926/4686)	
JNK/SAPK (54 kDa isoform)		1.52 (256/78)		-		-	
MKK7		2.44 (166/81)		-		-	
A-Raf		2.94 (240/141)		-		-	
MAPKAPK-5		4.45 (64/57)		-		-	
MDM2 (60 kDa isoform)		10.47 (43/90)		-		-	
DUSP6		11.29 (831/1876)		-		-	
DUSP9		-		1210.00 (11/2662)	+	-	
DUSP4		-		-		6.46 (4590/5930)	

Analyte Modification	untreated	+	CHIR 99021	+	MG132	+
Proteins associated with JAK/STAT signaling						
STAT3 (79 kDa isoform, TK # 054)	0.42 (862/73)		0.31 (761/47)		-	
Tumor markers						
Vimentin	16.38 (7346/24060)		25.05 (2818/14117)		16.49 (2763/9111)	
Cytokeratin (~46 kDa, # 0474)	65.33 (92/1202)		0.76 (8223/1257)		0.31 (10909/682)	
Cytokeratin (~60 kDa, # 0588)	-		5.00 (24510/24522)		-	
Cytokeratin (~55 kDa, # 0474)	-		-		23.35 (403/1882)	

After CHIR 99021 treatment both isoforms of Evi occurred as very strong interacting proteins (CF = 18.88 and 10.80) in the category of "proteins associated with the membranous Wnt signaling". The 60 kDa isoform was detected in the untreated sample and occurred after MG132 treatment as a very strong interactor, while the 50 kDa variant is only present in the CHIR 99021-treated sample. Wnt7b was an interactor, which appeared in all three conditions. For CHIR 99021 treatment, a five-fold increase (CF = 181.63) was seen, while MG132 caused no changes in the calculated CF. It has to be noted, that MG132 caused a strong drop in absolute signal of Wnt7b. Frizzeld4, a central regulator in the Wnt pathway [150, 226, 227], was detected as a very strong interactor (CF of 10.51) after MG132 treatment. Frizzled4 was also detectable in the other samples with a strong interaction, but the signals were eliminated from further analysis due to the defined cutoff criteria (see 3.4.3.3).

Five of the seven PPIs, participating in the β-catenin destruction complex, seen in the untreated sample, reappeared as interacting proteins after one or both treatments. Phosphorylated GSK3 α showed a strong increase after CHIR 99021 treatment and is classified as a very strong interactor (CF = 20.23). For MG132 the obtained CF was reduced, but it still remained as a strong interactor (CF = 3.38). The phosphorylated GSK3 β was detected after MG132 treatment, but not after CHIR 99021 application (strong interactor (CF = 5.42)). This is similar to GSK3 β, were the measured CF decreased for both treatments, but the interaction still remained strong (CFs of 5.72 and 4.84). CK1 α and Axin1 occurred only for one of the treatments each: CK1 α was detected after CHIR 99021 application as a strong interactor (CF of 1.31), while Axin represented a very strong PPI in the MG132-treated sample (CF of 40.39).

Both E-Cadherin and α-catenin interactions were found in the treated samples. The CF decreased for both proteins after CHIR 99021 treatment and classified them as strong interactors. For α-catenin the CF increased slightly after MG132 treatment compared to the untreated sample. On the other hand, it decreased for E-Cadherin; however, both remained very strong interactors, according to their CFs above 10.

In the category “transcriptional regulators and factors” four new interactions after treatment were detected. HNF1A remained a strong interactor, which increased for CHIR 99021 (CF = 2.68) and further for MG132 treatment (CF = 6.06). The CF for TCF4 (# 1727) decreased after treatment, since it was now already detectable in the input sample. Thus, the calculated ratio was smaller, but it remained as a very strong interactor after MG132 treatment, while it was classified only as a strong interactor for CHIR 99021 treatment. Smad5 and Src represent strong interacting proteins, which remained after CHIR 99021 with only a minor decrease (CF = 1.00 vs. 1.32 and 1.35 vs. 2.02), but disappeared after the application of MG132. Smad3 (# 0879) was seen after CHIR 99021 treatment, but the CF dropped to 0.25 and did not qualify it as a strong interactor anymore. This interacting protein didn’t appear after MG132 treatment. TAZ on the other side was not detectable after CHIR 99021 treatment, but MG132 led to an increased CF of 25.43. Besides the total Src, also phosphorylated variants were detected as strong or very strong interactors after both treatments. The inactive version, phosphorylated at Tyr527, showed high signals in the raw values, but the capturing rates were low (CF = 1.62 and 0.68). Src, phosphorylated at Tyr416, represents the active variant of the kinase. Here higher CFs are derived, especially after CHIR 99021 treatment (CF = 39.71). Elk-1 was a very strong interactor for both treatments, but not detectable in the untreated sample. The CFs were slightly above 18 in both cases. Additionally, ATF4 appeared after CHIR 99021 treatment as interacting protein. It occurred as a protein, which is only detectable in the bound sample with 839 AFI as a very strong interactor (CF = 381.36).

None of the earlier occurring PPIs associated with the MAPK pathways, were detected again after treatment. But three new interacting proteins were found: for both treatments DUSP1 was a very strong interactor; DUSP9 was detected as a very strong interactor after CHIR 99021 treatment, whereas DUSP4 was seen as a strong interactor after MG132 treatment. The raw values revealed, that DUSP1 was already detected in the untreated sample, but was eliminated based on the defined cutoff limits. DUSP9 showed no signal in the input sample, but a huge peak in the bound sample after CHIR 99021 treatment (2262 AFI), which resulted in an enormous CF of 1210.00. DUSP4 remained only for the MG132-treated cells as an interactor, although the obtained raw values were similar for all treatments, but the earlier mentioned cutoff limits (see 3.4.3.3) removed this protein as an interactor of β-catenin before calculating a CF for the other treatments.

STAT3 (79 kDa isoform, TK # 54) remained as a medium interactor after CHIR 99021 treatment (CF of 0.31), being assigned to the group of proteins associated with JAK/STAT signaling.

The capturing rate for the EMT marker Vimentin stayed unchanged for MG132 treatment compared to the untreated sample (CF = 16.38 vs. 16.49), but an increase through the application of CHIR 99021 (CF = 25.05) was detected. In all conditions, it represented a very strong interacting protein. Various Cytokeratins were measured after treatment. The very strong interaction of

Cytokeratin (~46 kDa, # 0474) in the untreated sample, decreased to a strong interaction in the CHIR 99021-treated (CF = 0.76) and even further in the MG132-treated sample (medium interaction; CF = 0.31). Additionally, two other Cytokeratins were detected: Cytokeratin (~60 kDa, # 0588), as a strong interacting protein after CHIR 99021 treatment (CF = 5.00), and Cytokeratin (~55 kDa, # 0474), as a very strong interactor after MG132 treatment (CF = 23.35). As described above for the DUSPs, again high signals were obtained for the Cytokeratins also in the remaining treatments, but were eliminated, because of the determined cutoff levels (see 3.4.3.3).

4.2.4.3 Modification of β-catenin interactions in HepG2 after drug treatment

In HepG2 cells frequently a rise in both, the CFs after treatment and the obtained raw values of β-catenin are observed. The increase of the CF was approximately five to eight fold after CHIR 99021 treatment and ten fold for MG132 for both antibodies detecting total β-catenin (BD and Millipore). The PPIs detected here, were classified in nine groups. The category six, eight and nine were newly added, as proteins assigned to these groups were occuring after treatment. 14 novel proteins were found and five reoccurring interactors from the untreated sample were detected (see 4.2.2.3).

Table 31: Co-immunoprecipitated proteins in HepG2 after treatment.
The CFs and raw values for cell line HepG2-specific β-catenin interacting proteins are represented. Calculation, representation and sorting were done analog to Table 21.

Analyte	Modification	untreated	+	CHIR 99021	+	MG132	+
Proteins associated with membranous Wnt signaling							
Evi (60 kDa isoform)		-		3.27 (124/81)		6.32 (288/364)	
LRP6 (180 kDa isoform, # 1567)	pSer1490	24.09 (11/53)	+	-		-	
Wnt7b		32.27 (11/71)	+	-		-	
Proteins comprising the β-catenin destruction complex							
GSK3 β		0.59 (2085/244)		2.95 (1072/632)		12.05 (1873/4515)	
GSK3 β	pTyr216	1.15 (278/64)		4.75 (61/58)		19.50 (239/932)	
CK1 δ		0.27 (867/46)		-		-	
Axin2 (98 kDa isoform, # 0956)		-		20.00 (12/48)		-	
GSK3 α	pTyr279	-		-		8.37 (181/303)	
Axin2 (95 kDa isoform, # 0956)		-		-		8.38 (40/67)	
Axin1		-		-		52.73 (11/116)	+

Analyte	Modification	untreated	+	CHIR 99021	+	MG132	+
Proteins associated with the membrane-associated β-catenin complex							
α-catenin		0.55 (1200/133)		6.64 (229/304)		6.67 (576/768)	
E-Cadherin		1.64 (679/223)		4.69 (533/500)		14.91 (1235/3683)	
β-Actin		-		-		0.16 (144040/4539)	
Transcriptional regulators and factors							
HNF1A		1.02 (293/60)		2.30 (816/375)		1.71 (924/316)	
TCF4 (60 kDa isoform, # 1481)		-		16.40 (43/141)		60.19 (52/626)	
eIF4E		0.14 (1930/54)		-		-	
FoxO3a	pSer413	24.55 (11/54)	+	-		-	
ATF4		41.82 (11/92)	+	-		-	
Snail		53.18 (11/117)	+	-		-	
TCF4 (70 kDa isoform, # 1481)		-		-		14.91 (53/158)	
TCF1		-		-		128.64 (11/283)	+
Proteins associated with MAPK pathway							
JNK/SAPK		-		-		1.88 (309/116)	
Proteins associated with JAK/STAT signaling							
STAT3 (79 kDa isoform, # 1736)		-		3.66 (1778/1303)		25.92 (2318/12015)	
STAT4		23.64 (11/52)	+	-		-	
Epigenetic regulators							
LSD1		-		0.66 (881/116)		0.48 (1758/170)	
Tumor markers							
Cytokeratin (~60 kDa, # 0588)		-		-		1.49 (196115/585144)	
Vimentin		-		-		14.00 (20/56)	

LRP6 (180 kDa isoform, # 1567) and Wnt7b defined as very strong interactors, yet with low absolute measured signals, were not found after treatment. An isoform of the Evi protein appeared newly as a strong interactor in the "membranous Wnt signaling" category that responded to CHIR 99021 and MG132 treatment. Its capturing rate was higher after MG132 treatment (CF of 6.32) than after CHIR 99021 treatment (CF = 3.27).

Two of the three interactors detected in the untreated sample classified as members of the β-catenin destruction complex, occurred after treatment. The CFs for GSK3 β and GSK3 β (pTyr216) showed a four- to five-fold rise after CHIR 99021 treatment and remained as strong interactors, while under MG132 treatment they increased further and represented very strong interactors (CF = 12.50 and 19.50). Several interactors were only detected for one of the treatments. The 98 kDa isoform of Axin2 was identified as very strong interactor after CHIR 99021 treatment (CF = 20.00). Three interacting proteins were only measured in the MG132-treated sample: the GSK3 α (pTyr279) as a strong interactor (CF of 8.37); the 95 kDa isoform of Axin2, a strong interacting protein (CF = 8.38) and Axin1 as a very strong PPI (CF = 52.73), which is only measurable in the bound sample.

A strong interaction for α-catenin and E-Cadherin was seen. The CFs for α-catenin were very similar after CHIR 99021 and MG132 treatment (CF = 6.64 and 6.67, representing a 12-fold change compared to the untreated sample). For E-Cadherin, a three-fold rise after CHIR 99021 treatment was seen and after MG132 the CF was more than nine times higher. That classified E-Cadherin as a strong interactor for CHIR 99021 (CF = 4.69) and a very strong interactor for MG132 treatment (CF = 14.91). In addition, β-Actin was captured as a medium interacting protein (CF of 0.16) for the MG132-treated samples.

Among the group of “transcriptional regulators and factors”, HNF1A was detected with an increased capturing rate after both treatments. It remained a strong interactor for both, CHIR 99021 (CF = 2.30) and MG132 treatment (CF = 1.71). TCF1 and TCF4 detected by different antibodies were the newfound PPIs after treatment. The 60 kDa isoform of TCF4 was seen for both treatments with CFs of 16.40 and 60.19 indicating a very strong interaction, while the 70 kDa isoform was visible only for the MG132-treated sample again as a very strong interactor (CF = 14.91). TCF1 only occurred as complex partner of β-catenin in the bound sample of the MG132-treated sample, representing another very strong PPI (CF of 128.64, obtained raw value of 283 AFI).

JNK/SAPK, the only protein occurring as associated to the MAPK pathway, appeared only after MG132 application as a strong interacting protein of β-catenin (CF of 1.88).

STAT3 was seen as a new strong PPI for the HepG2 cell line after CHIR 99021 treatment (CF = 3.66) and increased to a very strong interactor with a factor of approximately seven for MG132 treatment (CF = 25.92).

The epigenetic regulator LSD1 was caught as an interacting protein. For CHIR 99021 this interaction was classified as strong (CF of 0.66), while the capturing rate decreased for MG132 treatment and the interaction was rated as a medium one (CF = 0.48).

After MG132, treatment two different tumor markers were precipitated together with β-catenin in HepG2 cells. Cytokeratin (~60 kDa, # 0588) was detected as a strong interactor (CF of 1.49) and Vimentin as a very strong interacting protein (CF = 14.00).

4.2.4.4 Changed protein-protein interactions in HB35 by drug treatment

In HB35 cells CHIR 99021 treatment led to a decrease in the total amount of β-catenin detected for both antibodies targeting total β-catenin (BD and Millipore). For MG132, the amount of β-catenin stayed similar for the BD antibody, while the Millipore antibody showed an increase. The CFs in turn increased approximately three times after CHIR 99021 and MG132 treatment for both antibodies (see 4.2.3, Table 28). In the treated HB35 sample, nine induced and five known interaction partners (see 4.2.2.4) were seen and sorted into the six groups (see 4.2.2.1). The last group, comprising the tumor markers, was excluded here as no interacting proteins were detected after treatment.

Table 32: Co-immunoprecipitated proteins in HB35 after treatment.
The CFs and raw values for cell line HB35-specific β-catenin interacting proteins are represented. Calculation, representation and sorting were done analog to Table 21.

Analyte	Modification	untreated	+	CHIR 99021	+	MG132	+
Proteins associated with membranous Wnt signaling							
DVL1		-		21.36 (11/47)	+	28.18 (11/62)	+
Evi (60 kDa isoform)		-		9.31 (29/54)		-	
LRP6 (180 kDa isoform, # 1567)	pSer1490	-		-		14.25 (20/57)	
Proteins comprising the β-catenin destruction complex							
GSK3 β		10.80 (1868/4036)		0.77 (397/61)		0.93 (1113/208)	
GSK3 α	pTyr279	3.34 (295/197)		-		-	
GSK3 β	pTyr216	20.76 (204/847)		-		-	
Axin1		23.96 (48/230)		-		-	
Proteins associated with the membrane-associated β-catenin complex							
α-catenin		1.14 (350/80)		8.53 (112/191)		7.59 (1198/1819)	
E-Cadherin		4.32 (1246/1077)		11.99 (78/187)		9.77 (328/641)	
β-Actin		0.04 (140755/1250)		-		-	
Transcriptional regulators and factors							
HNF1A		-		4.50 (90/81)		15.56 (45/140)	
eIF4E		0.05 (6969/74)		-		-	
Src	pTyr527	0.10 (9362/188)		-		-	
Smad2		0.78 (598/93)		-		-	
cJUN (43 kDa isoform)		1.28 (301/77)		-		-	
TCF1		10.69 (29/62)		-		-	

Analyte	Modification	untreated	+	CHIR 99021	+	MG132	+
Transcriptional regulators and factors							
TAZ (HD)		15.19 (27/82)		-		-	
Snail		84.09 (11/185)	+	-		-	
cJUN (# 1162)	pSer63	-		-		1.93 (135/52)	
Smad5		-		-		5.00 (45/45)	
Bcl9		-		-		32.73 (11/72)	+
Proteins associated with JAK/STAT signaling							
STAT3 (79 kDa isoform, TK # 054)		0.17 (2679/92)		-		0.40 (870/70)	
STAT3 (86 kDa isoform, # 1736)		0.61 (475/58)		-		-	
STAT3 (79 kDa isoform, # 1736)		-		4.26 (685/583)		-	
Epigenetic regulators							
LSD1		0.16 (3015/97)		-		-	
HDAC6		-		-		1.21 (194/47)	

Proteins associated with the membranous Wnt signaling arose only after treatment. DVL1 occurred for both treatments as a very strong interactor (CF between 20 and 30). Signals were only obtained in the bound samples each (AFIs of 47 and 62). For CHIR 99021 treatment, Evi (60 kDa isoform) occurred as a strong interacting protein belonging to this group (CF of 9.31). LRP6 (pSer1490, 180 kDa isoform, # 1567) represented a very strong interactor of β-catenin after MG132 treatment (CF = 14.25).

Only one of the interacting proteins participating in the β-catenin destruction complex, measured in the untreated sample reoccurred after treatments, which is GSK3 β. Classified as a very strong interactor in the untreated sample, it still remained as a strong interactor after treatments, but the CF was decreased more than ten times to 0.77 for CHIR 99021 and 0.93 for MG132.

Both α-catenin and E-Cadherin reappeared with an increased CF after treatment. For α-catenin the CF rose for both treatments by a factor of approximately 7 (CF = 8.53 and 7.59). The CF for E-Cadherin in the CHIR 99021-treated classified it as a very strong interactor (CF = 11.99), while it was increased for MG132 as well, but stayed a strong interacting protein (CF of 9.77).

None of the PPIs, defined as “transcriptional regulators and factors”, detected for the untreated HB35 sample recurred after treatment. With HNF1A a strong interactor / very strong interactor (CF of 4.50 after CHIR 99021 treatment; CF of 15.56 after MG132 treatment) was found. Additionally, two strong and one very strong interactor occurred for the MG132 treatment. As strong interactors,

the phosphorylated cJUN (CF = 1.93) and Smad5 (CF = 5.00) were measured, while Bcl9 [36, 64, 228], the B-cell CLL/lymphoma 9 protein, was found an interaction partner of β-catenin for the first time. It appeared only in the MG132-treated, bound sample (72 AFI) as a very strong PPI (CF = 32.73).

STAT3 (79 kDa isoform, TK # 054) appeared as a medium interactor, with a slightly increased CF of 0.40 after MG132 treatment. In addition, STAT3 (79 kDa isoform, # 1736) a new isoform of STAT3 was detected as a strong interactor (CF = 4.26).

One protein, HDAC6 [229-231], assigned to the group of "epigenetic regulators", was captured in HB35 cells after MG132 treatment. HDAC6 belongs to the cytosolic histone deactylases and is able to deacetylase β-catenin directly. It represents a strong interactor (CF of 1.21). No PPIs, belonging to this category, were obtained after application of CHIR 99021.

4.2.5 Summary

Differences in between the cell lines appear for the different amounts of β-catenin detected by various antibodies after Co-IP and additionally after treatment (see 4.2.1 and 4.2.3). These differences can be obtained for the CFs as well. In general, antibodies against total β-catenin achieved higher raw signal intensities both for the untreated samples as well as after drug treatment. On the other hand, the CFs for the phosphorylated variants of the protein are increased in comparison to the CFs received by the antibodies detecting total β-catenin, although the raw values show a lower signal intensity. The signal intensity of the raw values for the detected β-catenin decrease generally after treatment, while the derived CFs normally rise. It can be assumed, that a higher portion of the different β-catenin variants were captured during Co-IP, although the treatment caused a decrease in the raw values.

All cell lines showed major differences in the precipitated interaction partners of β-catenin (see 4.2.2), both among each other and upon drug treatment. They all share, that proteins belonging to various well-known β-catenin-complexes were identified but vary in the individual proteins detected. The variation among the cell lines is increased after treatment (see 4.2.4).

By the possibility of covering a signaling cascade and its spatial cellular surrounding with antibodies, links to other important pathways, such as the MAPK pathway, as well as the identification of unknown crosstalks in between signaling pathways, are enabled. Additionally, the ability of screening for a multitude of potential PPIs and PTMs of these proteins, might lead to new insights into the cellular network. The huge differences observed for the chosen cell lines and the two treatments were not expected to this extent, but employing this novel screening approach to illustrate these differences will allow to gain a deeper understand of the cellular signaling network in the long run.

4.3 Immunoprecipitation with high-affinity nanobody

For the development of a novel way of detecting intracellular PPIs, two fundamental experimental conditions were changed: First, the cell line employed for performing the Co-IP was changed; HEK293T providing a more general cell model for the extracellular Co-IP (ECIP). Second, the capturing antibody was replaced by a high-affinity, β-catenin-specific nanobody. The employed capturing molecule BC1 binds β-catenin at the N-terminal region, targeting aa 61 – 87; a different epitope than the antibody that was used during the described immunoprecipitations (see 4.2). This approach uses the possibility to perform intracellular Co-IPs (ICIPs) for the first time (see 4.4). The properties of the nanobody BC1 in Western blots have been tested [112] and in a first step the comparability between the conventional Western blot approach and the DigiWest was tested. As control for the ECIP, a nanobody-specific for GFP (GFP-Nanotrap®) was employed.

The analysis of HEK293T cells treated with CHIR 99021 were included. The nanobody BC1 has a preference for binding β-catenin, which is unphosphorylated at the SSTS-motif; thus it seems to be particularly well suitable as a capturing molecule during Co-IP on CHIR 99021-treated cell lysates. The ability to screen for treatment-induced differences in the occurring β-catenin complexes seemed to be promising.

4.3.1 Comparison between classical Western blot and DigiWest

To compare the signals obtained in Western blots with signals received by the novel DigiWest approach, both approaches were used for sample analysis and detection of PPIs. Aliquots of the samples, generated by Co-IP employing the nanobody BC1 or the GFP-Nanotrap®, were applied to different gels and processed in Western blot and DigiWest individually. Antibodies against the Co-IP-target protein β-catenin and well-known interactors like α-catenin, GSK3 β, TCF1 and Axin2, as well as the housekeeping protein, GAPDH, as control, were used for the comparison. Figure 30 A shows the results obtained for the classical Western blot next to the bar graphs, resulting from the DigiWest (Figure 30 B). In addition, the DigiWest bar graphs were transformed into grayscale Western blot mimics (see Figure 30 C), as described in 3.4.2, to give a more familiar, Western blot alike, visual impression of the obtained results.

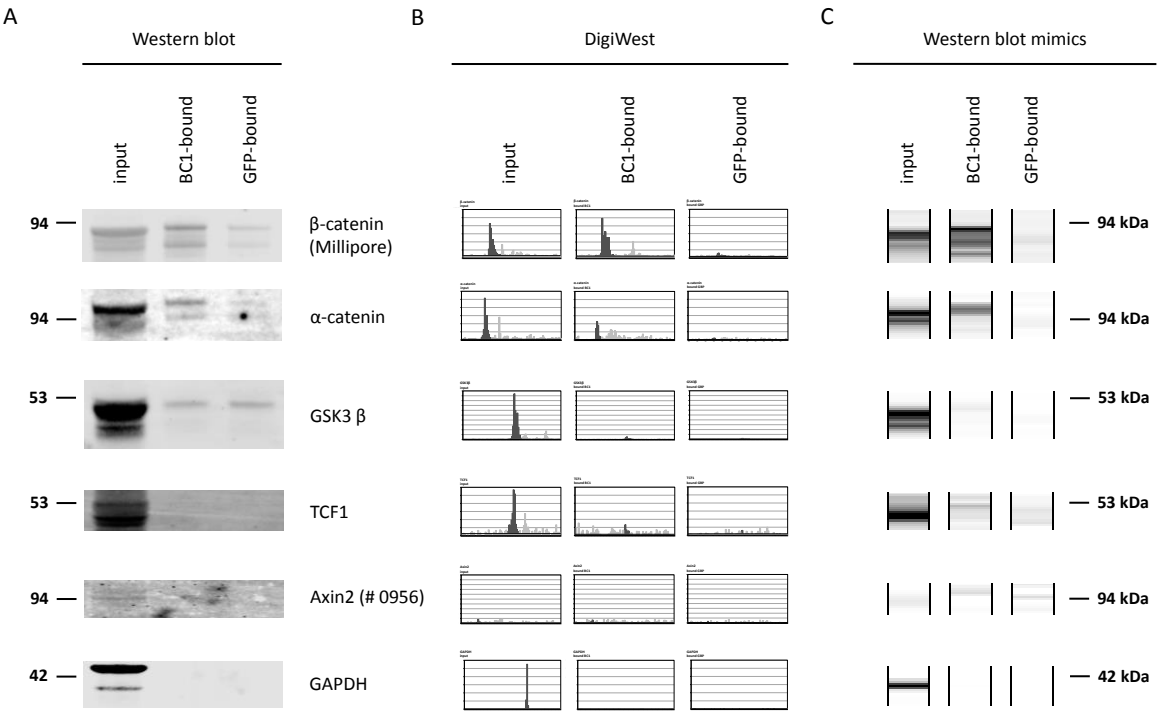

Figure 30: Direct comparison between conventional Western blot, digitalized Western blot and Western blot mimics.
Direct comparison between the same samples on conventional Western blot (A) and the DigiWest (B,C) is represented. The bar graphs of the digitalized Western blot (B) and after transforming the obtained AFI values into Western blot mimics (C) are shown.
Co-IP was performed with an anti-β-catenin nanobody, called BC1, or an unspecific nanobody recognizing GFP as a negative control. Besides the target protein β-catenin, various antibodies are presented: α-catenin, GSK3 β, TCF1 and Axin2 represent known interacting proteins of β-catenin, while GAPDH serves as a negative control. For the DigiWest bar graphs (B), the molecular weight between ~15 kDa and ~300 kDa is plotted on the x-axis, while the signal intensity is shown on the y-axis, as explained in Figure 10 in detail. The signal maxima for the different antibodies differ, thus for β-catenin it is defined at 1200 MFI, for α-catenin at 300 MFI, for GSK3 β at 2000 MFI, for TCF1 at 120 MFI, for Axin2 at 200 MFI and for GAPDH at 30000 MFI.

As it was difficult to directly compare the Western blot lanes Figure 30 A with the DigiWest bar graphs Figure 30 B, it was very helpful to have digitalized Western blot mimics Figure 30 C, which visualize the similarity between the individual antibodies. The target protein β-catenin showed intense lanes for the input and BC1-bound sample both in the conventional Western blots and the Western blot mimics. In addition, the side bands observed for the BC1-bound sample were visible and show a high similarity in all three representations. A low, unspecific signal for β-catenin in the control sample can be seen in both approaches as well. For α-catenin similar observations can be made: A strong signal in the input sample is received, while a lower one in the BC1-bound. The GFP-bound serves as a negative control, without any visible signal. For GSK3 β, the signals seem to differ slightly between Western blot and DigiWest, as the Western blot shows a low signal in both bound lanes and the DigiWest seems to show no signal in the bound lanes at all. A closer inspection of the raw data reveals a measured signal of 368 AFI (BC1-bound) and 117 AFI (control bound), which is not easily visible in the Western blot mimics (see Suppl. Table G).

TCF1 and Axin2 show no signal in the Western blot and the DigiWest; for Axin2 already in the input lane no signal is measurable. GAPDH, serving as negative control for the Co-IP, shows no signal in any of the bounds, neither in Western blot nor in the DigiWest.

One of the main advantages of the DigiWest is the easy obtainment of semi-quantitative intensity values, which can be used for further analysis. In order to compare these values to the signals obtained during the conventional Western blot, a densiometrical analysis was done, employing the Image Studio v4 software. For antibodies with measurable signals in both approaches, the ratio of input or BC1-bound values over the corresponding GFP-bound was calculated (data not included in this work). For TCF1 and Axin2 this was not possible, as there was no measurable signal in one of the approaches. Thus, these antibodies were not included in further calculations. The calculation showed similar fold changes for both approaches and indicated good comparability of both methods.

Based on these results, a wider ranging analysis of the immunoprecipitation was performed to identify further interaction partners. A set of 75 antibodies was screened on the samples (two replicas existing of input, BC1-bound and GFP-bound each). The antibodies are marked in the appendix (see Suppl. Table A) with "**". The duplicate samples were screened for PPIs with β-catenin, but as duplicates were used, the cutoff limits were adjusted as described in detail in 3.4.3.3, in order to make sure that no false positive interactions were picked up. As a result all peaks showing a signal intensity above 45 AFI were evaluated as specific signals. In addition, the sum of the duplicate signals had to be above 90 AFI with a deviation of smaller or equal to 10 AFI between individual signals, to guarantee stability among the replicas. Signals of proteins that bound unspecific to the immunoprecipitation matrix were identified and excluded from analysis by defining a specificity limit; a signal intensity of at least 1.5-fold above the negative control for an individual peak qualified a peak as specific. In addition, the sum of both individual ratios had to be above 2.9 with a deviation of the single ratios below 0.2, which led to a higher consistency in between the different replicas. For calculating the average of the CFs, the formula, described in 3.4.3.3, Equation 3, was applied to each individual replica and the mean was taken afterwards. All CFs for the duplicates, along with the obtained raw values for the different input and bound samples, are listed in the appendix (see Suppl. Table G).

During these experiments, it was possible to detect different β-catenin variants (see 4.3.2) and to define 21 proteins interacting with β-catenin in HEK293T cells (see 4.3.3 and 4.3.4).

4.3.2 Detection of different β-catenin variants

In analogy to chapter 4.2.1 the different β-catenin pools detected by different antibodies were viewed first. The capturing nanobody detects β-catenin preferably at an unphosphorylated epitope close to the N-terminally SSTS-motif. Therefore, the addressed β-catenin pools might differ from those, detected after precipitating with an antibody recognizing the C-terminus. Besides the same β-catenin antibodies as tested in previous experiments, an antibody against total β-catenin (8E7) was added. This monoclonal antibody recognizes β-catenin N-terminally (aa 36 – 44). To evaluate the amount of each precipitated β-catenin variant, the CFs were calculated (see Table 33).

Table 33: Caught β-catenin variants during ECIP on untreated and CHIR 99021-treated HEK293T cells.
The capturing rate is represented for the untreated sample and after CHIR 99021 treatment. For calculating the average of the CFs, the formula described in 3.4.3.3, Equation 3, was applied to each individual replica. Subsequently the mean of the duplicate was calculated. The different β-catenin variants detected, were sorted in an ascending order referring to their average CF obtained for the untreated sample. β-catenin variants, which were only detected in the bound sample, are marked with a "+". For one antibody no signal was obtained without treatment. This cell was marked with "-".

Analyte	Modification	untreated	+	CHIR 99021	+	increase (fold change)
β-catenin	pSer675	3.98		17.30		4.35
β-catenin (BD)		5.56		21.57		3.88
β-catenin	pSer552	6.47		91.07		14.08
β-catenin (Millipore)		7.60		36.29		4.78
β-catenin	non-p Ser33/ Ser37/Thr41	8.76		156.00		17.81
β-catenin (8E7)		-		3800.23	+	> 80

Two antibodies directed against total β-catenin were used (BD and Millipore), showing similar capturing rates in the untreated sample (CF = 5.56 and 7.6) and also a similar increase after CHIR 99021 treatment. For both an approximately four- to five-fold rise was observed, which led to a CF of 21.57 and 36.29 after treatment. Two antibodies directed against C-terminal phosphorylations (pSer552 and pSer675) showed CFs of 6.47 and 3.98 in the untreated sample. While for the Ser675 phosphorylated variant of β-catenin, the CF increased approximately four-fold after CHIR 99021 treatment, the increase for the pSer552-version was 14.08-fold. This corresponds to a CF of 91.07 after CHIR 99021 treatment detected by the anti-β-catenin pSer552 antibody. Anti-β-catenin non-phospho Ser33/Ser37/Thr41 and anti-β-catenin (8E7) address an active β-catenin variant, unphosphorylated at the SSTS-motif. Anti-β-catenin non-phospho Ser33/Ser37/Thr41 showed the highest CF (8.76) in the untreated sample and also the highest increase for CHIR 99021. Here a CF of 156.00 was detected, while the CHIR 99021 treatment led to an increase of a factor of 17.81. The antibody 8E7 recognizes β-catenin at the residues aa 36 – 44. It showed no signal in three of the samples: the untreated input, the untreated bound and the CHIR 99021-treated input; but a

substantial increase was obtained after the application of CHIR 99021 in the amount of β-catenin detected by this antibody in the bound sample after CHIR 99021 treatment (CF = 3800.23). As there is no signal obtained for the untreated sample, no fold change can be calculated that provides information about the increase by drug treatment. Thus, a new criteria was introduced to estimate and visualize this increase: The means of the background signals were calculated and their SD derived for each replica. The integrated peak values for the anti-β-catenin (8E7) antibody were devided by three times of their individual SD value, which led to an estimated increase of more than 80 compared with three times the SD.

4.3.3 Extracellularly detected interacting proteins on HEK293T

Besides the differences in precipitation of β-catenin variants, a variety of interacting proteins were identified. Nine interactors were detected both in the untreated and the CHIR 99021-treated HEK293T cells (see Table 34).

Table 34: Co-immunoprecipitated proteins in untreated and CHIR 99021-treated HEK293T cells.
The CFs for interacting proteins precipitated in untreated and CHIR 99021-treated HEK293T cells are represented, calculated with the formula described in 3.4.3.3, Equation 3. The colorized background stands for the strength of the PPI (see Table 19). Proteins were sorted referring to their CF in an ascending order in the untreated sample. The averaged CF of the duplicate is shown. In brackets the molecular weight and the distinct NMI number are listed, if the analytes need to be differentiated.

Analyte	Modification	untreated +	CHIR 99021 +	increase (fold change)
PCNA		0.02	0.02	1.00
PP2A C		0.11	0.14	1.27
GSK3 β		0.22	1.98	9.00
CDK2		0.22	0.41	1.86
Src	pTyr527	0.25	0.31	1.24
MTA2		0.29	0.25	0.86
LSD1		0.40	0.27	0.68
Src		0.65	1.22	1.88
α-catenin		2.48	9.29	3.75

PCNA showed up with a low CF of 0.02 in both, the untreated and the CHIR 99021 sample. It seems likely, that the PCNA signal is a weak false positive interactor, derived from a protein carry over into the bound sample. The signal obtained for the input is above 50000 AFI, while the measured signal in the precipitate is below 300 AFI indicating such an unspecific enrichment.

Six proteins showed a medium enrichment in the untreated sample, five of which stayed nearly unchanged after CHIR 99021 treatment, while one (GSK3 β) rose from a medium interaction (CF = 0.22) to a strong PPI (CF = 1.98) after treatment. This nine-fold increase was the largest observed effect of CHIR 99021 after ECIP on HEK293T cells. The other five medium interactors

(PP2A C, CDK2, Src pTyr527, MTA2 and LSD1) showed CFs between 0.11 and 0.40 in the untreated samples, remaining nearly unchanged after CHIR 99021 treatment (CFs between 0.14 and 0.41). It has to be pointed out, that only PP2A C, CDK2 and Src pTyr527 showed an increase between untreated and CHIR 99021 treatment, while for MTA2 and LSD1 a decrease was observed. Total Src and α-catenin were identified as strong interacting proteins of β-catenin. Src with a CF of 0.65, which increased to a CF of 1.22 after the application of CHIR 99021 (1.88-fold increase). The 3.75-fold increase obtained for α-catenin derived from the CF of 9.29 after CHIR 99021 treatment and a lower CF (CF = 2.48) for the untreated sample.

4.3.4 Protein interactions of β-catenin induced by drug treatment

Besides the nine interacting proteins detected in the untreated and the CHIR 99021-treated sample, twelve additional PPIs were identified only after treatment (see Table 35). One medium, nine strong and two very strong interacting proteins.

Table 35: Co-immunoprecipitated proteins only in CHIR 99021-treated HEK293T cells.
The averaged CFs for interacting proteins precipitated only after CHIR 99021 treatment in HEK293T cells, are represented. Calculation, representation and sorting was done analog to Table 34.

Analyte	Modification	untreated	+	CHIR 99021	+
HDAC2		-		0.21	
HELLS		-		0.51	
Smad1		-		0.52	
Pontin52		-		0.96	
HDAC3		-		1.18	
GSK3 β	pTyr216	-		1.93	
Smad2	pSer245/pSer250/ pSer255	-		2.04	
TCF1		-		3.13	
TCF4 (60 kDa isoform, # 1481)		-		3.34	
GSK3 α	pTyr279	-		8.16	
Axin1		-		10.82	
Axin2 (95 kDa isoform, # 0956)		-		35.88	

HDAC2 qualified as a medium strong interactor (CF = 0.21). Nine proteins appeared as strong interactors. Among these, HELLS (also called lymphoid-specific presumptive helicase (Lsh)), Smad1 and Pontin52 (also called Ruvbl1) showed a CF below one. HDAC3 had a CF of 1.18 and for Smad2 (pSer245/pSer250/pSer255) a CF of 2.04 was detected. The CFs of the transcription factors TCF1 and TCF4 were above three, which marked them as strong interacting proteins. GSK3 α (pTyr279) and GSK3 β (pTyr216), as the remaining of the strong interacting proteins, showed a CF of 1.93 for the β-variant, which is much lower than the CF for the α-polypeptide of the

GSK3 protein (CF = 8.16). Additionally, two very strong interactions were seen: Axin1 and Axin2. For Axin1 the CF was just above 10, while the CF of 35.88 for Axin2 was much higher.

4.3.5 Summary

Interacting proteins were precipitated during Co-IP against β-catenin with the employed high-affinity nanobody BC1. The number of interactors increased after CHIR 99021 treatment and frequently the CF increased accordingly.

The raw signal intensities measured for the different β-catenin antibodies rose after treatment. Especially the signal observed for the anti-β-catenin (8E7) antibody was striking. Signal for this antibody was only detected in the CHIR 99021-treated bound sample (see Table 33). The estimation of the CF gave a value of 80 or higher, if comparing the raw values with three times of the SD values of the averaged background signal (see 3.4.3.3).

Differences for the precipitated interaction partners of β-catenin were obvious when comparing the results to the cell line screening. Proteins like Pontin52, HDAC3 and MTA2 represent novel interactors after ECIP. This might be due to the HEK293T cell line. Besides these, still many of the well-known PPIs of β-catenin (GSK3 β, TCF4 and Axin) are seen (see 4.3.3 and 4.3.4).

The obtained results laid the basis to proceed with the development of the combination of intracellular Co-IP with DigiWest.

4.4 Intracellular Immunoprecipitation of transfected HEK293T cells

As shown above (see 4.3), the use of a nanobody as a capturing molecule in a conventional Co-IP approach is possible. It is also feasible to express the nanobody BC1 intracellularly to bind to the target protein β-catenin and its complex partners before cell lysis. This opens the possibility to perform intracellular Co-IPs (ICIPs). Therefore, a version of the nanobody fused to a fluorescent protein, resulting in the BC1-chromobody, was used and expressed inside living cells [112]. The intracellular expression leads to the advantage of the nanobody binding to native β-catenin complexes, before meeting other possible interacting proteins with a higher affinity during cell lysis, which are normally spatially separated.

A stable HEK293T cell line was generated (received from Björn Tränkle, Pharmaceutical biotechnology department, Eberhard Karls University of Tübingen), showing a good expression of the BC1-chromobody. It was shown, that the BC1-chromobody does not block the functional activity of β-catenin and still captures preferably unphosphorylated β-catenin. As a negative control, a HEK293T cell line expressing GFP only was used [112]. The growth conditions and treatment were comparable to the previous ECIP on HEK293T cells (see 3.2.1). Additionally, the same set of 75 antibodies was screened on the samples (three replicas, existing of BC1-input, BC1-bound, GFP-input and GFP-bound). This set of antibodies is marked in the appendix (see Suppl. Table A) with "**". In analogy to the evaluation done in 4.3, the performed triplicate experiments were screened for PPIs with β-catenin. The cutoff limits were adjusted according to the usage of triplicates (see 3.4.3.3) to avoid the identification of false positive interactions. Thus, all peaks showing a signal intensity above 45 AFI were treated as specific signals. Additionally, the sum of the triplicate signals had to be above 140 AFI with a deviation of smaller or equal to 10 AFI in between the individual signals, to guarantee more stability among the replicas. Signals of proteins, that bound unspecific to the immunoprecipitation matrix were eliminated by defining a specificity limit of the signal intensity being 1.5-fold above the negative control for an individual peak. In addition, the sum of all three ratios had to be above 4.3 with a deviation between the single ratios being beneath or equal to 0.2, which led to a higher consistency in between the different replicas. To classify the strength of a PPI, the mean of the individually CFs of the triplicates was calculated. For calculating the average of the CFs, the formula, described in 3.4.3.3, Equation 3, was applied to each individual replica and the mean was taken afterwards. All CFs for the triplicates, along with the obtained raw values for the different input and bound samples, are listed in the appendix (see Suppl. Table H).

4.4.1 Precipitation of β-catenin variants

Different β-catenin variants were detected by using the different anti-β-catenin antibodies on the immunoprecipitate. The relevant difference to the previous ECIP experiment on HEK293 was the intracellular binding of the β-catenin N-terminus by the BC1-chromobody. After calculating the CFs and sorting the antibodies in an ascending order according to the mean of the obtained CFs of the untreated samples, the same order was obtained as already seen for ECIP in 4.3.2.

Table 36: Caught β-catenin variants during ICIP on untreated and CHIR 99021-treated HEK293T cells.
The capturing rate is represented for the untreated sample and after CHIR 99021 treatment. For calculating the average of the CFs, the formula, described in 3.4.3.3, Equation 3, was applied to each individual replica. Subsequently the mean of the triplicate was calculated. The different β-catenin variants detected, were sorted in an ascending order referring to their average CF obtained for the untreated sample. β-catenin variants, which were only detected in the bound sample, are marked with a "+". For one antibody no signal was obtained without treatment. This cell was marked with "-".

Analyte	Modification	untreated	+	CHIR 99021	+	increase (fold change)
β-catenin	pSer675	6.83		14.05		2.06
β-catenin (BD)		9.66		18.16		1.88
β-catenin	pSer552	10.60		52.62		4.96
β-catenin (Millipore)		11.07		32.31		2.92
β-catenin	non-p Ser33/ Ser37/Thr41	31.49		136.82		4.34
β-catenin (8E7)		-		677.88	+	> 12

All antibodies directed towards different β-catenin variants showed much higher CFs on the untreated samples in the ICIP experiments than in comparison to the CFs calculated for ECIP (1.45 to 3.59-fold increase (see 4.3.2)). This might be caused by the earlier intracellular binding of the nanobody to its target protein β-catenin. The two antibodies detecting total β-catenin (BD and Millipore) showed similar CFs (9.66 and 11.07) in the untreated samples again and the increase after CHIR 99021 treatment is similar as well. A two- to three-fold increase was observable, which resulted in CFs of 18.16 and 32.31 for these two antibodies. The antibodies recognizing C-terminal phosphorylations at Ser675 and Ser552 of β-catenin, had CFs of 6.83 and 10.60 in the untreated sample. These CFs experienced a two to five-fold increase after CHIR 99021 treatment (CFs of 14.05 and 52.65). Anti-β-catenin non-phospho Ser33/Ser37/Thr41 was one of the antibodies identifying active β-catenin. As in the ECIP results previously, it showed the highest CF (31.49) in the untreated sample, but not the highest fold change after the application of CHIR 99021. Here the increase was 4.34-fold, which derived in a CF of 136.82 for the CHIR 99021-treated sample. Anti-β-catenin (8E7), the second antibody recognizing active β-catenin, showed again no signal in the untreated sample or in the input of the CHIR 99021-treated cells, but an enormous increase in the amount of recognized β-catenin by this antibody after CHIR 99021 treatment was visible

(CF = 677.88). The same difficulty of calculating a fold change arose. As seen before (see 4.3.2) the means of the background signals were calculated and their SDs derived to estimate the obtained increase. The integrated peak values for the anti-β-catenin (8E7) antibody in each replica were devided by three times their individual SD value. This led to an estimated increase of more than 12 of the measured peak compared to three times of the SDs of the averaged background signal.

4.4.2 Interacting proteins on HEK293T detected by ICIP

In comparison to the results obtained for the ECIP, for ICIP only one interacting protein was measurable in the untreated and the CHIR 99021-treated sample (see Table 37).

Table 37: Co-immunoprecipitated proteins in untreated and CHIR 99021-treated HEK293T cells.
The CFs for interacting proteins precipitated in untreated and CHIR 99021-treated HEK293T cells are represented, calculated with the formula described in 3.4.3.3, Equation 3. The colorized background stands for the strength of the PPI (see Table 19). Proteins were sorted referring to their CF in an ascending order in the untreated sample. The averaged CF of the triplicate is shown. In brackets the molecular weight and the distinct NMI number are listed, if the analytes need to be differentiated.

Analyte	Modification	untreated	+	CHIR 99021	+	increase (fold change)
α-catenin		4.38		10.89		2.49

α-catenin represented a strong interactor of β-catenin, with a high capturing rate for both the untreated sample (CF = 4.38) and the sample after CHIR 99021 treatment (CF = 10.89). After treatment, the interaction surmounted the cutoff limit of 10 and thus α-catenin was classified as a very strong interacting protein. Calculating the ratio between the two different treatments resulted in an 2.49-fold increase.

4.4.3 Modulation of β-catenin protein complexes after drug treatment

Also the number of PPIs detected after CHIR 99021 was lower than the interactors observed for ECIP. Only five interacting proteins were seen, of which three were classified as strong and two as very strong interactors.

Table 38: Co-immunoprecipitated proteins only in CHIR 99021-treated HEK293T cells.
The averaged CFs for interacting proteins precipitated only after CHIR 99021 treatment in HEK293T cells, are represented. Calculation, representation and sorting was done analog to Table 34.

Analyte	Modification	untreated	+	CHIR 99021	+
GSK3 β				2.62	
TCF1		-		3.16	
GSK3 β	pTyr216	-		3.28	
Axin1		-		50.44	
Axin2 (95 kDa isoform, # 0956)		-		113.79	

The three strong interacting proteins, GSK3 β, TCF1 and GSK3 β (pTyr216), showed very similar values for the CFs (between 2.62 and 3.28). Axin1 and Axin2 were categorized as very strong interactors of β-catenin, with CFs above 10. Axin1 had a CF of 50.44 after CHIR 99021 treatment, while for Axin2 the CF was even higher with a value of 113.79.

4.4.4 Comparison of extracellular and intracellular Immunoprecipitation

Comparing the interacting proteins received from ECIP and ICIP it became apparent, that less PPIs were detected by ICIP for both treatments. For ECIP it was possible to identify nine proteins as interactors in both samples and an additional 12 after CHIR 99021 treatment. In ICIP only one PPI was detected both in the untreated and the CHIR 99021-treated sample and five more after CHIR 99021 treatment. Furthermore, only already well-known interactors were seen during ICIP, while no novel ones were obtained.

Overall higher CFs were detected after ICIP for the untreated sample in comparison to the same interacting proteins captured during ECIP. After CHIR 99021 treatment the capturing rates were lower for the addressed β-catenin variants after ICIP compared to the ones calculated for ECIP. But, the obtained interacting proteins during ICIP still showed a rise in the derived CFs in comparison with the same interacting proteins in ECIP. The obtained raw values revealed, similar or slightly higher AFI values being derived for the different antibodies against β-catenin or β-catenin interacting proteins in the input samples for all replicas after ICIP compared to the AFI values received after ECIP.

4.4.5 Summary

In conclusion an increase after CHIR 99021 treatment, for antibodies detecting β-catenin, was visible. Additionally, the same interesting result as in 4.3.2 for the anti-β-catenin (8E7), was seen. This antibody generates signal only in the CHIR 99021-treated bound sample (see Table 36).

Surprisingly, much less interacting proteins were precipitated during ICIP with the intracellularly expressed BC1-chromobody in comparison to the earlier performed ECIP. Again, CHIR 99021 treatment led to an increase in the amount of PPIs detected and also in the CF detected for α-catenin, which is the only protein measured as an interactor already in the untreated sample (see 4.4.2 and 4.4.3). In addition, all detected interacting proteins were well-known β-catenin interactors, with a strong or very strong interaction. Thus, no novel PPIs were identified.

5. Discussion

5.1 Co-Immunoprecipitation and high throughput DigiWest

For the detection and discovery of protein-protein interactions, the Co-Immunoprecipitation is a straightforward and widely used approach [95, 112]. The Co-IP is derived from the classical immunoprecipitation. The experimental procedure is performed identically, yet during the subsequent analysis, proteins are identified, which are precipitated together with the target protein [135]. Interactions are typically confirmed directly in gel or after blotting on membranes by immunological methods, which is a gold standard [94, 136]. Mass spectrometric approaches (MS) [232, 233] have become important in recent years. Antibody-based detection allows only a limited testing and is usually employed to verify known or highly predicted interacting partners, while MS-based approaches allow wide ranging analyses, which are technically rather complex, but hold the advantage of being able to screen for unknown complex members or interacting proteins from the Co-IP products and to explicitly identify them. MS facilitates the unbiased analysis of samples and allows *de novo* identification of changes in the proteome. It thus has a massive impact on signaling research [234]. Hence, for identifying PPIs, Co-IP combined with MS became the method of choice lately [92-94], but is yet technically challenging. MS-based approaches show some major disadvantages: the limited throughput, the cost and complexity of the technique, the requirement of a higher amount of material and the difficulty of the reliable detection of differences in the phosphorylation states of signaling proteins.

To address and overcome these disadvantages, a novel and recently described, digitalized, high output Western blotting approach, termed DigiWest [91] was applied. In this approach, the conventional Western blot [235] is adapted to a bead-based microarray platform and thus adds advantages, such as high throughput and low material consumption [91], to the highly reliable and well-established classical technique. This new method was shown to be capable of providing high-resolution data on protein phosphorylation and expression. Among the advantages of this approach are the ability to run focused proteomic studies to detect differences in the activation states of cellular signaling cascades and the capability of performing multiple assays in parallel [91]. By linking this bead-based immunoassay to a previously carried out, conventional Co-IP, a new screening approach was generated. This linkage results in a high throughput tool to screen for PPIs and henceforth it is possible to functionally analyze the signaling state of intracellular pathways, as a highly parallel analysis of protein expression and modification status is enabled [91].

An additional benefit of combining these two techniques, Co-IP and DigiWest, is the possibility to distinguish a variety of posttranslational modified protein fractions from each other in parallel. The interrogation of activation states of regulatory cascades by PTMs, helps to provide a better

understanding of cellular processes [91]. Combining Co-IP with a target-specific antibody and a novel readout system for immunoblots provides a versatile approach to study endogenous complexes and to identify dynamic PPIs, e.g. in cancer relevant signaling pathways.

In this thesis, the focus is set on the detection of protein complexes comprising the central regulator of the canonical Wnt pathway, β-catenin, in various cell lines (55.1c, 70.4, HepG2, HB35 and HEK293T).

Canonical Wnt signaling is one of the most relevant regulatory circuits of cell fate during the lifetime of any animal [36]. Besides its participation in many developmental processes and the indispensable role in tissue homeostasis, it is crucially linked to carcinogenesis [25-27]. The key effector of the canonical Wnt signaling, β-catenin, is responsible for signal transduction into the nucleus and inducing the transcription of specific Wnt target genes there. Thereby, these genes are responsible for modulating cell fate in various cells and tissues [36]. Aberrations or imbalances in the structure of β-catenin or the characteristics of the Wnt/β-catenin signaling often lead to the formation of diseases and deregulated growth properties linked to cancer or metastasis [36]. β-catenin, as the main molecule in the canonical Wnt pathway, cooperates with a great variety of interaction partners, which are either able to affect transcriptional output, permit its direct crosstalk with other transcription factors or provide a linkage to signaling cascades [36]. Thus, it is of high interest to gain a deeper insight into this altered signaling cascade and the spatially / temporally coordinated PPIs of β-catenin occurring in multiple cellular processes [112].

As an initial approach, a conventional Co-IP approach was performed, in the beginning by employing a β-catenin-specific antibody for precipitating protein complexes. As the system to study PPIs of β-catenin, differently mutated hepatoma cell lines were chosen. The Wnt/β-catenin signaling plays a major role in liver development and homeostasis, thus these cell lines depict a suitable model to study aberrant liver signaling and its influence on disease/cancer formation [236].

I aimed at gaining a higher resolution picture of the precipitated and isolated β-catenin complexes as well as the various interaction partners of the target protein (e.g. α-catenin and GSK3 β) via probing the precipitate with hundreds of antibodies. Thereby, differences in the expressed amount of β-catenin were seen and additionally unknown and unfamiliar interaction partners of β-catenin were detected.

This workflow was further developed by changing the cell system from hepatoma cells to a well-established and good characterized cell line, the HEK293T cells. HEK293 is a human epithelial cell line, derived from embryonic kidney cells, which is suitable for transient transfection and protein expression. The cell line was transformed by the early region of adenovirus type 5 with an inserted gene for the temperature-sensitive SV40 T-antigen mutant tsA1609 [237, 238]. There are no known

mutations in proteins associated with the Wnt pathway and thus it should provide a relative undisturbed system for studying the mechanisms of this pathway [124].

In addition, the β-catenin-specific capturing antibody, directed towards a C-terminal epitope of the protein, was replaced by a nanobody, called BC1. This nanobody binds at the N-terminus of β-catenin with a high-affinity. By the usage of a nanobody, especially the limitations of antibodies used for Co-IP, which arise due to steric hindrances and large binding interfaces, can be overcome [112]. Another convincing characteristic of this binder is the ability of expressing it intracellularly, which enables the performance of intracellular Co-IPs [112]. The BC1 nanobody, used in this experimental setting, was recently designed and described in some detail. Additionally, its capability for Western blot was shown [112]. Among its characteristics are for example a detection level down to 1 ng/ml and it is assumed, that the binder detects preferably an unphosphorylated three-dimensional epitope of β-catenin. This epitope is located close to the N-terminal SSTS-motif, which regulates the stability of the protein. The ability to bind and precipitate a high level of β-catenin especially after inhibiting GSK3 β might be based on the simplified accessibility of the epitope or on posttranslational changes of the epitope, which induce an increased affinity [112].

5.1.1 Utilization of a novel intracellular binding molecule

To employ the BC1 nanobody, initially only used for conventional Co-IP, in intracellular IP, it was fused to the fluorescent protein tagGFP to detect endogenous β-catenin within living cells, resulting in the BC1-chromobody. A stable cell line, with a good expression of the BC1-chromobody, was generated [112]. After transfection and cellular expression of the chromobody, it becomes visible and can be used to trace the dynamic re-localization of β-catenin using fluorescence microscopy. Another interesting feature is the intracellular binding capacity and the possible use for ICIPs [112]. An advantage of an early intracellular binding might be the binding of protein complexes before encountering additional high affinity binding proteins during cell lysis, which are spatially separated in the original cellular structure. An exchange of low-affinity proteins to high-affinity proteins during lysis is still possible, but it was tried to be prevented this by using a very gentle lysis procedure during Co-IP.

It was shown, that the chromobody does not hinder the functional activity of β-catenin and still binds preferably diffusible, non-phosphorylated β-catenin. Additionally, it is possible to visualize the enrichment of β-catenin and its relocation into the nucleus upon compound treatment [112].

The combination of the conventional Co-IP approach linked to the earlier described DigiWest might provide a versatile approach to study endogenous complexes, to uncover dynamic PPIs and protein-protein modifications in general. This was exemplary shown for the cancer relevant Wnt signaling pathway, with its key player β-catenin in this work.

To establish the newly developed screening approach, consisting of Co-IP and DigiWest, four different hepatoma cell lines derived from two species were chosen. These cell lines seemed to be promising for the detection of a plethora of β-catenin interaction partners; three of them carrying a heterozygous activating mutation in the *CTNNB1* gene, encoding for β-catenin (55.1c, HepG2, HB35), while one presenting the wild type (70.4) (see 1.3.2 – 1.3.4). As mentioned before: The cell system was changed and HEK293T cells were selected, in order to use a more general cell model during the further development of the experimental design and the BC1 nanobody as capturing molecule was introduced.

For the establishment of a novel screening approach and showing its significant potential, the different Co-IP workflows (conventional Co-IP, ECIP and ICIP) were linked to the DigiWest. As the DigiWest provides a technique, which is able to visualize changes in the modification status of proteins and identifies dynamic variations in the PPIs, it is particularly suitable to detect differences upon compound treatment.

5.1.2 Modulation of complex composition by drug treatment

Two different inhibitors were chosen, which represent different cellular conditions: The first selected inhibitor, CHIR 99021, is a small organic molecule, which inhibits GSK3 α and GSK3 β by competing for their ATP-binding sites with a high specificity and potency [221, 222]. Inhibition of GSK3 plays an important role in the activation cascade of Wnt/β-catenin signaling. When Wnt signaling is active, GSK3 is inhibited [222]. After GSK3 loses its ability to phosphorylate β-catenin at the SSTS-motif, which marks it for ubiquitin-mediated degradation, unphosphorylated β-catenin is stabilized and accumulates in the cytosol. The accumulated β-catenin translocates to the nucleus and binds to transcription factors, mostly members of the TCF/LEF family. This leads to an active transcription of Wnt-regulated target genes [36]. During suppressed Wnt signaling, β-catenin is phosphorylated by GSK3 and targeted for ubiquitin-regulated degradation at the proteasome [44, 45]. Therefore, CHIR 99021 is an adequate tool to mimic the activated status of the canonical Wnt pathway [222]. As all used cell lines are either wild type according to their β-catenin expression or show a heterozygous deletion of the *CTNNB1* exon 3 gene, they should be susceptible for a stimulation of Wnt signaling with CHIR 99021. In comparison to CHIR 99021, which leads to an enrichment especially of the free cytosolic [222], non-phosphorylated β-catenin (sometimes also called “active” β-catenin) in the cell, as it induces a decrease in β-catenin phosphorylation [239], a second inhibitor was applied, called MG132. MG132 is a potent, reversible and cell-permeable proteasome inhibitor. It has a rapid influence on the ubiquitin-proteasome pathway and blocks the proteasomal degradation of ubiquitinated proteins [223, 224]. β-catenin is one of the proteins, which is degraded by this degradation pathway [45]. Hence, not only the activated, non-phosphorylated form of β-catenin

should be present and enriched in the MG132-treated cells, but also phosphorylated and in addition, ubiquitinated forms of β-catenin and other proteins, which are degraded via the ubiquitin-proteasome pathway, should be available in a higher quantity. Subsequently a general enrichment of proteins degraded through the proteasome in the cell was expected.

5.2 Captured posttranslational modified forms of β-catenin

Increasing evidence propose that PTMs, such as phosphorylation, ubiquitination, acetylation and others [36, 240], of key players of the Wnt/β-catenin pathway are crucial for its activation. PTMs play an essential role in a highly dynamic system, which does not require new protein synthesis, and facilitates a quick change of β-catenin's properties, by covalently adding functional groups or presenting altered binding platforms [62, 241]. By that, they enable positive or negative crosstalk between each other, which depicts an important regulatory mechanism for signal transduction [241-243]. The different added PTMs result in changed complexation of β-catenin, as they determine its location and its diverse cellular roles [244].

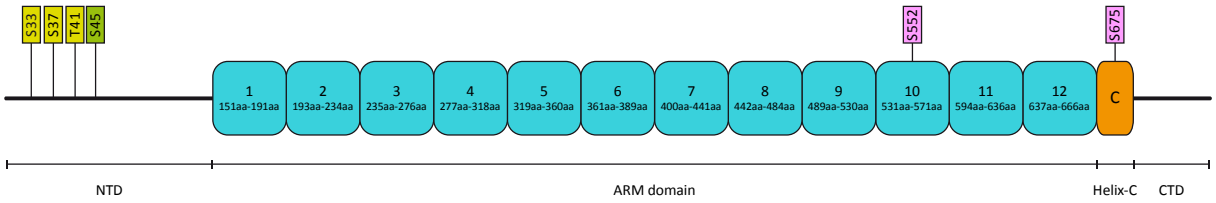

Figure 31: Structure of β-catenin and its phosphorylation sites.
A schematic diagram of β-catenin (781 aa) represents its structure, divided into the NTD, the ARM domain, composed of 12 ARM sequences (each approximately 40 aa long), the Helix-C and the CTD. Additionally, the phosphorylation sites are shown: those in green/yellow promote its degradation, while those in purple enhance the signaling activity. The kinases, responsible for phosphorylating at the marked positions, can be obtained in Table 39 (Figure adapted from [36]).

The operation mode of β-catenin can be regulated through phosphorylation by a large, yet defined set of different kinases (see Table 39) [36, 62]. Phosphorylations of β-catenin, especially at the C-terminal end, often result in the enhancement of signaling [36] and/or the stabilization of the protein as well as its nuclear accumulation [189, 245, 246]. On the contrary, phosphorylations at the N-terminal SSTS-motif introduced by kinases CK1 and GSK3 α/β, promote the degradation of β-catenin via β-TrCP-mediated proteolysis (see Figure 31) [43, 45, 62]. The weakening of the membrane-associated β-catenin complex, the catenin-cadherin interaction, and an impairment of the adhesive functions of β-catenin is also caused by phosphorylations [247-249]. Thus, β-catenin is guided towards an increased signaling and β-catenin driven transcription is induced [36, 250]. Phosphorylations of β-catenin towards the last ARM repeats enhance the possibility for additional interaction partners to bind. Causative is the development of a bond between the unphosphorylated, last ARM repeat and the partially flexible Helix-C, which prevents interacting proteins from binding [36]. The Helix-C is a specific conserved helix, which is located adjacent to the last ARM repeat, proximally to the CTD (see Figure 31) [36, 251]. As long as the CTD is folded and bound to the ARM repeats, interaction partners, such as transcriptional co-activators, cannot bind [251]. If the fold back of the C-terminal tail is prevented, the ARM region and the Helix-C are stabilized and stay open

[62, 250]. Hence, remain accessible for additional PTMs [250], which can lead to an increased recruitment of co-activators of β-catenin-mediated transcription [36, 58, 252].

Table 39: PTMs control the functional output of β-catenin.
Antibodies against all of the listed PTMs of β-catenin, which are summarized with their functional impacts, were tested during the experimental setup (Table adapted from [36]).

Modification	Sites	Enzyme	Function	Reference
Serine/threonine phosphorylation	S33, S37	GSK3	degradation, provides sites for β-TrCP	[253, 254]
	T41	GSK3	degradation, phosphorylation relay sites	[173]
	S45	CK1	degradation, priming for GSK3	[172]
	S552	Akt, PKA	signaling	[246]
	S675	PKA	signaling, enhancement of CBP binding	[246, 252]
	S675	PAK	signaling, promoting stability and transcription	[255]

As mentioned earlier (see 4.2.1 and 4.2.3), different β-catenin pools were addressed by the use of specific antibodies during detection. On the one hand, this served as a control for the success of the Co-IP, on the other hand, it was hoped to gain a deeper insight into the role of different β-catenin PTMs. Besides the listed phosphorylation sites in Table 39, which were screened throughout the experiments, various additional serine/threonine, but also tyrosine residues of β-catenin can be posttranslational phosphorylated by different enzymes, but weren't analyzed here, since no specific antibodies were available.

Nine different β-catenin-specific antibodies were used for the experiments of this thesis. Two of them recognizing total β-catenin (BD and Millipore), differing in their binding region (N- and C-terminal), while seven antibodies addressed different PTMs of the target protein.

The obtained differences in recognition of β-catenin by the BD and the Millipore antibody, might be explained by the polyclonality of the Millipore antibody. This antibody is intended to recognize not only one, but multiple epitopes on the β-catenin antigen, and can have a higher sensitivity than a monoclonal antibody, like the one purchased from BD Biosciences [256]. Both treatments, CHIR 99021 and MG132, usually lead to an increase of β-catenin, which is visible in the detected CFs. Although the raw data show a general decrease after treatment compared to the untreated samples (see Suppl. Table C – Suppl. Table H). This decrease can be caused by the cytotoxicity of MG132 [257] or by the enhanced proliferation after CHIR 99021 application and is seen for example in 70.4 or HB35 cells. The CFs for all different antibodies detecting β-catenin rise both after CHIR 99021 and MG132 application (fold changes of > 1.3 for 70.4 cells and > 1.8 for HB35 cells). However a distinct decrease in the raw data is obtainable for CHIR 99021 in HB35: The obtained raw input values are 0.1 – 0.6 times of the raw values detected for the untreated input sample. For MG132 the decrease is

best observable in 70.4 cells: The obtained raw input values are 0.15 – 0.6 times of the raw values detected for the untreated input sample. For CHIR 99021 an activation of Wnt signaling without a concomitant toxicity was shown [258]. The enhanced proliferation, caused by an active canonical Wnt pathway, could result in the enrichment of the protein entity in the cell. This enrichment might lead to a shift in the amount of detected β-catenin coupled to the bead surface in comparison to the remaining proteins.

As mentioned earlier, the anti-β-catenin (non-phospho Ser33/37/Thr41) antibody recognizes its target protein N-terminally and specifically detects the active β-catenin variant. β-catenin with an unphosphorylated SSTS-motif is not amendable to degradation, accumulates in the cytosol, is able to translocate into the nucleus and activates the transcription of Wnt/β-catenin target genes. The amount of β-catenin captured after CHIR 99021 treatment both for ECIP and ICIP on HEK293T cells is substantially higher than for the untreated cells: This indicates too the enrichment of non-phosphorylated β-catenin in the cytosol after GSK3 inhibition by CHIR 99021 treatment.

Antibody 8E7 and the anti-β-catenin (non-phospho Ser33/Ser37/Thr41) antibody recognize both an active form of β-catenin. The similar pattern observed for both the DigiWest bar graphs and the conventional Western blots after CHIR 99021 treatment for these antibodies supports this characteristic. The very high capture rate of the antibody 8E7 found only after CHIR 99021 treatment, is due to the fact that specific signal in the DigiWest is only obtained after treatment. This might be due to a lower affinity of the 8E7 antibody and accordingly a lower signal detected during readout. In untreated cells, the available amount of unphosphorylated β-catenin in the cytoplasm is known to be low, since a permanent degradation takes place. The antibody 8E7 might have difficulties to detect these low β-catenin levels in the untreated samples. After CHIR 99021 treatment the unphosphorylated β-catenin accumulates, but is still not detected in the input sample by the 8E7 antibody. This points to a low antibody affinity, which is supported by the much higher signals obtained for the non-phospho Ser33/Ser37/Thr41 antibody during ECIP and ICIP for all samples (see Suppl. Table G – Suppl. Table H).

The anti-β-catenin pThr41/pSer45 antibody yielded very low signals. A similar outcome was observed for antibodies directed towards other phosphorylations (pSer33/Ser37/Thr41 and pSer45) of the SSTS-motif. That can be due to a low affinity of these antibodies. An absence of one allele of *CTNNB1* exon 3, which results in an N-terminally truncated protein, is a characteristic trait in most of the screened cell lines. This heterozygous truncation might additionally lead to lower detected signals for these antibodies. Deletion of exon 3 and the expression of N-terminally truncated β-catenin leads to activated Wnt signaling, since a part of the SSTS-motif is deleted and the β-catenin can not be flagged for degradation. A higher amount of active β-catenin is available in cells carrying these variants, due to the lack of these specific phosphorylation sites.

Contrary to degradation-promoting phosphorylations at the N-terminal SSTS-motif, phosphorylations of β-catenin, especially if located at the C-terminus, lead to enhanced signaling activity [36]. Among these phosphorylation sites are Ser552 and Ser675 at the C-terminus of β-catenin. These lead to a stabilization of the unfolded ARM region and Helix-C, and a general enhancement of signaling activity [189, 245, 246]. The phosphorylation of β-catenin at Ser552 indicates that the protein is able to dissociate from the membrane bound protein complex that mediates cell-cell contacts and can accumulate in the nucleus [246]. Phosphorylation at Ser675 leads to an increased recruitment of co-activators of β-catenin-mediated transcription, such as CBP (CREB-binding protein) binding, and results in a promotion of transcription [36, 58, 255]. When Ser675 is phosphorylated, the β-catenin structure opens up, is stabilized and an increase in Wnt signaling by recruiting transcriptional activators, can be observed [252, 255]. It was shown for HEK293T cells that exposing the cells to a GSK3 inhibitor, such as CHIR 99021, results in the increased presence of β-catenin phosphorylated at Ser552 and Ser675. The level of β-catenin phosphorylated at these residues increases concomitantly with an increase of total β-catenin and free β-catenin [244]. It was postulated that the C-terminal phosphorylation of β-catenin is linked to canonical Wnt signaling, but still the regulatory functions of Ser552 and Ser675 phosphorylations are little characterized and need further investigation [244]. The increase of β-catenin phosphorylated C-terminally was observed after CHIR 99021 treatment accordingly. As MG132 also leads to a general rise in the cellular protein amount, an increase in the CF of precipitated β-catenin was expected and also observed here.

The increasing need for the availability of improved techniques, which are able to detect PTMs was expressed recently [62]. Here, such an approach was developed and shows its ability to provide insights about differently phosphorylated forms of the target protein β-catenin. However, still little is known about the effective and combinatory interaction of PTMs both in ON and OFF state of the Wnt signaling [62]. It is important to identify specific Wnt pathways inhibitors, as an aberrant activation of this signaling cascade results in the development of various diseases, such as cancer [62, 259]. Modulating PTMs of components of the Wnt pathway, like its key player β-catenin, might be a promising alternative for drug development, as Wnt signaling itself is too complex and thus difficult to target specifically, while the direct inhibition of β-catenin can’t be undertaken without destroying its various functions within the cellular context [28, 62, 260].

5.3 Detection of known PPIs for β-catenin in different cell lines

With the possibility to detect different β-catenin pools, a comprehensive search for proteins interacting with β-catenin was started. To obtain information about β-catenin protein complexes, a closer look at formerly published PPIs was taken. As MS-based approaches allow wide ranging analyses and result in large data sets, most of these PPIs were detected via MS. A common procedure is to list the detected interacting proteins in databases, such as BioGRID, UniProtKB and IntAct. For a broad characterization of the Wnt/β-catenin pathway and the complex partners of β-catenin, an extensive database and literature research was undertaken. The general description of the protein function was obtained at the UniProtKB database, which was used as a first reference. By that a plethora of antibodies (> 500) were identified and matched with more than 1000 available antibodies. This lead to a set of 344 particularly interesting protein antibodies, which covered the Wnt-/β-catenin pathway and allowed an additional glance at the spatial cellular surrounding, to display a possible crosstalk with other signaling cascades or novel protein interactions.

While a large number of proteins, known to interact directly with β-catenin, were precipitated by Co-IP, only one protein was detected consistantly in all analyzed cell lines under all treatment conditions: α-catenin. In the cytosol, α-catenin exists as a monomer or a homodimer [148] with different binding properties. The monomeric α-catenin binds strongly to E-Cadherin-β-catenin, whereas the dimer preferentially binds Actin filaments. There is no simultaneously binding between the adhesion molecule E-Cadherin and the Actin cytoskeleton via α-catenin [149, 155]. Depending on β-catenin, it can accumulate in the nucleus and interact with β-catenin and TCF there [261]. The high amount of signal obtained for α-catenin in 55.1c in comparison to other cell lines, can be explained by a high amount of α-catenin present in this cell line. The detected amount of α-catenin is already higher compared to the other cell lines, according to the raw input values.

Besides the presence of α-catenin in all analyzed samples, several other known complex partners of β-catenin were detected during the experiments in the different cell lines. Especially prominent are proteins, which are present in the membrane-associated β-catenin complex or participate in the β-catenin destruction complex (see Figure 2).

E-Cadherin, as a central interacting protein, is part of the membranous complex linked to β-catenin. This transmembrane glycoprotein and endogenous adhesion molecule is one of the best characterized interaction partners of β-catenin. It associates with cytoplasmic proteins like α-catenin and β-catenin at its specific cytoplasmic domain [174, 262, 263]. The complexation of cadherin-catenin provides a dynamic link to the Actin cytoskeleton [149, 174, 175] and plays an important role maintaining the epithelial integrity [264]. The dissociation of the E-cadherin/β-catenin adhesion complex represents a key step in EMT and promotes metastasis [265] as well as the development of HCC [266]. Without Wnt signaling, most of the available β-catenin is either bound to

E-Cadherin or phosphorylated and marked for degradation by the destruction complex in the cytoplasm [36].

Also part of the membrane-associated β-catenin complex is β-Actin, which is ubiquitously expressed in all eukaryotic cells and is involved in various types of cell motility. It is one of the cytoplasmic Actins and is an extremely well conserved structural protein [153, 154]. Therefore, it is considered as housekeeping protein. β-Actin binds to α-catenin, which could provide a link to β-catenin [149, 155]. But α-catenin is not able to bind simultaneously to β-catenin and β-Actin. Still the function of α-catenin as a molecular switch [149, 155] might create an additional explanation for precipitating small amounts of β-Actin together with β-catenin besides the possibility of detecting a weak false positive interaction due to a small carry over into the bound sample, as it was seen for GAPDH.

A second central regulatory complex associated with β-catenin is the β-catenin destruction complex. Seven proteins, which are part of this complex, occur repeatedly during the analysis of the different cell lines: APC, Axin1, Axin2, CK1 α, CK1 δ, GSK3 α and GSK3 β.

The tumor suppressor protein APC, represents a scaffold protein in the β-catenin destruction complex [151]. Newly synthesized β-catenin or already existing β-catenin, which is released from the adherens junctions, is captured by APC or Axin. Both proteins establish a basis for allowing other proteins like GSK3 β or CK1 to posttranslationally modify β-catenin [36, 41, 151, 267]. APC plays a key role in the β-catenin turnover by participating in the destruction complex and also via its own direct binding to β-catenin. Various functions for APC have been suggested, e.g. increasing the binding affinity of β-catenin to the destruction complex, but its actual role remains still enigmatic [41, 152].

Axin1 and its homolog Axin2 are scaffolding proteins, that contain separate binding sites for APC, β-catenin, GSK3 β, CK1 and possibly other proteins [36, 151, 152]. They act as the core protein of the β-catenin destruction complex [268], which is required for regulating β-catenin levels through phosphorylation and ubiquitination as well as modulating Wnt signaling [168].

CK1 α (Caseinkinase 1 α) and CK1 δ (Caseinkinase 1 δ) are members of the CK1 family. Caseinkinases are responsible for phosphorylating serine/threonine residues of their target proteins [49]. CK1 α is one isoform of the priming CK1 kinases, which phosphorylates β-catenin at Ser45 [169] and is strictly required for subsequent phosphorylation of Thr41, Ser37 and Ser33 by GSK3 β. A depletion of CK1 α leads to an inhibition of β-catenin phosphorylation, which is a prerequisite for the degradation process. This results in an increase of β-catenin and in excessive Wnt/β-catenin signaling [36, 172]. CK1 δ is a key regulator of various cellular growth and survival processes, including Wnt signaling [269]. This kinase was, like CK1 α, identified for being in charge of the initial Ser45 phosphorylation of β-catenin [49, 169] and can therefore also contribute to Wnt-induced β-catenin stabilization [187].

The other two found proteins, belonging to the β-catenin destruction complex, are the two homologous forms of GSK3: GSK3 α (52 kDa) and GSK3 β (47 kDa) [170]. GSK3s are involved in many cellular processes, including the Wnt pathway. Both mammalian homologues seem to function identically in Wnt signaling, the difference in size is caused by an amino-terminal glycine-rich extension of unknown function [270]. GSK3 binds Axin at a central region and phosphorylates β-catenin at Thr41 [173], Ser37 and Ser33 [172] subsequent to the initial phosphorylation by CK1 [169]. A tyrosine phosphorylation on the activation loop of GSK3, either at Tyr216 of GSK3 β or at Tyr279 of GSK3 α increases the enzyme's activity [171, 271, 272].

It can be assumed that the developed screening approach works reliably, as it was possible to identify and verify well-known interacting proteins of the addressed target protein β-catenin. Thus, we concluded that other detected PPIs are true and classified these as authentic interactions. Not all of the found interacting proteins, assigned to one of the two described complexes, are seen in all screened cell lines. In addition and after comparison to the results obtained for the untreated cell lines, some of the PPIs show a higher CF or are detected only after treatment with CHIR 99021 or MG132. This rise in capturing or in the amount of detected interacting proteins can be explained by the influences through treatment which might vary for the different cell lines as all of them possess a different genotype.

CHIR 99021 inhibits GSK3 and thereby prevents the phosphorylation of β-catenin. The binding of β-catenin to the remaining, now inactive destruction complex is not disabled. It can be assumed that after CHIR 99021 treatment, the existing destruction complexes get saturated with β-catenin. In the untreated cells a steady-state between binding of β-catenin to the destruction complex and its dissociation as well as its subsequent degradation is reached. Consequently, a proportionally higher amount of β-catenin can remain bound in the destruction complex after CHIR 99021 treatment as there are in total more available β-catenin molecules in the cytosol due to their CHIR 99021-dependent accumulation. Accordingly more proteins of the destruction complex are precipitated after CHIR 99021 treatment as β-catenin is still bound to them. The higher amount of cytololic, unphosphorylated β-catenin leads in addition to the distribution of β-catenin to other subcellular locations, as they for example its translocation into the nucleus. This simplifies the possibility for other proteins to form complexes and enhances the amount of precipitated interaction partners. MG132 on the other hand, as an inhibitor of the proteasome, causes a general enrichment of proteins, which use this degradation pathway. This presumably leads to an enrichment of β-catenin interactors, such as the membrane-associated complex partners or members of the destruction complex, which are degraded by the proteasome.

Hence, dynamical, intracellular changes emerging through the application of different drug treatments become visible in this approach. This offers the possibility of directly analyzing the effects

of compound treatment on various proteins and proximate modulation of signaling cascades at once. Additionally, the usage of diverse samples, such as cell lines, but also lysed tissues, etc. is feasible and make the approach very versatile.

5.4 Wnt proteins detected after Co-IP in hepatoma cells

19 Wnt proteins are encoded by the mammalian genome. It was suggested that Wnts can activate a variety of different signaling pathways, which again intersect with numerous other intracellular signal transduction pathways [150]. All mammalian Wnt proteins analyzed so far, can either activate or inhibit the canonical Wnt signaling pathway [38]. Wnts are grouped into so-called “canonical” Wnts and “noncanonical” Wnts, following the original assumption of being assigned either to “canonical” or “noncanonical” signaling pathways. Recent studies however showed, that the classification of Wnts into these two categories does not hold up to scrutiny. This is especially true, as Wnts themselves control and modulate multiple pathways [150]. All Wnt proteins are hydrophobic glycoproteins, which undergo heavy PTMs such as palmitoylation and glycosylation prior to transport and release into the extra-cellular milieu [35]. These lipid modifications are essential for their function [273]. Palmitoylation and glycosylation are needed to initiate the targeting of Wnt proteins to the plasma membrane to secret them, while palmitoylation also supports the binding of Wnts to their receptors [274]. After palmitoylation in the ER by the porcupine acyltransferase, Wnts are transported and packed in secretory vesicles, which is controlled by the multi-pass transmembrane protein Wntless/Evi. Wntless/Evi is present in the Golgi and/or the plasma membrane and was shown to interact with Wnts [273, 275, 276]. Once released into the extra-cellular milieu, they can pass signaling in an autocrine or paracrine manner (see Figure 32) [277].

Secreted Wnt proteins in the canonical Wnt signaling pathway initiate signaling by binding to their membrane receptors (FZDs) and their co-receptors (LRP5/6) [38]. This primary signaling leads to the phosphorylation of DVLs (DVL1, DVL2 and DVL3) [48, 49] and is further transduced to the multicomplex, consisting out of APC, GSK3, Axin and β-catenin. This complex dissociates as a result and β-catenin is stabilized [53]. As mentioned before, the stabilized β-catenin accumulates in the cytosol and translocates into the nucleus, where it is able to bind to transcription factors and activate transcription of Wnt/β-catenin pathway-specific target genes (see Figure 32) [36].

Wnt3a is the most prominent member of the “canonical” Wnts, which bind to the FZD receptor [53]. Yet, also Wnt7b, formerly classified as “noncanonical” Wnt, was shown to bind to two different FZD proteins: FZD1 (Frizzled1) and FZD10 (Frizzled10) [167]. Both were demonstrated to affect the canonical Wnt pathway in an activating manner [152, 167], but for Wnt3a a much higher activation was observed, than for Wnt7b in comparison [278]. Wnt11 is an example for a Wnt protein that holds dual signaling capabilities [150], on the one hand it was shown to inhibit the canonical β-catenin-dependent Wnt pathway [38], but it is also well-known for its ability to trigger noncanonical Wnt signaling [279]. All three mentioned Wnts were detected interactors of β-catenin in this work.

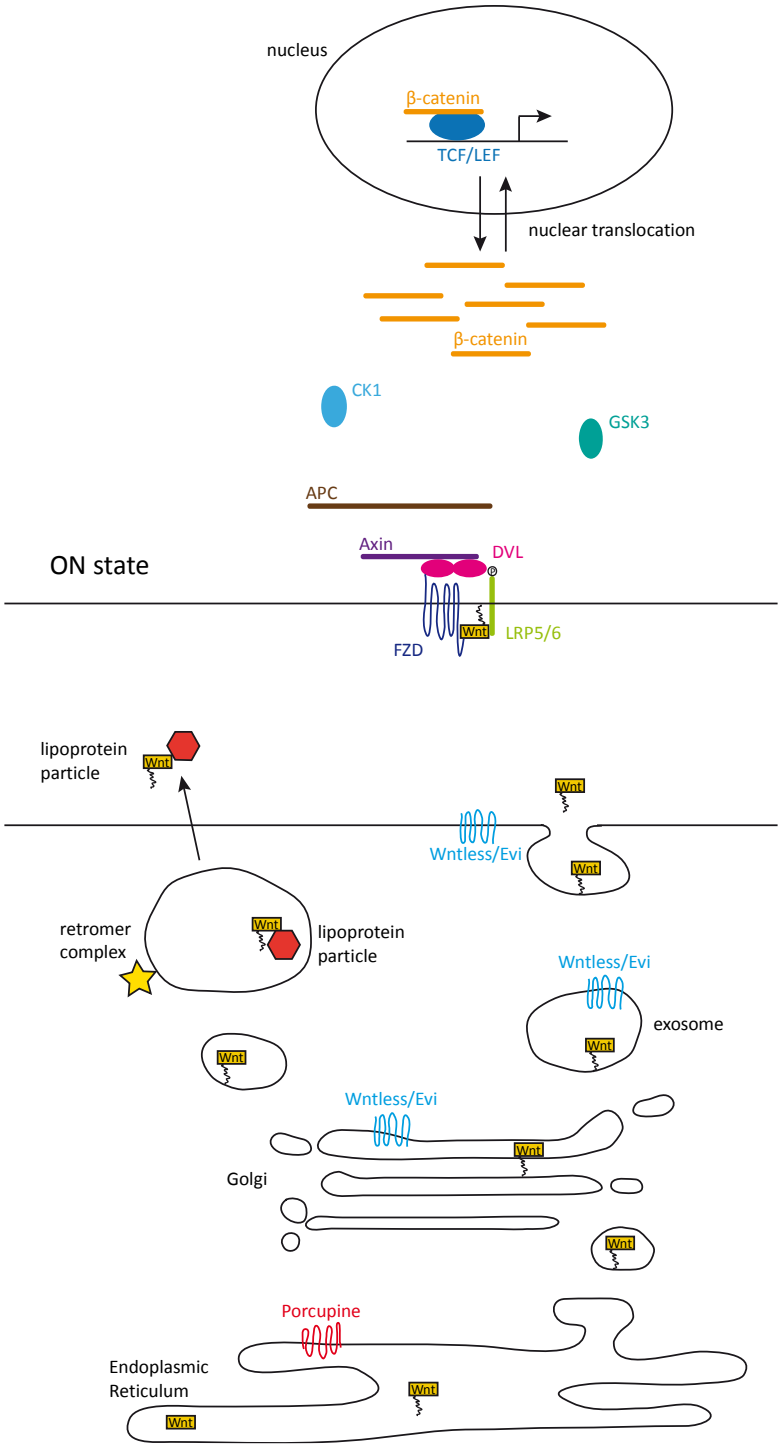

Figure 32: Wnt secretion and initiation of canonical Wnt signaling.
Wnt proteins become palmitoylated in the ER (Endoplasmic Reticulum) by the porcupine acyltransferase after being produced. The multi-pass transmembrane protein Wntless/Evi controls the further transport and secretion of the Wnt proteins in secretory vesicles, such as exosomes. Wntless/Evi is present in the Golgi and the plasma membrane. It is also suggested, that they can travel by a second mechanism: lipoprotein particles. The association with ligands, like lipoprotein particle, might be promoted by a retromer complex to transport these Wnt forms in endosomal trafficking vesicles outside the cell. After release into the extracellular gap, signaling is passed in an autocrine or paracrine fashion. Upon binding to their membrane receptors (FZD) and co-receptors (LRP5/6), DVL is recruited to the complex. After forming a signalosome, which in turn recruits Axin to the plasma membrane, the destruction complex gets destabilized and dissociates. The degradation of β-catenin is now prohibited and the protein accumulates in the cytosol, before translocating into the nucleus. In the nucleus, β-catenin binds to transcription factors, such as members of the TCF/LEF family, and enables gene expression (Figure adapted from [34, 36, 50, 51, 273]).

Very little is known about how Wnts orchestrate the β-catenin signaling by inhibiting its phosphorylation. A combination of various processes, like Axin degradation, alteration of the destruction complex or inhibiting the kinase activities of GSK3 or CK1, is possible [151].

A direct interaction between Wnts and β-catenin or a cytosolic occurrence of Wnt proteins is not reported by the current literature; thus no indication for their presence in the cytosol, without being packed into secretory vesicles, was found.

Hence the question arises, how Wnts can be co-immunoprecipitated with β-catenin and appear as interaction partners. Two explanations of the occurring phenomenon are likely: Co-IP of Wnts occurs via their link to the LRP5/6 and FZD receptor complex. This complex is able to bind via the DVL proteins to Axin, which is also part of the destruction complex, a place where β-catenin can be located [36]. Additionally, direct interaction for β-catenin with nuclear DVL was shown previously [219]. But no evidence for the relocation of members of this complex into the cytosol, where β-catenin would be able to bind directly, is available. Another possibility and a more likely explanation, is the generation of a protein complex after cell lysis. The occurrence of precipitated Wnts and members of the membranous Wnt signaling complex (LRP5/6 or FZD) as β-catenin interactors might be explained as result of the Co-IP procedure.

ICIP holds the possible advantage of preventing these interaction partners by an earlier binding to β-catenin complexes. A signal occuring during ECIP but not ICIP would support the assumption of detecting an artificial interaction, which does not occur *in vivo*, but emerges after destroying the original cellular context. Therefore, antibodies against several Wnt proteins were tested on the ECIP duplicates and the ICIP triplicates, but no PPIs were detected. As HEK293T cells are known to exhibit normal Wnt signaling and were shown to be suitable for studying this signaling cascade many times before [112, 124], the occurring differences can’t be attributed to the change in cell system (liver to kidney). Thus, the detection of an interaction between β-catenin and Wnts has to be led back to the differences during the cell lysis and has to be evaluated as an interaction emerging from lysis and/or Co-IP.

5.5 β-catenin interaction with transcriptional regulators

Several interactions of β-catenin with transcription factors or proteins, involved in the modulation of transcriptional activity, were tested and confirmed as such. Among these interacting proteins well-known interaction partners were detected, such as members of the TCF/Lef family [36, 54, 55], the proto-oncogenes Src [36, 185, 186, 252, 280, 281] and cJUN [36, 217-219]. In addition, interactions with other proteins, which can modulate the transcriptional activity, were identified. Below a discussion of some of these newly identified interactors (GLI1, FoxO3a, Smads and TAZ) is found and the result is put into a biological context.

The zinc finger protein GLI1 is active in the Hedgehog signaling pathway. Like the Wnt/β-catenin pathway, the Hedgehog pathway plays a pivotal role in directing growth and patterning during embryonic development in the liver [138]. Wnt/β-catenin signaling and Hedgehog signaling show similarities, which might indicate a common ancestral evolutionary pathway [282]. Among the similarities is also the shared use of proteins, such as GSK3 or CK1 [283, 284], in both pathways. GLI1 is an interactor of CK1 α/δ, that was found in this study [285, 286] and thus might provide a link to the β-catenin destruction complex. A physical interaction between GLI1 and stabilized β-catenin was shown recently by Co-IP and proximity ligation assay [156]. If the available amount of the stabilized form of β-catenin increases, for example through activated or mimicked Wnt/β-catenin signaling, the sequestration of GLI1 increases simultaneously and the transcriptional activity of GLI1 is inhibited. It was even suggested, that the interaction with β-catenin leads to the degradation of GLI1 and the inhibition of Hedgehog signaling [156].

An interacting transcription factor is FoxO3a (Forkhead box O3). FoxO3a belongs to the forkhead transcription factor family (FoxOs), which critically controls fundamental cellular processes, like proliferation, apoptosis and survival [210]. It was shown for both FoxO4 and FoxO3a, that they are co-immunoprecipitated with β-catenin, which indicates the existence of a physical interaction in mammalian cells [211]. β-catenin serves as a co-factor for FoxOs and is known to be implicated as a pivotal protein in the oxidative stress defense [287]. Via the binding between β-catenin and FoxOs, their transcriptional activity is enhanced [211, 288]. Another crosstalk link between Wnt/β-catenin signaling and other signaling pathways is provided [289] by the competition of FoxOs with TCF for β-catenin [36]. This competition might influence various diseases, like diabetes [287], or developmental processes, such as bone development [290]. Besides the interaction of FoxOs with β-catenin, an interaction with many other transcription factors was shown for this protein family, like their complex formation with Smad3 and Smad4 [290] in a TGF-β-dependent manner [291].

Several Smads are known interaction partners of β-catenin. They were detected as interactors throughout the analysis of the different cell lines. Smads are signal transducers, which facilitate signaling of the TGF-β (transformation growth factor-β) superfamily inside the cell [292]. Interactions

between TGF-β signaling and the Wnt/β-catenin pathway are central in many biological processes, while their alterations are associated with diseases, like cancer [293]. Smads can be divided into three groups: the receptor-regulated Smads (R-Smads, e.g. Smad 2, 3 and 5) [216], the common-mediator Smad (only Smad 4) [180] and some inhibitory Smads, which act antagonistic to the former two Smad groups [294]. Smad 2 and Smad 3 are structurally highly similar and both mediate TGF-β signals. Smad 4 is distantly related to Smad 2 and 3 and can form a heteromeric complex with both of them [178, 179]. After phosphorylation upon ligand stimulation, Smads translocate from the cytosol to the nucleus. While R-Smads do not require the association with Smad 4 to be able to translocate into the nucleus, the nuclear accumulation of Smad 4 is driven by the heterodimerization with R-Smads [292]. The heteromeric complex, formed out of Smad 2/3 together with Smad 4 is able to associate with transcription factors in the nucleus after translocating [181]. Besides that complexation, Smad 2 is already able to associate with cytoplasmic β-catenin to mediate the increased activation of TGF-β target genes [177, 295]. It was shown by Co-IP, that Smad 3, Smad 4 [296], TCF4 and GSK3 β are also present in this complex [297, 298]. While Smad 2 and 3 are active in TGF-β signaling, Smad 5 is part of the BMP (bone morphogenetic proteins) signaling. It also interacts with Smad 4 and accumulates in the nucleus to bind and regulate target gene expression there [182].
The last transcriptional regulator, described in this chapter, is TAZ (WW domain-containing transcription regulator protein 1). TAZ is a transcriptional co-activator of the Hippo pathway. One of the cytoplasmic functions of TAZ is constraining Wnt/β-catenin signaling by inhibiting CK1 δ/ε-mediated phosphorylation of DVL and thus promoting an interaction between TAZ and DVL. The phosphorylation of DVL precedes the stabilization and activation of β-catenin, which is now restrained [187]. Additionally it was shown, that TAZ can bind directly to β-catenin and by that retain it in the cytoplasm to suppress Wnt/β-catenin signaling [299, 300]. TAZ therefore provides a direct molecular link between Hippo and Wnt signaling pathways (see Figure 33) [187]. In the Hippo pathway, the tumor suppressor Mst1/2 is regulated by upstream molecules, which often transduce signals from the membrane. Mst1/2 activates LATS1/2 via phosphorylation [301, 302], before LATS1/2 in turn phosphorylates TAZ, which leads to the inhibition of its transcriptional co-activator activity and its cytoplasmic localization [301]. Therefore, many proteins participating in the Hippo signaling are identified as tumor suppressors [302].

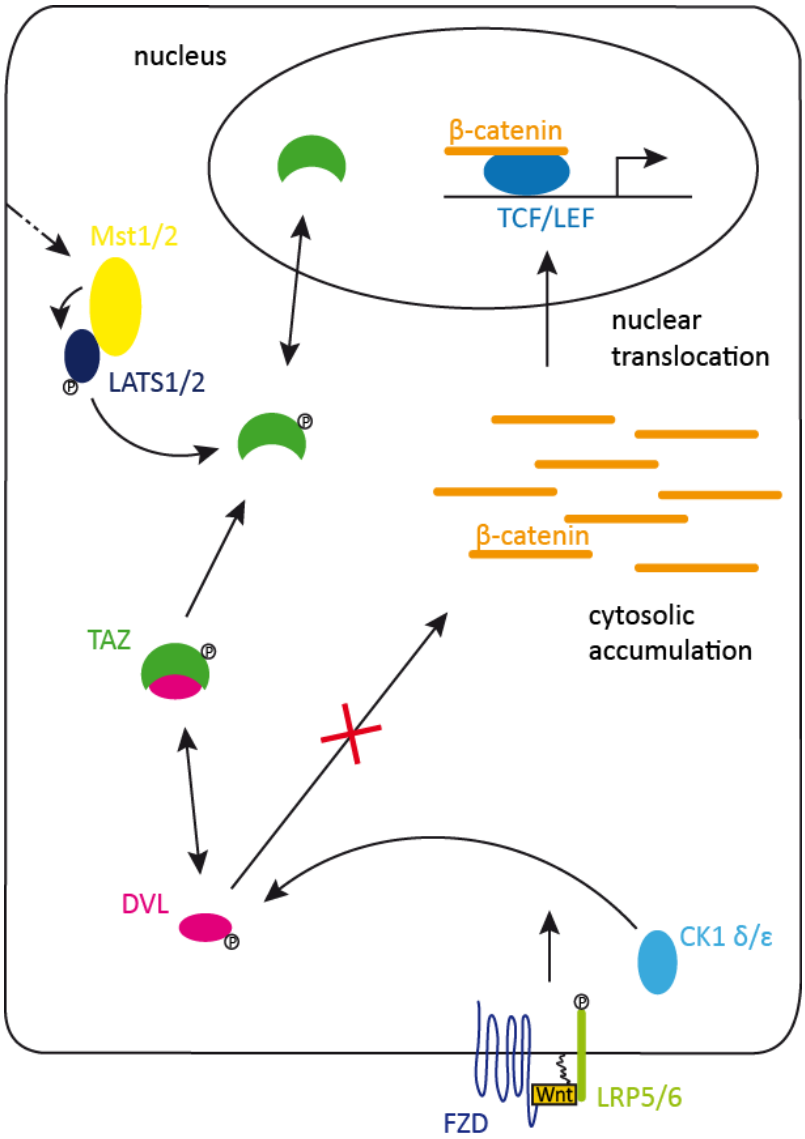

Figure 33: Schematic overview of the Hippo pathway-mediated inhibition of Wnt signaling.
The cytoplasmic localization of TAZ is induced by the Hippo pathway, which leads to an enhanced interaction between TAZ and DVL. Interaction with TAZ inhibits the binding of DVL to CK1 δ/ε and prevents the transcriptional activity induced through activated Wnt signaling. Thus, Hippo is able to modulate Wnt signaling, by limited responses to Wnt signals (Figure adapted from [187]).

β-catenin as a known transcriptional co-activator [152] is not only found in complexes with its major partners, but also associated with several other transcriptional co-activators, such as the FoxO proteins [211, 288] and the transcription factors from the TCF/LEF family [303, 304]. The detection of other transcriptional regulators showed, that the combinatory screening approach developed in this work is capable to detect new interactions of β-catenin with proteins, which are known to modulate transcription, but have not been brought into direct connection with β-catenin. Enabled by the identification of these PPIs, effects across different signaling cascades were detected and have to be interpreted in future. The possibility to add further, target-oriented screenings for specific proteins or to cover defined pathways completes the application spectrum of the developed screening approach.

5.6 β-catenin and MAPK signaling in hepatoma line 55.1c

The analysis of the mouse hepatoma cell line 55.1c, showed several clearly interacting proteins, that were not seen consistently in the other screened cell lines. Interestingly these are frequently associated with the MAPK pathways.

The MAPK pathways transduce signals from the cell membrane to the nucleus as a response to various stimuli. Thus, they participate in many intracellular signaling cascades [305]. They regulate many central processes, such as cell differentiation, proliferation, inflammation, cell growth and death [158, 306]. Hence, they also contribute to the pathology of various human diseases, like cancer or several neurodegenerative disorders [307]. The role of MAPKs in cancer is as pleiotropic as cancer itself [188, 308]. In total approximately 20 % of all human tumors show an activating mutation in a member of the RAS family (see Figure 34). Thus, both signaling cascades, Wnt/β-catenin and MAPK are subject to mutational activation in a large number of tumor types [29]. Gaining a deeper insight in the crosstalk between the two pathways, is of high interest. This crosstalk is rapidly emerging as more and more underlying, molecular details are unraveled [29].

The MAPK kinase family represents a group of four distinct subgroups, whereby the subsignaling cascades are named after their main MAP kinases: 1. MAPK/ERK pathway, 2. JNK/SAPK signaling, 3. p38/MAPK pathway and 4. BMK1 signal cascade (see Figure 34) [306]. In the following, the interacting proteins belonging to the first three subgroups will be described exemplarily. The MAPK/ERK cascade is activated by mitogens and growth factors, while the JNK and p38 pathways are cytokine- and stress-response-dependent [157, 307, 309]. Each of the MAPK signaling axes comprises three or more components: MAPK kinase kinases (MAP3Ks), which phosphorylate and activate MAPK kinases (MAPK2Ks). These in turn phosphorylate and activate MAPKs. Subsequently activated MAPKs are enabled to phosphorylate various substrate proteins, including transcription factors and downstream effectors, such as Elk-1 or the DUSPs [158, 309]. Selected PPIs detected in 55.1c cells, belonging to the MAPK pathway, are illustrated below and are shown in Figure 34.

A-Raf is a member of the Raf kinase family, which consists of three structurally similar kinases (A-Raf, B-Raf and C-Raf) and constitutes a family of Ser/Thr-protein kinases [196]. A-Raf mutations have not been found in human cancer [310], which can be explained by the fact that A-Raf requires two mutations for its oncogenic activation, while B-Raf, which is frequently mutated in cancer [311], only needs a single amino acid exchange [196]. Raf kinases are MAP3Ks and as such belong to the MAPK/ERK (extracellular signal-regulated kinase) pathway [197], but no direct physical interaction of A-Raf with β-catenin was shown so far.

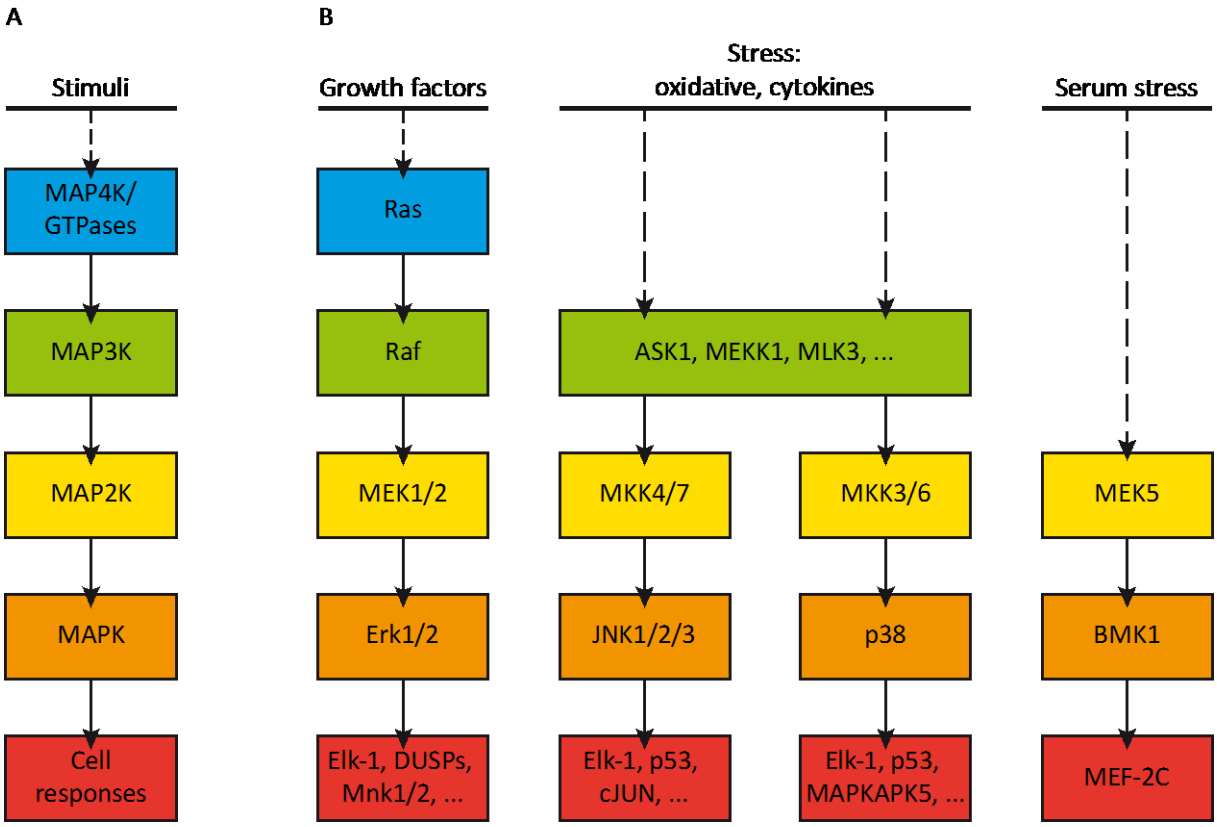

Figure 34: MAPK signaling pathways.
A: MAP4Ks or GTPases are stimulated via extracellular or intracellular stimuli and activate MAP3Ks. These mediate the phosphorylation and activation of MAP2Ks, which in turn phosphorylate and activate MAPKs. Activated MAPKs are able to phosphorylate various substrate proteins, including transcription factors. This results in the modulation of several cellular responses, such as cell proliferation, inflammatory responses, cell growth and death.
B: Erk1/2, p38, JNK1/2/3 and BMK1 belong to the mammalian MAPKs and name the distinct subgroups of the MAPK family. The specific upstream kinases and stimuli, as well as the cellular responses for each pathway, are pictured (Figure adapted from [309, 312]).

MKK7 belongs to the family of the Mitogen-activated protein kinase kinases (MAP2K) and is able to selectively activate only JNKs by phosphorylating preferably threonine but also tyrosine residues on the protein [190-194]. No direct physical interaction with β-catenin is known from literature so far, although it was identified as interactor here.

JNK/SAPKs (cJUN N-terminal kinases and stress activated protein kinases, also called MAPK8) belong to the group of MAP kinases [190]. They are activated by cytokines or environmental stress [313]. Additionally, they participate in various cellular functions, like the regulation of cellular proliferation or the binding and phosphorylating of cJUN [313, 314]. Several isoforms exist, of which JNK1 and JNK2 proteins are ubiquitously expressed, while JNK3 is only found in brain [190]. Both, JNK1 and JNK2, can induce the nuclear translocation of β-catenin by directly phosphorylating the protein [189]. Furthermore JNK can be activated directly through dual phosphorylation by MKK7 [202, 313] or DVL [195, 315], while the JNK cascade can be activated via Axin [195, 316]. This provides a possibility, how

Wnt signaling can mediate JNK/SAPK signaling. It has been shown, that JNK activity can be induced by Wnts, but it is still unclear, how this mechanism works [317].

MAPKAPK5 (MAP kinase-activated protein kinase 5, also known as PRAK) also belongs to the Ser/Thr kinase family [318]. It acts as a tumor suppressor presumably by directly phosphorylating and thereby modulating p53 activity [198]. As part of the p38/MAPK pathway, it is activated in response to cellular stress and proinflammatory cytokines by phosphorylation at Thr182 [318]. It is also known to directly interact with FoxO3a and by phosphorylating this protein, it is promoting its nuclear localization [319].

For the transcription factor Elk-1, no direct interaction with β-catenin is described in literature, still it was detected as an interacting protein of β-catenin here. Elk-1 is activated in the cytoplasm via phosphorylation by three classes of MAPKs: JNK, p38/MAPK and Erk [157, 320]. Based on its phosphorylation by Erks [321], Elk-1 is enabled to translocate from the cytoplasm into the nucleus [29]. There it promotes chromatin remodeling via the acetylation and phosphorylation of histones and recruits transcriptional co-activators [157].

The dual-specificity phosphatases (DUSPs) have been established as important negative regulators of the MAPK pathway [322]. They are part of the auto-inhibitory feedback loop in the MAPK signaling, where they dephosphorylate Erk1/2 [312, 323]. Besides that, they represent important mediators of crosstalk between the two pathways, MAPK and Wnt/β-catenin [29], since the murine DUSP6 gene is a transcriptional target of the β-catenin pathway [158]. Hence, the activity of MAPK signaling can be negatively regulated by the β-catenin-dependent induction of DUSPs [29]. For DUSP1, DUSP4 and DUSP9 no direct or distant interaction with the Wnt/β-catenin pathway was found in literature.

Besides the interaction between β-catenin and proteins of the MAPK pathways in 55.1c cells, also the other screened cell lines showed interacting proteins, which were assigned to the category “associated with MAPK pathway”. For example DUSP6 detected in untreated 70.4 cells, A-Raf found in CHIR 99021-treated 70.4 cells and JNK/STAT precipiated in HepG2 cells after MG132 treatment.

It was shown that by usage of this combinatory screening approach, it is possible to perform a targeted screening, searching for specific interactions between the Wnt/β-catenin and the MAPK pathways. Beyond that, the used approach can easily be transferred to generally identify PPIs and thereby confirming links between two or more determined pathways.

5.7 Analysis of the human HCC cell line HB35

The HB35 cell line is a recently established novel human hepatocellular carcinoma cell line. Its characterization was first published in 2012, with only little further investigations done so far. As the cell line is derived from a pediatric HCC, with no indication of viral hepatitis or cirrhosis, and since it shows a heterozygous deletion in the exon 3 of β-catenin [83], it serves as an interesting model to study Wnt/β-catenin signaling. During the analysis of the results obtained for the four different, screened liver cell lines, two proteins occurred as individual interaction partners of β-catenin only in HB35 cells. Furthermore, both proteins, histone deacetylase 6 (HDAC6) and Bcl9 (B-cell CLL/lymphoma 9 protein), solely appear after MG132 treatment.

HDAC6 belongs to the histone deacetylases, which catalyze the removal of acetyl groups from lysine residues in a variety of proteins and change the protein function in diverse ways [229]. 18 human histone deacetylases are known and sorted into three groups, according to their homology to the respective yeast proteins. HDAC6 has two catalytic sites and is member of the class II HDACs. As a protein belonging to class II, HDAC6 is able to shuttle between the cytoplasm and the nucleus [231]. In the cytoplasm, it can bind directly to β-catenin and deacetylates the Lys49 residue of β-catenin. This deacetylation has been shown to result in an inhibitory effect on the β-catenin phosphorylation at Ser45 [324]. HDAC6 also associates physically in a ternary complex with CD133 and β-catenin and stabilizes β-catenin via its deacetylase activity. If HDAC6 is down-regulated, β-catenin acetylation and degradation increases. Additionally, it was shown that HDAC6 is the deacetylase responsible for regulating the acetylation level of β-catenin [325], but it can also promote proliferation in cancer cell lines [326].

The Bcl9 protein, on the other side, is an important transcriptional co-activator of β-catenin [36]. It binds N-terminally to the first ARM repeats of β-catenin [327] and is able to shuttle, like other proteins, e.g. APC and TCF4, in and out of the nucleus. Additionally, it was suggested that both TCFs and Bcl9 might act as nuclear import factors, whereas APC and Axin may take part in actively exporting β-catenin into the cytoplasm [328]. Bcl9 could subsequently convey β-catenin from the cytoplasm to the TCF-target genes [64, 329] and is recruited by β-catenin to stimulate gene transcription [330, 331]. As Bcl9 is additionally able to directly interact with other transcriptional co-activators of β-catenin and strengthen their association with the TCF/β-catenin complex, it is implicated in signal transduction through the Wnt pathway [36, 228]. In addition, human tumor tissue expresses high levels of Bcl9 and the β-catenin/Bcl9 complex has become an interesting target for cancer therapy [332].

Hence, both identified interacting proteins, Bcl9 and HDAC6, are important partners of β-catenin. HDAC6 as well as Bcl9 can shuttle between the cytosol and the nucleus. Both are capable of binding β-catenin already in the cytosol, while for Bcl9 an interaction with β-catenin in the nucleus was

shown. It is striking, that most interacting partners were found in the untreated HB35 cells, while the amount of detected PPIs decreased after MG132 treatment and for CHIR 99021 only a low number of PPIs are obtained. Only three interactions remained detectable and four new ones were seen after CHIR 99021 treatment. For MG132 treatment seven novel interactions and five former ones recurred in comparison to the untreated sample.

5.8 Comparison of extracellular and intracellular IP

In this thesis an interesting novel approach, that reaches beyond the classical Co-IP, was applied to a defined experimental system, HEK293T cells. The possibility to express the BC1 nanobody intracellularly holds the advantage to detect endogenous β-catenin complexes *in vivo*. By connecting this novel approach to a screening tool like the DigiWest the idea of performing a wide ranging comparison between the conventional Co-IPs and intracellular Co-IP is self-evident. This was possible for ECIP and ICIP on HEK293T cells, as monogenetic cells were used and the identical nanobody was employed for capturing during Co-IP. Differences in the precipitated protein complexes of varying cell lines (derived from various tissues (e.g. liver, kidney) or diverse species (e.g. human, mouse)) would lead to difficulties during interpretation of the results in order not to miss important insights and connections among intracellular signaling cascades. In addition, the use of different antibodies (conventional antibody in the beginning and high affinity nanobody in posterior experiments) for the Co-IP experiments in this thesis introduces an additional variability in the precipitated β-catenin complexes. This variability is difficult to evaluate, especially as the capturing antibodies were directed towards oppositional ends of β-catenin. The characteristics of the nanobody (small size; recognition of the target protein β-catenin at the regulatory domain, the N-terminal SSTS-motif) might prevent the loss of complexes due to steric hindrances, but they might also promote the loss of interaction partners by competing for N-terminally located binding sites. On the other side, it is known, that the C-terminus of β-catenin serves as a platform for the recruitment of transcriptional co-activators [36, 327]. Therefore, a binding of a nanobody on the opposite end of β-catenin, might facilitate the formation of complexes with transcriptionally regulating interactors.

Introducing both a new cell line, HEK293T, and a new capturing molecule, led to the detection of four novel interacting proteins after ECIP, which were not obtained during the examination of the four different hepatoma cell lines.

CDK2 (Cyclin-dependent kinase 2) is a Ser/Thr kinase, which is involved in the control of the cell cycle [333, 334]. It is known to directly interact and phosphorylate β-catenin specifically at the same phosphorylation sites as GSK3 β (Ser33, Ser37, Thr41 and Ser45), but also other serine or threonine residues, which are followed by a proline residue [335]. In contrast to GSK3 β, CDK2 needs no priming phosphorylation at Ser45 [169]. Also other proteins, like p53 [336] or Ezh2 [337, 338], are known to be phosphorylated by CDK2.

MTA2 (Metastasis-associated protein) belongs to the metastasis tumor-associated family of transcriptional regulators. Together with other members of its family, it acts as core scaffold of the nucleosome remodeling and histone deacetylation (NuRD) complex [339]. So far no physical interaction between MTA2 and β-catenin is known from literature. It was shown, that a member of the MTA protein family, MTA3, is involved in controlling the E-Cadherin/β-catenin-complex and thus

maintaining the epithelial adhesion junctures and regulating EMT [340]. EMT being a process, which enables metastasizing of cancer cells [341].

Pontin52, also called RuvBL1 (RuvB-Like 1), is a protein, predominately localized in the nucleus. A direct, physical interaction with β-catenin was shown [342]. It may be involved in modulating the nuclear functions of β-catenin, independent of its interaction with LEF-1/TCF. *In vivo* a multiprotein complex composed of Pontin52, TCF and β-catenin exists, which suggests a stimulating role for Pontin52 in the activation of Wnt target genes [343, 344]. Reptin52, also called RuvBL2, as an interacting partner of Pontin52, is also known to bind β-catenin, but represses gene activation. This antagonistically mode of action on target gene activation constitutes a mechanism for controlling the Wnt/β-catenin pathway [344].

PP2A C is the abbreviation for the catalytic subunit of the Ser/Thr-protein phosphatase 2A. The PP2A family represent the most abundant Ser/Thr phosphatases in mammals and plays an important role in various biological processes [345, 346], like regulation of cell growth and division. PP2A has been shown to be part of the β-catenin destruction complex [36, 41]. In general, a suppressive effect of PP2A on the phosphorylation of Akt, which subsequently leads to the activation of GSK3 β and the phosphorylation, respectively degradation of β-catenin, has been described [347]. On the other hand, if N-terminally phosphorylated β-catenin is not associated with APC after leaving the destruction complex, PP2A dephosphorylates it immediately [348]. PP2A has been suggested to play both a positive and negative role in Wnt signaling. A regulatory role of PP2A, which promotes the phosphorylation and degradation of β-catenin, has been shown, as well as a direct interaction of the regulatory subunit PR55α of PP2A with β-catenin, which regulated the PP2A-mediated dephosphorylation of β-catenin [349]. Additionally, an interference with the destruction complex via Axin was shown [349]. This interference might provide an additional possibility of modulating Wnt signaling, if a loss of function for PP2A occurs [350]. Furthermore, PP2A C is a potent tumor suppressor, whose expression is decreased for example in prostate cancer and a correlation of the down-regulated expression with the tumor stage was shown [351].

As explained earlier (see 5.1) it is very interesting to be able to detect endogenous protein complexes directly and to discover dynamic PPIs related to Wnt/β-catenin signaling in a way that is as close to the natural cellular occurrence as possible. By the expression of a functional β-catenin-specific BC1-chromobody in living HEK293T cells, the investigation of already intracellularly existing β-catenin complexes via subsequent ICIP became possible. Hence, it was expected to precipitate low-affinity protein complexes, which are bound in the authentic cellular context, while additional binding proteins, with a higher affinity, but a spatial separation, can be largely avoided. Thus, it was assumed to obtain differences in the received interacting proteins after performance of the ICIP and at least a similar number of interaction partners as measured after ECIP.

The interaction of proteins was confirmed for several well-known interaction partners, such as GSK β, TCF1 and Axin. All three were detected both during ICIP and ECIP and were classified as strong or very strong interacting proteins. This can be seen as validation for the ICIP approach. Interestingly, less PPIs were detected via ICIP in the untreated and the CHIR 99021-treated HEK293T samples in general than in comparison to the interactors detected after ECIP. For ECIP in total 21 proteins were obtained, while for ICIP an entity of six proteins remained. Aside from that, only well-known interacting proteins arose after ICIP and the assumption of achieving novel, lower affinity complex partners could not be confirmed. A possible reason for that might be the difference in the performed duplicate or triplicate experiments. Both DigiWest and Co-IP have been shown to be reliable technical approaches before [89, 112], thus they can be excluded as cause for the obtained differences and the creation of artifacts in between multiple replicas. Biological replicas are known to show differences, thus it is the most probable remaining explanation for these artifacts is to trace their occurence back to cell culturing.

Fundamental and stable complex partners were detected with both approaches (ECIP and ICIP), while for lower affinity or less abundant interactors differences among the replicas occurred. These weaker interaction partners can disappear, as they might not always be detected due to a broken binding or an overlay by other, stronger signals. This phenomenon looks similar to difficulties in creating reliable data replicas, but is de facto a side effect of generating biological replicas in cell culture and not necessarily a shortcoming of the Co-IP or the DigiWest approach. On the contrary the obtained variations between the biological replicas support the DigiWest approach, as it illustrates its high sensitivity by being able to detect, distinguish and visualize even minor differences between varying samples. Already among the hepatoma cell lines (70.4, 55.1c, HepG2 and HB35) high differences in the amount of captured proteins are visible. In addition, these cells are known to be tumor cells which hold the characteristics of uncontrolled cell growth and proliferation. Thus, a decrease in the precipitated interaction partners in HEK293T cells can be explained. The application of increasingly harsh elimination criteria (see 3.4.3.3) simoultaneous to the introduction of additional replicas led to a further natural decrease in the number of confirmed interaction partners during subsequent analysis, although the high number of interacting proteins for a single replica is not reduced. The raw data obtained for each replica and using the identical elimination criteria for a single replica (see 4.2.2), 13 additional interacting proteins are revealed for ECIP, while eight more interactors are identified for ICIP. This results in an equally high amount of PPIs detected for ECIP and a small decrease for ICIP in comparison to conventional Co-IP on the hepatoma cell lines. A higher amount of PPIs detected for ECIP in comparison to ICIP remains. This correlates with an observation of detecting more interacting proteins after ECIP than for ICIP in preliminary experiments (data not included in this thesis). A possible reason for a smaller amount of PPIs detected for ICIP might be,

that for capturing and precipitating protein complexes during ICIP, one additional interaction between the GFP and the capturing molecule, addressing GFP, is required. In ECIP, the β-catenin-specific nanobody BC1 is directly coupled to the capturing beads used during Co-IP. Therefore, only two interaction points must endure a possible breakage during ECIP performance: the link between the nanobody and the target protein β-catenin as well as the bond between β-catenin and its interacting proteins (see Figure 35 A). For ICIP the possible breaking sites are increased by one, as one more physical connection has to be formed during Co-IP. Not only the interacting proteins have to remain linked to β-catenin and the bond between the intracellularly expressed BC1-chromobody and the target protein β-catenin has to stay together, but also the interaction between the GFP-Nanotrap® and the GFP, attached to the BC1-chromobody, needs to survive the washing steps during separation of input and bound sample after Co-IP (see Figure 35 B).

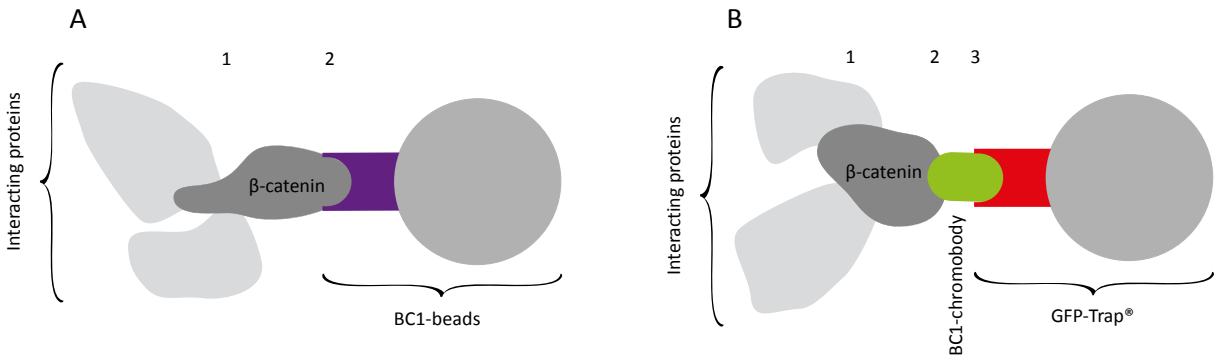

Figure 35: Possible breaking points during ECIP and ICIP.
The possible interaction points, which are built during ECIP (A) and ICIP (B) are represented.
A: Two possible break points are shown, which have to endure ECIP procedure. The first between the interacting proteins and β-catenin, and the second between the BC1 nanobody coupled to the bead surface and the target protein.
B: For ICIP in total three point have to remain after performing the Co-IP. First the link between β-catenin and the interacting proteins, second the intracellularly bond between β-catenin and the BC1-chromobody and third the binding between the GFP of the BC1-chromobody and the GFP-Trap®.

While comparing ECIP and ICIP results, it was additionally striking, that the CFs for the β-catenin variants, detected by the same antibodies, were overall higher after ICIP than after performing ECIP, both on the untreated and CHIR 99021-treated samples. The same phenomenon occurred for interacting proteins. Here, the CFs were also higher in the ICIP results. After CHIR 99021 treatment however, this result only recurred for the obtained PPIs, while for the differently addressed β-catenin pools the phenomenon was reversed. Thus, in comparison the CFs for ECIP were higher than the ones calculated for ICIP.

The higher CFs and proportionally higher raw values for the bound samples after ICIP might be based on the earlier and maybe still better intracellular binding of the BC1-chromobody to the target protein β-catenin. The few interaction partners, which were confirmed for ICIP, can be evaluated as

more authentic, not only because they are well-known from literature, but also because the ICIP approach with the former intracellular binding of protein complexes by the BC1-chromobody reflects a system, which is closer to the *in vivo* conditions. In addition, PPIs, which occur after destruction of the spatial separation within the cell, can largely be prevented.

5.9 Conclusion and outlook

The gained and presented results show that the combinatory approach of different Co-IP techniques and a novel readout system for immunoblots provides a versatile tool to examine protein complexes and their dynamic interactions. By employing target-specific antibodies and nanobodies towards β-catenin, the cancer relevant Wnt/β-catenin signaling was addressed and monitored in this thesis.

Co-IP is considered to be a gold standard for the detection and investigation of endogenous PPIs [94]. Especially the intracellular expression of binding molecules, as a further development of the conventional Co-IP approach, might lead to knowledge about the *in vivo* interactions between proteins and their crosstalk. The DigiWest shows the advantages of the classical Western blot, such as a high reliability, combined with features, like high throughput and low material consumption. The combination of both techniques facilitates the run of focused proteomic studies and the facile detection of differences in the activation states of cellular signaling cascades.

The ability of visualizing the modulation of available proteins by drug treatment in different cell lysates was shown. Differences occurring between screened cell lines and their individual response to treatment were illustrated (see 4.1) and classified the DigiWest as a valuable screening tool to uncover alterations in between various samples and upon drug treatment. In connection with the Co-IP approach, it was possible to precipitate β-catenin, the key player of the canonical Wnt signaling, and different posttranslational modified variants of the target protein. The modulation of these differently modified variants of β-catenin after drug treatment with CHIR 99021 and MG132 was visible. Additionally, major differences in between the screened cell lines were seen according to the precipitated interaction partners of β-catenin (see 4.2). Besides the identification of proteins, participating in well-known β-catenin complexes, such as GSK3, E-Cadherin and α-catenin, also various other possible interacting proteins were classified.

The application of a high-affinity nanobody against β-catenin and the exchange of the cell system, led to changes in the detected interaction partners. Besides newly identified PPIs, many of the well-known interactors, like TCF4, GSK3 β and Axin, were seen by using ECIP (see 4.3). By employing a nanobody as capturing molecule, it was moreover possible to use it as an intracellularly expressed captor to perform ICIPs. It was shown, that the combination of ICIP with the DigiWest constitutes an useful screening tool, which precipitated and detected highly affine proteins (see 4.4). In addition, the effects of CHIR 99021 treatment were visible both for ECIP and ICIP and resulted in general in an increase of the precipitated proteins.

By classifying a large variety of interacting proteins during performance of the different combinatory screening approaches, the possibility of covering the Wnt signaling cascade and its spatial cellular surrounding with specific antibodies was enabled. This provides an opportunity to both reveal links to other important signaling cascades, such as the MAPK pathway, as well as to identify entirely

unknown crosstalks in between pathways. It was possible to show the suitability of employing this novel screening approach to illustrate differences between samples and upon treatment. Additionally, the opportunity to screen for a multitude of potential PPIs of β-catenin and for specific PTMs of the analyzed proteins, facilitates new insights into cellular networks. These will allow a to gain a deeper understanding of the cellular signaling crosstalk in the long run.

Still, several validation experiments (e.g. generating replicas of the hepatoma cell lines) have to be performed. A confirmation of the results using different experimental approaches would be possible, such as targeted MS analyses, immunohistochemistry (IHC) or mRNA expression analyses. It also seems possible, to expand the gained knowledge about HCCs and HBs by comparing the generated results to identical performed experiments on primary hepatocytes. Primary hepatocytes are closest to the real system and might provide a better reflection of the actual signaling in the liver, thus occurring changes due to cell culturing might be prevented. Since the nanobody for capturing β-catenin in ECIP and ICIP used in this thesis can be stably expressed inside the living cell, additional cell lines could be transfected and compared in order to complete the so far gained knowledge. In addition, many of the obtained results have to be put into biological context, which includes further target-oriented screenings to round off the gained information.

The combinatory high throughput screening approach of Co-IP and DigiWest offers several promising ways of application, such as the observation of dynamic changes of PPIs dependent on time point, drug treatment or the examined sample tissue. The importance of achieving a deeper understanding of the PPIs and the crosstalk between two pathways, e.g. between Wnt/β-catenin and MAPK signaling (see 5.6), becomes clear, as many diseases such as cancer result from disturbed or unusual forms of inter- and intracellular communication. These disturbances are caused by mutational changes or the deregulation of cellular pathways [352]. A way of deciphering these aberrant cellular communications needs to be learned in order to target and modulate the altered signaling cascades [308]. Thereby is the identification of proteins, which modulate the activation state of various pathways as well as the understanding of their mode of action, of high relevance, as it provides a possibility for identifying biomarkers. Biomarkers in turn may not only help to diagnose diseases, but also to design effective drugs for therapy [352].

In this thesis, a possible way of achieving deeper insights into the cellular network was shown for addressing β-catenin, as one of the main molecules in the canonical Wnt signaling, and precipitating its complex partners. Proteins, which caught attention in research recently, such as TAZ (the transcriptional co-activator of the Hippo pathway) [187, 299, 300], E-cadherin (playing an important role in cell adhesion and preventing tumor metastasis) [265, 266, 353] or HDAC6 (a deacetylase modifying β-catenin and regulating its acetylation, active at various subcellular locations) [324-326] were detected as interaction partners in this work. All of them link β-catenin to different pathways or

complexes and thereby create the basis for its influence on a variety of signaling cascades and disease progression [62, 259, 354, 355]. An understanding of the physical interaction between β-catenin and other proteins or pathways might point to central connections which might help to identify specific Wnt pathways inhibitors. These inhibitors are important, as an aberrant activation of this signaling cascade results in the development of various diseases, such as cancer [62, 259]. Additionally, the modulation of PTMs of Wnt pathway components might depict a promising alternative in drug development, as these modifications have a high impact on the signaling state.

Taken together, this combinatory screening approach was developed, verified and applied in this thesis. Beyond that, PPIs published in research recently were detected and provided an additional confirmation of the approach. Furthermore, the approach is not limited to the canonical Wnt signaling or β-catenin as the addressed Co-IP molecule, but can easily be transferred and applied to other signaling cascades and their key proteins. By usage of this combinatory screening approach, it is possible to perform a targeted screening, searching for specific interactions between two or more determined pathways. Thereby it provides a versatile high throughput tool for the analysis of protein networks and signaling cascade interactions in general. The obtained results may be seen as a first impression, although validation and explanation of the biological mechanisms behind the generated knowledge remain challenging and will need further experimental studies.

6. Literature

1. Braun, P. and A.C. Gingras, *History of protein-protein interactions: from egg-white to complex networks.* Proteomics, 2012. **12**(10): p. 1478-98.
2. Hamers-Casterman, C., et al., *Naturally occurring antibodies devoid of light chains.* Nature, 1993. **363**(6428): p. 446-8.
3. Venter, J.C., et al., *The sequence of the human genome.* Science, 2001. **291**(5507): p. 1304-51.
4. Lander, E.S., et al., *Initial sequencing and analysis of the human genome.* Nature, 2001. **409**(6822): p. 860-921.
5. Yamada, K., et al., *Empirical analysis of transcriptional activity in the Arabidopsis genome.* Science, 2003. **302**(5646): p. 842-6.
6. Versteeg, R., et al., *The human transcriptome map reveals extremes in gene density, intron length, GC content, and repeat pattern for domains of highly and weakly expressed genes.* Genome Res, 2003. **13**(9): p. 1998-2004.
7. Weintz, G., et al., *The phosphoproteome of toll-like receptor-activated macrophages.* Mol Syst Biol, 2010. **6**: p. 371.
8. Wilkins, M.R., et al., *From proteins to proteomes: large scale protein identification by two-dimensional electrophoresis and amino acid analysis.* Biotechnology (N Y), 1996. **14**(1): p. 61-5.
9. James, P., *Protein identification in the post-genome era: the rapid rise of proteomics.* Q Rev Biophys, 1997. **30**(4): p. 279-331.
10. Kirik, U., *Development of Computational Methods for Cancer Research - Strategies for closing the feedback loop in omics workflows*, in *Faculty of Engineering*. 2015, Lund University: Lund.
11. Kholodenko, B.N., *Cell-signalling dynamics in time and space.* Nat Rev Mol Cell Biol, 2006. **7**(3): p. 165-76.
12. Ning, Z., et al., *Detecting protein-protein interactions/complex components using mass spectrometry coupled techniques.* Methods Mol Biol, 2014. **1164**: p. 1-13.
13. Genomes Project, C., et al., *A map of human genome variation from population-scale sequencing.* Nature, 2010. **467**(7319): p. 1061-73.
14. Martin, G.S., *Cell signaling and cancer.* Cancer Cell, 2003. **4**(3): p. 167-74.
15. Ivanov, A.A., F.R. Khuri, and H. Fu, *Targeting protein-protein interactions as an anticancer strategy.* Trends Pharmacol Sci, 2013. **34**(7): p. 393-400.
16. De Las Rivas, J. and C. Fontanillo, *Protein-protein interactions essentials: key concepts to building and analyzing interactome networks.* PLoS Comput Biol, 2010. **6**(6): p. e1000807.
17. Torre, L.A., et al., *Global cancer statistics, 2012.* CA Cancer J Clin, 2015. **65**(2): p. 87-108.
18. Ferlay, J., et al., *Cancer incidence and mortality worldwide: sources, methods and major patterns in GLOBOCAN 2012.* Int J Cancer, 2015. **136**(5): p. E359-86.
19. Kaatsch, O., et al., *Krebs in Deutschland 2011/2012*. Vol. 10. Ausgabe. 2015, Berlin: Robert Koch-Institut, Gesellschaft der epidemiologischen Krebsregister in Deutschland e.V.
20. Hanahan, D. and R.A. Weinberg, *Hallmarks of cancer: the next generation.* Cell, 2011. **144**(5): p. 646-74.
21. Hanahan, D. and R.A. Weinberg, *The hallmarks of cancer.* Cell, 2000. **100**(1): p. 57-70.
22. Mantovani, A., *Cancer: Inflaming metastasis.* Nature, 2009. **457**(7225): p. 36-7.
23. Nusse, R., *Wnt signaling in disease and in development.* Cell Res, 2005. **15**(1): p. 28-32.
24. Zeller, E., *The Role of Gtl2 in Hepatocarcinogenesis*, in *Mathematisch-Naturwissenschaftliche Fakultät*. 2015, Eberhard Karls Universität: Tübingen.
25. Reya, T. and H. Clevers, *Wnt signalling in stem cells and cancer.* Nature, 2005. **434**(7035): p. 843-50.
26. Logan, C.Y. and R. Nusse, *The Wnt signaling pathway in development and disease.* Annu Rev Cell Dev Biol, 2004. **20**: p. 781-810.

27. van Amerongen, R. and R. Nusse, *Towards an integrated view of Wnt signaling in development.* Development, 2009. **136**(19): p. 3205-14.
28. Anastas, J.N. and R.T. Moon, *WNT signalling pathways as therapeutic targets in cancer.* Nat Rev Cancer, 2013. **13**(1): p. 11-26.
29. Zeller, E., et al., *Mechanisms of RAS/beta-catenin interactions.* Arch Toxicol, 2013. **87**(4): p. 611-32.
30. Luckert, K., *Snapshots of protein dynamics and posttranslational modifications in one experiment – beta-catenin and its functions*, in *Mathematisch-Naturwissenschaftliche Fakultät*. 2010, Eberhard Karls Universität: Tübingen.
31. Behrens, J. and B. Lustig, *The Wnt connection to tumorigenesis.* Int J Dev Biol, 2004. **48**(5-6): p. 477-87.
32. Moon, R.T., et al., *WNT and beta-catenin signalling: diseases and therapies.* Nat Rev Genet, 2004. **5**(9): p. 691-701.
33. Polakis, P., *Wnt signaling and cancer.* Genes Dev, 2000. **14**(15): p. 1837-51.
34. Erdmann, G., *Evi/Wls Mediated Wnt Secretion is Required for Colon Cancer Growth and Survival Despite APC or β-catenin Mutations* in *Combined Faculties of Natural Sciences and for Mathematics*. 2012, Ruperto-Carola University: Heidelberg. p. 115.
35. Komiya, Y. and R. Habas, *Wnt signal transduction pathways.* Organogenesis, 2008. **4**(2): p. 68-75.
36. Valenta, T., G. Hausmann, and K. Basler, *The many faces and functions of beta-catenin.* EMBO J, 2012. **31**(12): p. 2714-36.
37. Grumolato, L., et al., *Canonical and noncanonical Wnts use a common mechanism to activate completely unrelated coreceptors.* Genes Dev, 2010. **24**(22): p. 2517-30.
38. Railo, A., et al., *Wnt-11 signaling leads to down-regulation of the Wnt/beta-catenin, JNK/AP-1 and NF-kappaB pathways and promotes viability in the CHO-K1 cells.* Exp Cell Res, 2008. **314**(13): p. 2389-99.
39. Takigawa, Y. and A.M. Brown, *Wnt signaling in liver cancer.* Curr Drug Targets, 2008. **9**(11): p. 1013-24.
40. Clevers, H., *Wnt/beta-catenin signaling in development and disease.* Cell, 2006. **127**(3): p. 469-80.
41. Kimelman, D. and W. Xu, *beta-catenin destruction complex: insights and questions from a structural perspective.* Oncogene, 2006. **25**(57): p. 7482-91.
42. Cadigan, K.M. and M. Peifer, *Wnt signaling from development to disease: insights from model systems.* Cold Spring Harb Perspect Biol, 2009. **1**(2): p. a002881.
43. Hart, M., et al., *The F-box protein beta-TrCP associates with phosphorylated beta-catenin and regulates its activity in the cell.* Curr Biol, 1999. **9**(4): p. 207-10.
44. Papkoff, J. and M. Aikawa, *WNT-1 and HGF regulate GSK3 beta activity and beta-catenin signaling in mammary epithelial cells.* Biochem Biophys Res Commun, 1998. **247**(3): p. 851-8.
45. Aberle, H., et al., *beta-catenin is a target for the ubiquitin-proteasome pathway.* EMBO J, 1997. **16**(13): p. 3797-804.
46. Gonzalez-Sancho, J.M., et al., *Wnt proteins induce dishevelled phosphorylation via an LRP5/6-independent mechanism, irrespective of their ability to stabilize beta-catenin.* Mol Cell Biol, 2004. **24**(11): p. 4757-68.
47. Gonzalez-Sancho, J.M., et al., *Functional consequences of Wnt-induced dishevelled 2 phosphorylation in canonical and noncanonical Wnt signaling.* J Biol Chem, 2013. **288**(13): p. 9428-37.
48. Boutros, M. and M. Mlodzik, *Dishevelled: at the crossroads of divergent intracellular signaling pathways.* Mech Dev, 1999. **83**(1-2): p. 27-37.
49. Knippschild, U., et al., *The casein kinase 1 family: participation in multiple cellular processes in eukaryotes.* Cell Signal, 2005. **17**(6): p. 675-89.
50. Bilic, J., et al., *Wnt induces LRP6 signalosomes and promotes dishevelled-dependent LRP6 phosphorylation.* Science, 2007. **316**(5831): p. 1619-22.

51. Schwarz-Romond, T., C. Metcalfe, and M. Bienz, *Dynamic recruitment of axin by Dishevelled protein assemblies.* J Cell Sci, 2007. **120**(Pt 14): p. 2402-12.
52. Zeng, X., et al., *Initiation of Wnt signaling: control of Wnt coreceptor Lrp6 phosphorylation/activation via frizzled, dishevelled and axin functions.* Development, 2008. **135**(2): p. 367-75.
53. Bryja, V., G. Schulte, and E. Arenas, *Wnt-3a utilizes a novel low dose and rapid pathway that does not require casein kinase 1-mediated phosphorylation of Dvl to activate beta-catenin.* Cell Signal, 2007. **19**(3): p. 610-6.
54. Najdi, R., R.F. Holcombe, and M.L. Waterman, *Wnt signaling and colon carcinogenesis: beyond APC.* J Carcinog, 2011. **10**: p. 5.
55. Archbold, H.C., et al., *How do they do Wnt they do?: regulation of transcription by the Wnt/beta-catenin pathway.* Acta Physiol (Oxf), 2012. **204**(1): p. 74-109.
56. Voronkov, A. and S. Krauss, *Wnt/beta-catenin signaling and small molecule inhibitors.* Curr Pharm Des, 2013. **19**(4): p. 634-64.
57. Xu, W. and D. Kimelman, *Mechanistic insights from structural studies of beta-catenin and its binding partners.* J Cell Sci, 2007. **120**(Pt 19): p. 3337-44.
58. Taurin, S., et al., *Phosphorylation of beta-catenin by cyclic AMP-dependent protein kinase.* J Biol Chem, 2006. **281**(15): p. 9971-6.
59. Olsen, J.V., et al., *Global, in vivo, and site-specific phosphorylation dynamics in signaling networks.* Cell, 2006. **127**(3): p. 635-48.
60. Cohen, P., *The role of protein phosphorylation in human health and disease. The Sir Hans Krebs Medal Lecture.* Eur J Biochem, 2001. **268**(19): p. 5001-10.
61. Pawson, T. and P. Nash, *Assembly of cell regulatory systems through protein interaction domains.* Science, 2003. **300**(5618): p. 445-52.
62. Gao, C., G. Xiao, and J. Hu, *Regulation of Wnt/beta-catenin signaling by posttranslational modifications.* Cell Biosci, 2014. **4**(1): p. 13.
63. Daugherty, R.L. and C.J. Gottardi, *Phospho-regulation of Beta-catenin adhesion and signaling functions.* Physiology (Bethesda), 2007. **22**: p. 303-9.
64. de la Roche, M., et al., *An intrinsically labile alpha-helix abutting the BCL9-binding site of beta-catenin is required for its inhibition by carnosic acid.* Nat Commun, 2012. **3**: p. 680.
65. Daniels, D.L., K. Eklof Spink, and W.I. Weis, *beta-catenin: molecular plasticity and drug design.* Trends Biochem Sci, 2001. **26**(11): p. 672-8.
66. Monga, S.P., et al., *Beta-catenin antisense studies in embryonic liver cultures: role in proliferation, apoptosis, and lineage specification.* Gastroenterology, 2003. **124**(1): p. 202-16.
67. Hussain, S.Z., et al., *Wnt impacts growth and differentiation in ex vivo liver development.* Exp Cell Res, 2004. **292**(1): p. 157-69.
68. Thompson, M.D. and S.P. Monga, *WNT/beta-catenin signaling in liver health and disease.* Hepatology, 2007. **45**(5): p. 1298-305.
69. Nejak-Bowen, K. and S.P. Monga, *Wnt/beta-catenin signaling in hepatic organogenesis.* Organogenesis, 2008. **4**(2): p. 92-9.
70. Calvisi, D.F., et al., *Ubiquitous activation of Ras and Jak/Stat pathways in human HCC.* Gastroenterology, 2006. **130**(4): p. 1117-28.
71. Gedaly, R., et al., *Targeting the Wnt/beta-catenin signaling pathway in liver cancer stem cells and hepatocellular carcinoma cell lines with FH535.* PLoS One, 2014. **9**(6): p. e99272.
72. Llovet, J.M., A. Burroughs, and J. Bruix, *Hepatocellular carcinoma.* Lancet, 2003. **362**(9399): p. 1907-17.
73. Monga, S.P., *beta-Catenin Signaling and Roles in Liver Homeostasis, Injury, and Tumorigenesis.* Gastroenterology, 2015. **148**(7): p. 1294-310.
74. de La Coste, A., et al., *Somatic mutations of the beta-catenin gene are frequent in mouse and human hepatocellular carcinomas.* Proc Natl Acad Sci U S A, 1998. **95**(15): p. 8847-51.
75. Koch, A., et al., *Childhood hepatoblastomas frequently carry a mutated degradation targeting box of the beta-catenin gene.* Cancer Res, 1999. **59**(2): p. 269-73.

76. Kress, S., et al., *p53 mutations are absent from carcinogen-induced mouse liver tumors but occur in cell lines established from these tumors.* Mol Carcinog, 1992. **6**(2): p. 148-58.
77. Aydinlik, H., et al., *Selective pressure during tumor promotion by phenobarbital leads to clonal outgrowth of beta-catenin-mutated mouse liver tumors.* Oncogene, 2001. **20**(53): p. 7812-6.
78. Braeuning, A., et al., *Coordinate regulation of cytochrome P450 1a1 expression in mouse liver by the aryl hydrocarbon receptor and the beta-catenin pathway.* Toxicol Sci, 2011. **122**(1): p. 16-25.
79. Aden, D.P., et al., *Controlled synthesis of HBsAg in a differentiated human liver carcinoma-derived cell line.* Nature, 1979. **282**(5739): p. 615-6.
80. Knowles, B.B., C.C. Howe, and D.P. Aden, *Human hepatocellular carcinoma cell lines secrete the major plasma proteins and hepatitis B surface antigen.* Science, 1980. **209**(4455): p. 497-9.
81. Qiu, G.-H., et al., *Distinctive pharmacological differences between liver cancer cell lines HepG2 and Hep3B.* Cytotechnology, 2015. **67**(1): p. 1-12.
82. Lopez-Terrada, D., et al., *Hep G2 is a hepatoblastoma-derived cell line.* Hum Pathol, 2009. **40**(10): p. 1512-5.
83. Armeanu-Ebinger, S., et al., *Characterisation of the cell line HC-AFW1 derived from a pediatric hepatocellular carcinoma.* PLoS One, 2012. **7**(5): p. e38223.
84. Adesina, A.M., et al., *Gene expression profiling reveals signatures characterizing histologic subtypes of hepatoblastoma and global deregulation in cell growth and survival pathways.* Hum Pathol, 2009. **40**(6): p. 843-53.
85. Cagatay, T. and M. Ozturk, *P53 mutation as a source of aberrant beta-catenin accumulation in cancer cells.* Oncogene, 2002. **21**(52): p. 7971-80.
86. Baur, N., *Multiplexe Immunoassays zur Quantifizierung von biogenen Aminen*, in *Mathematisch-Naturwissenschaftliche Fakultät*. 2013, Eberhard Karls Universität: Tübingen.
87. Wellhausen, R. and H. Seitz, *Facing current quantification challenges in protein microarrays.* J Biomed Biotechnol, 2012. **2012**: p. 831347.
88. Templin, M.F., et al., *Protein microarray technology.* Trends Biotechnol, 2002. **20**(4): p. 160-6.
89. Treindl, F., *DigiWest: a high throughput Western-Blot and its application for comprehensive signaling analysis of microdissected liver tissue*, in *Mathematisch-Naturwissenschaftliche Fakultät*. 2015, Eberhard Karls Universität: Tübingen.
90. dupont, N.C., et al., *Validation and comparison of luminex multiplex cytokine analysis kits with ELISA: determinations of a panel of nine cytokines in clinical sample culture supernatants.* J Reprod Immunol, 2005. **66**(2): p. 175-91.
91. Treindl, F., et al., *A bead-based Western for high-throughput cellular signal transduction analyses.* Nature communications, 2016. **in review**.
92. Huang, B.X. and H.Y. Kim, *Effective identification of Akt interacting proteins by two-step chemical crosslinking, co-immunoprecipitation and mass spectrometry.* PLoS One, 2013. **8**(4): p. e61430.
93. Kocher, T. and G. Superti-Furga, *Mass spectrometry-based functional proteomics: from molecular machines to protein networks.* Nat Methods, 2007. **4**(10): p. 807-15.
94. Mohammed, H. and J.S. Carroll, *Approaches for assessing and discovering protein interactions in cancer.* Mol Cancer Res, 2013. **11**(11): p. 1295-302.
95. Hermey, G., et al., *Analyse von Proteinen*, in *Der Experimentator: Neurowissenschaften*. 2010, Spektrum Akademischer Verlag.
96. Kohler, G. and C. Milstein, *Continuous cultures of fused cells secreting antibody of predefined specificity.* Nature, 1975. **256**(5517): p. 495-7.
97. Deffar, K., et al., *Nanobodies - the new concept in antibody engineering.* African Journal of Biotechnology, 2009. **8**(12): p. 2645-2652.
98. Reichert, J. and A. Pavolu, *Monoclonal antibodies market.* Nat Rev Drug Discov, 2004. **3**(5): p. 383-4.

99. Pavlou, A.K. and M.J. Belsey, *The therapeutic antibodies market to 2008.* Eur J Pharm Biopharm, 2005. **59**(3): p. 389-96.
100. Kurien, B.T. and R.H. Scofield, *Western blotting.* Methods for Analyzing Cytokines, 2006. **38**(4): p. 283-293.
101. Williams, N.E., *Immunoprecipitation Procedures*, in *Methods in Cell Biology*. 1999. p. 449-453.
102. Harmsen, M.M. and H.J. De Haard, *Properties, production, and applications of camelid single-domain antibody fragments.* Appl Microbiol Biotechnol, 2007. **77**(1): p. 13-22.
103. Conrath, K.E., et al., *Emergence and evolution of functional heavy-chain antibodies in Camelidae.* Dev Comp Immunol, 2003. **27**(2): p. 87-103.
104. Muyldermans, S., *Single domain camel antibodies: current status.* J Biotechnol, 2001. **74**(4): p. 277-302.
105. Van Audenhove, I., et al., *Mapping cytoskeletal protein function in cells by means of nanobodies.* Cytoskeleton (Hoboken), 2013. **70**(10): p. 604-22.
106. Muyldermans, S., *Nanobodies: natural single-domain antibodies.* Annu Rev Biochem, 2013. **82**: p. 775-97.
107. Schmidthals, K., et al., *Novel antibody derivatives for proteome and high-content analysis.* Anal Bioanal Chem, 2010. **397**(8): p. 3203-8.
108. Rothbauer, U., et al., *Targeting and tracing antigens in live cells with fluorescent nanobodies.* Nat Methods, 2006. **3**(11): p. 887-9.
109. Burgess, A., T. Lorca, and A. Castro, *Quantitative live imaging of endogenous DNA replication in mammalian cells.* PLoS One, 2012. **7**(9): p. e45726.
110. Zolghadr, K., et al., *Chromobodies: Forschung und Diagnostik mit fluoreszierenden Nanosonden.* BIO*spektrum*, 2009. **15**(3): p. 3.
111. Revets, H., P. De Baetselier, and S. Muyldermans, *Nanobodies as novel agents for cancer therapy.* Expert Opin Biol Ther, 2005. **5**(1): p. 111-24.
112. Traenkle, B., et al., *Monitoring interactions and dynamics of endogenous beta-catenin with intracellular nanobodies in living cells.* Mol Cell Proteomics, 2015. **14**(3): p. 707-23.
113. Kirchhofer, A., et al., *Modulation of protein properties in living cells using nanobodies.* Nat Struct Mol Biol, 2010. **17**(1): p. 133-8.
114. Helma, J., et al., *Direct and dynamic detection of HIV-1 in living cells.* PLoS One, 2012. **7**(11): p. e50026.
115. Saeed, A.I., et al., *TM4 microarray software suite.* Methods Enzymol, 2006. **411**: p. 134-93.
116. Saeed, A.I., et al., *TM4: a free, open-source system for microarray data management and analysis.* Biotechniques, 2003. **34**(2): p. 374-8.
117. Chatr-Aryamontri, A., et al., *The BioGRID interaction database: 2015 update.* Nucleic Acids Res, 2015. **43**(Database issue): p. D470-8.
118. Kotlyar, M., et al., *In silico prediction of physical protein interactions and characterization of interactome orphans.* Nat Methods, 2015. **12**(1): p. 79-84.
119. Hermjakob, H., et al., *IntAct: an open source molecular interaction database.* Nucleic Acids Res, 2004. **32**(Database issue): p. D452-5.
120. Kerrien, S., et al., *The IntAct molecular interaction database in 2012.* Nucleic Acids Res, 2012. **40**(Database issue): p. D841-6.
121. UniProt, C., *UniProt: a hub for protein information.* Nucleic Acids Res, 2015. **43**(Database issue): p. D204-12.
122. Hoh, A., et al., *The activity of gammadelta T cells against paediatric liver tumour cells and spheroids in cell culture.* Liver Int, 2013. **33**(1): p. 127-36.
123. Pear, W.S., et al., *Production of high-titer helper-free retroviruses by transient transfection.* Proc Natl Acad Sci U S A, 1993. **90**(18): p. 8392-6.
124. Tan, C.W., et al., *Analysis of Wnt signaling beta-catenin spatial dynamics in HEK293T cells.* BMC Syst Biol, 2014. **8**: p. 44.
125. Galvao, J., et al., *Unexpected low-dose toxicity of the universal solvent DMSO.* FASEB J, 2014. **28**(3): p. 1317-30.

126. Petzuch, B., et al., *Application of HC-AFW1 Hepatocarcinoma Cells for Mechanistic Studies: Regulation of Cytochrome P450 2B6 Expression by Dimethyl Sulfoxide and Early Growth Response 1.* Drug Metab Dispos, 2015. **43**(11): p. 1727-33.
127. Yakulov, T., et al., *Wnt3a-dependent and -independent protein interaction networks of chromatin-bound beta-catenin in mouse embryonic stem cells.* Mol Cell Proteomics, 2013. **12**(7): p. 1980-94.
128. Laemmli, U.K., *Cleavage of structural proteins during the assembly of the head of bacteriophage T4.* Nature, 1970. **227**(5259): p. 680-5.
129. Rothbauer, U., et al., *A versatile nanotrap for biochemical and functional studies with fluorescent fusion proteins.* Mol Cell Proteomics, 2008. **7**(2): p. 282-9.
130. Littlehales, W.J., *Electroblotting technique for transferring specimens from a polyacrylamide electrophoresis or like gel onto a membrane*. 1989, Google Patents.
131. Schutz-Geschwender, A., et al., *Quantitative, Two-Color Western Blot Detection With Infrared Fluorescence.* LI-COR Bioscience, 2004: p. 1-7.
132. Green, N.M., *Avidin.* Adv Protein Chem, 1975. **29**: p. 85-133.
133. Angeloni, S., et al., *xMAP® Cookbook*. 2nd ed. 2014: Luminex Corporation.
134. D'Haeseleer, P., *How does gene expression clustering work?* Nat Biotechnol, 2005. **23**(12): p. 1499-501.
135. Kaboord, B. and M. Perr, *Isolation of proteins and protein complexes by immunoprecipitation.* Methods Mol Biol, 2008. **424**: p. 349-64.
136. Bonifacino, J.S., E.C. Dell'Angelica, and T.A. Springer, *Immunoprecipitation*. Curr Protoc Neurosci. Vol. Chapter 5. 2006. Unit 5 24.
137. Polakis, P., *Wnt signaling in cancer.* Cold Spring Harb Perspect Biol, 2012. **4**(5).
138. Taipale, J. and P.A. Beachy, *The Hedgehog and Wnt signalling pathways in cancer.* Nature, 2001. **411**(6835): p. 349-54.
139. Yang, K., et al., *The evolving roles of canonical WNT signaling in stem cells and tumorigenesis: implications in targeted cancer therapies.* Lab Invest, 2016. **96**(2): p. 116-36.
140. Zhu, J., et al., *On the nature of human housekeeping genes.* Trends Genet, 2008. **24**(10): p. 481-4.
141. Tan, S.C., et al., *Identification of valid housekeeping genes for quantitative RT-PCR analysis of cardiosphere-derived cells preconditioned under hypoxia or with prolyl-4-hydroxylase inhibitors.* Mol Biol Rep, 2012. **39**(4): p. 4857-67.
142. Schmitz, S., *Zellkulturen, Zelllinien und deren Einsatzmöglichkeiten*, in *Der Experimentator: Zellkultur*. 2011, Spektrum Akademischer Verlag: Heidelberg.
143. Latchman, D.S., *Transcription factors: an overview.* Int J Biochem Cell Biol, 1997. **29**(12): p. 1305-12.
144. Lois, S., et al., *The functional modulation of epigenetic regulators by alternative splicing.* BMC Genomics, 2007. **8**: p. 252.
145. Cohen, P. and S. Frame, *The renaissance of GSK3.* Nat Rev Mol Cell Biol, 2001. **2**(10): p. 769-76.
146. Jaitovich, A., et al., *Ubiquitin-proteasome-mediated degradation of keratin intermediate filaments in mechanically stimulated A549 cells.* J Biol Chem, 2008. **283**(37): p. 25348-55.
147. Wong, C.M., S.T. Fan, and I.O. Ng, *beta-Catenin mutation and overexpression in hepatocellular carcinoma: clinicopathologic and prognostic significance.* Cancer, 2001. **92**(1): p. 136-45.
148. Han, S.P. and A.S. Yap, *An alpha-catenin deja vu.* Nat Cell Biol, 2013. **15**(3): p. 238-9.
149. Drees, F., et al., *Alpha-catenin is a molecular switch that binds E-cadherin-beta-catenin and regulates actin-filament assembly.* Cell, 2005. **123**(5): p. 903-15.
150. van Amerongen, R., A. Mikels, and R. Nusse, *Alternative wnt signaling is initiated by distinct receptors.* Sci Signal, 2008. **1**(35): p. re9.
151. He, X., et al., *LDL receptor-related proteins 5 and 6 in Wnt/beta-catenin signaling: arrows point the way.* Development, 2004. **131**(8): p. 1663-77.

152. MacDonald, B.T., K. Tamai, and X. He, *Wnt/beta-catenin signaling: components, mechanisms, and diseases.* Dev Cell, 2009. **17**(1): p. 9-26.
153. Gunning, P.W., et al., *The evolution of compositionally and functionally distinct actin filaments.* J Cell Sci, 2015. **128**(11): p. 2009-19.
154. Hanukoglu, I., N. Tanese, and E. Fuchs, *Complementary DNA sequence of a human cytoplasmic actin. Interspecies divergence of 3' non-coding regions.* J Mol Biol, 1983. **163**(4): p. 673-8.
155. Yamada, S., et al., *Deconstructing the cadherin-catenin-actin complex.* Cell, 2005. **123**(5): p. 889-901.
156. Zinke, J., et al., *beta-Catenin-Gli1 interaction regulates proliferation and tumor growth in medulloblastoma.* Mol Cancer, 2015. **14**: p. 17.
157. Besnard, A., et al., *Elk-1 a transcription factor with multiple facets in the brain.* Front Neurosci, 2011. **5**: p. 35.
158. Zeller, E., et al., *Dual-specificity phosphatases are targets of the Wnt/beta-catenin pathway and candidate mediators of beta-catenin/Ras signaling interactions.* Biol Chem, 2012. **393**(10): p. 1183-91.
159. Visconti, R., et al., *Importance of the MKK6/p38 pathway for interleukin-12-induced STAT4 serine phosphorylation and transcriptional activity.* Blood, 2000. **96**(5): p. 1844-52.
160. Satelli, A. and S. Li, *Vimentin in cancer and its potential as a molecular target for cancer therapy.* Cell Mol Life Sci, 2011. **68**(18): p. 3033-46.
161. Leader, M., et al., *Vimentin: an evaluation of its role as a tumour marker.* Histopathology, 1987. **11**(1): p. 63-72.
162. Gilles, C., et al., *Transactivation of vimentin by beta-catenin in human breast cancer cells.* Cancer Res, 2003. **63**(10): p. 2658-64.
163. Chaw, S.Y., et al., *Epithelial to mesenchymal transition (EMT) biomarkers--E-cadherin, beta-catenin, APC and Vimentin--in oral squamous cell carcinogenesis and transformation.* Oral Oncol, 2012. **48**(10): p. 997-1006.
164. Yu, H.M., et al., *Expression of Gpr177, a Wnt trafficking regulator, in mouse embryogenesis.* Dev Dyn, 2010. **239**(7): p. 2102-9.
165. Liu, G., et al., *A novel mechanism for Wnt activation of canonical signaling through the LRP6 receptor.* Mol Cell Biol, 2003. **23**(16): p. 5825-35.
166. Liang, J., et al., *Transmembrane protein 198 promotes LRP6 phosphorylation and Wnt signaling activation.* Mol Cell Biol, 2011. **31**(13): p. 2577-90.
167. Wang, Z., et al., *Wnt7b activates canonical signaling in epithelial and vascular smooth muscle cells through interactions with Fzd1, Fzd10, and LRP5.* Mol Cell Biol, 2005. **25**(12): p. 5022-30.
168. Kikuchi, A., *Modulation of Wnt signaling by Axin and Axil.* Cytokine Growth Factor Rev, 1999. **10**(3-4): p. 255-65.
169. Amit, S., et al., *Axin-mediated CKI phosphorylation of beta-catenin at Ser 45: a molecular switch for the Wnt pathway.* Genes Dev, 2002. **16**(9): p. 1066-76.
170. Woodgett, J.R., *Molecular cloning and expression of glycogen synthase kinase-3/factor A.* EMBO J, 1990. **9**(8): p. 2431-8.
171. Hughes, K., et al., *Modulation of the glycogen synthase kinase-3 family by tyrosine phosphorylation.* EMBO J, 1993. **12**(2): p. 803-8.
172. Liu, C., et al., *Control of beta-catenin phosphorylation/degradation by a dual-kinase mechanism.* Cell, 2002. **108**(6): p. 837-47.
173. Wu, G. and X. He, *Threonine 41 in beta-catenin serves as a key phosphorylation relay residue in beta-catenin degradation.* Biochemistry, 2006. **45**(16): p. 5319-23.
174. Chen, Y.T., D.B. Stewart, and W.J. Nelson, *Coupling assembly of the E-cadherin/beta-catenin complex to efficient endoplasmic reticulum exit and basal-lateral membrane targeting of E-cadherin in polarized MDCK cells.* J Cell Biol, 1999. **144**(4): p. 687-99.
175. Ozawa, M., H. Baribault, and R. Kemler, *The cytoplasmic domain of the cell adhesion molecule uvomorulin associates with three independent proteins structurally related in different species.* EMBO J, 1989. **8**(6): p. 1711-7.

176. Proud, C.G., *Mnks, eIF4E phosphorylation and cancer.* Biochim Biophys Acta, 2015. **1849**(7): p. 766-73.
177. Decarlo, L., et al., *Eukaryotic Translation Initiation Factor 4E Is a Feed-Forward Translational Coactivator of Transforming Growth Factor beta Early Protransforming Events in Breast Epithelial Cells.* Mol Cell Biol, 2015. **35**(15): p. 2597-609.
178. Nakao, A., et al., *TGF-beta receptor-mediated signalling through Smad2, Smad3 and Smad4.* EMBO J, 1997. **16**(17): p. 5353-62.
179. Wu, R.Y., et al., *Heteromeric and homomeric interactions correlate with signaling activity and functional cooperativity of Smad3 and Smad4/DPC4.* Mol Cell Biol, 1997. **17**(5): p. 2521-8.
180. Shi, Y., et al., *A structural basis for mutational inactivation of the tumour suppressor Smad4.* Nature, 1997. **388**(6637): p. 87-93.
181. Lebrun, J.J., et al., *Roles of pathway-specific and inhibitory Smads in activin receptor signaling.* Mol Endocrinol, 1999. **13**(1): p. 15-23.
182. Guo, X. and X.F. Wang, *Signaling cross-talk between TGF-beta/BMP and other pathways.* Cell Res, 2009. **19**(1): p. 71-88.
183. Soutoglou, E., et al., *Transcriptional activation by hepatocyte nuclear factor-1 requires synergism between multiple coactivator proteins.* J Biol Chem, 2000. **275**(17): p. 12515-20.
184. Karni, R., et al., *Active Src elevates the expression of beta-catenin by enhancement of cap-dependent translation.* Mol Cell Biol, 2005. **25**(12): p. 5031-9.
185. Brown, M.T. and J.A. Cooper, *Regulation, substrates and functions of src.* Biochim Biophys Acta, 1996. **1287**(2-3): p. 121-49.
186. Roskoski, R., Jr., *Src kinase regulation by phosphorylation and dephosphorylation.* Biochem Biophys Res Commun, 2005. **331**(1): p. 1-14.
187. Varelas, X., et al., *The Hippo pathway regulates Wnt/beta-catenin signaling.* Dev Cell, 2010. **18**(4): p. 579-91.
188. Orton, R.J., et al., *Computational modelling of the receptor-tyrosine-kinase-activated MAPK pathway.* Biochem J, 2005. **392**(Pt 2): p. 249-61.
189. Wu, X., et al., *Rac1 activation controls nuclear localization of beta-catenin during canonical Wnt signaling.* Cell, 2008. **133**(2): p. 340-53.
190. Davis, R.J., *Signal transduction by the JNK group of MAP kinases.* Cell, 2000. **103**(2): p. 239-52.
191. Lawler, S., et al., *Synergistic activation of SAPK1/JNK1 by two MAP kinase kinases in vitro.* Curr Biol, 1998. **8**(25): p. 1387-90.
192. Tournier, C., et al., *Mitogen-activated protein kinase kinase 7 is an activator of the c-Jun NH2-terminal kinase.* Proc Natl Acad Sci U S A, 1997. **94**(14): p. 7337-42.
193. Tournier, C., et al., *The MKK7 gene encodes a group of c-Jun NH2-terminal kinase kinases.* Mol Cell Biol, 1999. **19**(2): p. 1569-81.
194. Moriguchi, T., et al., *A novel SAPK/JNK kinase, MKK7, stimulated by TNFalpha and cellular stresses.* EMBO J, 1997. **16**(23): p. 7045-53.
195. Zou, H., et al., *Differential requirement of MKK4 and MKK7 in JNK activation by distinct scaffold proteins.* FEBS Lett, 2007. **581**(2): p. 196-202.
196. Gotz, R., *Inter-cellular adhesion disruption and the RAS/RAF and beta-catenin signalling in lung cancer progression.* Cancer Cell Int, 2008. **8**: p. 7.
197. Yun, M.S., et al., *Both ERK and Wnt/beta-catenin pathways are involved in Wnt3a-induced proliferation.* J Cell Sci, 2005. **118**(Pt 2): p. 313-22.
198. Sun, P., et al., *PRAK is essential for ras-induced senescence and tumor suppression.* Cell, 2007. **128**(2): p. 295-308.
199. Moll, U.M. and O. Petrenko, *The MDM2-p53 interaction.* Mol Cancer Res, 2003. **1**(14): p. 1001-8.
200. Alarcon-Vargas, D. and Z. Ronai, *p53-Mdm2--the affair that never ends.* Carcinogenesis, 2002. **23**(4): p. 541-7.
201. Ibrahem, S., et al., *STAT3 paradoxically stimulates beta-catenin expression but inhibits beta-catenin function.* Int J Exp Pathol, 2014. **95**(6): p. 392-400.

202. Lim, C.P. and X. Cao, *Serine phosphorylation and negative regulation of Stat3 by JNK.* J Biol Chem, 1999. **274**(43): p. 31055-61.
203. Aaronson, D.S. and C.M. Horvath, *A road map for those who don't know JAK-STAT.* Science, 2002. **296**(5573): p. 1653-5.
204. Chen, S., et al., *Histone deacetylase 1 and 2 regulate Wnt and p53 pathways in the ureteric bud epithelium.* Development, 2015. **142**(6): p. 1180-92.
205. Liu, C., et al., *p15RS/RPRD1A (p15INK4b-related sequence/regulation of nuclear pre-mRNA domain-containing protein 1A) interacts with HDAC2 in inhibition of the Wnt/beta-catenin signaling pathway.* J Biol Chem, 2015. **290**(15): p. 9701-13.
206. Ye, F., et al., *HDAC1 and HDAC2 regulate oligodendrocyte differentiation by disrupting the beta-catenin-TCF interaction.* Nat Neurosci, 2009. **12**(7): p. 829-38.
207. Li, H. and W.D. Richardson, *Genetics meets epigenetics: HDACs and Wnt signaling in myelin development and regeneration.* Nat Neurosci, 2009. **12**(7): p. 815-7.
208. Shi, B., et al., *Integration of estrogen and Wnt signaling circuits by the polycomb group protein EZH2 in breast cancer cells.* Mol Cell Biol, 2007. **27**(14): p. 5105-19.
209. Barak, V., et al., *Clinical utility of cytokeratins as tumor markers.* Clin Biochem, 2004. **37**(7): p. 529-40.
210. Tao, G.Z., et al., *Wnt/beta-catenin signaling protects mouse liver against oxidative stress-induced apoptosis through the inhibition of forkhead transcription factor FoxO3.* J Biol Chem, 2013. **288**(24): p. 17214-24.
211. Essers, M.A., et al., *Functional interaction between beta-catenin and FOXO in oxidative stress signaling.* Science, 2005. **308**(5725): p. 1181-4.
212. Greer, E.L., et al., *The energy sensor AMP-activated protein kinase directly regulates the mammalian FOXO3 transcription factor.* J Biol Chem, 2007. **282**(41): p. 30107-19.
213. Yang, X. and G. Karsenty, *ATF4, the osteoblast accumulation of which is determined post-translationally, can induce osteoblast-specific gene expression in non-osteoblastic cells.* J Biol Chem, 2004. **279**(45): p. 47109-14.
214. Yu, S., et al., *atf4 promotes beta-catenin expression and osteoblastic differentiation of bone marrow mesenchymal stem cells.* Int J Biol Sci, 2013. **9**(3): p. 256-66.
215. Stemmer, V., et al., *Snail promotes Wnt target gene expression and interacts with beta-catenin.* Oncogene, 2008. **27**(37): p. 5075-80.
216. Wu, J.W., et al., *Crystal structure of a phosphorylated Smad2. Recognition of phosphoserine by the MH2 domain and insights on Smad function in TGF-beta signaling.* Mol Cell, 2001. **8**(6): p. 1277-89.
217. Sancho, R., et al., *JNK signalling modulates intestinal homeostasis and tumourigenesis in mice.* EMBO J, 2009. **28**(13): p. 1843-54.
218. Toualbi, K., et al., *Physical and functional cooperation between AP-1 and beta-catenin for the regulation of TCF-dependent genes.* Oncogene, 2007. **26**(24): p. 3492-502.
219. Gan, X.Q., et al., *Nuclear Dvl, c-Jun, beta-catenin, and TCF form a complex leading to stabilization of beta-catenin-TCF interaction.* J Cell Biol, 2008. **180**(6): p. 1087-100.
220. Huang, Z., et al., *Lysine-specific demethylase 1 (LSD1/KDM1A) contributes to colorectal tumorigenesis via activation of the Wnt/beta-catenin pathway by down-regulating Dickkopf-1 (DKK1) [corrected].* PLoS One, 2013. **8**(7): p. e70077.
221. Kramer, T., B. Schmidt, and F. Lo Monte, *Small-Molecule Inhibitors of GSK-3: Structural Insights and Their Application to Alzheimer's Disease Models.* Int J Alzheimers Dis, 2012. **2012**: p. 381029.
222. Bennett, C.N., et al., *Regulation of Wnt Signaling during Adipogenesis.* The Journal of Biological Chemistry, 2002. **277**(34): p. 30998 - 31004.
223. Lee, D.H. and A.L. Goldberg, *Selective inhibitors of the proteasome-dependent and vacuolar pathways of protein degradation in Saccharomyces cerevisiae.* J Biol Chem, 1996. **271**(44): p. 27280-4.
224. Li, V.S., et al., *Wnt signaling through inhibition of beta-catenin degradation in an intact Axin1 complex.* Cell, 2012. **149**(6): p. 1245-56.

225. Lee, Y.N., Y. Gao, and H.Y. Wang, *Differential mediation of the Wnt canonical pathway by mammalian Dishevelleds-1, -2, and -3.* Cell Signal, 2008. **20**(2): p. 443-52.
226. Bhanot, P., et al., *A new member of the frizzled family from Drosophila functions as a Wingless receptor.* Nature, 1996. **382**(6588): p. 225-30.
227. MacDonald, B.T. and X. He, *Frizzled and LRP5/6 receptors for Wnt/beta-catenin signaling.* Cold Spring Harb Perspect Biol, 2012. **4**(12).
228. Sustmann, C., et al., *Cell-type-specific function of BCL9 involves a transcriptional activation domain that synergizes with beta-catenin.* Mol Cell Biol, 2008. **28**(10): p. 3526-37.
229. Choudhary, C., et al., *Lysine acetylation targets protein complexes and co-regulates major cellular functions.* Science, 2009. **325**(5942): p. 834-40.
230. Valenzuela-Fernandez, A., et al., *HDAC6: a key regulator of cytoskeleton, cell migration and cell-cell interactions.* Trends Cell Biol, 2008. **18**(6): p. 291-7.
231. Dokmanovic, M., C. Clarke, and P.A. Marks, *Histone deacetylase inhibitors: overview and perspectives.* Mol Cancer Res, 2007. **5**(10): p. 981-9.
232. Moresco, J.J., P.C. Carvalho, and J.R. Yates, 3rd, *Identifying components of protein complexes in C. elegans using co-immunoprecipitation and mass spectrometry.* J Proteomics, 2010. **73**(11): p. 2198-204.
233. Oeljeklaus, S., H.E. Meyer, and B. Warscheid, *New dimensions in the study of protein complexes using quantitative mass spectrometry.* FEBS Lett, 2009. **583**(11): p. 1674-83.
234. Wilhelm, M., et al., *Mass-spectrometry-based draft of the human proteome.* Nature, 2014. **509**(7502): p. 582-7.
235. Fujioka, A., et al., *Dynamics of the Ras/ERK MAPK cascade as monitored by fluorescent probes.* J Biol Chem, 2006. **281**(13): p. 8917-26.
236. Behari, J., *The Wnt/beta-catenin signaling pathway in liver biology and disease.* Expert Rev Gastroenterol Hepatol, 2010. **4**(6): p. 745-56.
237. Graham, F.L., et al., *Characteristics of a human cell line transformed by DNA from human adenovirus type 5.* J Gen Virol, 1977. **36**(1): p. 59-74.
238. DuBridge, R.B., et al., *Analysis of mutation in human cells by using an Epstein-Barr virus shuttle system.* Mol Cell Biol, 1987. **7**(1): p. 379-87.
239. Ying, Q.L., et al., *The ground state of embryonic stem cell self-renewal.* Nature, 2008. **453**(7194): p. 519-23.
240. Jensen, O.N., *Interpreting the protein language using proteomics.* Nat Rev Mol Cell Biol, 2006. **7**(6): p. 391-403.
241. Deribe, Y.L., T. Pawson, and I. Dikic, *Post-translational modifications in signal integration.* Nat Struct Mol Biol, 2010. **17**(6): p. 666-72.
242. Hunter, T., *The age of crosstalk: phosphorylation, ubiquitination, and beyond.* Mol Cell, 2007. **28**(5): p. 730-8.
243. Murr, R., *Interplay between different epigenetic modifications and mechanisms.* Adv Genet, 2010. **70**: p. 101-41.
244. Luckert, K., et al., *Snapshots of protein dynamics and post-translational modifications in one experiment--beta-catenin and its functions.* Mol Cell Proteomics, 2011. **10**(5): p. M110 007377.
245. Hino, S., et al., *Phosphorylation of beta-catenin by cyclic AMP-dependent protein kinase stabilizes beta-catenin through inhibition of its ubiquitination.* Mol Cell Biol, 2005. **25**(20): p. 9063-72.
246. Fang, D., et al., *Phosphorylation of beta-catenin by AKT promotes beta-catenin transcriptional activity.* J Biol Chem, 2007. **282**(15): p. 11221-9.
247. Piedra, J., et al., *p120 Catenin-associated Fer and Fyn tyrosine kinases regulate beta-catenin Tyr-142 phosphorylation and beta-catenin-alpha-catenin Interaction.* Mol Cell Biol, 2003. **23**(7): p. 2287-97.
248. Brembeck, F.H., et al., *Essential role of BCL9-2 in the switch between beta-catenin's adhesive and transcriptional functions.* Genes Dev, 2004. **18**(18): p. 2225-30.

249. Bustos, V.H., et al., *The first armadillo repeat is involved in the recognition and regulation of beta-catenin phosphorylation by protein kinase CK1.* Proc Natl Acad Sci U S A, 2006. **103**(52): p. 19725-30.
250. Piedra, J., et al., *Regulation of beta-catenin structure and activity by tyrosine phosphorylation.* J Biol Chem, 2001. **276**(23): p. 20436-43.
251. Xing, Y., et al., *Crystal structure of a full-length beta-catenin.* Structure, 2008. **16**(3): p. 478-87.
252. van Veelen, W., et al., *beta-catenin tyrosine 654 phosphorylation increases Wnt signalling and intestinal tumorigenesis.* Gut, 2011. **60**(9): p. 1204-12.
253. Liu, C., et al., *beta-Trcp couples beta-catenin phosphorylation-degradation and regulates Xenopus axis formation.* Proc Natl Acad Sci U S A, 1999. **96**(11): p. 6273-8.
254. Winston, J.T., et al., *The SCFbeta-TRCP-ubiquitin ligase complex associates specifically with phosphorylated destruction motifs in IkappaBalpha and beta-catenin and stimulates IkappaBalpha ubiquitination in vitro.* Genes Dev, 1999. **13**(3): p. 270-83.
255. Zhu, G., et al., *A Rac1/PAK1 cascade controls beta-catenin activation in colon cancer cells.* Oncogene, 2012. **31**(8): p. 1001-12.
256. Lipman, N.S., et al., *Monoclonal versus polyclonal antibodies: distinguishing characteristics, applications, and information resources.* ILAR J, 2005. **46**(3): p. 258-68.
257. Zanotto-Filho, A., et al., *Proteasome inhibitor MG132 induces selective apoptosis in glioblastoma cells through inhibition of PI3K/Akt and NFkappaB pathways, mitochondrial dysfunction, and activation of p38-JNK1/2 signaling.* Invest New Drugs, 2012. **30**(6): p. 2252-62.
258. Naujok, O., et al., *Cytotoxicity and activation of the Wnt/beta-catenin pathway in mouse embryonic stem cells treated with four GSK3 inhibitors.* BMC Res Notes, 2014. **7**: p. 273.
259. Nusse, R. and H. Varmus, *Three decades of Wnts: a personal perspective on how a scientific field developed.* EMBO J, 2012. **31**(12): p. 2670-84.
260. Polakis, P., *Drugging Wnt signalling in cancer.* EMBO J, 2012. **31**(12): p. 2737-46.
261. Daugherty, R.L., et al., *alpha-Catenin is an inhibitor of transcription.* Proc Natl Acad Sci U S A, 2014. **111**(14): p. 5260-5.
262. Kemler, R., *Classical cadherins.* Semin Cell Biol, 1992. **3**(3): p. 149-55.
263. Kemler, R., *From cadherins to catenins: cytoplasmic protein interactions and regulation of cell adhesion.* Trends Genet, 1993. **9**(9): p. 317-21.
264. Tian, X., et al., *E-cadherin/beta-catenin complex and the epithelial barrier.* J Biomed Biotechnol, 2011. **2011**: p. 567305.
265. Chen, H.N., et al., *PDLIM1 Stabilizes the E-Cadherin/beta-Catenin Complex to Prevent Epithelial-Mesenchymal Transition and Metastatic Potential of Colorectal Cancer Cells.* Cancer Res, 2016. **76**(5): p. 1122-34.
266. Rogacki, K., A. Kasprzak, and A. Stepinski, *Alterations of Wnt/beta-catenin signaling pathway in hepatocellular carcinomas associated with hepatitis C virus.* Pol J Pathol, 2015. **66**(1): p. 9-21.
267. Roberts, D.M., et al., *Deconstructing the sscatenin destruction complex: mechanistic roles for the tumor suppressor APC in regulating Wnt signaling.* Mol Biol Cell, 2011. **22**(11): p. 1845-63.
268. Polakis, P., *Casein kinase 1: a Wnt'er of disconnect.* Curr Biol, 2002. **12**(14): p. R499-R501.
269. Cheong, J.K., et al., *IC261 induces cell cycle arrest and apoptosis of human cancer cells via CK1delta/varepsilon and Wnt/beta-catenin independent inhibition of mitotic spindle formation.* Oncogene, 2011. **30**(22): p. 2558-69.
270. Doble, B.W., et al., *Functional redundancy of GSK-3alpha and GSK-3beta in Wnt/beta-catenin signaling shown by using an allelic series of embryonic stem cell lines.* Dev Cell, 2007. **12**(6): p. 957-71.
271. Dajani, R., et al., *Structural basis for recruitment of glycogen synthase kinase 3beta to the axin-APC scaffold complex.* EMBO J, 2003. **22**(3): p. 494-501.

272. Stamos, J.L. and W.I. Weis, *The beta-catenin destruction complex.* Cold Spring Harb Perspect Biol, 2013. **5**(1): p. a007898.
273. Mikels, A.J. and R. Nusse, *Wnts as ligands: processing, secretion and reception.* Oncogene, 2006. **25**(57): p. 7461-8.
274. Kurayoshi, M., et al., *Post-translational palmitoylation and glycosylation of Wnt-5a are necessary for its signalling.* Biochem J, 2007. **402**(3): p. 515-23.
275. Willert, K. and R. Nusse, *Wnt proteins.* Cold Spring Harb Perspect Biol, 2012. **4**(9): p. a007864.
276. Bartscherer, K. and M. Boutros, *Regulation of Wnt protein secretion and its role in gradient formation.* EMBO Rep, 2008. **9**(10): p. 977-82.
277. Nusse, R. and H.E. Varmus, *Wnt genes.* Cell, 1992. **69**(7): p. 1073-87.
278. Davis, E.K., Y. Zou, and A. Ghosh, *Wnts acting through canonical and noncanonical signaling pathways exert opposite effects on hippocampal synapse formation.* Neural Dev, 2008. **3**: p. 32.
279. Rao, T.P. and M. Kuhl, *An updated overview on Wnt signaling pathways: a prelude for more.* Circ Res, 2010. **106**(12): p. 1798-806.
280. Zheng, X.M., R.J. Resnick, and D. Shalloway, *A phosphotyrosine displacement mechanism for activation of Src by PTPalpha.* EMBO J, 2000. **19**(5): p. 964-78.
281. Yang, W., et al., *Nuclear PKM2 regulates beta-catenin transactivation upon EGFR activation.* Nature, 2011. **480**(7375): p. 118-22.
282. Nusse, R., *Wnts and Hedgehogs: lipid-modified proteins and similarities in signaling mechanisms at the cell surface.* Development, 2003. **130**(22): p. 5297-305.
283. Kalderon, D., *Similarities between the Hedgehog and Wnt signaling pathways.* Trends Cell Biol, 2002. **12**(11): p. 523-31.
284. Chen, Y. and J. Jiang, *Decoding the phosphorylation code in Hedgehog signal transduction.* Cell Res, 2013. **23**(2): p. 186-200.
285. Price, M.A. and D. Kalderon, *Proteolysis of the Hedgehog signaling effector Cubitus interruptus requires phosphorylation by Glycogen Synthase Kinase 3 and Casein Kinase 1.* Cell, 2002. **108**(6): p. 823-35.
286. Schittek, B. and T. Sinnberg, *Biological functions of casein kinase 1 isoforms and putative roles in tumorigenesis.* Mol Cancer, 2014. **13**: p. 231.
287. Manolagas, S.C. and M. Almeida, *Gone with the Wnts: beta-catenin, T-cell factor, forkhead box O, and oxidative stress in age-dependent diseases of bone, lipid, and glucose metabolism.* Mol Endocrinol, 2007. **21**(11): p. 2605-14.
288. Almeida, M., et al., *Oxidative stress antagonizes Wnt signaling in osteoblast precursors by diverting beta-catenin from T cell factor- to forkhead box O-mediated transcription.* J Biol Chem, 2007. **282**(37): p. 27298-305.
289. Jin, T., I. George Fantus, and J. Sun, *Wnt and beyond Wnt: multiple mechanisms control the transcriptional property of beta-catenin.* Cell Signal, 2008. **20**(10): p. 1697-704.
290. Almeida, M., *Unraveling the role of FoxOs in bone--insights from mouse models.* Bone, 2011. **49**(3): p. 319-27.
291. van der Vos, K.E. and P.J. Coffer, *FOXO-binding partners: it takes two to tango.* Oncogene, 2008. **27**(16): p. 2289-99.
292. Whitman, M., *Smads and early developmental signaling by the TGFbeta superfamily.* Genes Dev, 1998. **12**(16): p. 2445-62.
293. Labbe, E., et al., *Transcriptional cooperation between the transforming growth factor-beta and Wnt pathways in mammary and intestinal tumorigenesis.* Cancer Res, 2007. **67**(1): p. 75-84.
294. Itoh, F., et al., *Promoting bone morphogenetic protein signaling through negative regulation of inhibitory Smads.* EMBO J, 2001. **20**(15): p. 4132-42.
295. Kim, K.K., et al., *Epithelial cell alpha3beta1 integrin links beta-catenin and Smad signaling to promote myofibroblast formation and pulmonary fibrosis.* J Clin Invest, 2009. **119**(1): p. 213-24.

296. Massague, J., J. Seoane, and D. Wotton, *Smad transcription factors.* Genes Dev, 2005. **19**(23): p. 2783-810.
297. Clifford, R.L., K. Deacon, and A.J. Knox, *Novel regulation of vascular endothelial growth factor-A (VEGF-A) by transforming growth factor (beta)1: requirement for Smads, (beta)-CATENIN, AND GSK3(beta).* J Biol Chem, 2008. **283**(51): p. 35337-53.
298. Hirota, M., et al., *Smad2 functions as a co-activator of canonical Wnt/beta-catenin signaling pathway independent of Smad4 through histone acetyltransferase activity of p300.* Cell Signal, 2008. **20**(9): p. 1632-41.
299. Imajo, M., et al., *A molecular mechanism that links Hippo signalling to the inhibition of Wnt/beta-catenin signalling.* EMBO J, 2012. **31**(5): p. 1109-22.
300. Kang, W., et al., *Emerging role of Hippo pathway in gastric and other gastrointestinal cancers.* World J Gastroenterol, 2016. **22**(3): p. 1279-88.
301. Zhao, B., L. Li, and K.L. Guan, *Hippo signaling at a glance.* J Cell Sci, 2010. **123**(Pt 23): p. 4001-6.
302. Pan, D., *The hippo signaling pathway in development and cancer.* Dev Cell, 2010. **19**(4): p. 491-505.
303. Arce, L., N.N. Yokoyama, and M.L. Waterman, *Diversity of LEF/TCF action in development and disease.* Oncogene, 2006. **25**(57): p. 7492-504.
304. Hoppler, S. and C.L. Kavanagh, *Wnt signalling: variety at the core.* J Cell Sci, 2007. **120**(Pt 3): p. 385-93.
305. Munshi, A. and R. Ramesh, *Mitogen-activated protein kinases and their role in radiation response.* Genes Cancer, 2013. **4**(9-10): p. 401-8.
306. Ono, K. and J. Han, *The p38 signal transduction pathway: activation and function.* Cell Signal, 2000. **12**(1): p. 1-13.
307. Kim, E.K. and E.J. Choi, *Compromised MAPK signaling in human diseases: an update.* Arch Toxicol, 2015. **89**(6): p. 867-82.
308. Dhillon, A.S., et al., *MAP kinase signalling pathways in cancer.* Oncogene, 2007. **26**(22): p. 3279-90.
309. Kim, E.K. and E.J. Choi, *Pathological roles of MAPK signaling pathways in human diseases.* Biochim Biophys Acta, 2010. **1802**(4): p. 396-405.
310. Lee, J.W., et al., *Mutational analysis of the ARAF gene in human cancers.* APMIS, 2005. **113**(1): p. 54-7.
311. Davies, H., et al., *Mutations of the BRAF gene in human cancer.* Nature, 2002. **417**(6892): p. 949-54.
312. Camps, M., A. Nichols, and S. Arkinstall, *Dual specificity phosphatases: a gene family for control of MAP kinase function.* FASEB J, 2000. **14**(1): p. 6-16.
313. Ip, Y.T. and R.J. Davis, *Signal transduction by the c-Jun N-terminal kinase (JNK)--from inflammation to development.* Curr Opin Cell Biol, 1998. **10**(2): p. 205-19.
314. Derijard, B., et al., *JNK1: a protein kinase stimulated by UV light and Ha-Ras that binds and phosphorylates the c-Jun activation domain.* Cell, 1994. **76**(6): p. 1025-37.
315. Zhang, Y., et al., *Dimerization choices control the ability of axin and dishevelled to activate c-Jun N-terminal kinase/stress-activated protein kinase.* J Biol Chem, 2000. **275**(32): p. 25008-14.
316. Luo, W., et al., *Axin utilizes distinct regions for competitive MEKK1 and MEKK4 binding and JNK activation.* J Biol Chem, 2003. **278**(39): p. 37451-8.
317. Veeman, M.T., J.D. Axelrod, and R.T. Moon, *A second canon. Functions and mechanisms of beta-catenin-independent Wnt signaling.* Dev Cell, 2003. **5**(3): p. 367-77.
318. New, L., et al., *PRAK, a novel protein kinase regulated by the p38 MAP kinase.* EMBO J, 1998. **17**(12): p. 3372-84.
319. Kress, T.R., et al., *The MK5/PRAK kinase and Myc form a negative feedback loop that is disrupted during colorectal tumorigenesis.* Mol Cell, 2011. **41**(4): p. 445-57.
320. Cavigelli, M., et al., *Induction of c-fos expression through JNK-mediated TCF/Elk-1 phosphorylation.* EMBO J, 1995. **14**(23): p. 5957-64.

321. Seger, R. and E.G. Krebs, *The MAPK signaling cascade.* FASEB J, 1995. **9**(9): p. 726-35.
322. Owens, D.M. and S.M. Keyse, *Differential regulation of MAP kinase signalling by dual-specificity protein phosphatases.* Oncogene, 2007. **26**(22): p. 3203-13.
323. Bluthgen, N., et al., *A systems biological approach suggests that transcriptional feedback regulation by dual-specificity phosphatase 6 shapes extracellular signal-related kinase activity in RAS-transformed fibroblasts.* FEBS J, 2009. **276**(4): p. 1024-35.
324. Li, Y., et al., *HDAC6 is required for epidermal growth factor-induced beta-catenin nuclear localization.* J Biol Chem, 2008. **283**(19): p. 12686-90.
325. Wang, S.H., et al., *beta-catenin deacetylation is essential for WNT-induced proliferation of breast cancer cells.* Mol Med Rep, 2014. **9**(3): p. 973-8.
326. Mak, A.B., et al., *Regulation of CD133 by HDAC6 promotes beta-catenin signaling to suppress cancer cell differentiation.* Cell Rep, 2012. **2**(4): p. 951-63.
327. Mosimann, C., G. Hausmann, and K. Basler, *Beta-catenin hits chromatin: regulation of Wnt target gene activation.* Nat Rev Mol Cell Biol, 2009. **10**(4): p. 276-86.
328. Krieghoff, E., J. Behrens, and B. Mayr, *Nucleo-cytoplasmic distribution of beta-catenin is regulated by retention.* J Cell Sci, 2006. **119**(Pt 7): p. 1453-63.
329. Townsley, F.M., A. Cliffe, and M. Bienz, *Pygopus and Legless target Armadillo/beta-catenin to the nucleus to enable its transcriptional co-activator function.* Nat Cell Biol, 2004. **6**(7): p. 626-33.
330. Li, J., et al., *LATS2 suppresses oncogenic Wnt signaling by disrupting beta-catenin/BCL9 interaction.* Cell Rep, 2013. **5**(6): p. 1650-63.
331. Kramps, T., et al., *Wnt/wingless signaling requires BCL9/legless-mediated recruitment of pygopus to the nuclear beta-catenin-TCF complex.* Cell, 2002. **109**(1): p. 47-60.
332. Takada, K., et al., *Targeted disruption of the BCL9/beta-catenin complex inhibits oncogenic Wnt signaling.* Sci Transl Med, 2012. **4**(148): p. 148ra117.
333. Sherr, C.J., *Mammalian G1 cyclins.* Cell, 1993. **73**(6): p. 1059-65.
334. Morgan, D.O., *Cyclin-dependent kinases: engines, clocks, and microprocessors.* Annu Rev Cell Dev Biol, 1997. **13**: p. 261-91.
335. Park, C.S., et al., *Modulation of beta-catenin phosphorylation/degradation by cyclin-dependent kinase 2.* J Biol Chem, 2004. **279**(19): p. 19592-9.
336. Price, B.D., L. Hughes-Davies, and S.J. Park, *Cdk2 kinase phosphorylates serine 315 of human p53 in vitro.* Oncogene, 1995. **11**(1): p. 73-80.
337. Yang, C.C., et al., *Phosphorylation of EZH2 at T416 by CDK2 contributes to the malignancy of triple negative breast cancers.* Am J Transl Res, 2015. **7**(6): p. 1009-20.
338. Zeng, X., S. Chen, and H. Huang, *Phosphorylation of EZH2 by CDK1 and CDK2: a possible regulatory mechanism of transmission of the H3K27me3 epigenetic mark through cell divisions.* Cell Cycle, 2011. **10**(4): p. 579-83.
339. Covington, K.R. and S.A. Fuqua, *Role of MTA2 in human cancer.* Cancer Metastasis Rev, 2014. **33**(4): p. 921-8.
340. Zhang, H., L.C. Stephens, and R. Kumar, *Metastasis tumor antigen family proteins during breast cancer progression and metastasis in a reliable mouse model for human breast cancer.* Clin Cancer Res, 2006. **12**(5): p. 1479-86.
341. Heerboth, S., et al., *EMT and tumor metastasis.* Clin Transl Med, 2015. **4**: p. 6.
342. Feng, Y., N. Lee, and E.R. Fearon, *TIP49 regulates beta-catenin-mediated neoplastic transformation and T-cell factor target gene induction via effects on chromatin remodeling.* Cancer Res, 2003. **63**(24): p. 8726-34.
343. Bauer, A., O. Huber, and R. Kemler, *Pontin52, an interaction partner of beta-catenin, binds to the TATA box binding protein.* Proc Natl Acad Sci U S A, 1998. **95**(25): p. 14787-92.
344. Bauer, A., et al., *Pontin52 and reptin52 function as antagonistic regulators of beta-catenin signalling activity.* EMBO J, 2000. **19**(22): p. 6121-30.
345. Perrotti, D. and P. Neviani, *Protein phosphatase 2A: a target for anticancer therapy.* Lancet Oncol, 2013. **14**(6): p. e229-38.
346. Mumby, M., *PP2A: unveiling a reluctant tumor suppressor.* Cell, 2007. **130**(1): p. 21-4.

347. Bhardwaj, A., et al., *Restoration of PPP2CA expression reverses epithelial-to-mesenchymal transition and suppresses prostate tumour growth and metastasis in an orthotopic mouse model.* Br J Cancer, 2014. **110**(8): p. 2000-10.
348. Su, Y., et al., *APC is essential for targeting phosphorylated beta-catenin to the SCFbeta-TrCP ubiquitin ligase.* Mol Cell, 2008. **32**(5): p. 652-61.
349. Zhang, W., et al., *PR55 alpha, a regulatory subunit of PP2A, specifically regulates PP2A-mediated beta-catenin dephosphorylation.* J Biol Chem, 2009. **284**(34): p. 22649-56.
350. Seeling, J.M., et al., *Regulation of beta-catenin signaling by the B56 subunit of protein phosphatase 2A.* Science, 1999. **283**(5410): p. 2089-91.
351. Singh, A.P., et al., *Genome-wide expression profiling reveals transcriptomic variation and perturbed gene networks in androgen-dependent and androgen-independent prostate cancer cells.* Cancer Lett, 2008. **259**(1): p. 28-38.
352. Liu, K.Q., et al., *Identifying dysregulated pathways in cancers from pathway interaction networks.* BMC Bioinformatics, 2012. **13**: p. 126.
353. Beavon, I.R., *The E-cadherin-catenin complex in tumour metastasis: structure, function and regulation.* Eur J Cancer, 2000. **36**(13 Spec No): p. 1607-20.
354. Giakoustidis, A., et al., *Molecular signalling in hepatocellular carcinoma: Role of and crosstalk among WNT/ss-catenin, Sonic Hedgehog, Notch and Dickkopf-1.* Can J Gastroenterol Hepatol, 2015. **29**(4): p. 209-17.
355. Winczewska-Wiktor, A., et al., *A de novo CTNNB1 nonsense mutation associated with syndromic atypical hyperekplexia, microcephaly and intellectual disability: a case report.* BMC Neurol, 2016. **16**(1): p. 35.

7. Appendix

7.1 Supplementary tables

Suppl. Table A: List of all used primary antibodies.
All antibodies tested within this thesis are listed with their individual properties. If they belong to the defined antibody set, tested on the Co-IP samples derived from the different liver cell lines (see 0), they are marked with "*". If they were screened on the ECIP captured with the BC1 binder (see 4.3) or the ICIP samples (see 4.4), the antibodies are marked with "**".

Antigen	Mod.	Spec.	Reactivity	Distributor	Product number	NMI number	*/**
14-3-3 ε		rb	hu, ms, rt	Cell Signaling	9635	# 1554	*
14-3-3 ζ δ		rb	hu, ms, rt	Cell Signaling	9639	TK # 009	*
4E-BP1	pSer65	rb	hu, ms	Epitomics	2206-1	# 0428	
4E-BP1		rb	hu, ms, rt	Epitomics	1557-1	# 0446	
ABL2		rb	hu, ms, rt	abcam	ab134134	# 1343	
Akt		rb	hu, ms, rt	Cell Signaling	9272	# 0548	
AML1		rb	hu, ms, rt	Cell Signaling	8229	# 1540	
Androgen receptor		rb	hu	Cell Signaling	3202	# 1161	
Apaf-1		rb	hu, ms, rt	Cell Signaling	8723	# 1544	*
APC		rb	hu, ms, rt	Cell Signaling	2504	TK # 025	*/**
A-Raf		rb	hu, ms, rt	Cell Signaling	4432	# 1145	*
ATF3		rb	hu	Sigma	HPA001562	# 1353	
ATF4		gt	hu ms, rt	Acris	AP15940PU-N	# 0725	*
ATF6 α		rb	hu	Acris	AP17892PU-N	# 0726	
Axin1		rb	hu, ms, rt	Cell Signaling	3323	# 0690	*/**
Axin2		rb	hu	Cell Signaling	2151	# 1724	*
Axin2		rb	hu	Cell Signaling	5863	# 0956	*/**
Bax		rb	hu, ms, rt	Cell Signaling	2772	# 1173	*
Bcl2		rb	hu, ms, rt	Cell Signaling	2870	# 0682	*
Bcl9		ms		ABNOVA		# 1743	*
Bcl9l		rb	hu, ms, rt	Thermo Scientific	PA5-21111		
Bcl-xL		rb	hu, ms, rt	Cell Signaling	2764	# 0435	*
Biotin		gt	all spec.s	Cell Signaling	7075	# 0303	
BMP4		rb	hu	Epitomics	5163-1	# 0936	*
b-Raf		rb	hu, rt, ms	Upstate	07-453	# 1692	*
BRCA1		rb	hu	Cell Signaling	9010	# 1003	
BRCA1	pSer1524	rb	hu	Cell Signaling	9009	# 1018	
Caveolin-1		rb	hu, ms, rt	Cell Signaling	3238	# 1188	
CBP		rb	hu, ms, rt	Cell Signaling	7389	# 1095	
CD133		rb	hu	Cell Signaling	3663	# 0460	*
CD36		rb	ms, rt, hu	abcam	ab133625	# 1400	
CD44		rb	hu, ms, rt	abcam	ab51037	# 1413	*
CD45		rb	hu	Epitomics	1577-1	# 0444	
CD45		ms		BD Biosciences	610266	# 0500	
CD51		ms	hu, rt, ms	BD Biosciences	611012	# 0501	
CDK2		rb	hu, ms, rt	Cell Signaling	2546	# 1479	*/**
CDK4		ms	hu, ms	Cell Signaling	2906	# 1272	
CDK5		rb	hu, ms, rt	Cell Signaling	2506	# 1478	
CDK6		ms	hu, ms, rt	Cell Signaling	3136	# 1305	
CDK6	pTyr24	rb	hu, ms	biorbyt	orb15014	# 1340	
CDK6	pTyr13	rb	hu, ms	biorbyt	orb15013	# 1341	
CDKN2B		rb	hu, ms, rt	Cell Signaling	4822	# 0412	

Antigen	Mod.	Spec.	Reactivity	Distributor	Product number	NMI number	*/**
c-Fos		rb	hu, ms, rt	Cell Signaling	4384	TK # 011	
CHD3		rb	hu, ms	Cell Signaling	4241		**
CHD4		rb	hu, ms, rb	Cell Signaling	11912		**
CITED2		rb	hu, ms, rt	Epitomics	3297-1	# 0934	
cJUN	pSer63	rb	hu, ms, rt	Cell Signaling	2361S	# 1744	*
cJUN	pSer63	rb	hu, ms, rt	Cell Signaling	2361	# 1162	*/**
cJUN		rb	hu, ms, rt	Cell Signaling	9165	# 1187/HD	*/**
CK 1 α		rb	hu, ms, rt	Cell Signaling	2655	TK # 035	*
CK 1 δ		ms	hu, ms, rt	abcam	ab85320	# 0719	*
CK 1 ε		rb	hu, ms, rt	Invitrogen	487600	# 0340	*
CK 2 α		rb	hu, ms	Cell Signaling	2656	TK # 034	*
c-Met		ms	hu, ms, rt	Cell Signaling	3127	# 0434	*
c-myc		rb	hu, ms, rt	Cell Signaling	9402	TK # 023	
c-Raf		rb	hu, ms, rt	Cell Signaling	9422	TK # 029	*
CREB		rb	hu, ms, rt	Cell Signaling	9197	BG # 005	
CREB	pSer133	rb	hu, ms, rt	Cell Signaling	9198	# 1043	
Cytokeratin Pan		ms	hu, ms, rb	Dako	M0821	# 0261	*
Cytokeratin Pan		ms	hu, rt	Cell Signaling	4545	# 0474	*
Cytokeratin Pan		ms	hu	Ventana	760-2135	# 0588	*
DKK1		rb	hu, ms, rt	Biorbyt	orb27676	# 1593	*
DKK1		rb	hu, ms, rt	Biorbyt	orb13376	# 1594	*
DKK2		rb	hu	Cell Signaling	4683	# 1522	*
DNMT1		rb	hu, ms, rt	Cell Signaling	5032	# 1066	*
DUSP1		rb	hu, ms	Millipore	07-535	TK # 081	*
DUSP10		rb	hu, ms, rt	Cell Signaling	3483	# 0406	*
DUSP14		gt	hu, ms	Santa Cruz	sc-48039	# 0487	*
DUSP16		rb	hu, ms	abcam	ab65151	# 0391	*
DUSP2		gt	ms, rt	Santa Cruz	sc-1622	# 0394	*
DUSP4		rb	hu, ms, rt	abcam	ab72593	# 1568	*
DUSP5		rb	hu, ms	Sigma	D8819	# 0417	*
DUSP6		rb	hu, ms	ProteinTech Group	10433-1-AP	# 0335	*
DUSP7		gt	hu, ms, rt	Santa Cruz	sc-47667	# 0497	*
DUSP9		rb	hu, ms	ProteinTech Group	14484-1-AP	# 0337	*
DVL1		ms	ms, rt, hu	Santa Cruz	sc-8025	# 1729	*
DVL2		rb	hu, ms, rt	Cell Signaling	3224	# 0687	*
DVL2		rb	hu, ms, rt	Cell Signaling	3224S	# 1739	*
DVL3		rb	hu, ms, rt	Cell Signaling	3218	# 1182	*
DVL3		ms	ms, rt, hu	Santa Cruz	sc-8027	# 1731	*
E-Cadherin	pSer838/ pSer840	rb	hu, ms, rt	Epitomics	2239-1	# 0203	
E-Cadherin		gt	ms	R&D	AF748	# 0742	
E-Cadherin		rb	hu, ms	Cell Signaling	3195	# 1180	*/**
EGFR		rb	hu, ms, rt	Cell Signaling	2232	BG # 034	
EGR1		rb	hu, ms, rt	Cell Signaling	4153	# 1226	
eIF2 α		rb	hu, ms, rt	Cell Signaling	9722	# 1691	*
eIF2 α	pSer51	rb	hu, ms, rt	Cell Signaling	3398	# 1204	*
eIF4E	pSer209	rb	hu, ms, rt	Cell Signaling	9741	# 1221	
eIF4E		rb		Cell Signaling	2067	# 0441	*
Elk-1		rb	hu, ms, rt	Cell Signaling	9182	TK # 021	*
Erk1/2		rb	hu, ms, rt	Cell Signaling	4695	# 1071	*
Erk3		rb	hu, ms, rt	Epitomics	2030-1	# 0248	*
ER β		gt		Santa Cruz	sc-6820	# 0845	
Evi		rb		Protein Tech		# 1740	*
Ezh2		gt	hu, ms	R&D	AF4767	# 0743	

Antigen	Mod.	Spec.	Reactivity	Distributor	Product number	NMI number	*/**
Ezh2		rb	hu, ms, rt	Cell Signaling	5246	# 1454	*/**
FAK		rb	hu, ms, rt	Cell Signaling	3285	# 1451	*
FAK1		rb	hu, ms, rt	Epitomics	2146-1	# 0223	
FAS		ms	hu	Calbiochem	AM01	# 0314	*
FoxM1		rb	hu	Cell Signaling	5436	# 1196	
FoxM1		rb	hu, ms	Cell Signaling	3948	# 0949	*
FoxO1/ O3a/O4	pThr24/ pThr32/ pThr28	rb	hu, ms	Cell Signaling	2599	# 1483	*
FoxO3a	pSer413	rb	hu	Cell Signaling	8174	# 1539	*
Frizzled1		rb	hu	abcam	ab71342	# 1417	*
Frizzled4		rb	ms, hu, rt	abcam	AB83042	# 1733	*
Frizzled7		rb	ms, rt, hu	abcam	AB64636	# 1734	*
Fyn		rb	hu, ms	Cell Signaling	4023	# 1326	
GAPDH		rb	hu, ms, rt	abcam	ab9485	# 1648	*/**
GATA4		gt	ms, rt, hu	Santa Cruz	sc-1237	# 1725	*
GCN5L2		rb	hu, ms, rt	Cell Signaling	3305	# 1022	
GFP (3H9)		rt		ChromoTek			
GLI1		rb	hu, ms, rt	Cell Signaling	2534	# 1434	*
Gpr49		rb	hu, ms, rt	Epitomics	2495-1	# 0200	
Gpr49 P2 T1		rb	ms	NMI	P2 T1	TK # 125	
GSK3 α/β	pTyr279/ pTyr216	rb	hu, ms, rt	Epitomics	2309-1	# 1714	*/**
GSK3 β		rb	hu, ms, rt	Cell Signaling	9315	# 1627	*/**
GSK3 β	pSer9	rb	hu, ms, rt	Cell Signaling	9336	# 1665	*/**
Ha-ras		rb	hu, ms, rt	Upstate	05-775	TK # 002	*
HDAC1		ms	hu, ms, rb	Cell Signaling	5356	# 1629	
HDAC1		rb	hu, ms, rt	Cell Signaling	2062	# 1165	*/**
HDAC2		rb	hu, ms	Cell Signaling	2545	# 1637	*
HDAC2		rb	hu, ms, rt	Epitomics	1603-1	# 1680	**
HDAC3		rb	hu, ms, rt	Epitomics	1580-1	# 0734	*/**
HDAC6		rb	hu, ms	Upstate	07-732	# 1666	
HDAC6		rb	hu, ms	Millipore	07-732	# 0739	*/**
HELLS		rb	hu, ms	Cell Signaling	7998	# 1070	*/**
Her2		rb	hu	Cell Signaling	2242	# 1276	
Her3		rb	hu	Santa Cruz	sc-285	# 1076	
HIF1 α		rb	hu	Cell Signaling	3716	# 0694	*
Histone H3	me3Lys4	ms	hu	Millipore	05-1339	# 1040	
Histone H3	acLys27	rb	hu	Millipore	07-360	# 1041	
HMGCS1		rb	hu, ms	biorbyt	orb36826	# 1127	
HNF-1		rb	hu, rt, ms	Santa Cruz	sc-8986		
HNF1A		rb	hu, ms, rt	abcam	ab96777	# 1563	*
HNF-1 α		ms	ms, rt, hu	Santa Cruz	sc-135939		
HNF-1 α		gt	ms, rt, hu	Santa Cruz	sc-6548		
HNF-4 α		gt		Santa Cruz	sc-6556	# 0889	
HSP 90		ms	hu, ms, rt	abcam	ab1429-50	# 0266	
IKK α		rb	hu, ms, rt	Cell Signaling	2682	# 0670	
IKK α/β	pSer176/pSer180	rb	hu, ms, rt	Cell Signaling	2697	# 1267	
IKK β		rb	hu, ms, rt	Cell Signaling	2370	# 0671	
ILK1	pSer259	rb	hu, ms, rt	biorbyt	orb6215	# 1300	
ILK1		rb	hu, ms, rt	Cell Signaling	3862	TK # 112	*/**
IMP		ms	hu, ms, rt	Santa Cruz	sc-166012	# 0396	*
Integrin α1 subunit		rb	hu, ms, rt	Chemicon	AB1934	BG # 126	
Integrin α5		ms	hu	BD Biosciences	610634	# 0515	

Antigen	Mod.	Spec.	Reactivity	Distributor	Product number	NMI number	*/**
Integrin β1		ms	hu	BD Biosciences	610468	# 0516	
Integrin β3		ms	hu	BD Biosciences	611141	# 0517	
JNK/SAPK		rb	hu, ms, rt	Cell Signaling	9252	# 1319	*
JNK/SAPK 1/2/3	pTyr185/ pTyr223	rb	hu, ms, rt	Epitomics	2155-1	# 0215	
JNK1		ms	hu, ms, rt	Cell Signaling	3708	# 1686	*
JNK3		rb	hu, ms, rt	Cell Signaling	2305	# 1690	*
KLF4		rb	ms, hu	Millipore	09-821	# 0928	
KLF4		rb	hu	Cell Signaling	12173S	# 1283	
KLF5		rb	hu	Sigma	HPA040398	# 1700	*
LATS1	pSer909	rb	hu, ms, rt	Cell Signaling	9157	# 1547	*
LATS1	pThr1079	rb	hu, ms, rt	Cell Signaling	8654	# 1250	*/**
LATS1		rb	hu, ms	Cell Signaling	3477	# 1251	*/**
LATS2		rb	hu	Cell Signaling	5888	# 1306	*
LEF1		rb	hu, ms	Cell Signaling	2286	# 0426	
LEF1		rb	hu, ms, rt	Cell Signaling	2230	# 1470	
LGR5		gt	hu, ms	Santa Cruz	sc-68580	# 1696	*
LRP6		rb	hu, ms, rt	Cell Signaling	3395	# 0691	*
LRP6	pSer1490	rb	hu, ms	Cell Signaling	2568	# 1567	*
LRP6	pSer1490	rb	hu, ms	Cell Signaling	2568S	# 1750	*
LRP6		rb	hu, rt	Cell Signaling	2560	HD	*
LSD1		rb	hu, ms, rt	Cell Signaling	2184	# 1640	*/**
MAPKAPK-2		rb	hu, ms, rt	Cell Signaling	12155	# 1685	*
MAPKAPK-3		rb	hu, ms, rt	Cell Signaling	7421	# 1693	*
MAPKAPK-5		rb	hu, rt	Cell Signaling	7419	# 1694	*
MBD2		rb	hu, ms	bethyl laboratories	A301-633A		**
MBD3		rb	hu, ms, rt	Cell Signaling	3896	# 1632	
MBD3		rb	hu	abcam	ab91458	# 1639	**
MDM2	pSer166	rb	hu, ms, rt	Cell Signaling	3521	TK # 015	
MDM2		ms	ms, rt, hu	Santa Cruz	sc-965	# 1083	*
MEK1		rb	hu, ms, rt	Cell Signaling	9124	TK # 005	*
MEK2		rb	hu, ms, rt	Cell Signaling	9125	TK # 004	*
MEKK3		ms	hu, rt, ms	BD Biosciences	611102	# 0502	*
MKK4		rb	hu, ms, rt	Epitomics	1658-1	# 0241	*
MKK6		rb	hu, ms, rt	Epitomics	1821-1	# 0247	*
MKK7		rb	hu, ms, rt	Cell Signaling	4172	# 1225	*
Mnk1		rb	hu, ms	Cell Signaling	2195	# 0422	*
MOB1	pThr35	rb	hu, ms, rt	Cell Signaling	8699	# 1252	*/**
MOB1		rb	hu, ms, rt	Cell Signaling	3863	# 1253	*/**
MSK1	pThr589	rb	hu, ms	Cell signaling	9595P	# 1752	*
Mst1		rb	hu, ms, rt	Cell Signaling	3682	# 1254	*/**
Mst2		rb	hu, ms, rt	Cell Signaling	3952	# 1255	*/**
MTA1		rb	hu, ms, rt	Cell Signaling	5646	# 1633	**
MTA2		rb	hu, ms, rt	Sigma	HPA006214	# 1631	*/**
MUC1		ms	hu	Cell Signaling	4538	# 0445	
N-Cadherin		ms	rt	BD Biosciences	610920	# 0762	
N-Cadherin		rb	hu, ms, rt	Cell Signaling	4061	# 1227	*
NDRG1	pThr346	rb	hu, ms, rt	Cell Signaling	3217	# 1181	
NF-κB p100/p52		rb	hu, ms, rt	Cell Signaling	4882	# 0667	
NF-κB p50		rb	hu, ms, rt	Santa Cruz	sc-7178		
NF-κB p65		rb	hu	Epitomics	2229-1	# 0205	
NF-κB p65	pSer468	rb	hu, ms, rt	Cell Signaling	3039	# 0465	
NF-κB p65		rb	hu, ms, rt	Santa Cruz	sc-372		
NIK		rb	hu, ms, rt	Cell Signaling	4994	# 0668	

Antigen	Mod.	Spec.	Reactivity	Distributor	Product number	NMI number	*/**
NR5A2		rb	hu, ms, rt	Epitomics	5450-1	# 1110	
Oct-4		ms	hu, ms	Cell Signaling	4286	# 0696	
p15		rb	hu, ms, rt	Santa Cruz	sc-67279	# 1622	**
p21		rb	hu	Cell Signaling	2947	# 1102	*
p300	pSer89	rb	hu	biorbyt	orb34489	# 1285	
p300	pSer1834	rb	hu, ms, rt	biorbyt	orb6262	# 1299	
p38/MAPK		rb	hu, ms, rt	Cell Signaling	9212	# 0350	*
p38/MAPK α		rb	hu, ms, rt	Cell Signaling	9218	# 1684	*
p38/MAPK β		rb	hu	Cell Signaling	2339	# 1688	*
p38/MAPK γ		rb	hu, ms, rt	Cell Signaling	2307	# 1695	*
p38/MAPK δ		rb	hu, rt	Cell Signaling	2308	# 1689	*
p53		rb	hu, rt	Cell Signaling	9282	# 1121	
p53	acLys305	rb	hu, ms, rt	abcam	ab109396	# 1274	
p53	pSer46	rb	hu	Cell Signaling	2521	BG # 101	
p53	acLys382	rb	hu	Cell Signaling	2525	# 1269	
p53	pSer392	rb	hu, ms	Cell Signaling	9281	# 1549	
p53	pSer6	rb	hu, ms	Cell Signaling	9285	BG # 103	
p53	pSer9	rb	hu	Cell Signaling	9288	BG # 105	
p53	pSer37	rb	hu	Cell Signaling	9289	BG # 106	
p53	pSer15	rb	hu, ms, rt	Cell Signaling	9284	# 1164	*
p53	pSer20	rb	hu, ms	Cell Signaling	9287	# 1213	*
p53		gt	hu, ms, rt	R&D	af1355	TK # 001	*
PARP	cleAsp214	rb	hu	Cell Signaling	9541	# 1044	
PARP		rb	hu, ms, rt	Cell Signaling	9542	# 1358	*
PARP		rb	hu, ms, rt	Cell Signaling	9532	# 0708	**
PARP1		ms	hu, ms, rt	BD Biosciences	611038		
PCAF		rb	hu,ms,rt	Cell Signaling	3378	# 1052	
PCNA		rt	hu, ms, rt	Kremmer		# 0256	*/**
PI3-kinase p110 α		rb	hu, ms, rt	Cell Signaling	4255	# 1160	
PI3-kinase p110 β		rb	hu	Millipore	04-400	# 1049	
PI3-kinase p85 α		rb	hu, rt	Epitomics	1675-1	# 0240	
PI3-kinase γ		ms	hu, ms	Jena Bioscience	ABD-026S	# 1051	
PI3-kinase δ		rb		Santa Cruz	sc-7176	# 0533	
Pontin52		rb	hu, ms, rt	Cell Signaling	12300	# 1634	*/**
PP2A C	pTyr307	rb	hu, ms, rt	R&D	AF3989	TK # 105	**
PP2A C		rb	hu, ms, rt	Cell Signaling	2259	TK # 093	*/**
PRMT1		rb	hu, ms, rt	Cell Signaling	2449	# 1093	
PRMT4		rb	hu, ms, rt	Cell Signaling	3379	# 1094	*
PTCH1		rb	hu	Cell Signaling	2468	# 1437	*
PTCH2		rb	hu	Cell Signaling	2470	# 1436	*
PTEN		rb	hu, ms, rt	Cell Signaling	9552	TK # 031	
PTEN	pSer380	rb	hu, ms, rt	Cell Signaling	9551	# 1045	
PTPN7		rb	hu, ms	ProteinTech Group	15286-1-AP	# 0336	
PTP-PEST		ms	hu, ms, rt	Cell Signaling	4864	# 0407	
Rac1	pSer71	rb	hu, ms, rt	Cell Signaling	2461	# 1476	
Rac1		rb	hu, ms, rt	Cell Signaling	4651	# 1521	
RACK1		ms	hu, ms, rt	BD Biosciences	610177	# 1590	
Ras		rb	hu, ms, rt	Cell Signaling	8955	# 1545	*
Rb	pSer807/ pSer811	rb	hu, ms, rt	Cell Signaling	8516	# 1270	
Rb	pSer608	rb	hu	Cell Signaling	8147	# 1271	
Rb		ms	hu	Cell Signaling	9309	BG # 046	*
RelB		rb	hu, ms, rt	Cell Signaling	4954	# 0672	
RelB	pSer552	rb	hu, ms, rt	Cell Signaling	5025	# 1280	

Antigen	Mod.	Spec.	Reactivity	Distributor	Product number	NMI number	*/**
RPTP β		ms	hu, ms, rt	BD Biosciences	610179	# 0526	
Sav1		rb	hu, rt	Cell Signaling	3507	# 1256	*/**
SFRP2		rb	ms, rt, hu	abcam	ab111874	# 1404	*
SFRP2		rb	hu, ms, rt	abcam	ab92667	# 1414	*
SHP-2	pTyr582	rb	hu	Epitomics	2165-1	# 0214	
SHP-2		rb	hu, ms, rt	Epitomics	1609-1	# 0239	
SHP-2	pTyr542	rb		Cell Signaling	3751	BG # 112	
Slug		rb	hu, ms	Cell Signaling	9585	# 1355	
Smad1		rb	hu, ms,	Cell Signaling	6944	# 0955	*/**
Smad2	pSer245/ pSer250/ pSer255	rb	hu, ms, rt	Cell Signaling	3104	# 0880	*/**
Smad2/3		rb	hu, ms, rt	Cell Signaling	3102	# 0879	*/**
Smad3	pSer423/ pSer425	rb	hu, ms, rt	Cell Signaling	9520	# 0953	*/**
Smad3		rb	hu, ms, rt	abcam	ab40854	# 1237	*/**
Smad4		rb	hu, ms, rt	Cell Signaling	9515	# 1552	*
Smad5		rb	hu, rt	Cell Signaling	9517	# 0954	*
Smad9		gt	hu	R&D	AF2309	# 0916	
Snai1		rb	hu, ms, rt	Santa Cruz	sc-28199		
Snail		rb	hu, ms, rt	Cell Signaling	3879	# 1375	*/**
SOX17		ms		Sigma		# 1741	*
Sox2		rb	hu	Cell Signaling	3579	# 0946	
Sox9		rb	hu, ms, rt	Millipore	AB5535	# 0919	
SP1		rb	hu	Cell Signaling	9389	# 1550	
SPRY2		rb	hu, rt, ms	Millipore	07-524	# 0342	*
Src	pTyr527	rb	hu, ms, rt	Cell Signaling	2105	# 1189	*/**
Src	pTyr416	rb	hu, ms, rt	Cell Signaling	6943	# 1262	*/**
Src		rb	hu, ms, rt	Cell Signaling	2108	# 1359	*/**
SRC-3		rb	hu, ms, rt	Cell Signaling	2126	# 1097	
SRC-3	pThr24	rb	hu	Cell Signaling	2979	# 1096	
STAT1		rb	hu	Cell Signaling	9175	# 1186	
STAT1		rb	hu, ms, rt	Cell Signaling	9172	TK # 038	
STAT3		rb	hu, ms, rt	Cell Signaling	9132	# 0358	
STAT3		rb		Cell Signaling		# 1736	*
STAT3	pTyr705	ms	hu, ms, rt	Cell signaling	9138S	# 1745	*
STAT3	pTyr705	rb	hu, ms, rt	Cell Signaling	9145	# 1192	*/**
STAT3		rb	hu, ms, rt	Cell Signaling	4904	TK # 054	*/**
STAT3	pSer727	rb	hu, ms, rt	Cell Signaling	9134	# 1606	*/**
STAT4		ms	hu	Cell signaling	5097S	# 1735	*
STAT4	pTyr693	rb	hu, ms, rt	Cell signaling	4134S	# 1749	*
STEP		rb	ms, rt, hu	Cell Signaling	4817	# 0405	
Tag(CGY)FP		rb		evrogen	AB122	# 1565	**
TAK1	pSer412	rb	hu, ms, rt	Cell Signaling	9339	TK # 089	
TAK1	pThr187	rb	hu, ms, rt	Cell Signaling	4536	TK # 091	
TAK1		rb	hu, ms, rt	Cell Signaling	4505	TK # 090	*
TAZ		ms	hu, ms	BD Biosciences	560235	# 1626	*
TAZ		rb		Novus		# 1737	*
TAZ		rb	hu	Cell Signaling	2149	# 1184	**
TBP		rb	hu, ms, rt	Cell Signaling	8515	# 1104	
TCF1		ms		Upstate		# 1746	*
TCF1		rb	hu, ms, rt	Cell Signaling	2206	# 1673	*/**
TCF4		rb	hu	Epitomics	2114-1	# 0226	
TCF4		rb	hu, ms, rt	Cell Signaling	2565	# 0939	

Antigen	Mod.	Spec.	Reactivity	Distributor	Product number	NMI number	*/**
TCF4		rb	hu	Sigma	AV100775	# 1148	
TCF4		ms		Upstate		# 1753	*
TCF4		rb	hu	Santa Cruz	sc-13027	# 1727	*
TCF4		rb	hu, ms	Cell Signaling	2569	# 1481	*/**
TCF7L2		ms	hu	Abgent	AT4192a	# 1730	*
Topo 2 α		rb		Santa Cruz	sc-13058	# 0892	
Vimentin		rb	hu, ms, rt	Cell Signaling	5741	# 1376	*/**
Wnt1		gt	ms, rt, hu	Santa Cruz	sc-6266	# 1728	*/**
Wnt11		rb	hu, rt	abcam	ab31962	HD	*
Wnt16		rb	hu, ms	GeneTex	GTX128468	# 1751	*/**
Wnt2		rb	ms, rt, hu	Santa Cruz	sc-50361	# 1726	*/**
Wnt3A		rb	hu, ms, rt	Millipore	09-162	# 0741	*/**
Wnt5a		rb	ms, rt, hu	Santa Cruz	sc-30224	# 1732	*/**
Wnt7a		rb	hu, ms	abcam	ab100792	# 1738	*/**
Wnt7b		rb		GeneTex	GTX11488	# 1742	*/**
YAP		ms	hu, ms, rt	Santa Cruz	sc-271134	# 1625	
YAP	pSer127	rb		Cell Signaling		# 1747	*
YAP		rb		Cell Signaling		# 1748	*
YAP	pSer127	rb	hu, ms, rt	Cell Signaling	4911	# 1260	*/**
YAP		rb	hu, ms, rt	Cell Signaling	4912	# 1605	*/**
YAP/TAZ		rb	hu, ms	Cell Signaling	8418	# 1258	*/**
Yes		rb	hu	Cell Signaling	3201	# 1261	*/**
ZO-1		rb	hu	Cell Signaling	8193	# 1383	
α-catenin		ms	hu, ms, rt	USBiological	C2069-44H	# 1678	*/**
α-Tubulin		ms	hu, ms, rt	Synaptic Systems	302211	# 1086	
β-Actin		ms		Sigma	A1978	# 1284	*/**
β-catenin		rb	hu, ms	Biosource	AHO0462	# 0802	
β-catenin		rb	hu, ms	Invitrogen	AHO0462	# 1361	
β-catenin		rb	hu, ms, rt	Santa Cruz	sc-7199	H102	
β-catenin		ms	hu, ms, rt	Santa Cruz	sc-65484	7A7	
β-catenin	pSer45	rb	hu, ms, rt	Cell Signaling	9564	# 0952	*
β-catenin	acLys49	rb	hu, ms, rt	Cell Signaling	9534	# 0982	*
β-catenin	pSer33/ pSer37/ pThr41	rb	hu, ms, rt	Cell Signaling	9561		*
β-catenin		ms	hu, ms, rt	Upstate	05-665	8E7	**
β-catenin	pThr41/pSer45	rb	hu, ms	Cell Signaling	9565	# 0763	*/**
β-catenin		rb	hu, ms, rb	Millipore	06-734	# 0917	*/**
β-catenin		ms	hu	BD Biosciences	610154	BD	*/**
β-catenin	pSer675	rb	hu, rt, ms	Cell Signaling	9567	# 0950	*/**
β-catenin	pSer552	rb	hu, ms, rt	Cell Signaling	9566	# 1001	*/**
β-catenin	non-p Ser33/ pSer37/ pThr41	rb	hu, ms, rt	Cell Signaling	8814	# 1356	*/**
γ-catenin		rb	hu, ms, rt	Cell Signaling	2309	# 1472	

Suppl. Table B: Antibodies, detecting isoforms of the same protein or several ones.
All antibodies detecting different isoforms and cleaved versions of one protein or binding to more than one protein are listed and separated into their different peaks assigned to different MWs.

Antigen	Modification	NMI number	MW	Protein/Isoform
Axin2		# 0956	95	isoform
			98	isoform
cJUN		# 1187	43	isoform
			48	isoform
Cytokeratin Pan		# 0474	ca. 46	Krt-13 or -18
			ca. 55	Krt-4, -8 or -10
Erk1/2		# 1071	42	Erk2
			44	Erk1
Evi		# 1740	50	isoform
			60	isoform
FoxO1/O3a/O4	pThr24/pThr32/ pThr28	# 1483	65	FoxO4
			95	FoxO3a
GSK3 α/β	pTyr279/pTyr216	# 1714	47	GSK3 β
			51	GSK3 α
JNK1		# 1686	46	isoform
			54	isoform
JNK/SAPK		# 1319	46	isoform
			54	isoform
LRP6	pSer1490	# 1567	180	isoform
			210	isoform
LRP6	pSer1490	# 1750	180	isoform
			210	isoform
MDM2		# 1083	90	isoform
			60	isoform
MSK1	pThr589	# 1752	61	isoform
			85	isoform
PARP		# 1358	24	isoform
			116	isoform
Smad2/3		# 0879	52	Smad3
			60	Smad2
SOX17		# 1741	30	isoform
			44	isoform
STAT3	pTyr705	# 1192	79	isoform
			86	isoform
STAT3		TK # 054	79	isoform
			86	isoform
STAT3		# 1736	79	isoform
			86	isoform
TCF4		# 1481	60	isoform
			70	isoform
TCF4		# 1753	60	isoform
			50	isoform
TCF4		# 1727	60	isoform
			50	isoform
TCF7L2		# 1730	30	isoform
			50	isoform

Suppl. Table C: Co-immunoprecipitated proteins with β-catenin in 70.4 cells.
All different β-catenin variants and proteins precipitated with β-catenin, after eliminating unspecific signals, are illustrated and sorted alphabetically. The respective raw data values for input and bound in the differently treated samples, as well as the calculated CFs, can be obtained. Proteins which only occur as a signal in the bound sample, thus represent complex partners of β-catenin, which are enriched during Co-IP, are marked with a "+". The corresponding raw values for other treatments of these proteins are included in the table, albeit the calculation of a CF. If these signals were eliminated by earlier cutoff limits, the cell "-" was inserted into the cell.

		untreated				CHIR 99021				MG132			
Analyte	**Modification**	**input**	**bound**	**CF**	**+**	**input**	**bound**	**CF**	**+**	**input**	**bound**	**CF**	**+**
α-catenin		120	175	7.29		21	107	25.48		68	205	15.07	
APC		17	89	26.18		11	11	-		11	11	-	
A-Raf		73	11	-		11	48	21.82	+	43	21	-	
β-Actin		60390	57646	4.77		34895	3304	0.47		39159	81	0.01	
β-catenin	non-p Ser33/ Ser37/Thr41	354	4706	66.47		44	2201	250.11		52	2408	231.54	
β-catenin	pSer552	353	2916	41.30		181	2022	55.86		96	1715	89.32	
β-catenin	pSer675	572	4726	41.31		163	2209	67.76		86	1446	84.07	
β-catenin	pThr41/pSer45	20	55	13.75		11	22	-		11	27	-	
β-catenin (BD)		2596	9349	18.01		1239	7437	30.01		1519	13598	44.76	
β-catenin (Millipore)		2434	11812	24.26		846	6459	38.17		1076	8672	40.30	
CK1 δ		856	26	-		336	72	1.07		615	198	1.61	
cJUN (# 1744)	pSer63	11	16	-		11	12	-		56	86	7.68	
cJUN (HD)		11	11	-		11	16	-		84	137	8.15	
Cytokeratin Pan (~46 kDa, # 474)		11	84	-		44	60	6.82		1055	11	-	
Cytokeratin Pan (~55 kDa, # 474)		2762	121	-		11	58	-		73	614	42.05	
Cytokeratin Pan (~60 kDa, # 588)		1301	840	-		567	5626	-		2665	36739	68.93	
DUSP6		160	82	2.56		116	11	-		41	11	-	
DVL1		11	11	-		11	88	40.00	+	11	11	-	
DVL2 (# 1739)		11	32	-		11	33	-		11	305	138.64	+
Elk-1		107	191	8.93		54	28	-		116	11	-	
Evi (50 kDa isoform)		75	25	-		193	29	-		175	52	1.49	
GLI1		32	48	7.50		11	11	-		16	17	-	
GSK3 β		2315	13	-		397	11	-		694	60	0.43	
LRP6 (210 kDa isoform, # 1567)	pSer1490	11	11	-		11	11	-		11	47	21.36	+
STAT3 (79 kDa isoform, # 1736)		71	151	-		31	346	-		11	5489	2495.00	+
STAT3 (86 kDa isoform, # 1736)		81	11	-		110	54	2.45		206	19497	473.23	
STAT4		11	63	28.64	+	11	78	35.45	+	11	53	24.09	+
Vimentin		343	465	6.78		871	153	0.88		2688	20	-	
Wnt11		11	45	20.45	+	11	11	-		11	11	-	
Wnt7b		11	11	-		11	123	-		11	69	31.36	+

Suppl. Table D: Co-immunoprecipitated proteins with β-catenin in 55.1c cells.
All different β-catenin variants and proteins precipitated with β-catenin, after eliminating unspecific signals, are illustrated. The respective raw data values for input and bound in the differently treated samples, as well as the calculated CFs, can be obtained. Data representation was done analog to Suppl. Table C.

		untreated				CHIR 99021				MG132			
Analyte	**Modification**	**input**	**bound**	**CF**	**+**	**input**	**bound**	**CF**	**+**	**input**	**bound**	**CF**	**+**
α-catenin		888	2878	16.20		968	1504	7.77		732	2764	18.88	
APC		23	54	11.74		11	11	-		22	11	-	
A-Raf		240	141	2.94		505	42	-		344	11	-	
ATF4		742	370	-		11	839	381.36	+	226	628	-	
Axin1		50	758	75.80		14	11	-		38	307	40.39	
Axin2 (# 1724)		11	90	40.91	+	11	11	-		11	11	-	
β-Actin		167362	535130	-		176674	467673	13.24		138494	335905	12.13	
β-catenin	pSer552	2497	23560	47.18		1114	6343	28.47		2206	18517	41.97	
β-catenin	pSer675	2491	30807	61.84		810	6157	38.01		1317	14049	53.34	
β-catenin	non-p Ser33/ Ser37/Thr41	48	1088	113.33		255	5570	109.22		82	2555	155.79	
β-catenin (BD)		14047	63725	22.68		15515	37887	12.21		20615	74652	18.11	
β-catenin (Millipore)		969	5525	28.51		2955	12880	21.79		1320	8773	33.23	
CK1 α		480	223	2.32		360	94	1.31		206	57	-	
Cytokeratin Pan (~46 kDa, # 474)		92	1202	65.33		8223	1257	0.76		10909	682	0.31	
Cytokeratin Pan (~55 kDa, # 474)		51241	628	-		9941	2089	-		403	1882	23.35	
Cytokeratin Pan (~60 kDa, # 588)		28948	7650	-		24510	24522	5.00		30185	22750	-	
DUSP1		1324	9861	-		1236	6724	27.20		926	4686	25.30	
DUSP4		5500	3468	-		7361	5433	-		4590	5930	6.46	
DUSP6		831	1876	11.29		349	39	-		270	20	-	
DUSP9		226	8781	-		11	2662	1210.00	+	143	326	-	
E-Cadherin		781	3328	21.31		1191	1493	6.27		1102	2511	11.39	
eIF4E		8820	189	0.11		5043	118	-		2534	11	-	
Elk-1		1155	6119	-		742	2740	18.46		428	1604	18.74	
Evi (50 kDa isoform)		147	165	-		209	789	18.88		323	556	-	
Evi (60 kDa isoform)		503	452	4.49		193	417	10.80		254	618	12.17	
Ezh2		1435	109	0.38		598	41	-		657	47	-	
Frizzled4		1085	1219	-		8081	12505	-		4960	10430	10.51	
GSK3 β	pTyr216	696	2100	15.09		233	281	-		493	534	5.42	
GSK3 α	pTyr279	436	746	8.56		22	89	20.23		312	211	3.38	
GSK3 β		3653	8018	10.97		2442	2795	5.72		2856	2767	4.84	
HDAC2		49	83	8.47		15	72	-		41	12	-	
HNF1A		1211	391	1.61		228	122	2.68		726	880	6.06	
JNK/SAPK (54 kDa isoform)		256	78	1.52		638	133	-		779	45	-	
LRP6 (180 kDa isoform, # 1750)	pSer1490	58	67	5.78		65	25	-		64	16	-	
MAPKAPK-5		64	57	4.45		263	53	-		165	48	-	
MDM2 (60 kDa isoform)		43	90	10.47		44	45	-		49	20	-	
MKK7		166	81	2.44		174	29	-		141	34	-	
Smad3		618	189	1.53		2394	119	0.25		522	71	-	
Smad4		387	72	0.93		572	22	-		988	28	-	
Smad5		355	94	1.32		902	181	1.00		549	84	-	
Src		9241	3738	2.02		4022	1085	1.35		4374	501	-	
Src	pTyr416	144	11	-		17	135	39.71		25	51	10.20	
Src	pTyr527	5370	3097	-		2982	968	1.62		4024	550	0.68	
STAT3 (79 kDa isoform, TK # 054)		862	73	0.42		761	47	0.31		362	11	-	
TAZ		3726	10502	14.09		38	27	-		58	295	25.43	
TCF4 (60 kDa isoform, # 1727)		11	294	133.64	+	234	388	8.29		227	531	11.70	
TCF4 (70 kDa isoform, # 1481)		30	77	12.83		11	21	-		12	12	-	
Vimentin		7346	24060	16.38		2818	14117	25.05		2763	9111	16.49	
Wnt3a		11	105	47.73	+	11	11	-		78	11	-	
Wnt7b		70	537	38.36		135	4904	181.63		11	84	38.18	+

Suppl. Table E: Co-immunoprecipitated proteins with β-catenin in HepG2 cells.
All different β-catenin variants and proteins precipitated with β-catenin, after eliminating unspecific signals, are illustrated. The respective raw data values for input and bound in the differently treated samples, as well as the calculated CFs, can be obtained. Data representation was done analog to Suppl. Table C.

		untreated				CHIR 99021				MG132			
Analyte	**Modification**	**input**	**bound**	**CF**	**+**	**input**	**bound**	**CF**	**+**	**input**	**bound**	**CF**	**+**
α-catenin		1200	133	0.55		229	304	6.64		576	768	6.67	
ATF4		11	92	41.82	+	11	11	-		11	11	-	
Axin1		24	25	-		11	23	-		11	116	52.73	+
Axin2 (95 kDa isoform, # 956)		18	17	-		14	22	-		40	67	8.38	
Axin2 (98 kDa isoform, # 956)		11	11	-		12	48	20.00		14	11	-	
β-Actin		131914	606	-		129705	442	-		144040	4539	0.16	
β-catenin	non-p Ser33/ Ser37/Thr41	24	17	-		108	4150	192.13		81	2313	142.78	
β-catenin	pSer552	2775	2384	4.30		303	2593	42.79		422	8789	104.14	
β-catenin	pSer675	2161	1994	4.61		159	1193	37.52		245	3703	75.57	
β-catenin (BD)		8037	4464	2.78		8021	25290	15.76		16848	92633	27.49	
β-catenin (Millipore)		410	232	2.83		1752	8796	25.10		1271	7972	31.36	
CK1 δ		867	46	0.27		1298	40	-		2290	73	-	
Cytokeratin Pan (~60 kDa, # 588)		189398	572	-		116755	9825	-		196115	58514	1.49	
E-Cadherin		679	223	1.64		533	500	4.69		1235	3683	14.91	
eIF4E		1930	54	0.14		1608	20	-		3580	11	-	
Evi (60 kDa isoform)		922	39	-		124	81	3.27		288	364	6.32	
FoxO3a	pSer413	11	54	24.55	+	11	11	-		12	11	-	
GAPDH		138556	386	0.01		172504	11	-		157497	2896	-	
GSK3 β	pTyr216	278	64	1.15		61	58	4.75		239	932	19.50	
GSK3 α	pTyr279	397	36	-		11	11	-		181	303	8.37	
GSK3 β		2085	244	0.59		1072	632	2.95		1873	4515	12.05	
HNF1A		293	60	1.02		816	375	2.30		924	316	1.71	
JNK/SAPK (46 kDa isoform)		317	22	-		231	25	-		309	116	1.88	
LRP6 (180 kDa isoform, # 1567)	pSer1490	11	53	24.09	+	27	25	-		65	43	-	
LSD1		1160	15	-		881	116	0.66		1758	170	0.48	
Snail		11	117	53.18	+	38	11	-		11	141	-	
STAT3 (79 kDa isoform, # 1736)		2249	168	-		1778	1303	3.66		2318	12015	25.92	
STAT4		11	52	23.64	+	46	11	-		11	34	-	
TCF1		32	24	-		26	28	-		11	283	128.64	+
TCF4 (60 kDa isoform, # 1481)		56	14	-		43	141	16.40		52	626	60.19	
TCF4 (70 kDa isoform, # 1481)		17	14	-		16	12	-		53	158	14.91	
Vimentin		39	13	-		13	11	-		20	56	14.00	
Wnt7b		11	71	32.27	+	11	11	-		313	64	-	

Suppl. Table F: Co-immunoprecipitated proteins with β-catenin in HB35 cells.
All different β-catenin variants and proteins precipitated with β-catenin, after eliminating unspecific signals, are illustrated. The respective raw data values for input and bound in the differently treated samples, as well as the calculated CFs, can be obtained. Data representation was done analog to Suppl. Table C.

		untreated				CHIR 99021				MG132			
Analyte	**Modification**	**input**	**bound**	**CF**	**+**	**input**	**bound**	**CF**	**+**	**input**	**bound**	**CF**	**+**
α-catenin		350	80	1.14		112	191	8.53		1198	1819	7.59	
Axin1		48	230	23.96		11	13	-		11	19	-	
β-Actin		140755	1250	0.04		78367	32	-		124953	76	-	
Bcl9		11	11	-		11	11	-		11	72	32.73	+
β-catenin	non-p Ser33/ Ser37/Thr41	40	78	9.75		27	294	54.44		59	1257	106.53	
β-catenin	pSer552	2102	6121	14.56		212	1264	29.81		1166	6061	25.99	
β-catenin	pSer675	1179	3107	13.18		147	1069	36.36		497	3222	32.41	
β-catenin (BD)		12678	13472	5.31		2710	8423	15.54		12872	34538	13.42	
β-catenin (Millipore)		680	764	5.62		401	1394	17.38		1098	4313	19.64	
cJUN (43 kDa isoform, # 1187)		301	77	1.28		29	16	-		477	118	-	
cJUN (# 1162)	pSer63	22	14	-		20	14	-		135	52	1.93	
Cytokeratin Pan (~55 kDa, # 474)		140930	277	0.01		2884	11	-		48554	154	-	
DVL1		11	38	-		11	47	21.36	+	11	62	28.18	+
E-Cadherin		1246	1077	4.32		78	187	11.99		328	641	9.77	
eIF4E		6969	74	0.05		100	17	-		585	23	-	
Evi (60 kDa isoform)		55	11	-		29	54	9.31		11	11	-	
GAPDH		178263	848	0.02		27760	11	-		121293	232	0.01	
GSK3 β	pTyr216	204	847	20.76		33	16	-		154	22	-	
GSK3 α	pTyr279	295	197	3.34		11	15	-		141	66	-	
GSK3 β		1868	4036	10.80		397	61	0.77		1113	208	0.93	
HDAC6		3675	57	-		112	11	-		194	47	1.21	
HNF1A		1348	11	-		90	81	4.50		45	140	15.56	
LRP6 (180 kDa isoform, # 1567)	pSer1490	11	11	-		12	24	-		20	57	14.25	
LSD1		3015	97	0.16		70	11	-		374	35	-	
Smad2		598	93	0.78		11	11	-		154	11	-	
Smad5		11	11	-		33	22	-		45	45	5.00	
Snail		11	185	84.09	+	42	11	-		11	190	-	
Src	pTyr527	9362	188	0.10		1205	13	-		3692	27	-	
STAT3 (79 kDa isoform, # 1736)		1465	212	-		685	583	4.26		1279	9210	-	
STAT3 (79 kDa isoform, TK # 054)		2679	92	0.17		269	11	-		870	70	0.40	
STAT3 (86 kDa isoform, # 1736)		475	58	0.61		536	11	-		1990	11	-	
TAZ (HD)		27	82	15.19		41	96	-		61	39	-	
TCF1		29	62	10.69		11	22	-		17	55	-	

Suppl. Table G: Proteins precipitated in HEK293T cells during ECIP.
All different β-catenin variants and proteins precipitated with β-catenin, after eliminating unspecific signals, are illustrated. The respective raw data values for inputs and bounds of the two replicas in the differently treated samples, as well as the calculated CFs and their mean, can be obtained. Data representation was done analog to Suppl. Table C.

		untreated								CHIR 99021							
Analyte	Modification	input		bound		CF			+	input		bound		CF			+
		1. Repl.	2. Repl.	1. Repl.	2. Repl.	1. Repl.	2. Repl.	AM		1. Repl.	2. Repl.	1. Repl.	2. Repl.	1. Repl.	2. Repl.	AM	
α-catenin		1077	701	585	315	2.72	2.25	2.48		1553	898	3003	1599	9.67	8.90	9.29	
Axin1		51	15	28	30	-	-	-		58	37	171	51	14.74	6.89	10.82	
Axin2 (95 kDa isoform, # 0956)		16	27	17	19	-	-	-		33	46	323	210	48.94	22.83	35.88	
β-catenin	non-p Ser33/ Ser37/Thr41	161	270	379	311	11.77	5.76	8.76		2281	1471	57383	54784	125.78	186.21	156.00	
β-catenin	pSer552	178	94	343	62	9.63	3.30	6.47		1109	582	18188	11656	82.00	100.14	91.07	
β-catenin	pSer675	488	400	465	256	4.76	3.20	3.98		1039	800	3728	2665	17.94	16.66	17.30	
β-catenin (8E7)		11	11	11	11	-	-	-		11	11	8850	7871	4022.73	3577.73	3800.23	+
β-catenin (BD)		3641	3193	4666	3008	6.41	4.71	5.56		20850	16206	82797	75472	19.86	23.29	21.57	
β-catenin (Millipore)		2519	2975	4247	4029	8.43	6.77	7.60		14506	11152	90439	92357	31.17	41.41	36.29	
CDK2		2244	1838	112	72	0.25	0.20	0.22		2029	1700	117	178	0.29	0.52	0.41	
GSK3 β	pTyr216	836	742	21	52	-	-	-		133	210	59	69	2.22	1.64	1.93	
GSK3 α	pTyr279	1437	1176	11	28	-	-	-		52	58	115	61	11.06	5.26	8.16	
GSK3 β		6286	6365	196	368	0.16	0.29	0.22		4523	4881	1739	1992	1.92	2.04	1.98	
HDAC2 (# 0238)		5627	5069	104	117	-	-	-		5450	5104	147	296	0.13	0.29	0.21	
HDAC3		665	533	53	29	-	-	-		425	392	76	115	0.89	1.47	1.18	
HELLS		3741	2532	164	11	-	-	-		3792	3172	381	324	0.50	0.51	0.51	
LSD1		3592	2221	259	196	0.36	0.44	0.40		4282	2984	189	191	0.22	0.32	0.27	
MTA2		6807	6735	240	538	0.18	0.40	0.29		9085	7528	438	400	0.24	0.27	0.25	
PCNA		53848	51143	288	142	0.03	0.01	0.02		57406	50808	235	107	0.02	0.01	0.02	
Pontin52		4040	5100	146	339	-	-	-		2858	3715	439	859	0.77	1.16	0.96	
PP2A C		7425	6676	169	135	0.11	0.10	0.11		7373	7407	174	243	0.12	0.16	0.14	
Smad1		1434	1127	48	78	-	-	-		1266	1313	138	132	0.55	0.50	0.52	
Smad2	pSer245/pSer250/ pSer255	287	359	18	38	-	-	-		185	134	50	73	1.35	2.72	2.04	
Src	pTyr527	7121	5551	424	231	0.30	0.21	0.25		6703	5994	230	536	0.17	0.45	0.31	
Src		7594	7983	1042	970	0.69	0.61	0.65		6224	6404	880	2223	0.71	1.74	1.22	
TCF1		517	382	43	53	-	-	-		1543	1510	703	1200	2.28	3.97	3.13	
TCF4 (60 kDa isoform, # 1481)		88	56	11	19	-	-	-		117	114	65	89	2.78	3.90	3.34	

Suppl. Table H: Proteins precipitated with β-catenin in HEK293T cells during ICIP.
All different β-catenin variants and proteins precipitated with β-catenin, after eliminating unspecific signals, are illustrated. The respective raw data values for inputs and bounds of the two replicas in the differently treated samples, as well as the calculated CFs and their mean, can be obtained. Data representation was done analog to Suppl. Table C.

		untreated										
Analyte	**Modification**	**input**			**bound**			**CF**				**+**
		1. Repl.	**2. Repl.**	**3. Repl.**	**1. Repl.**	**2. Repl.**	**3. Repl.**	**1. Repl.**	**2. Repl.**	**3. Repl.**	**AM**	
α-catenin		2047	1672	775	1529	1979	541	3.73	5.92	3.49	4.38	
Axin1		82	58	11	42	43	18	-	-	-	-	
Axin2 (95 kDa isoform, # 0956)		13	11	12	59	28	11	-	-	-	-	
β-catenin	non-p Ser33/ Ser37/Thr41	25	62	62	286	311	151	57.20	25.08	12.18	31.49	
β-catenin	pSer552	183	232	329	426	679	364	11.64	14.63	5.53	10.60	
β-catenin	pSer675	391	396	210	516	665	231	6.60	8.40	5.50	6.83	
β-catenin (8E7)		11	11	11	11	11	11	-	-	-	-	
β-catenin (BD)		2728	3179	1532	5997	6948	2162	10.99	10.93	7.06	9.66	
β-catenin (Millipore)		1065	1328	935	2430	3383	1694	11.41	12.74	9.06	11.07	
GSK3 β	pTyr216	1054	1066	775	213	20	117	-	-	-	-	
GSK3 β		7462	6418	4880	1510	1057	907	-	-	-	-	
TCF1		296	312	109	65	51	70	-	-	-	-	

		CHIR 99021										
Analyte	**Modification**	**input**			**bound**			**CF**				**+**
		1. Repl.	**2. Repl.**	**3. Repl.**	**1. Repl.**	**2. Repl.**	**3. Repl.**	**1. Repl.**	**2. Repl.**	**3. Repl.**	**AM**	
α-catenin		2084	1909	907	3490	6510	1317	8.37	17.05	7.26	10.89	
Axin1		106	52	17	454	831	170	21.42	79.90	50.00	50.44	
Axin2 (95 kDa isoform, # 0956)		126	32	16	629	1567	229	24.96	244.84	71.56	113.79	
β-catenin	non-p Ser33/ Ser37/Thr41	1225	611	414	15607	29052	9027	63.70	237.74	109.02	136.82	
β-catenin	pSer552	1500	1203	987	9880	19991	8260	32.93	83.09	41.84	52.62	
β-catenin	pSer675	1240	972	528	2041	4435	1174	8.23	22.81	11.12	14.05	
β-catenin (8E7)		11	11	11	1430	2347	697	650.00	1066.82	316.82	677.88	+
β-catenin (BD)		22554	14505	7706	43443	74633	29463	9.63	25.73	19.12	18.16	
β-catenin (Millipore)		8973	5822	4298	34660	57757	24092	19.31	49.60	28.03	32.31	
GSK3 β	pTyr216	390	90	216	155	87	130	1.99	4.83	3.01	3.28	
GSK3 β		6612	5792	4527	2433	4485	1945	1.84	3.87	2.15	2.62	
TCF1		1088	809	534	527	757	255	2.42	4.68	2.39	3.16	

7.2 List of figures

7.3 List of tables

7.4 List of publications

articles:

Haeussler R.S., Treindl F., Schwarz M., Templin M.F. (2015) *Characterisation of β-catenin complexes by co-immunoprecipitation and high output Western blotting in different cell lines.* Toxicol Lett. 2015 Oct; **238**(2): S243.doi:10.1016/ j.toxlet.2015.08.716

Traenkle B, Emele F, Anton R, Poetz O, Haeussler RS, Maier J, Kaiser PD, Scholz AM, Nueske S, Buchfellner A, Romer T, Rothbauer U. (2015). *Monitoring interactions and dynamics of endogenous β-catenin with intracellular nanobodies in living cells.* Mol Cell Proteomics. 2015 Mar;14(3):707-23. doi: 10.1074/ mcp.M114.044016.

presentations:

Personalised Medicine Congress 2016, Tübingen, 2016
poster: *"Translational oncology: Identification of biomarkers from primary ovarian cancer tissue using DigiWest multiple protein profiling technology"*

51.*Congress of the European Societies of Toxicology*, Porto, 2015
poster: *„Characterisation of β-catenin complexes by co-immunoprecipitation and high output Western blotting in different cell lines"*

13.*Human Proteome Organization World Congress*, Madrid, 2014
poster: „*Characterisation of β-catenin complexes by intracellular co-immunoprecipitation and high output Western blotting*"

7. junior scientist-Meeting: „*Young Scientists meet Experience*", Günzburg, 2014
poster: *„Characterisation of β-catenin containing protein complexes by intracellular co-immunoprecipitation and high output Western blotting*"

β-catenin Symposium, Natural and Medial Sciences Institute at the University Tübingen, Reutlingen, 2013
talk: „*Detecting β-catenin and its interaction partners*."

attendances: *GBM-Bioanalytic annual meeting*, Natural and Medial Sciences Institute at the University Tübingen, Reutlingen, 2015

Mini-Symposium: Frontiers in Proteome Research,
Eberhard Karls Universität Tübingen, 2015

posters: Advances in Cell Based Screening in Drug Discovery, Mölndal, 2015
poster: *„Characterisation of β-catenin complexes by Chromobody-based intracellular co-immunoprecipatation and DigiWest protein profiling“*

Drug Discovery 2015, Telford, 2015
poster: *„Characterisation of β-catenin complexes by Chromobody-based intracellular co-immunoprecipatation and DigiWest protein profiling“*

trainings: Personal Cancer Genomics: Next generation sequencing:
from basics to clinical application,
Personalised Medicine Congress 2016, Tübingen, 2016

Removing Obstacles on the Way to Implement 3R Methods in Toxicology,
51. *Congress of the European Societies of Toxicology*, Porto, 2015

Workshop – Trends in Diagnostics,
Eberhard Karls Universität Tübingen, 2013

7.5 Curriculum vitae

For reasons of data protection, the Curriculum vitae is not included and published in the online version.